Cranfield University

D. Zdebski

The Impact of Tool Performance on Micromachining Capability

School of Applied Sciences

PhD Thesis

Academic Year: 2011 - 2012

Supervisors: Prof. D. J. Stephenson and Prof. D. M. Allen

June 2012

Cranfield University

School of Applied Sciences

PhD Thesis

Academic Year 2011 - 2012

Daniel Zdebski

The Impact of Tool Performance on Micromachining Capability

Supervisor: Prof. D. J. Stephenson and Prof. D. M. Allen

June 2012

This thesis is submitted in partial fulfilment of the requirements for the degree of PhD.

Abstract

Micro-milling represents a versatile and fast manufacturing process suitable for production of fully 3D micro-components. Such components are demanded for a vast number of industrial applications including safety systems, environmental sensors, personalized medical devices or micro-lenses and mirrors. The ability of micro-milling to process a wide range of materials makes it one of the best candidates to take a leading position in micro-manufacturing. However, so far it does not seem to happen. By discussion with various industrialists, low predictability of micro-milling process was identified as the major limiting factor. This is mainly because of strong effects of the tool tolerances and process uncertainties on machining performance. Although, these issues are well known, they are not reflected by the current modelling methods used in micro-milling.

Therefore, the research presented in this thesis mainly concentrates on development of a method allowing a prediction of the tool life in manner of tool breakage probability. Another important criterion which must be fulfilled is the method applicability to industrial applications. This means that the method must give sufficiently accurate prediction in reasonable time with minimum effort and interactions with day-to-day manufacturing process.

The criteria listed above led to development of a new method based on analytically/numerical modelling techniques combined with an analysis of real tool variations and process uncertainty. Although, the method is presented in a relatively basic form, without considering some of the important factors, it shows high potential for industrial applications. Possibility of further implementation of additional factors is also discussed in this thesis.

Additionally, some of the modelling techniques presented in this thesis are assumed to be suitable for application during designing of micro end-mills. Therefore, in the last part of this thesis is presented a systematic methodology for designing of micro end-mills. This method is based on knowledge and experience gained during this research.

Key words:

Micro end-milling, cutting force modelling, tool life prediction, tool design

Acknowledgements

First of all I would like to show my gratitude to my supervisors: Prof. David J. Stephenson and Prof. David M. Allen for their interest, guidance and support during my PhD course.

I also would like to thank to all of the technicians from Precision Engineering Centre in Cranfield University. My special gratitude is to Mr. John Hedge for his invaluable help during my PhD. It would be much more difficult to succeed without his help and advice in many aspects of my work.

I am also grateful for all the support of all PhD students and researchers from Precision Engineering Centre in Cranfield University.

My work was sponsored from two EPSRC projects. Hence, I would like to thank EPSRC for supporting IMRC 110 and 3D-Minteration (the design and manufacture of 3D integrated miniaturised products, EP/C534212/1) Grand Challenge project. Details about 3D-Mintegration can be accessed at www.3d-mintegration.com.

Finally, I would also like to show my gratitude to my dear partner Blanka Chovancová and my parents: Dana Zdebská and Svatopluk Zdebski for their support during my PhD course.

Daniel Zdebski

Cranfield, June 2012

Table of contents

List of figures

Nomenclature

A	Area	mm^2
a_e	Width of cut	µm
a_p	Depth of cut	µm
d	Diameter	mm
D_c	Cutting diameter	mm
d_s	Shank diameter	mm
E	Modulus of elasticity	MPa
F	Force	N
F_t, F_r, F_a	Tangential, radial and axial force component	N
F_x, F_y	Force components in cutting and perpendicular direction	N
$\dot{F}$	Unity force increment	$N \cdot mm^{-1}$
f_z	Feed per tooth	µm/tooth
h	Reduction of the cutting diameter	µm
$\dot{h}$	Wear rate	$\mu m \cdot mm^{-1}$
I	Moment of inertia	mm^4
K	Force/wear coefficient	$\mu m \cdot N^{-1} \cdot mm^{-1}$
K_m	Specific cutting force	$N \cdot mm^{-2}$
l	Length, distance	mm
l_c	Cutting length	mm
$P(f)$	Cumulative probability function	-
$p(f)$	Probability function	
q	Proportional constant	-
s	Sliding distance	mm
S_a	Average surface deviation	µm
V	Volume	mm^3
v_c	Cutting speed	$m \cdot min^{-1}$
β	Helix angle	°
ψ	Neck angle	°
σ	Stress	MPa

Abbreviations

2D	Two-dimensional
3D	Three-dimensional
AFM	Atomic force microscopy
ALE	Arbitrary Lagrangian-Eulerian
BUE	Build-up-edge
CAD	Computer-aided design
CAM	Computer-aided manufacturing
CNC	Computer numerical control
DOF	Degree of freedom
ECM	Electrochemical machining
EDM	Electro discharge machining
EDS	Energy dispersive X-ray spectroscopy
FE, FEA, FEM	Finite element, Finite element analysis, Finite element method
FIB	Focus Ion Beam
ICT	Information & communication technologies
LBM	Laser beam machining
MCT	Minimum chip thickness
MEMS	Micro electro-mechanical system
MRR	Material removal rate
SEM	Scanning electron microscopy
SLS	Selective laser sintering
TRS	Transverse rupture strength
WLI	White light interferometer

1. Introduction

Micro manufacturing processes can be classified into four main groups based on their abilities, requirements and historical development.

The first group, which is the oldest one, covers **silicon-based processes** originally developed for needs of semi-conductor industry [1, 2]. These processes are able to produce large arrays of 2D micro components (features) with low unit costs. However, the initial costs are usually very high as these processes require expensive masters and clean/controlled environment. Because of this, the flexibility of production is low and majority of products has only a low-added value.

The second group of micro manufacturing processes is completely different. The processes within this group were mainly developed by scaling down of macro manufacturing processes. Some authors classify these processes as **ultra-precision processes** [3]. Typical examples are: micro electro discharge machining (micro-EDM) [4], micro mechanical cutting (e.g. micro milling, micro drilling or ultra-precision turning) [5-7], laser beam machining (LBM) [8] or micro electrochemical machining (micro-ECM). These processes are usually not directly applicable in mass-production because of their low material removal rates (MRR) and high unit costs. However, their advantages are in ability of processing a wide range of materials, producing fully 3D products and relatively low initial costs (compared to silicon-based processes). Hence, their place is in manufacturing of masters and tools for replication methods. They can also be applied in low- to medium-scale production, where high-added value and high flexibility are usually desired.

The third group covers non-silicon-based **replication processes**. Typical representatives of this group are micro-injection moulding, micro-embossing (hot or cold), forming and, in some extend, also micro-EDM (sinking variation of this process). These processes usually produce a negative shape of the master prepared by some of the processes covered in the previous groups. They are typically able to process wide range of materials (e.g. micro-injection moulding can be used for production of polymer, ceramic or metal micro-components).

The fourth group covers so called **rapid prototyping processes [9]**. These processes are based on building up the product by adding an extra material. Originally these processes were limited to a range of product materials which are not suitable for real applications. Therefore, these technologies were used only for demonstration of new products. This has, however, changed with development of new processes, such as selective laser sintering (SLS), which are able to produce parts from metals, ceramics, polymers etc. [9].

IHS Isuppli report [10] had estimated the total MEMS market in 2006 to be worth $6 billion. The report has also predicted 10% growth of the market between years 2010 and 2015, and in 2015 the market is expected to reach approximately $11.5 billion. This report has also predicted a growth of high added-value markets from $1 billion in 2006 to $2.5 billion in 2015. The results of the IHS Isuppli report are illustrated in fig. 1.1.

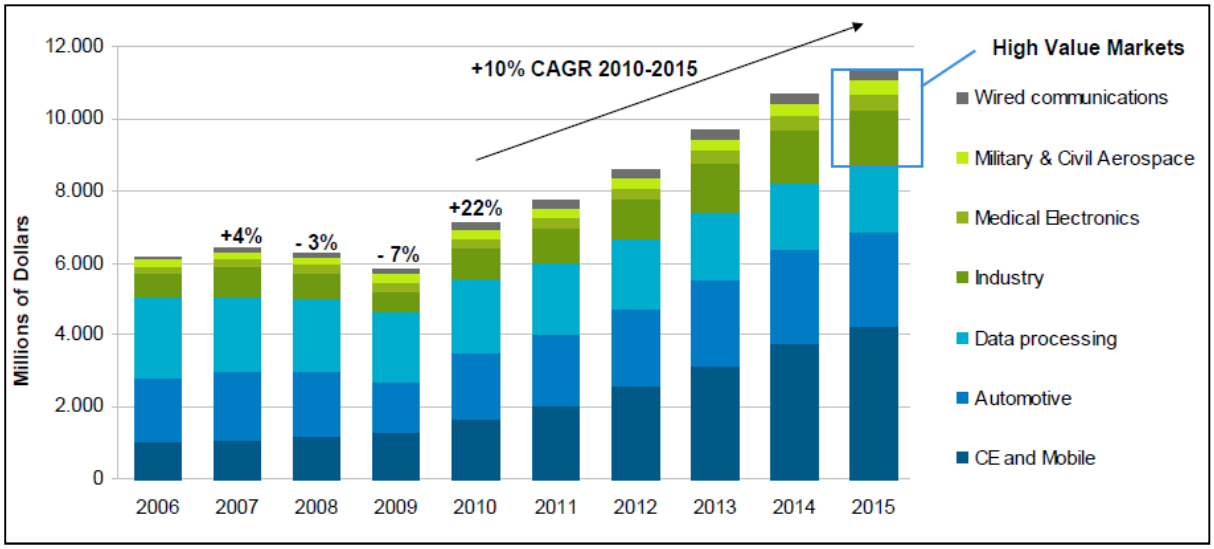

Fig. 1.1: Estimation of MEMS market [10]

Another interesting market research is presented in MINAM 2.0 strategic research agenda [11]. MINAM 2.0 consortium has investigated shares of different sectors on the total micro and nano manufacturing market. The report states that manufacturing & production equipment is the most vital sector. It is followed by healthcare & biochemistry, energy generation & storage, information & communication technologies (ICT) and other 8 sectors with less than 10% shares, see fig. 1.2. Furthermore, MINAM 2.0 has predicted a growing importance of healthcare & biochemistry sector. On the other hand, ICT sector is expected to

experience the most dramatic reduction of its share of the total market. The prediction of the market shares in 2015 is illustrated in fig. 1.3.

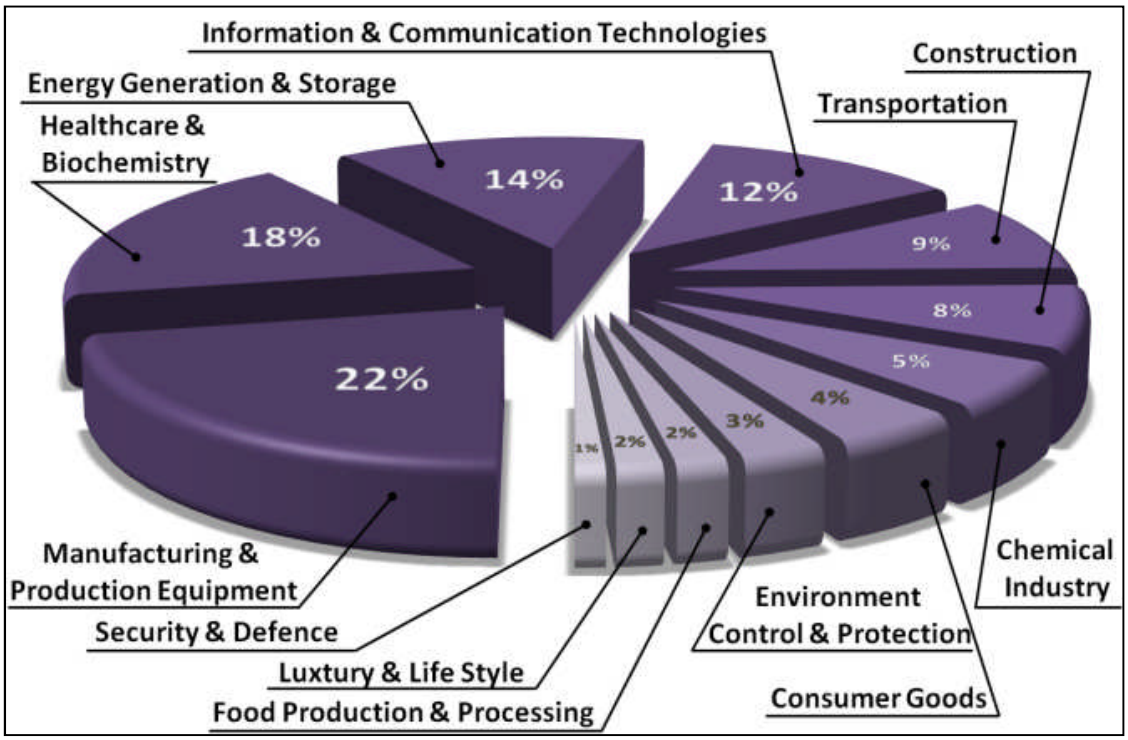

Fig. 1.2: Current market shares of micro and nano manufacturing industry [11]

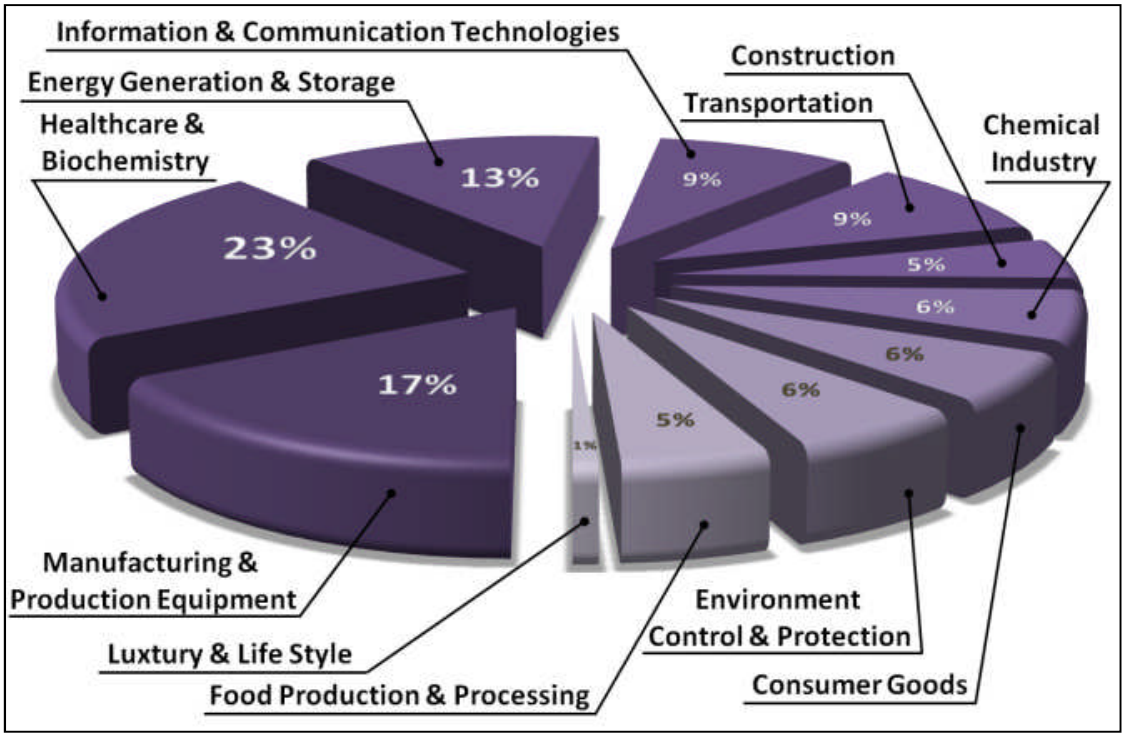

Fig. 1.3: Prediction of market shares of micro and nano manufacturing industry in 2015 [11]

The conclusions from these reports can be summarized as:

- Fast growth of the micro manufacturing market is expected,
- New fields of applications increase their importance,
- Increasing individualisation of micro products is expected,
- Increasing demands on quality and complexity of new emerging micro products.

These findings indicate a need of new manufacturing solutions which will be able to fulfil the arising demands. It is assumed, that many of the future products will not be makeable with the traditional silicon-based processes, and therefore, the processes from the other three groups will become more important. It is also expected that the new products will require multiple manufacturing processes to be employed during their production. In this sense, especially ultra-precision processes (micro-EDM, LBM, micro cutting etc.) are expected to play the key role. This because they are typically involved in any manufacturing chain used for production of 3D, high quality micro products. Two examples of the manufacturing solutions involving ultra-precision processes are:

- **Applications in sequence with rapid prototyping methods.** In this case, a near net shape is produced by some of the rapid prototyping processes, and then, the final product is finished by some of ultra-precision processes. Such methods are popular in macro manufacturing because of their ability of efficient production of complex and accurate products. It is suitable for manufacturing of small and medium batches of micro components.
- **Applications in sequence with replication processes.** In this case is first produced a master by some of ultra-precision processes, and then it is replicated by some of the replication processes. This solution facilitates manufacturing of large batches of 3D high quality components with low unit costs.

From processes classified in the second group, micro milling is one of the most promising ones. It is based on mature conventional milling with which it shares majority of its characteristics. It also has an ability of manufacturing complex 3D shapes with high accuracy and high surface quality [5-7]. Unlike comparable LBM or micro-EDM (both are based on melting and evaporation) micro milling is based on mechanical cutting. Therefore, it has not as significant effect on material properties in near-to-surface layers and on sub-surface

damage. Furthermore, according to Bigot et. al. [12] the micro milling unit cost in medium batch size production is approximately 80% lower than in the case of LBM (see fig. 1.4).

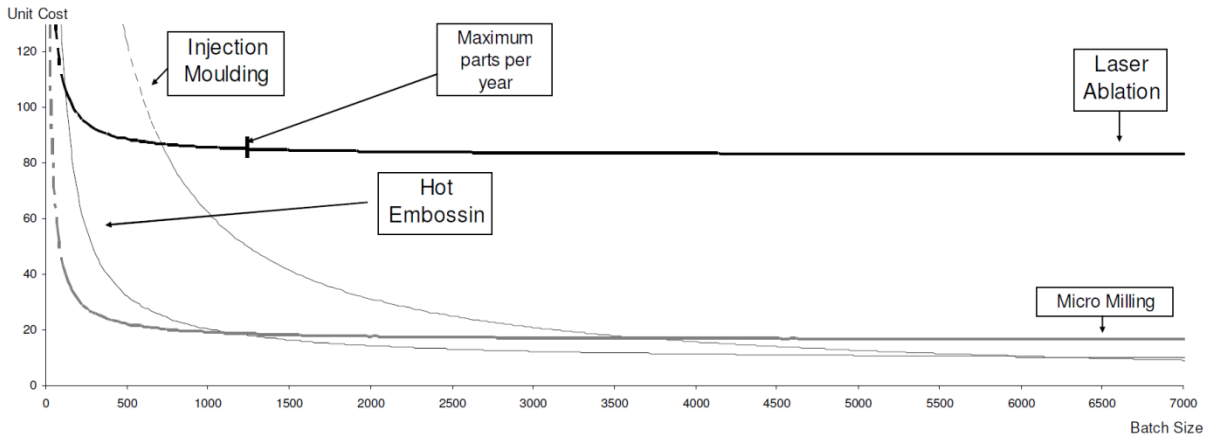

Fig. 1.4: Unit cost as a function of batch size [12]

All the above mentioned reasons make micro milling extremely competitive process. However, although this process is derived from well established conventional milling, it is affected by various scaling factors. These factors affect tool performance, the final product quality and most importantly process predictability. Furthermore, because of very small dimensions, high complexity and high rotational speeds typical for micro milling, it is very difficult to monitor it. Most of the current monitoring techniques are insufficient for the required dimensions.

Hence, the main drawback of this process is its low predictability. Without reliable methods it is unlikely that industry will accept micro milling. Therefore, the main objective of this research is to develop a tool performance prediction method applicable in industrial applications. This method should:

- be applicable to the smallest micro end-mills available on the market,
- be applicable to different machining strategies (different cutting parameters, materials, tool geometries etc.),
- have minimum interactions with day-to-day production.

The author assumes that theoretical modelling represents the best possible solution. However, the models must respect various scaling effects which are influencing micro

milling. Especially process tolerances and uncertainties are expected to be highly influential. The proposed method is, to the author's best knowledge, the first one respecting these issues.

Another important factor affecting micro milling is tool design. It is assumed that by an appropriate design, tool performance predictability and also tool life can be significantly increased. This, however, does not seem to be reflected by currently available micro end-mills. Although the tool design is not the main topic of this research, some of the techniques used for prediction of tool life seem to be applicable in the designing process. Therefore, it seems to be logical to apply the knowledge gained in this research on designing of micro end-mills. Hence, the second main objective of this research is to introduce a systematic tool designing method reflecting the main micro milling challenges.

Each of these methods concentrates on some of the aspects of micro milling. The first one helps to plan suitable milling strategies and estimate the final costs, as the second one is assumed to facilitate designing of new tools with longer life and more predictable performance. Hence, application of both of these methods may help to increase popularity of micro milling in industry.

2. Literature review

2.1 Micro-milling and its components

Milling is a traditional chip removal process. First references about applications of milling can be tracked already since the industrial revolution in 19th century [13]. It was quickly recognized as extremely powerful manufacturing process capable of producing 3D parts from wide range of technical materials. Increasing industrial demands have led to continuous improvements of the process; especially increasing accuracy, repeatability and reduction of product dimensions were always highly desirable. This had resulted in situation, when in the late nineties of the twentieth century the process dimensions became as small as the relations developed for conventional milling were no longer valid. Since that time some researchers have started to speak about micro-milling. Perhaps the first one whom used the term "micro-milling" was I. Tansel in his paper published in 1998 [14].

As mentioned above, micro-milling has been developed from well established conventional (macro) milling process. Generally, it may be stated that micro-milling is simply a scaled down version of conventional milling. Hence, all the kinematics is the same. The basic movements are: tool rotation and simultaneous feeds in x, y and z directions [15]. Recent developments in computer numeric control (CNC) systems enable also multi-axis milling with increased number of degrees-of-freedom (DOF). Most usual are two additional rotational axes facilitating production of very complex 3D parts with freeform surfaces. However, increased number of DOFs increases the complexity of the process and introduces new challenges in process modelling, control and monitoring.

Because micro-milling was derived from conventional milling by continuous reduction of dimensions, it is obvious, that it is very difficult to identify clear boundary between these two cases. In the reality, all mechanisms remain the same in both cases. The main difference is in relative effects of process variables on machining performance, and not in different principles. Importance of the effects continuously increases with reduction of tool dimensions up to a moment when it cannot be any longer ignored. However, there is also an important "shadow" zone, in which the effects are not negligible, but they are not yet critical. This zone was identified by Sandia National Report titled "Meso-machining capabilities" to be

approximately between the tool diameters of 0.5 mm and 1 mm [16]. However, it is important to mention, that the decision of classifying some process as micro-milling is affected by many factors and it cannot be simply stated that all processes with tools smaller than Ø0.5 mm are definitely micro.

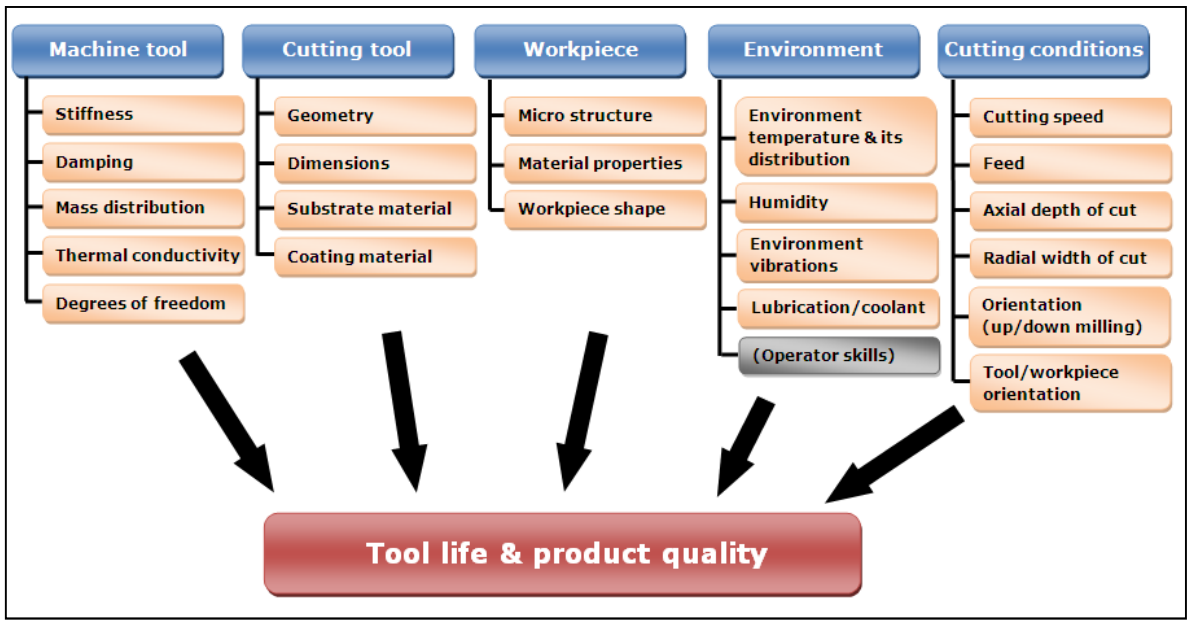

Fig. 2.1: Main factors affecting micro milling process

Hence, the remaining question is: what are the factors affecting milling process? This is not a simple question because there is a large number of such factors. Fig. 2.1 summarizes and logically classifies the most important ones. Evidently all hardware components involved in milling process have an important influence on the process. These include machine tool, cutting tool and workpiece. Another important group of factors is classified as environmental effects. This group of factors has an increasing effect in the case of micro scaled and high precision milling. The last group of factors includes different interactions between the tool and the workpiece. In its entirety, these factors can be called cutting conditions. Although, some of the factors listed in fig. 2.1 play more important role than the others, they all must be assumed as ineligible in real micro milling. Hence, it is worth to have a brief insight to the current state-of-the-art of each of these groups individually.

2.2 Machine tools

It is obvious that machine tool strongly affects the machining process. Especially its stiffness, damping and mass distribution have enormous effects on process dynamics and

stability [17]. However, these are not only factors affecting the process stability. Another important factor is obviously machine tool thermal performance. Although, micro-milling process does not generate large amount of heat, the moving parts of the machine tool, especially spindle, can do so [17]. This can lead to unexpected machine tool deformations, which negatively affect machining accuracy. Last, but not least is the effect of driving and control systems. Evidently inaccurate driving system does not facilitate high machining accuracy and repeatability desired for successful micro manufacturing. Another issue of driving and control systems can appear, if it is not appropriately designed from the point of view of thermal distribution. All current machining systems are based on transfer of electrical energy to mechanical energy. Due to electrical resistance, these systems often generate ineligible heat, which can cause further machine tool deformations. This can be solved by location of majority of electrical components outside of the machine tool as it is done for example by KERN Precision inc. [18]. Another solution is minimization of electrical energy needed for machine tool functionality and good electro/thermal design of all electrical systems. Advanced measurement systems should be a standard for micro-milling machines. High resolution and fast response are greatly desirable because: “what cannot be measured cannot be improved”. Furthermore, these systems facilitate back-loop process control which can in near-to-real time optimize the process input parameters in order to increase machining performance.

In the early stage of micro milling research no specialized machine tools were available. Therefore, all research at turn of the century was performed on conventional high speed milling centres. This includes for example early research of I. Tansel [14, 19, 20], W. Y. Bao [21-23] and M. Rahman [24].

However, researchers have quickly identified unsuitability of the conventional machine tools. This led to extensive research and development of new, more suitable, machine tools in last decade. According to Chae et. al. [25] two main directions of machine tool development can be distinguished as:

- Continuous improvements of conventional machine tools. These improvements include increasing stiffness, improvements of control and monitoring systems and implementation of more accurate and stable machine tool components such as spindles,

positioning systems, brackets etc. However, as these machine tools are developed on the same basis as conventional machine tools they are commonly unreasonably large. This direction can be observed mainly in industry. Some of the typical examples of commercial machine tools are shown in fig. 2.2.

- New miniaturized micro-milling machine tools, which are often used in research institutions. These machine tools are characterized by a desktop size, which better reflects dimensions of usual micro-products. Benefits of these machine tools are mainly in reduction of energy, space, material and costs. Although the first miniaturized micro-milling machine tools appeared already in very beginning of 21st century (e.g. Takeuchi's 5-axis milling centre presented in 2000 [26]), they still did not gain their position in market. To the author's best knowledge, the only commercial producer of such type of milling centres is Nanowave. Some examples of desktop machine tools, including the one from Nanowave, are shown in fig. 2.3.

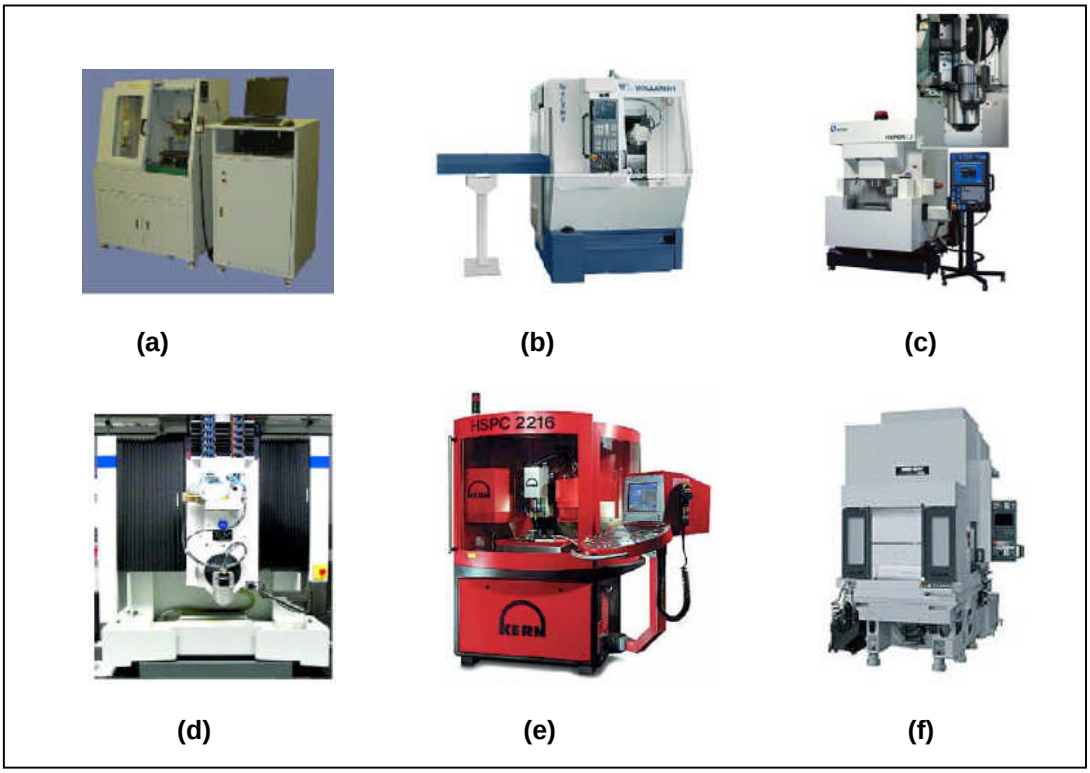

Fig. 2.2: Commercial micro-milling centres: (a) Mikrotool DT-110 [27], (b) Willemin-Macodel W-408MT [28], (c) Makino Hyper2j [29], (d) Kugler [30], (e) KERN evo [18], (f) Mori-Seiki [31]

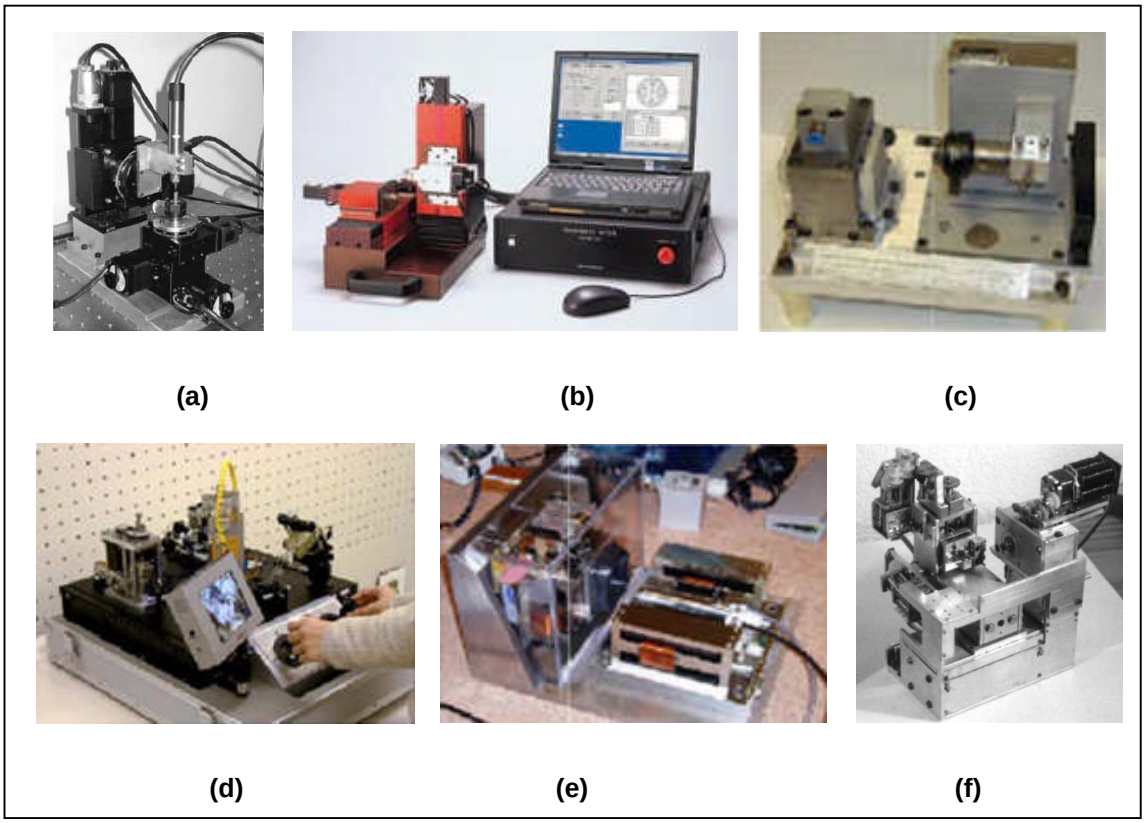

Fig. 2.3: Examples of micro-machines (a) miniature machine [32], (b) commercial miniature machine from Nanowave [33], (c) micro-factory [34], (d) micro-factory [35], (e) second generation miniature machine [34], (f) micro-machine tool [36]

2.3 Micro end-mill

Cutting tool (micro end-mill) is the second hardware component presented in micro milling. Because the tool is usually the smallest part introduced in micro milling process, it represents the weakest point of the whole setup. Therefore, a special attention must be paid to its design, properties and performance. In this section is summarized the current state of the research of this topic.

2.3.1 Micro end-mill dimensions

Currently a great variety of micro end-mills with diameters down to tens of micrometers is available in the market. In fig. 2.4 is shown an example of one of the smallest tools provided by Performance Micro Tool [37]. This example represents a dual helix micro end-mill with the cutting diameter of only 10 μm. Other suppliers also offer very small tools with diameters bellow 100 μm (e.g. UNION TOOL provides micro end-mills with diameters of 60 μm [38]).

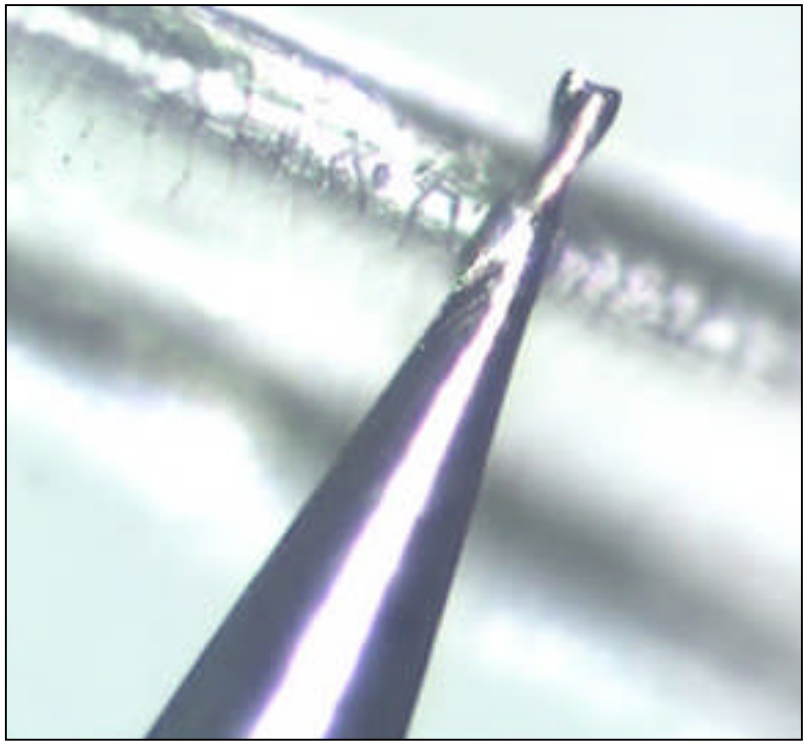

Fig. 2.4: Micro end-mill with cutting diameter of 10 μm next to a human hair; Performance Micro Tool [37]

However, the smallest available tools are very rarely used in both research and industry. Majority of tools used in recently published research have cutting diameters in a range of 0.3 mm to 1 mm (e.g. [19-24, 39-41]).

2.3.2 Micro end-mill design

Although the manufacturers continuously reduce tool dimensions, tool geometry remains identical for both micro and macro end-mills. For example Kyocera offers the same tool model with diameters from 100 μm up to 6 mm [42] and UNION TOOL offers its C-CES2000 tool model with diameters from 100 μm up to 20 mm [38].

The situation in research is not significantly different. There is only a limited number of publications related to micro end-mill design. Fang et. al. [43] compared a commercial dual-helix tool with four other geometries, namely straight and tapered Δ-type tools and straight and tapered D-type tools (see fig. 2.5). The study consists of a theoretical modelling (FEM) followed by an experimental verification. Both Δ-type and D-type tools show higher rigidity and wear resistance than the standard tool. Fang has concluded that D-type tool is the most

suitable for micro-milling. These tool designs are, however, orthogonal, and therefore, they generates higher cutting forces. Hence, it is disputable, whereas the newly developed tools will have as significantly longer tool life as predicted.

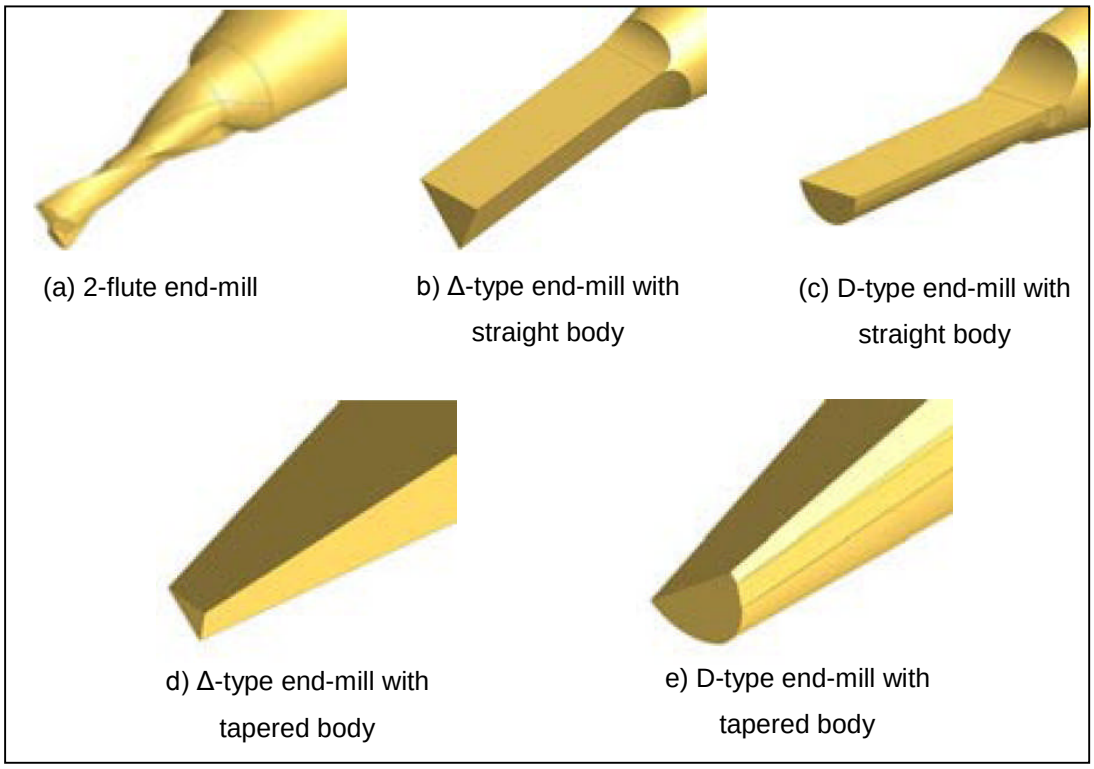

Fig. 2.5: Tool geometries studied by F. Z. Fang et.al. [43]

On the other hand Uhlmann and Schauer have concentrated on optimization of the tool dimensions [44]. They have not compared different concepts, but they optimised the under-neck length and diameter. The longer length of under-neck was achieved by a reduction of the flute length. This variation of the tool geometry leads to smoothing of the tool geometry in the critical zone (the zone where are the highest bending stresses). Their analysis was based on FE stress analysis and then experimentally verified. In fig. 2.6 are shown examples of the commercial tool and the optimised one. By the optimisation was achieved reduction of bending stresses of 1 190 MPa (~30%). The experimental tests have confirmed that the optimised tools last longer than the commercial ones. However, the improvement was not as significant as expected (the total machining length achieved by the optimised tool was only 10% longer than the one achieved by the commercial tool). This shows that not only bending stresses affects the tool life, but also other effects must be taken in consideration.

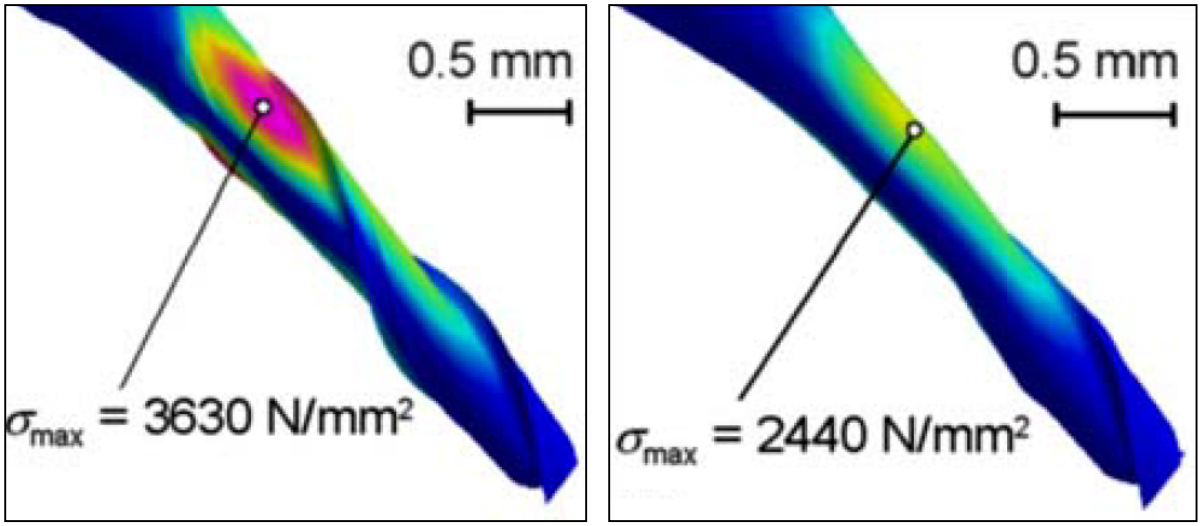

(a) Commercial end-mill (b) Optimized end-mill

Fig. 2.6: Stress distribution in commercial and optimized end-mill, Uhlmann and Schauer [44]

Another interesting work about micro end-mill design was published by P. Li et.al. [45]. P. Li has concentrated on a design of the tool cross-section. The main effort of this work was put on reduction of tool wear. P. Li has proposed and experimentally validated two new tool designs (2-flutes and 4-flutes micro end-mills) as they are shown in fig. 2.7. P. Li has concluded that the rake angle is not as critical in micro milling as it is in conventional milling. Hence, he proposed to prioritize robustness of the cutting edge over the effort of achieving high positive rake angles. Both of the newly developed tools show approximately 3.5 times lower tool wear than the commercial one. This reduction of the tool wear was dominantly achieved by prevention of initial cutting edge chipping.

Some research on the topic of micro end-mill design was also presented by Fleischer et. al. on 4M conference 2008 [46]. In this work, three different tool designs were numerically analysed. Proposed designs, however, show significant drawbacks. The first two presented designs seem to have inappropriate geometries with very low stiffness and high number of stress concentrators (see fig. 2.8a and 2.8b). Furthermore, all proposed designs are orthogonal. Such tools are, however, likely to generate higher cutting forces. The third tool geometry (fig. 2.8c) shows high stiffness. A possible issue of this geometry is, however, in conduction of the removed chip away from the cutting zone. Because the proposed geometry has no helix angle, it is unlikely that the chip would be “pushed” upward as it is typical in oblique cutting. In combination with the proposed geometric features, it can result in a

"suction" of the chip below the tool where it may stick. This can result in a build-up-edge (BUE). However, because neither experimental nor theoretical analysis of this effect was presented, it cannot be proved or disproved. It should be also mentioned that all geometries proposed by Fleischer are a single tooth. This seems as a good idea for designing of micro end-mills which can help to eliminate dangerous run-out effects and also help to increase the tool stiffness. However, before the concept of a single tooth micro end-mill can be applied, an effect of tool unbalance should be investigated.

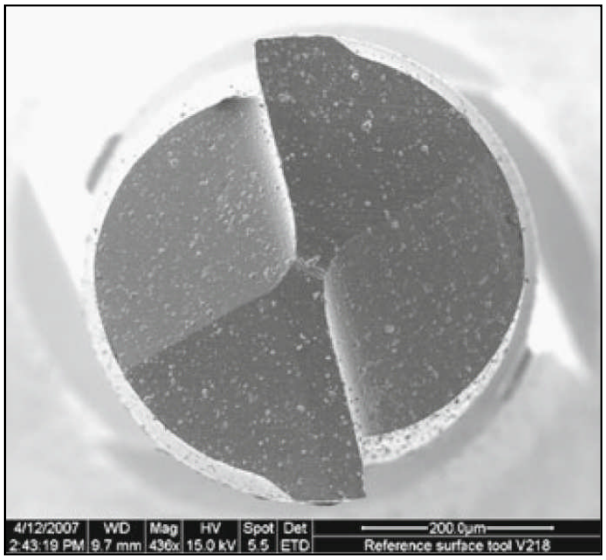

(a) Commercial tool

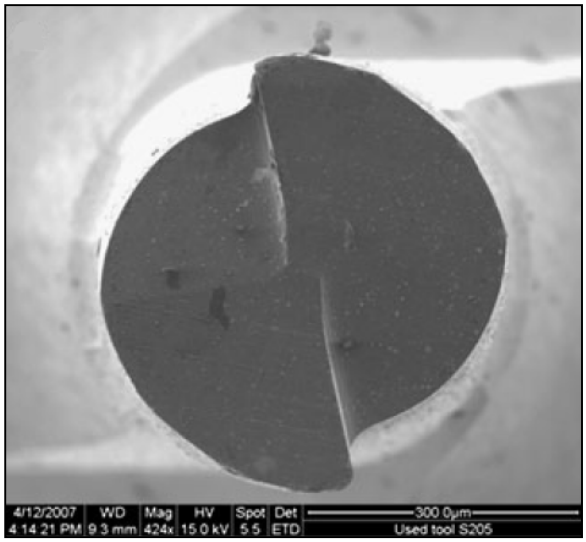

(b) Newly developed 2-flutes design

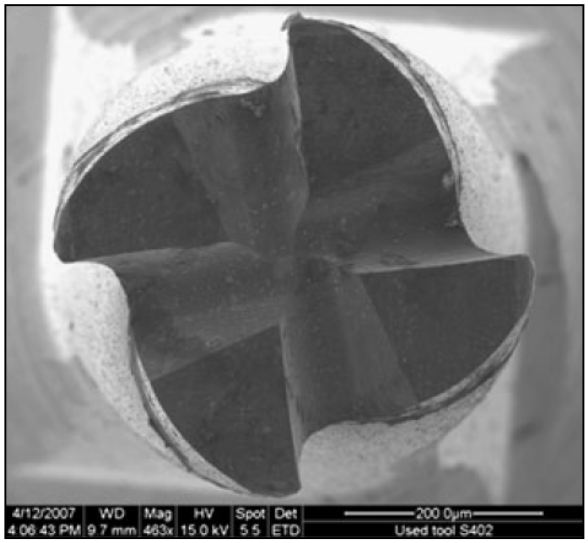

(c) Newly developed 4-flutes design

Fig. 2.7: New micro end-mills designs proposed by P. Li [45]

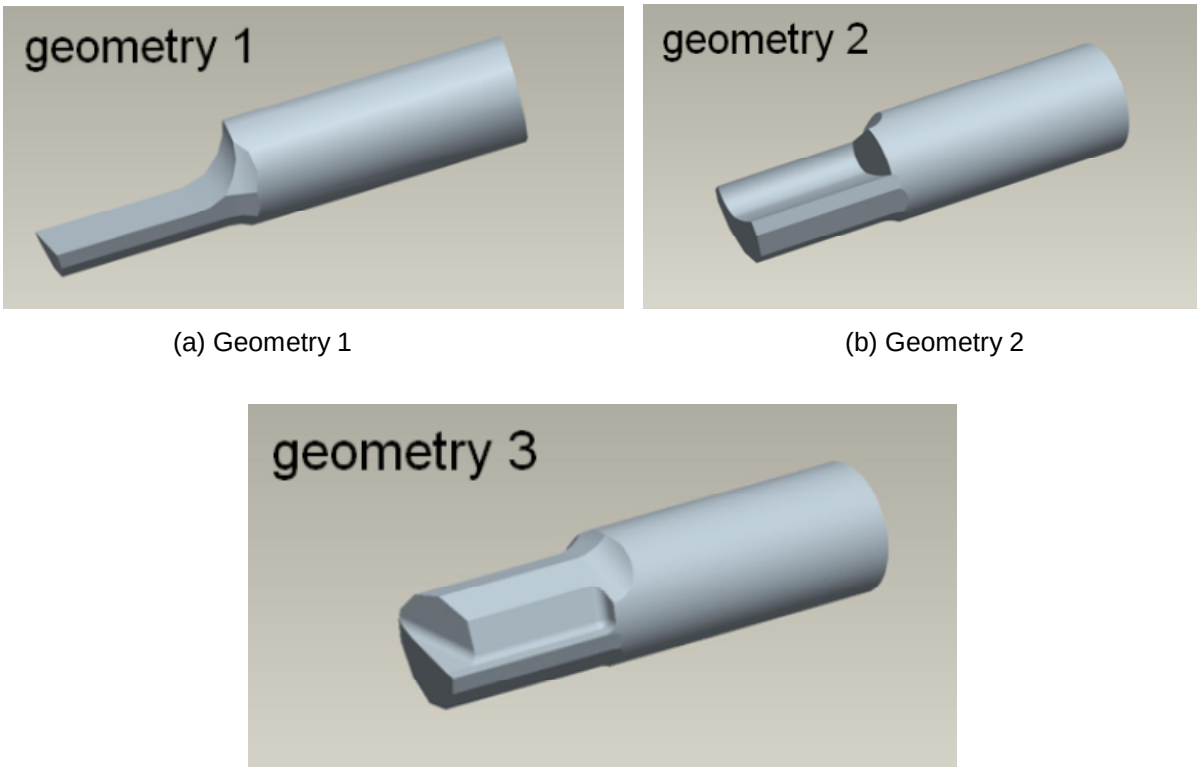

(a) Geometry 1

(b) Geometry 2

(c) Geometry 3

Fig. 2.8: Micro end-mills proposed by Fleischer et. al. [46]

Each of the published works related to the tool design concentrates on different issues. P. Li has concentrated on tool cross-section and tool wear, Uhlmann on bending stresses and parametric optimisation of under-neck, Fang on simplicity of tool manufacutring and high stiffness and Fleischer on elimination of tool run-out effect. However, none of the researchers has proposed a systematic method for tool design which would reflect whole scope of challenges arising from tool scaling down. However, it is assumed that in the future the micro end-mills will be designed specialy for different types of applications (varius tools for machining soft and hard materials, roughing and finishing operations etc.). This specialisation of the tools for different applications is expected to be more important in micro scale than it is in macro scale. This is becasuse of higher liability of micro tools performance to be affected by various effects than it is in conventional milling. Therefore, a designing method is assumed to be more valuable than a new design itself.

2.3.3 Micro end-mill material & coatings

Same as conventional cutting tools, micro end-mills are usually made from fine grain tungsten carbide with cobalt binder (WC-Co). This material is typically used for cutting tools

because of its high melting temperature and very high hardness [47]. The WC-Co tools are more wear resistant than tools made from high speed steels [47]. However, also in the case of WC-Co tools, tool wear remains an issue which leads to reduction of final product quality, cutting force growth and in micro milling to premature tool breakage. Therefore, tool producers as well as researchers pay an attention to reduction of tool wear. Except of application of suitable lubrication, an application of protective coatings is the most usual method.

In commercial practice TiN, TiAlN and CrN coatings are the most usual coating materials [38, 42]. However, these coatings were developed for protection of conventional tools and not for micro tools. Therefore, it is essential to verify the effects of these coatings in micro milling applications. As mentioned above, the performance of micro end-mills differs from conventional milling due to various size effects. Therefore, special attention should be paid to the appropriate coating design for micro end-mills. This task is, however, extremely demanding. This is due to the numerous complications in coating of micro tools. Hence, only a limited research in this field has been done so far [41, 48, 49].

Aramcharoen et. al. has compared five different coatings in micro milling [48]. The coatings used in this research were: TiN, TiCN, TiAlN, CrN, CrTiAlN. These coatings were deposited by magnetron sputtering method. All of these coatings had too layers. The bounding layer was formed by Ti and the following layer by TiN, TiCN, TiAlN or by Cr and then followed by CrN. Total thickness of all coatings was 1.5 μm. The tools used in this research were Ø0.5 mm micro end-mills, and the machined material was hardened steel. The resistance to different wear mechanisms was evaluated for all the tested coatings. Authors claim all these coatings to be extremely resistant against cutting edge chipping. All the tested coatings have shown significantly reduced chipping as well as flank wear. Although TiN has lower hardness than all the other tested coatings, it has shown the highest resistance against tool wear. This may be because of good adhesive properties and good surface quality of this type of coating. The research has shown that in micro milling extra hard coatings are not the most effective ones, and that tougher and softer coatings may be better protection.

Another interesting research on different coating systems applied in micro milling, was published by Kim et. al. [49]. In this research Ø0.2 mm micro end-mills were used to

machine brass (soft material). Four different coatings were used in this research: single-layered CrN, CrCN, CrSiN and CrSiCN. This research has shown that the CrSiN and CrSiCN have the best wear resistance. These two coatings are claimed to have the highest micro-hardness from the tested coatings. This observation is, however, inconsistent with the Aramcharoen's observations [48].

Recently were also published some initial tests of diamond-like coatings. Torres et. al. [41] tested CVD diamond-like coatings. Coatings with ultra fine diamond grains (500 – 1000 nm and 200 – 300 nm) were tested. The tools used in this research were Ø0.3 mm micro end-mills and the machined material was aluminium (soft material). Both tested coatings showed a great cutting force reduction in comparison with uncoated tools. Furthermore, a significant improvement of the surface quality was recorded during the cutting tests. The authors claim coating with finer grain size to be more suitable for micro milling due to a smaller cutting edge radius, lower friction and better wear resistance.

Except of the coating material, the coating structure is also very important. An interesting research on the coating structuring was published by C. Ducros et. al. [50, 51]. Different coating structures studied by Ducros are shown in fig. 2.9. Ducros claims the nano-layered coating to generate lower friction. This leads to lower cutting forces, lower wear and also a better surface finish. Nano-layered coatings also show better fracture resistance. Because tool breakage is one of the most dangerous phenomena observed in micro milling, this finding is very important for future direction of research in micro milling coating systems.

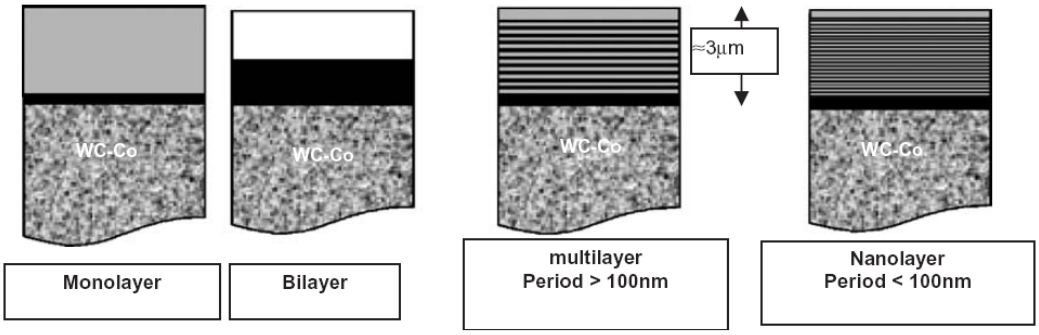

Fig. 2.9: Scheme of different coatings architectures [50]

Another important work on the evaluation of coating structure effect on wear resistance was published by L. Settineri et. al. [52]. In this research was compared wear resistance of AlSiTiN, AlSiCrN, AlCrN and AlTiN coatings. All these coatings were deposited as mono-layered and multi-layered (5 layers). The conclusions of this research are, however, inconsistent with Ducros et. al. The single-layered coatings have generally shown higher wear resistance than multi-layered ones. Based on Settineri et. al. research, the best wear resistance at low temperatures has the mono-layered AlSiCrN coating.

2.3.4 Manufacturing of micro end-mills

Majority of WC-Co micro end-mills are currently manufactured by micro-grinding [53]. The quality of the final micro end-mills crucially depends on grinding wheel properties such as wheel-size and grid-size, the grinding wheel wear, and chosen cutting conditions. Furthermore, grinding is mechanical machining process which generates high machining forces. Because a typical micro end-mill has low bending stiffness, it is evident, that by application of cutting forces the accuracy will reduce. The accuracy of the produced tools can obviously be increased by application of less aggressive cutting conditions. This, however, results in longer machining times and consequently in high production costs. Therefore, it is unlikely that commercial tool manufacturers would reduce the cutting conditions and produce more accurate tools.

Micro electrical discharge machining (micro EDM) is another process suitable for manufacturing of micro end-mills. This method is based on melting and vaporization of workpiece material. Temperatures of 5 000-12 000°C [54, 55] are generated by electrical sparkling between the electrode and the workpiece. According to Pham et. al. [4] four different variation of micro EDM can be distinguished as:

- Die-sinking micro EDM, where an electrode is used to produce its mirror image in a workpiece.
- Micro-wire EDM, where a wire of diameter down to 0.01 mm is used to cut through a workpiece.
- Micro EDM milling, where a rod electrode with diameter down to 0.005 mm is used to produce 3D shape by controlled movement (similarly as in mechanical milling).

- Micro EDM drilling, where the rod electrode is used to produce holes through the workpiece.

However, only micro-wire EDM and micro-EDM milling are suitable for manufacturing of micro end-mills. Cheng et. al. has published a theoretical work showing a possibility of manufacturing a dual helix tool with micro-wire EDM [56]. The graphical interpretation of his simulation is shown in fig. 2.10. Cheng has concluded that such a tool can be manufactured on a six-axis machine tool and also suggested three different designs of suitable machine tools. The solution shows a great potential, however, the concept has not yet been experimentally verified. The main advantages of micro EDM are: very small dimensions (wires down to 10 μm are available) and negligible machining forces. Hence, the accuracy of micro EDM can be higher than accuracy of micro grinding. On the other hand, the potential risk of micro EDM is in its thermal nature. It typically generates heat affected zones with different properties than the bulk material. Furthermore, this process is usually slower than commercially used grinding.

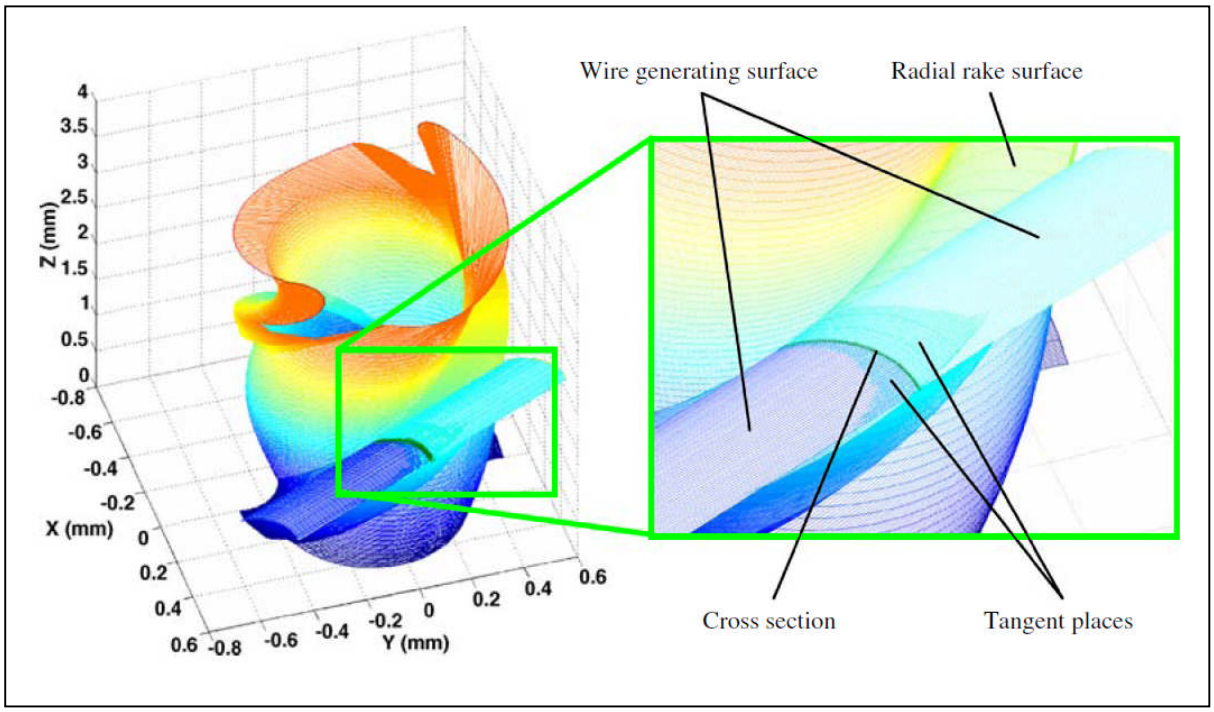

Fig. 2.10: Simulation of tool manufacturing by micro-wire EDM [56]

An interesting research on application of wire-EDM on manufacturing of micro end-mills was also published by Jiwang et.al. in 2009 [57]. In this paper is presented a fabrication of a D-type micro end-mill with a nominal cutting diameter of 50 μm, see fig. 2.11. The manufactured tool was measured and the cutting diameter was found 3.3 μm smaller than expected. This is significantly lower than the tolerance of typical ground micro end-mills (as it will be shown later in this thesis, the commercial Ø0.2 mm tools have tolerances of approximately ±10 μm). Furthermore, Jiwang clams that the tool has improved wear characteristics. This may be caused by the presence of the heat affected zone, which has typically higher hardness than the bulk material. This effect is, however, not further discussed in the presented paper, and therefore, the hypothesis cannot be confirmed. Another, possibly positive effect of micro-EDM is the produced surface micro structure, see fig. 2.12a. Jiwang assumes that this surface structure is able to keep lubricant within the cutting zone as it is shown in fig. 2.12b.

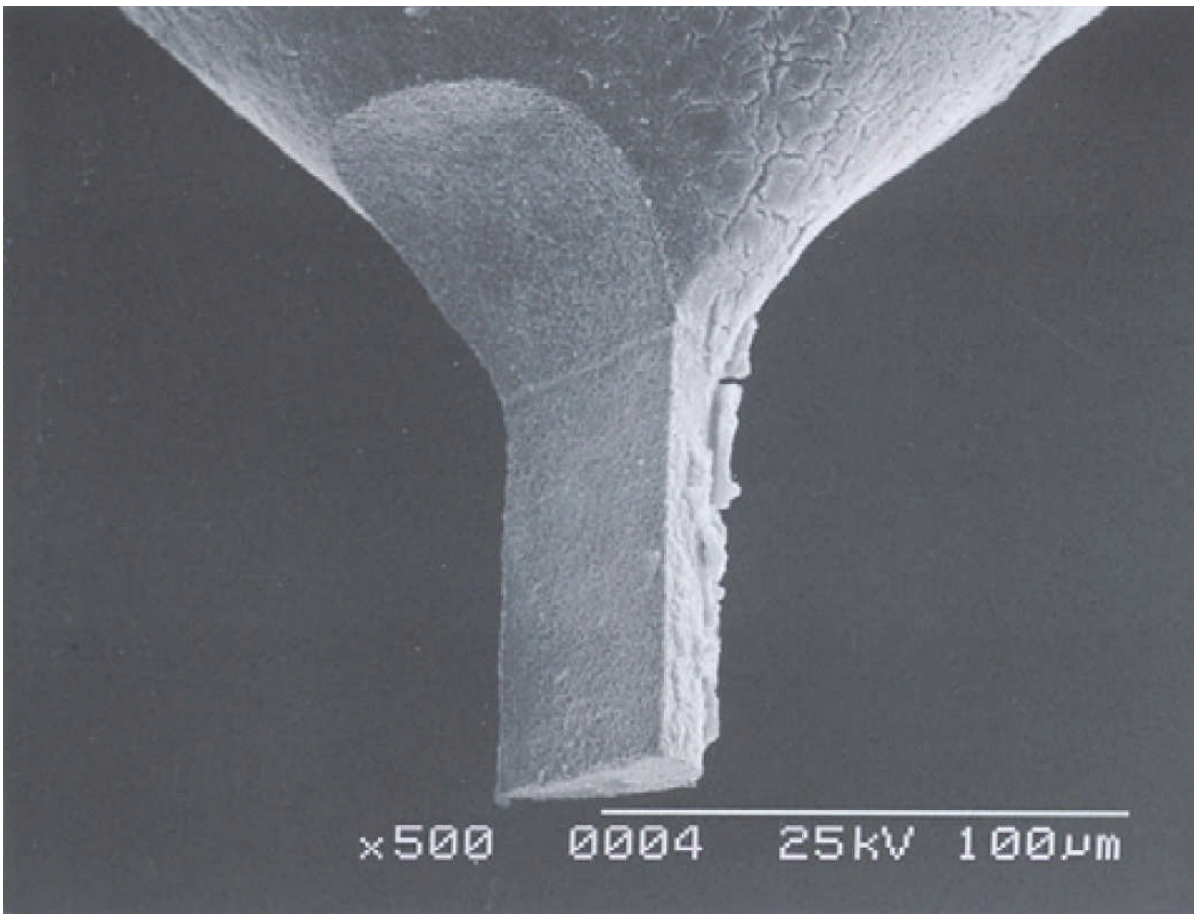

Fig. 2.11: Micro end-mill manufacture by micro-wire EDM [57]

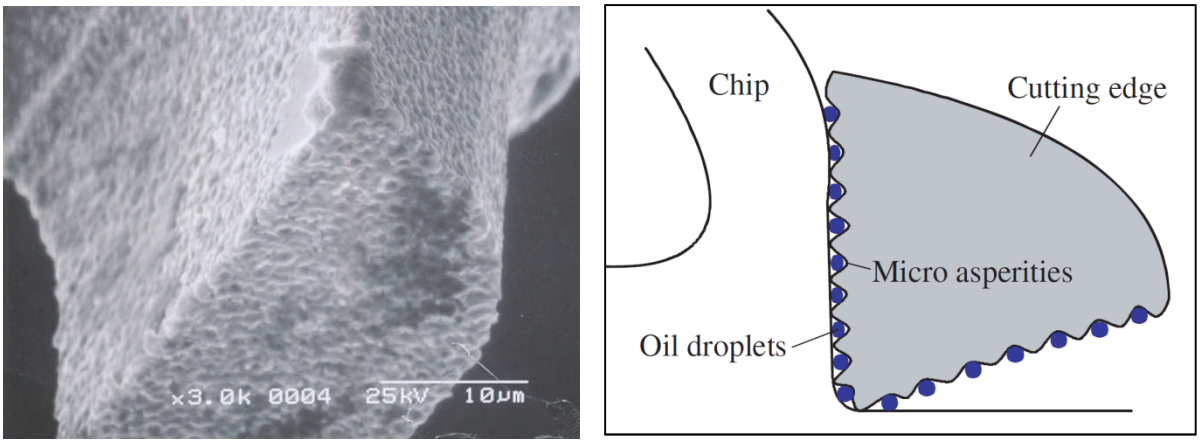

(a) Detail of EDM surface

(b) Schematic illustration of the effect of EDMed on lubrication

Fig. 2.12: Schematic model of material removal during cutting by EDMed micro end-mill [57]

Another manufacturing technology which has been used for manufacturing of micro end-mills in research is Focus Ion Beam (FIB) machining. Adams et. al. manufactured and tested diverse micro end-mills with diameter of 25 µm as they are shown in fig. 2.13 [58]. These tools were successfully used for machining of slots in brass and hardened steel, see fig. 2.14. Because of poor tool design (all tools have large negative rake angles) the slots machined by these tools show large burrs. This, however, does not mean that FIB would not be suitable for manufacturing of micro end-mills. The advantage of this manufacturing technology is its high resolution and high accuracy. However, very low MRRs limit this manufacturing process only for manufacturing tools with diameters below ~100 µm [58].

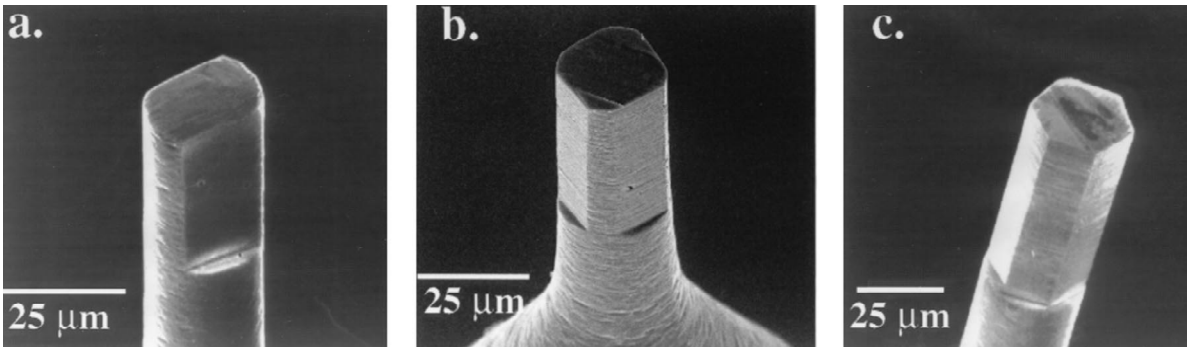

Fig. 2.13: Micro end-mills manufactured by FIB [58]

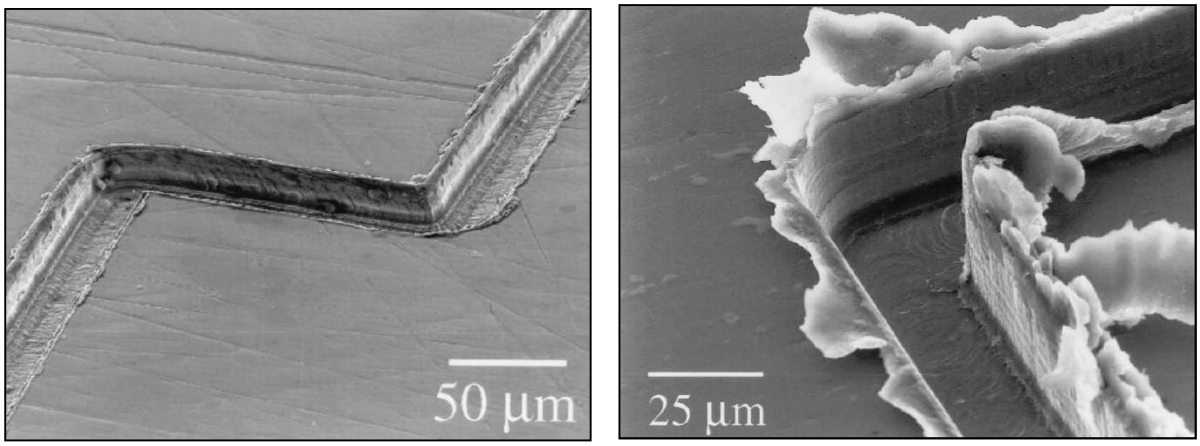

(a) An example of a slot machined in brass (b) An example of a slot machined in steel

Fig. 2.14: Slots machined by FIBed micro end-mills [58]

2.4 Workpiece materials

One of the great advantages of micro milling is its ability of machining a broad range of materials such as aluminium alloys [19-23, 39, 58-60], steels [19-23, 39, 60-63], copper and its alloys [24, 43, 64, 65], polymers [66], ceramics [21-23, 58, 66] or graphite [19, 20, 39, 67].

It is evident that machinability of each of the materials is different. This is because of different material properties; especially workpiece hardness. However, it is difficult to compare the results published by different researchers. The main issue is that each of the researchers uses different tools and different experimental procedures. It is also difficult to compare results achieved on different machine tools (this is because of different characteristics of various machine tools).

2.5 Cutting mechanism

For research in micro milling it is fundamental to understand cutting mechanism. However, due to complexity of micro end-mills, very small dimensions and high speeds, it is difficult to study cutting mechanism directly in micro milling. Therefore, most of the knowledge about cutting mechanism in micro milling is derived from orthogonal cutting, mainly from micro turning (e.g. [68-72]) and ultra-precision diamond turning (e.g. [25, 73-76]). It is assumed that this knowledge can be transferred to micro milling because of comparable uncut chip thicknesses.

In micro cutting, the magnitude of the uncut chip thickness is comparable with the cutting edge radius. This causes significant changes in cutting mechanisms [77, 78]. Due to this size effect, ploughing becomes more dominant than shearing and it has undesirable effects on machined surfaces, subsurface damage and cutting forces. The illustration of micro and macro cutting are shown in fig. 2.15. In the case of micro cutting, the springback effect becomes more important and cannot be neglected. The springback effect can be described as an elastic recovery of the material, and is greatly affected by the cutting edge radius. In micro cutting sometimes, a situation arises, when the springback is the same as the uncut chip thickness. Hence, no material is removed. This critical chip thickness is called: Minimum chip thickness (MCT). Great effort to predict MCT was spend, both experimentally [79, 80] and theoretically [81, 82]. For example, the MCT for steel was recorded by Yuan et. al. to be between 20% and 30% of the cutting edge radius [81].

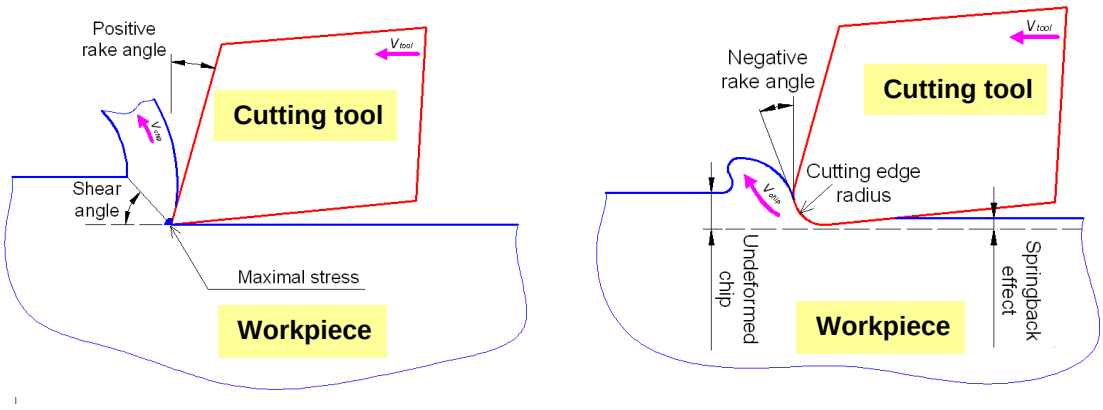

(a) Macro cutting (b) Micro cutting

Fig. 2.15: Illustration of macro scale and micro scale cutting

The MCT effect greatly influences the cutting forces. It is evident that if in one cut no material is removed in the next cut the uncut chip thickness will be twice as large. This phenomenon is commonly observed in measured force-signal as dominancy of first sub-harmonic of the tooth-passing frequency[82, 83].

2.6 Heat generation

S. Afazov has used coupled structural-thermal Finite Element Analysis (FEA) of chip formation. Although his model represents only 2-dimensional orthogonal cutting and it was

not experimentally verified, it gives an important indication about the heat generated in micro milling [84]. In fig. 2.16 are plotted resulting maximum temperatures for various cutting speeds and uncut chip thicknesses. The temperatures predicted by S. Afazov are in a good correlation with temperatures measured in conventional milling by M. Sato et.al. [85]. Hence, the theoretical results achieved by Afazov can be assumed as reliable.

The maximum feed recommended by UNION TOOL for Ø0.2 mm tools is ~7 μm/tooth [38]. If the recommended axial width of cut is used (20 μm) the resulting maximum uncut chip thickness will be approximately 3 μm. Furthermore, in the case of micro milling with Ø0.2 mm tools are realistically achievable only the first two speeds analysed in [84] (104.7 mm/s corresponds to 10 000 rpm and 523.7 mm/s corresponds to 50 000 rpm). Hence, the maximum temperatures in micro milling are approximately between 50° and 120°. Such temperatures are not high enough to have any significant effect on machining process. Therefore, the heat is not assumed to be an issue in micro milling.

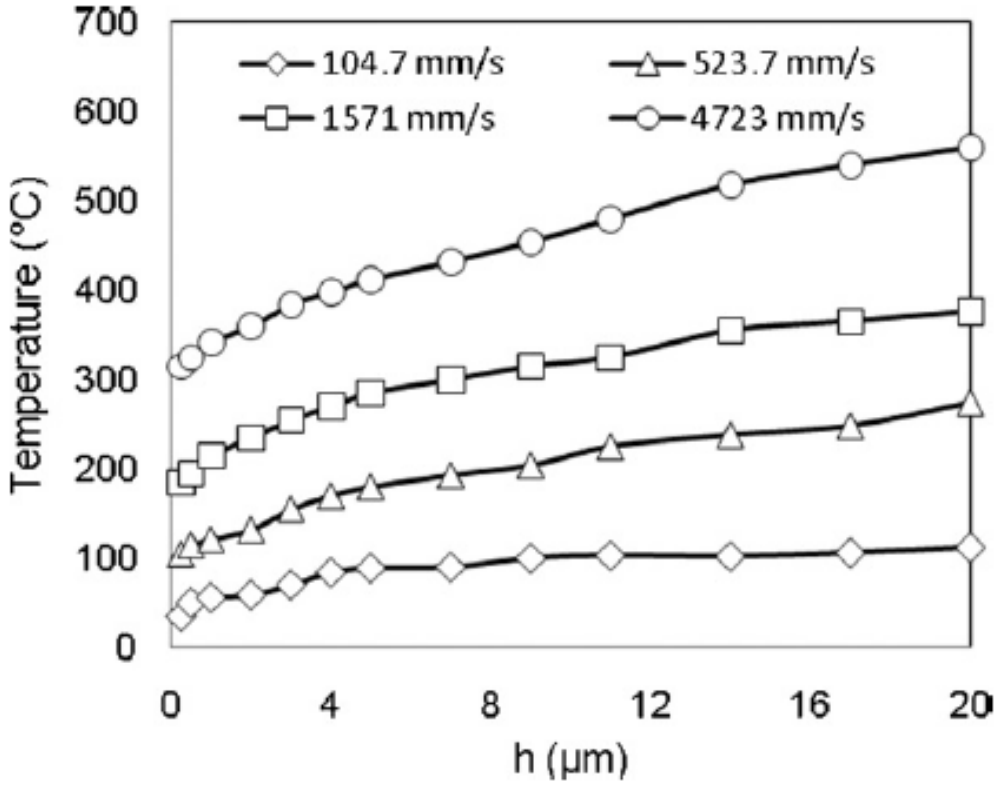

Fig. 2.16: Maximum cutting temperatures predicted by S. Afazov [84]

2.7 Modelling of micro-milling

2.7.1 Cutting forces and chip formation

The monitoring of micro milling process gives only limited information about tool performance (e.g. cutting force distribution over the cutting edge or tool stresses cannot be measured in real process etc.). Furthermore, reliable measurements in micro milling are very challenging because of very small dimensions, complexity of the tool geometry and high rotational speeds. Furthermore, in many cases the measured signal is of the same magnitude as the noise.

Therefore, reliable modelling is essential for understanding of different effects. Proper modelling also helps to speed up the procedure and makes the whole developing process less expensive [5, 86, 87]. In this section is discussed the current state of cutting forces modelling. In the researches published in this field, three main streams can be identified [5, 86, 87] as:

- Analytical force modelling.
- Mechanistic force modelling.
- Numerical chip formation modelling.

Analytical force modelling

These models try to link the cutting forces with some geometric characteristics and empirically obtained data. All these models are fundamentally based on J. Tlusty and P. MacNeil's [88] milling force model. The original J. Tlusty and P. MacNeil model is, however, insufficient for the micro milling process due to omission of the axial force component and the substitution of a tool path by a series of circles. Furthermore, J. Tlusty and P. MacNeil have assumed specific cutting energy to be a constant. However, according to T. Jin et.al. [89] this assumption is invalid in the case of micro milling. The specific cutting energy is affected by scaling effect and with reduction of uncut chip thickness has a tendency to grow. This is because of increasing effect of the cutting edge radius, which is typically negligible can in conventional cutting. Other models based on the J. Tlusty and P. MacNeil work were presented by Gygax [90] and Kline [91]. However, the first analytical model for micro milling was suggested W. Y. Bao and I. Tansel in 2000 [22]. Bao considered new expression of the trajectory of the tool tip. The drawback of his model is its 2-dimensionality

and use of a constant specific cutting energy. Therefore, this model gives good results for higher feed rates, but the accuracy of the predicted forces for low feed rates is significantly lower.

The first 3-dimensional model which links radial and tangential force to axial force, is a model proposed by Zaman et. al. in 2005 [61]. The model uses uncut chip area instead of uncut chip thickness and considers the tangential cutting force component to be normal to the cutting edge. Hence, the tangential cutting force component can be further resolved to axial component and component perpendicular to the tool axis. The model, however, uses an unrealistic calculation of theoretical chip areas, and therefore, The results achieved by this model do not fit with experimental data (see fig. 2.17).

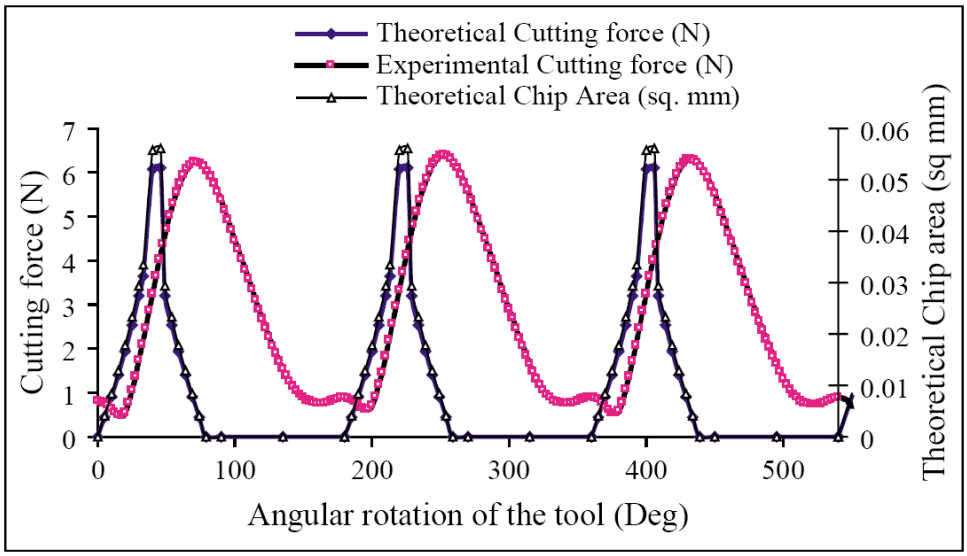

Fig. 2.17: Comparison of theoretical and experimental force by Zaman [92]

Another three-dimensional cutting force model in micro milling was proposed by Li et. al. in 2007 [93]. This model uses a much more realistic trochoidal tool tip path. In advance, the cutting mechanism is split into two phases: plastic-elastic and shearing-ploughing mechanisms. The model gives a very precise estimation of cutting forces with an error of up to 10%.

Mechanistic force modelling

This group of models is also based on a relation between the cutting force and the uncut chip thickness. An example of the sort of model is [94]. This model is the only attempt to use

this sort of models in micro milling found in literature. The model uses complicated relation between cutting forces and mechanical aspects, such as material properties, friction, and tool and workpiece geometries. It is, however, very difficult to achieve all the necessary properties in micro-scale. Another drawback of these models is the concept of slip-line theory. It is impossible to determine the shearing plane experimentally in micro milling. At the reality it is difficult to determine the plain even in orthogonal cutting. For these reasons these models require much more effort than analytical models and are considered to be tricky. Furthermore, the effort does not seem to lead to improvement of the accuracy of the predicted forces, see fig. 2.18.

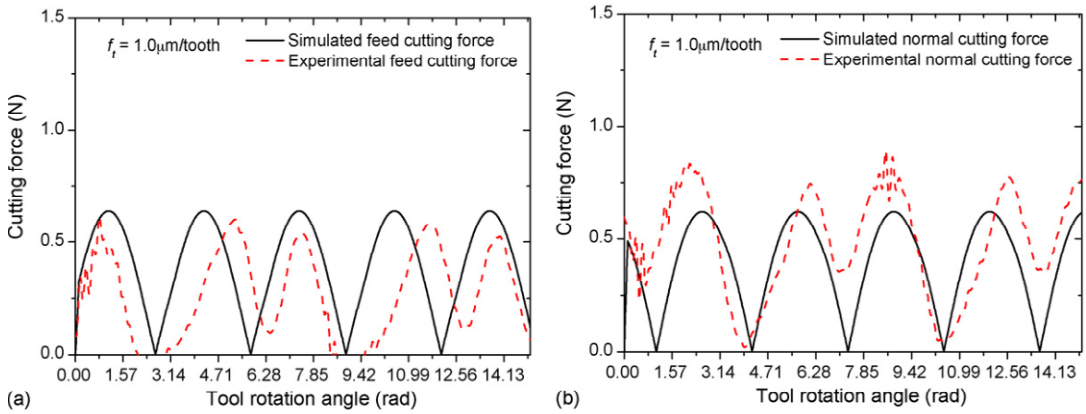

Fig. 2.18: Comparison of theoretical and experimental force by Feng [94]

Numerical approaches for chip formation analysis

Majority of the methods used for chip formation analysis use FEA. These methods may be based on three different formulations: Eulerian formulation, Lagrangian formulation and methods combining advantages of both of these formulations (Arbitrary Lagrangian-Elerian formulation). The difference between Lagrantial and Eulerian formulation is illustrated in fig. 2.19. In Lagrangian formulation the mesh deforms with the physical material. The advantages of this formulation are that process can be simulated from some initial state to a steady state. Furthermore, the chip formation can be simulated together with residual stress. However, large element deformations resulting in distorted elements have been always a matter of concern. This formulation was used for example be the following researchers: Umbrello et. al. [95], Outeiro et. al. [96] or Özel et.al. [97].

On the other hand, Eulerian formulation uses fixed mesh. This eliminates issues with element distortion. However, simulations based on Eulerian formulation require knowledge about chip geometry in advance. Therefore, the range of cutting conditions which can be analysed is restricted. Because of its restrictions this formulation is much less popular for chip formation analysis. However, some researchers have used it for analysis of steady state chip formation in orthogonal cutting [98-100].

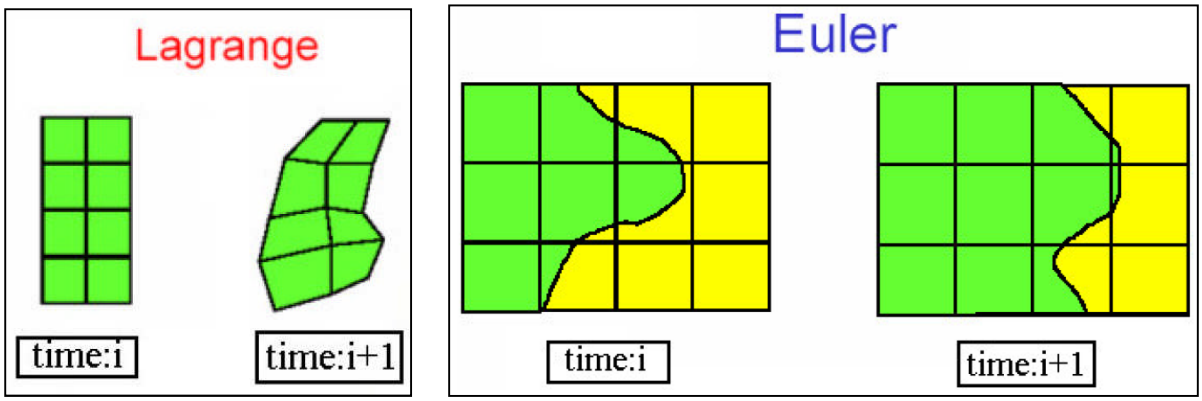

Fig. 2.19: Illustration of Elerian and lagrangian formulations [101]

Arbitrary lagrangian-euelerian formulation (ALE) combines advantages of both of the previous formulations. In this case, the mesh follows the physical material deformation (step 1) and then the mesh is smoothed and the calculated values remapped (step 2). Advantage of this formulation is in elimination of element distortion issues. Therefore, the models based on this formulation are more stable than the models based on purely lagrangian formulation. This formulation was used for example by Pantalé et.al. for fully 3D simulation of face milling, as it is shown in fig. 2.20 [102]. This work is, however, only example found in literature where FEA was used directly in milling. Other researchers using ALE formulation are for example: M.R. Movahedy et. al. [103, 104], P. J. Arrazola et. al.[105] or L. Olovson et. al. [106].

Apart from issues with large number of DOFs and large deformations (potentially leading to element distortions), the numerical models also suffer from great difficulties of achieving realistic material models. Umbrello et. al. [95] has compared effects of different material models on the resulting quantities (stresses and displacements). In his work five different material models of AISI 316L from different literature sources are used. The resultant chip

shapes achieved from these simulations are shown in fig. 2.21. It is evident, that the material models greatly influence the chip shape. This issue is even more challenging in the case of micro cutting because the material properties on the micro level can be significantly different than on the macro level.

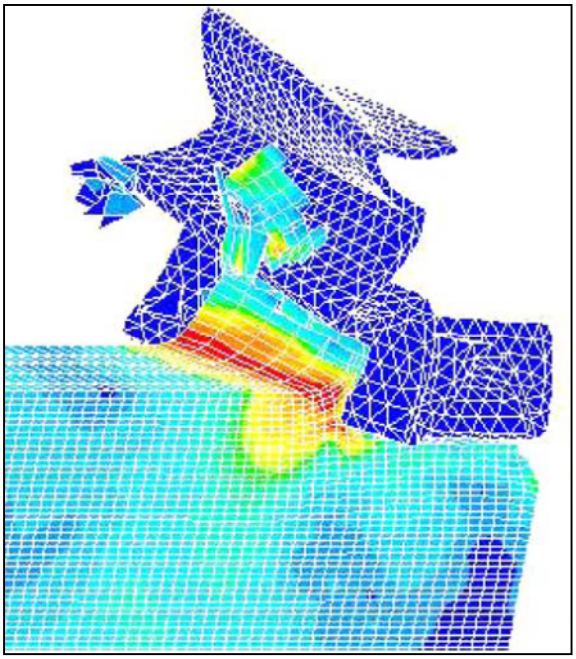

Fig. 2.20: Illustration of 3-dimensional FE simulation of milling process, [102]

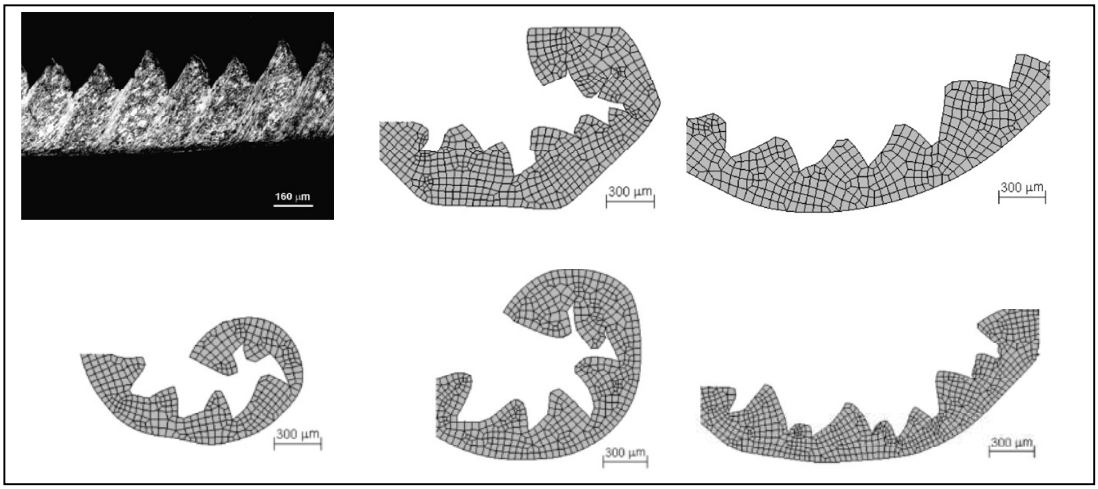

Fig. 2.21: Simulation of chip formation with different material models of AISI 316L [95]

It should also be mentioned that application of FEA in micro milling is very difficult. This is because of very complex chip formation process requiring 3D models (oblique cutting with

unsteady uncut chip thickness). Furthermore the computational time of usually used explicit numerical methods is related to mass of the smallest element (lower mass results in longer computational time) [107]. Hence, it is evident that the computational times of micro cutting simulations are extremely long. Therefore, chip formation FEA does not seem as the right tool for prediction of cutting forces in methods used for estimation of production costs, quality and time. However, its place seems to be in tool design, where a comprehensive knowledge about different effects is needed.

2.7.2 Analysis of tool deformations

The forces acting on the tool during micro milling process results in complex deformations. Generally three types of deformations can be identified as: bending, torsion and axial buckling. From these three types of deformations bending is the most important. It is a well known fact that bending stiffness decreases with reducing cross-sectional areas. A common way of estimating end-mill bending stiffness is by the employment of cantilever beam theory [108-110]. Based on this theory, the stiffness is proportional to the 4^{th} power of the tool diameter. However, the simplified analytical solutions give only a very rough estimation of the tool deformations. Thus, it is not very suitable for micro milling where the stiffness is very low and needs to be estimated much more accurately than in conventional milling, and therefore, the actual tool geometry should be considered.

Hence, some researchers use FEA instead of analytical solutions (e.g. all researches related to the tool design in section 2.3.2 use FEA). Another analysis of micro end-mills with cutting diameters bellow 0.3 mm was presented by Uriarte et. al. [111]. In this research, stiffness of Ø0.3 mm tool was found to be 0.056 $N \cdot \mu m^{-1}$. This means that a cutting force of 1 N will deflect the tool by approximately 18 µm. However, such deflection is significantly larger than uncut chip thicknesses typical for this type of tools. Even worse situation is in the case of Ø0.1 mm micro end-mill which shows stiffness of 0.008 $N \cdot \mu m^{-1}$. Hence, it is clear that the reduction of tool diameter has an enormous effect on tool stiffness and high attention must be paid to this topic.

2.8 Summary

This literature review shows a broad variety of challenges presented in micro milling. In the first part are summarised all the main factors affecting micro milling. The first group of

factors is related to the machine tool. The review of currently available machine tools has identified two main streams. The first stream, more usual for commercial machine tools, is in continuous improvements of machine tool stiffness, thermal stability and dynamic characteristics. These improvements, however, often lead to increasing dimensions. The second stream, more usual in research, is in reduction of machine tool dimensions. The experimental machine tools have often desktop dimensions. Furthermore, these machine tools often use high speed air-bearing spindles which have higher stability than conventional bearing spindles used in commercial machine tools. However, the experimental machine tools are often limited in their capabilities and are not yet ready for commercial production.

In the second part of this chapter is reviewed the current state of the micro end-mills. Micro end-mills represent the weakest point of the whole system. The smallest available micro end-mills have cutting diameters below 0.1 mm. The absolutely smallest commercially available tool is a dual-helix micro end-mill with the cutting diameter of 0.01 mm. All commercial micro end-mills were found to have the identical geometry as their conventional ancestors. The low interest in the tool design is also proven by absence of any patents related to micro end-mill design. The situation in research is not significantly better. Although many researchers have claimed necessity of improvements of micro end-mills, only four publications related to this topic were identified. Each of the publications targets different topic (e.g. tool wear, evaluation of new micro end-mills concepts or dimensional optimisation). However, a systematic methodology dealing with whole scale of micro end-mill design was not found. However, it is also assumed that if micro milling shall be competitive manufacturing technology, much higher flexibility of tool designs will be desired. This is because of an extreme sensitivity of the tools to various factors. Hence, a development of a systematic methodology and spreading it over micro manufacturing community is one of the greatest challenges.

Other topics which were reviewed are: state of the development of coatings for micro end-mills and effects of tool manufacturing technologies. In both cases only a limited research was identified. The coatings currently used in micro milling are identical with coatings originally developed for conventional cutters. It is, however, questionable if micro end-mills could not be protected by different, specially designed coatings. One of potential solutions is application of nano-layered tough-hard coatings. However, the research on these types of

protective coatings for micro end-mills is in its beginning phase. Another big issue, which was identified, is inconstancy of published results (e.g. TiN coating claimed by one researcher as the best one, is claimed as the worst one by another researcher). This may be caused by inconstancy of research techniques, but also by inadequate quality of the experimentally developed coatings.

Another big challenge is manufacturing of micro end-mills. Commercial micro end-mills are typically manufactured by micro grinding. These tools, however, show large inaccuracies. This is caused by application of aggressive cutting conditions, which are preferred by industry because of economical matters. The question is, whether some other more accurate manufacturing technologies could be used for production of micro end-mills. As the most promising was identified wire EDM (proven to be able to machine dual helix micro end-mills). This process, however, produce significant damages on the machined surface and further research is needed. Another process used for manufacturing of micro end-mills with diameters of 25 μm is FIB. Disadvantage of this process is, however, its low MRR. Therefore, it is assumed not to be applicable in industry. Other too potentially applicable manufacturing processes are micro-ECM and micro LBM. However, no applications of these two processes on manufacturing of micro end-mills were identified in literature.

In the last part of this chapter is reviewed current state of modelling in micro milling. This includes mainly chip formation, cutting forces and tool stiffness. Chip formation is mainly studied by FEA. However, majority of the research in this field is not done directly in micro milling, but in orthogonal cutting. This is because of extreme computational times of simulating 3D chip formation. Furthermore, the methods have often problems to solve processes involving large deformations. As the most promising method seems FEM ALE formulation which is currently the fastest and the most stable one. However, it is disputable whether this type of simulations will ever be applicable in micro milling.

Cutting forces are modelled by two different methods: analytical or mechanistic. Both of these methods are based on relating cutting forces to uncut chip thickness. However, because of difficulties of determination of shearing plane needed for mechanics models, analytical solutions are much more popular. Therefore, this type of models is also going to be used in this research.

3. Research aim and approach

In this chapter are identified the main objectives and described the structure and approach of this research. This chapter is divided into two separate sections. The research aim and objectives are addressed in the first section. In the second section are described the research structure and approach.

3.1 Research aim and objectives

Micro milling was found a capable manufacturing process. However, its low predictability prevents it from wider industrial applications. According to literature review no suitable prediction and planning methods applicable in industry are currently available. Hence, it is important to increase the knowledge of this process and use it for development of a new reliable and feasible machining strategies and methods. Therefore, the main aim of this research may be defined as:

To increase reliability of micro milling process through better understanding of tool performance.

To achieve this aim four different objectives are set for this research:

1. Identify the main factors affecting tool performance and develop an understanding of them.
2. Based on the knowledge, propose a tool life prediction method.
3. Investigate possibilities of tool life extension through improvements of the tool geometry.
4. Develop a systematic methodology suitable for designing of micro end-mills.

3.2 Working approach and the structure of this research

The basic approach used in this research is illustrated in fig. 3.1. It is divided into four main stages. In the first stage is justified this research. Furthermore, relevant research publications are reviewed and identified current stage of the knowledge. This stage forms chapters 1 and 2 of this thesis.

The information achieved in the first stage is then used to set the main objectives and approaches. To support the objectives an experimental study is included in this stage. The main aim of this study is to identify research challenges and the main factors affecting micro milling. The objectives are defined in this chapter and the experimental study in chapters 4 and 5.

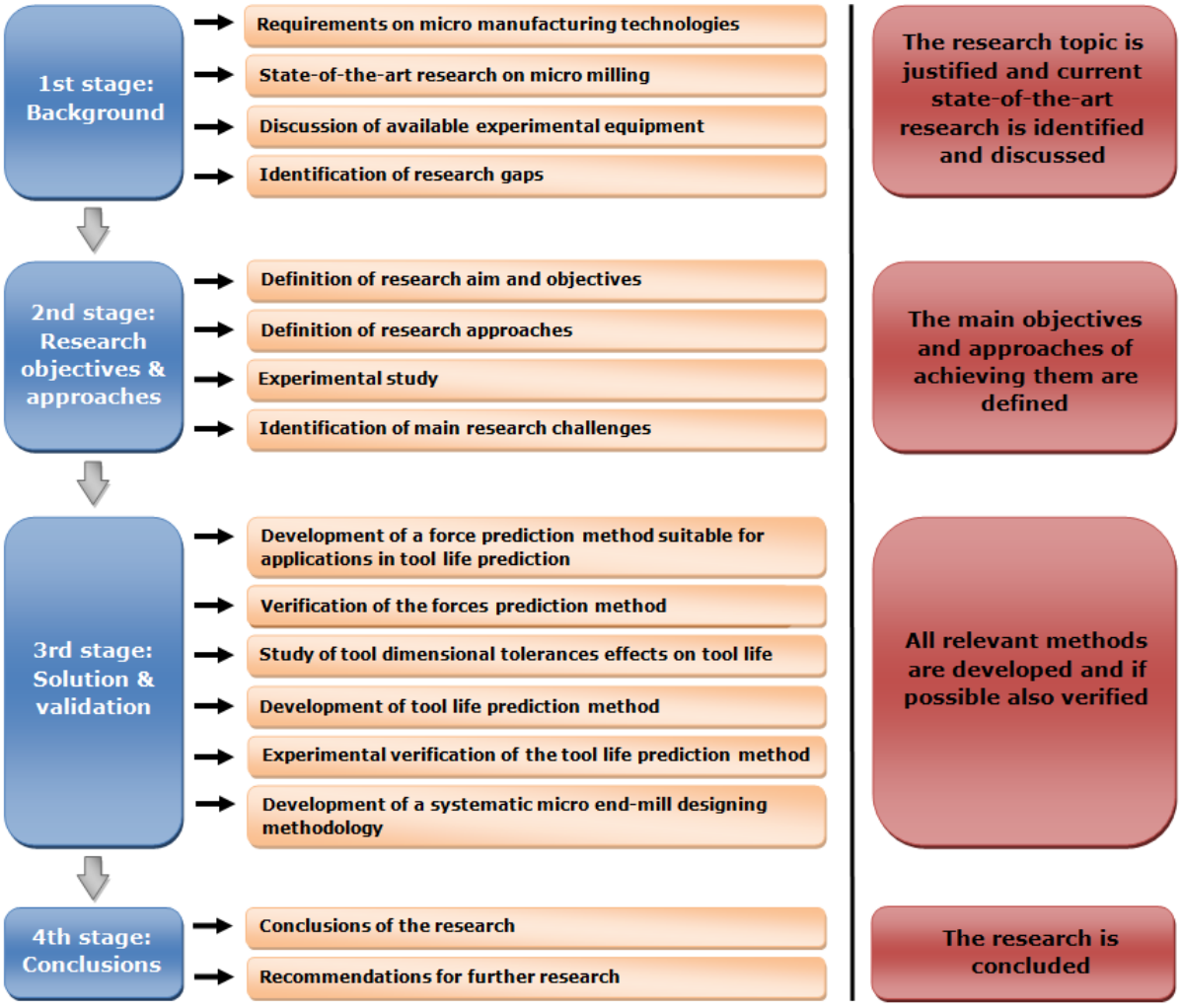

Fig. 3.1: Illustration of working approach and structure of this research

The third stage (solution & validation) is the most important one of the whole research. All the methods are developed in this stage. In this particular research are proposed two different methods. The first one links the input cutting parameters with tool life. The main novelty of this method is in its statistical character. It is also the first method which tries to predict tool breakage for real life applications. The second method developed in this research is a micro end-mill designing method. This method tries to identify suitable designing rules

and approaches applicable in micro milling. Because of the special character of micro milling, the future micro end-mills are likely to be more specialised than it is now. It is assumed that the new, more specialised, micro end-mills will be designed with respect to its proposed applications. Hence, a general systematic method is assumed to be more valuable than a new tool design. The solution stage is presented in chapters 6, 7, 8 and 9.

Finally, in the last stage the research is reviewed and its achievements summarized. In this stage is discussed the main contribution of knowledge achieved during this work and new topics arising from this research are formulated. This stage is presented in the last chapter of this thesis.

4. Experimental equipment

In this chapter is introduced all experimental equipment used in the current research. In section 4.1 is described KERN EVO precision manufacturing centre. The section 4.2 gives the basic information about micro end-mills used in this research. This is followed by description and justification of workpiece material in the section 4.3. Finally, in the section 4.4 is discussed all the measurement equipment used in this research.

4.1 Machine tool

The machine tool used in this research is KERN EVO CNC precision machining centre [18], see fig. 4.1. To secure the highest possible stability of machining process the machine tool was located in temperature and humidity controlled environment. The temperature was maintained on 20°C with maximum fluctuations within 1°C. The humidity was kept on 50 ±5% RH. Furthermore, the machine tool was placed on separated floor segment. This solution provides sufficient insulation from disruptive vibrations which may be induced by other work performed within the laboratory.

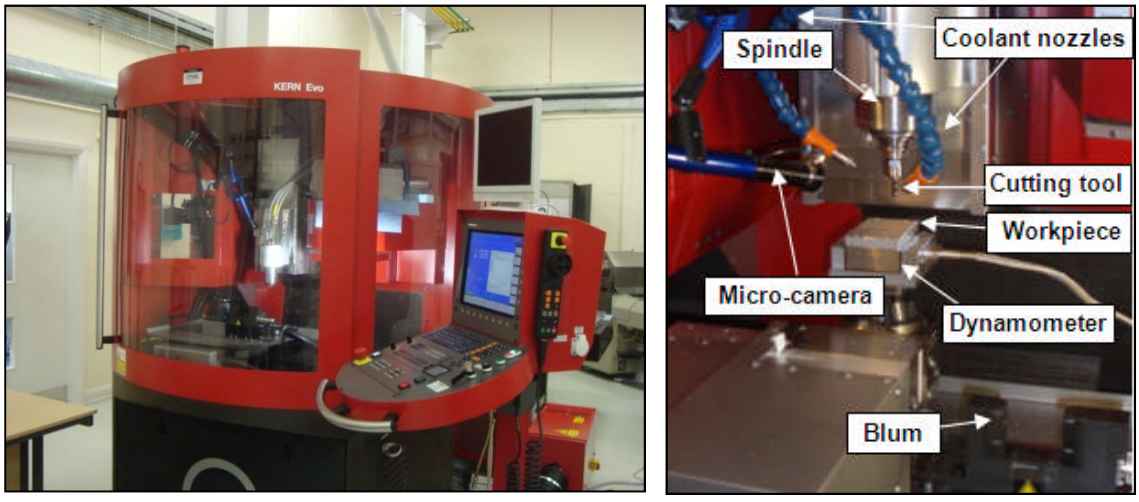

(a) KERN EVO (b) KERN EVO - cutting area

Fig. 4.1: Kern Evo CNC machining centre

KERN EVO represents a state-of-the-art machining centre widely used in research institutions as well as in industry. The basic description of the machine tool is given in tab. 4.1. The machine tool itself shows excellent stability and positioning accuracy. The machine

tool provider quotes the positioning accuracy of 1 μm and positioning resolution of 0.1 μm. This is considered sufficient for all experiments performed during this research.

Table 4.1: Main specification of KERN Evo CNC machining centre [18]

Machine type	Micro milling CNC machine
Axes	X, Y, Z, B, C
Spindle type	Precise hybrid bearing
Spindle speed	0-50000 rpm
Clamping interface	HSK-E25
Tool holder	Collets
Tool setting	BLUM nano
Workpiece setting	Touch probe
Resolution	0.1 μm
Positioning tolerance	±1 μm
Feed rate in X, Y, Z	16 $m \cdot min^{-1}$
Automatic thermal compensation	Yes
Lubrication system	MQL
Control unit	Heidenhain iTNC 530

The machine tool located in Cranfield University is equipped with two different spindles:

1) a hybrid bearing spindle with maximum speed of 50 000 rpm,
2) a hybrid bearing high speed spindle with maximum speed of 160 000 rpm.

However, only the first spindle is used during all experiments covered in this research. This is because of two main reasons. Firstly, the changing of spindles can affect machining process. Different spindles can have different dynamic performance, stiffness, run-outs etc. This could influence the experimental results, and therefore, it is not convenient to use different spindles. Secondly, each spindle is equipped with different types of collets. The second spindle has collets which can accommodate only tools with maximum shank diameters of 3 mm. However, the tools used in this research, have shank diameters of 4 mm. Hence, only the first spindle could be used.

According to spindles, it is good to mention, that recently two novel Westwind air-bearing spindles were tested in Cranfield University. These spindles are considered to give better stiffness and machining stability [112]. Therefore, they seem to be good solution for high speed micro-manufacturing.

The machine tool is additionally equipped with a micro-camera which allows real time process monitoring, thermal compensation system and state-of-the-art BLUM nano [113] laser measurement system for fast tool setting. The BLUM nano laser system is also used for fast inspection of the tool diameter during all experiments included in this research. The capabilities of the system itself are further discussed in section 4.4.

4.2 Micro end-mills

End-mills used in this research are commercial tungsten-carbide square micro end-mills with diameters of 0.2 mm and 1 mm respectively. The manufacturer of the tools is UNION TOOL [38]. UNION TOOL is one of the leading micro tools manufacturers and its tools are widely used in research as well as in industry. The tools with 1 mm diameter were used only in the initial stage of this research to identify main differences between real micro end-milling and meso/macro end-milling. The material of the tools is tungsten-carbide with a cobalt binder (WC-Co). The average grain size of the material is between 0.6 μm to 1 μm. Some of the tools used in this research were uncoated, some others coated by commercial coating (TiAlN). Main tool nominal dimensions as given by manufacturer are listed in tab. 4.2.

Table 4.2: Nominal dimensions of tools used in this research

Component	Symbol	Values	
		Ø0.2 mm tool	Ø1 mm tool
Total length	l	45 mm	45 mm
Shank diameter	D_s	4 mm	4 mm
Cutting part length	l_c	0.4 mm	2 mm
Cutting diameter	D_c	0.2 mm	1 mm
Neck angle	ψ	15°	15°
Helix angle	β	30°	30°

The quality of all tools used in this research was checked by SEM to avoid any damaged or non-standard tools. The geometry of a typical Ø0.2 mm micro-end mill is shown in fig. 4.2. Because of verification of the dimensions declared by the manufacturer, some of the main dimensions of 10 randomly chosen tools were measured using SEM micrographs and compared with declared dimensions. The measured dimensions are: the cutting diameter, the core diameter, the rake angle, the relief angle, the neck angle and the distance from the tool tip to the neck. For clarity reasons these dimensions are highlighted in fig. 4.3. Average values together with minimum and maximum measured values are listed in tab. 4.3.

(a) View 1 - Overall side view

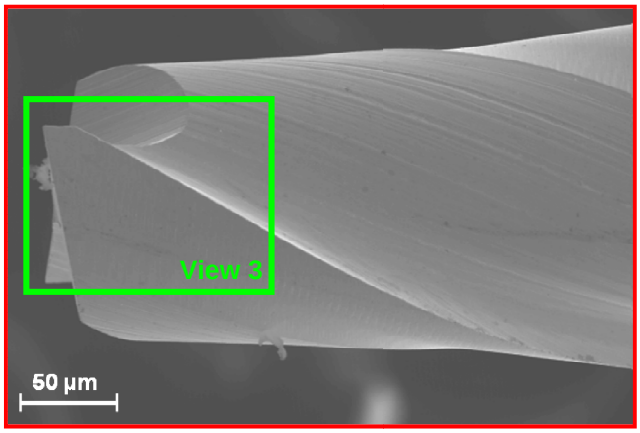

(b) View 2 - detail of the tool tip

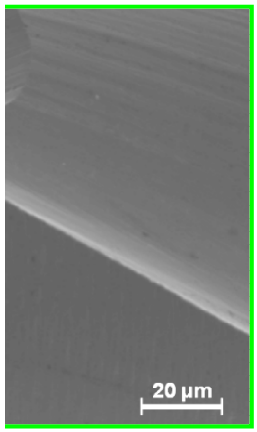

(c) View 3 - detail of the cutting edge

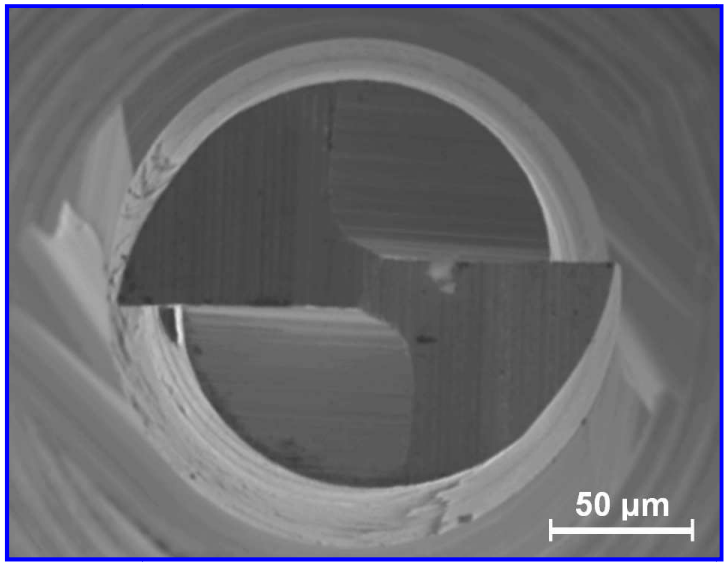

(d) View 4 - front view

Fig. 4.2: SEM micrographs of uncoated Ø0.2 mm micro end-mills

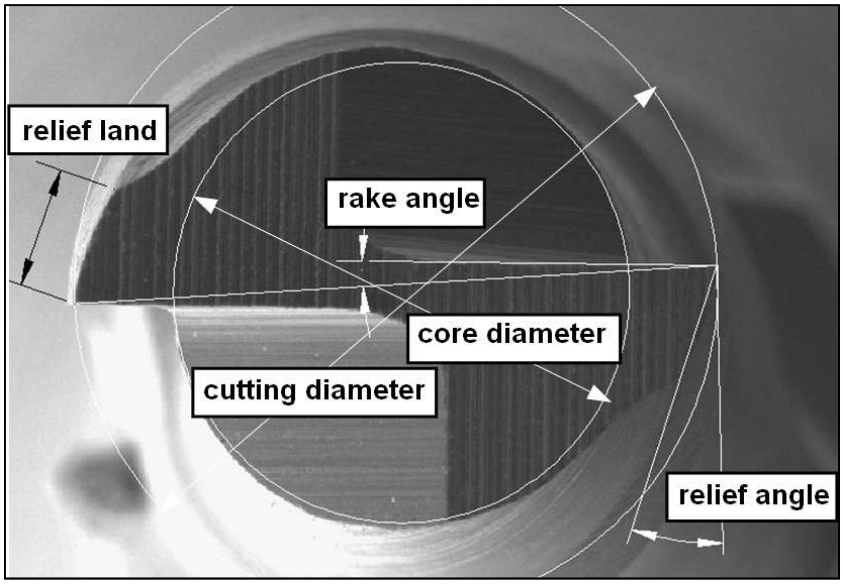

(a) Front view

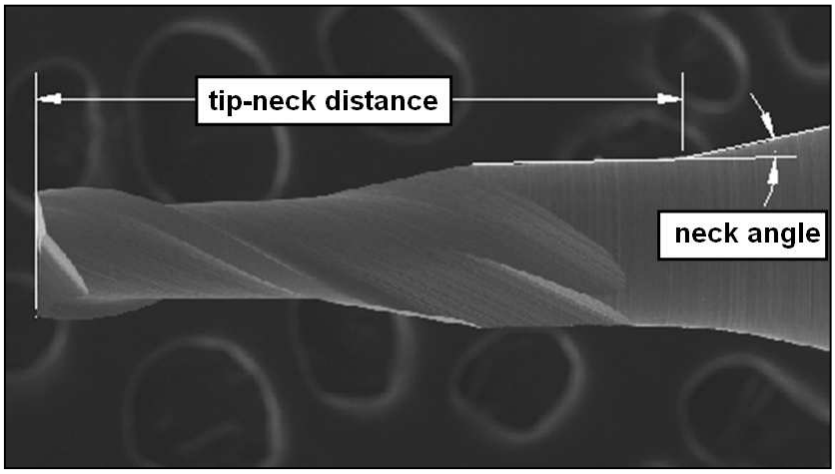

(b) Side view

Fig. 4.3: Illustration of dimensions measured on Ø0.2 mm micro end-mills

Table 4.3: Tools geometry check

	Ø0.2 mm (uncoated)	**Ø0.2 mm (TiAlN)**	**Ø1 mm (uncoated)**	**Ø1 mm (TiAlN)**
Cutting diameter (µm)	$180\ \binom{183}{178}$	$184\ \binom{187}{181}$	$977\ \binom{980}{971}$	$979\ \binom{983}{974}$
Core diameter (µm)	$130\ \binom{133}{128}$	$132\ \binom{133}{128}$	$675\ \binom{680}{668}$	$677\ \binom{683}{670}$
Rake angle (°)	$-4.5\ \binom{-6}{-3}$	$-4.3\ \binom{-5}{-3}$	$-3.8\ \binom{-5}{-3}$	$-4.0\ \binom{-6}{-3}$
Relief angle (°)	$18.3\ \binom{20}{16}$	$17.9\ \binom{20}{16}$	$17.8\ \binom{19}{16}$	$18.1\ \binom{19}{15}$
Neck angle (°)	$13.5\ \binom{16}{11}$	$14.1\ \binom{16}{12}$	$14.0\ \binom{15}{11}$	$13.8\ \binom{15}{10}$
Tip-neck distance (mm)	$952\ \binom{955}{944}$	$958\ \binom{960}{949}$	$3950\ \binom{3961}{3947}$	$3956\ \binom{3978}{3950}$

All the measured tools were found to have smaller than declared dimensions. The coated tools were found to have generally larger core and cutting diameters. This was expected, as an extra material is added onto the finished tool. On the other hand the coating has no effect on any of the tool angles. It was also found that the measured angles (rake angle, relief angle and neck angle) are the same for both Ø0.2 mm and Ø1 mm tools.

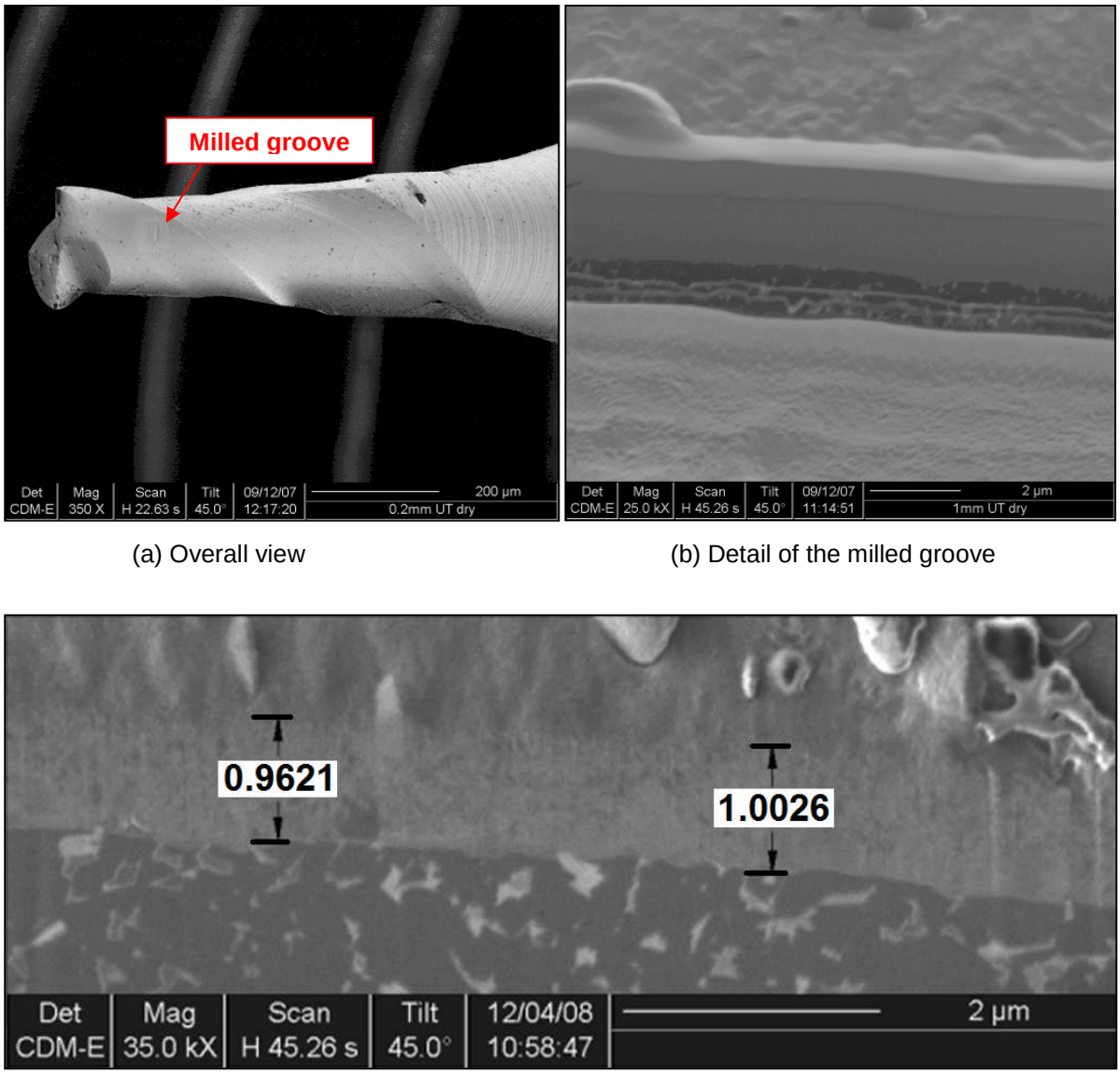

(a) Overall view

(b) Detail of the milled groove

(c) Illustration of the measured coating thickness

Fig. 4.4: Ø0.2 mm Micro end-mill milled by FIB

Three randomly chosen uncoated tools were analysed by Energy Dispersive X-ray spectrometry (EDS) for identification of the real chemical composition. Details of the EDS

analysis are covered in Appendix B. Material density of the tool core material (WC-Co) was also experimentally analysed. The measured chemical composition and density were used for identification of material properties relevant for FEA. These properties were taken from www.matweb.com and www.generalcarbide.com [114, 115] and are summarized in tab. 4.4.

Table 4.4: Material properties of WC-Co

Content of tungsten (W)	83% (measured by EDX)
Content of carbon (C)	11% (measured by EDX)
Content of cobalt (Co)	6% (measured by EDX)
Grain size	0.6 - 1.0 µm
Average Density	14 653 $kg \cdot m^3$ (measured)
Average modulus of elasticity	645 GPa
Average Poisson's ratio	0.22
Average transverse rupture strength	2.9 GPa
Coefficient of thermal expansion	$4.8 \cdot 10^{-6}\ K^{-1}$
Specific heat capacity	$340\ J \cdot kg^{-1} \cdot K^{-1}$
Thermal conductivity	$70\ W \cdot m^{-1} \cdot K^{-1}$

In the case of the coated tools, the only information from the supplier is the coating chemical composition (TiAlN). Therefore, three coated tools were milled and measured by FIB as shown in fig. 4.4. By this analyses, the tool coating was found to be mono-layered and approximately 1 µm thick.

4.3 Workpiece

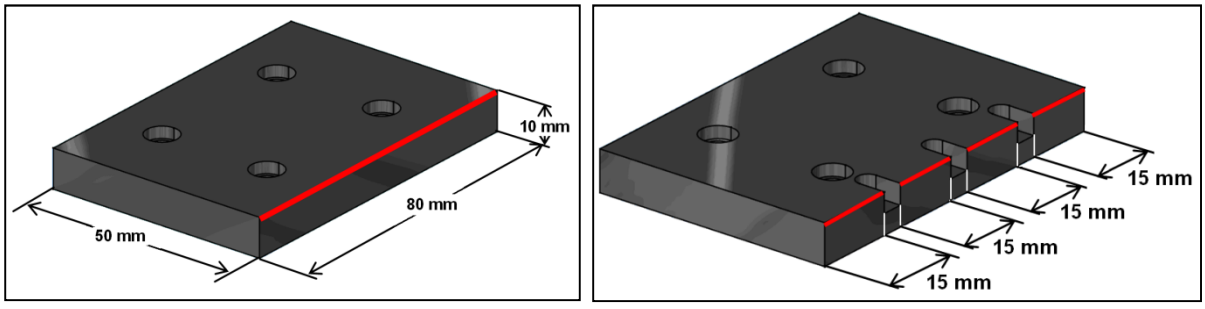

(a) Workpiece for tests with Ø1 mm tools (b) Workpiece for tests with Ø0.2 mm tools

Fig. 4.5: Workpiece geometry used in this research

The workpiece material used in this research is tooling steel Toolox 33 [116]. Toolox 33 is quenched and tempered steel with high impact toughness and low residual stresses. Therefore, Toolox 33 is suitable for plastic or rubber micro moulds and machine components.

Relatively low hardness (27 – 35 HRC) makes this material easily machinable. Therefore, it is in a great demand in different industrial fields.

Material supplied was cut into blocks of 50×80×10 mm^3 as it is shown in fig. 4.5a. The surface of these blocks was ground in order to achieve a suitable flatness and roughness for micro milling experiments. Such blocks were used for all experiments with Ø1 mm tools. In the case of the experiments with Ø0.2 mm tools, the side of the workpiece was segmented as it is shown in fig. 4.5b. This was done because of shorter tool life of Ø0.2 mm tools, and therefore, necessity of a higher frequency of tool inspections. The workpiece was mounted to a KISTLER dynamometer (see section 4.4.1) by four screws and the whole setup was clamped within the KERN EVO as it is shown above in fig 4.1b.

Table 4.5: Chemical composition of Toolox 33

Chemical component	Content declared by supplier (%)	Measured content (weight %)
Fe	95.2 - 97.0	92.03
C	0.22 - 0.24	0.43
Si	0.60 - 1.10	0.63
Mn	0.80	0.91
P	max 0.01	-
S	max 0.003	-
Cr	1.00 - 1.20	1.00
Mo	0.30	0.39
V	0.10 - 0.11	0.15
Ni	max 1.00	0.46

Chemical composition of the workpiece material was analysed by EDS and compared with the composition given by the supplier, see tab 4.5. All values, except content of carbon, are in a good agreement with the declared values. The measured content of carbon is almost twice as high as the declared one. This is assumed to be because of possible contamination of the sample surface during handling and preparation. However, as all the experiments in this thesis are comparative (either comparing different types of tools or used for model verification), this difference is considered as unimportant and can be accepted.

4.4 Measurement equipment

In this section is summarized and briefly discussed all measurement equipment used during this research. This includes:

- KISTLER dynamometer used for all cutting force measurements,
- Scanning electron microscope (SEM) and energy dispersive X-ray spectrometer (EDS) used for tool inspection,
- BLUM nano laser setting system used for wear monitoring of the tools,
- Talysurf CCI white light interferometer used for analyses of generated surfaces.

4.4.1 Force measurements

Cutting forces were measured by a piezoelectric force sensor Kistler MiniDyn 9256C2 [117], which is shown in fig. 4.6a. The force sensor measures three force components in *x*, *y* and *z* directions. The sensitivity of the sensor is -26 pC/N in *x* and *z* direction and -13 pC/N in *y* direction and the threshold 0.002 N. First natural frequency of the sensor is 4 kHz. The measured signal was amplified and transformed from an electrical charge to a voltage by a Kistler 4-chanell charge amplifier 5070A [117], which is shown in fig. 4.6b. The range of the output voltage is ±10 V. The acquisition board used in this research was NI 9215A [118] with a maximum sampling rate of 100 kHz and a resolution of ~0.003 V.

Two different measuring ranges were used for experiments with Ø1 mm tools and Ø0.2 mm tools. In the first case the measuring range was setup to ±20 N whereas in the second case the measuring range was only ±10 N. These ranges were chosen with attempt to maximize measuring resolution and with respect to forces measured during few initial tests. Both ranges are expected to be high enough to prevent a cut-off of the maximum cutting forces during the planned experiments.

The measurement system total resolution was calculated for each of the above cases from the relation 4.1.

$$\text{Total resolution} = \frac{\text{Resolution of acquisition board}}{\text{Amplifier output voltage}} \cdot \text{Force range} \tag{4.1}$$

In the case of ±20 N range the calculated resolution is 0.006 N, whereas in the case of ±10 N range the calculated resolution is 0.003 N.

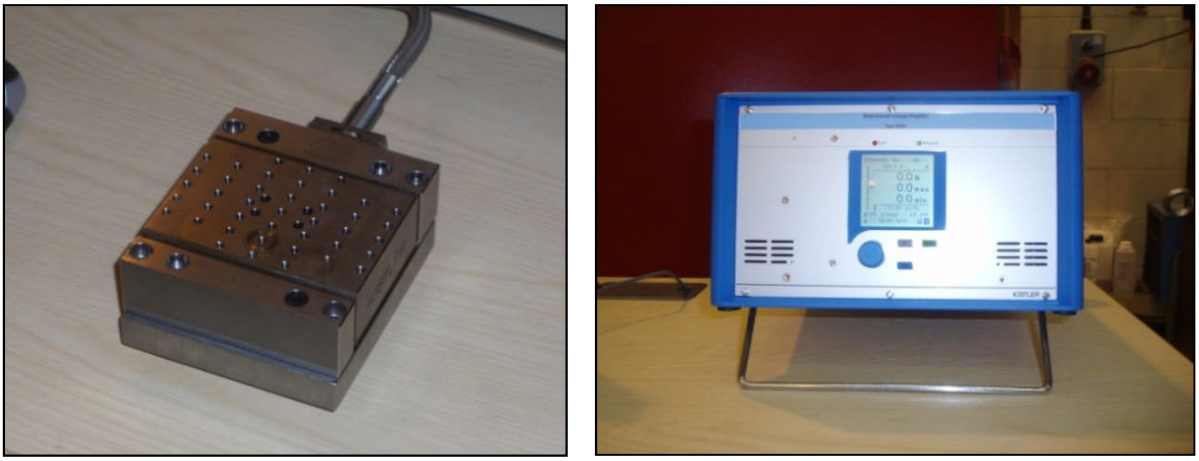

(a) Force sensor Kistler MiniDyn Type9256C2 (b) Kistler 4-chanell charge amplifier type 5070A

Fig. 4.6: Dynamometer KISTLER MiniDyn 9256C

The sampling frequency used in all experiments was set to 40 000 samples per second. This high sampling frequency was chosen with respect to rotational speeds usually used in micro milling (between 10 000 rpm and 40 000 rpm). Lower sampling rate per tool rotation would increase a risk of missing the maximum force, and therefore, significantly decrease the confidence in the measured data. An example of a typical force signal measured during this research is shown in fig. 4.7. In all cases presented in this thesis the measurement was started before and stopped after cutting process as it is shown in fig. 4.7a. This is because of identification and, if necessary, a compensation of any signal drift. In fig. 4.7b is shown a detail of the measured signal with highlighted data points. It is evident that the chosen sampling frequency is sufficiently high for the intended measurements.

Another important factor affecting the measurement accuracy is a signal noise. This noise may be produced either by environmental fluctuations or electrical noise. By location of the machine tool in an environmentally controlled room should be minimized the effects of the temperature and the humidity fluctuations. Furthermore, as the machine tool is located on an isolated floor block, the effect of environmental vibrations is also assumed to be negligible. The noise induced by the measuring system itself was analysed by running a measurement without any physical load. The amplitude of the measured signal was less than 0.007 N. This is in good agreement with a noise measured by M. Malekian who had used the same measuring system in his research and measured the noise of approximately 0.005 N [119]. Such noise level is insignificant compared to the cutting forces.

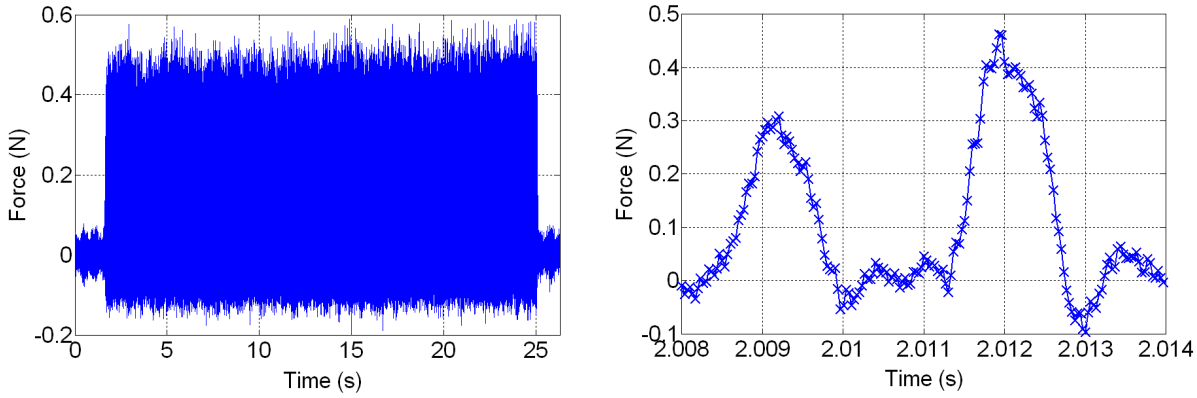

Fig. 4.7: An example of a measured force signal measured during experiments with Ø0.2 mm tools (30 000 rpm, f_z = 2 µm/tooth, a_p = 100 µm and a_e = 20 µm)

4.4.2 Scanning electron microscope and energy dispersive X-ray spectrometer

All tools were inspected by a scanning electron microscope (SEM). The SEM is based on scanning of a sample surface by a narrow electron beam. The electrons interact with the surface atoms and so produce different signals which can be used for characterisation of the material composition, the surface topography or electrical conductivity. The main advantages of the SEM compared with optical microscopes are: very high resolution (typically 1nm to 20 nm), magnifications from 10x up to 500 000x and large depth of field.

The SEM used in this research is equipped with backscattered and secondary electron detectors. The first one is used mainly for an easy differentiation between various materials. An example of backscattered image is shown in fig. 4.8a. In this particular case two different materials can be identified. The first material is WC-Co (appears as brighter) and the second material is the workpiece steel (appears as darker). On the other hand, secondary electron detector is more useful for imaging of surface topography. An example of this type of image is shown in fig. 4.8b.

Furthermore, the SEM used in this research is equipped with an energy dispersive X-ray spectrometer (EDS). EDS is a technique used for chemical characterisation of a sample. It relies on an analysis of an interaction of X-rays with the sample. EDS represents a non-destructive, reliable and fast method. In this research it was mainly used for an identification of the tool and the workpiece materials.

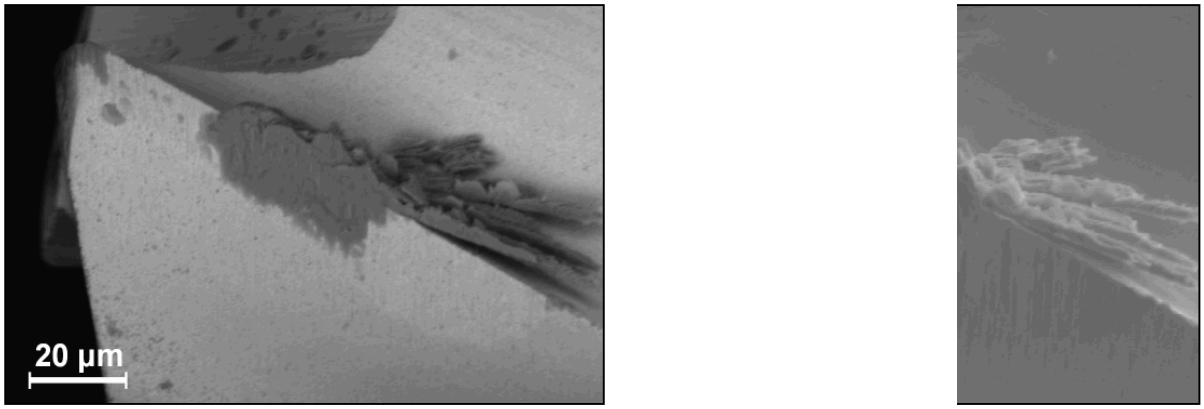

(a) Backscattered electron image (b) Secondary electron image

Fig. 4.8: Examples of SEM images

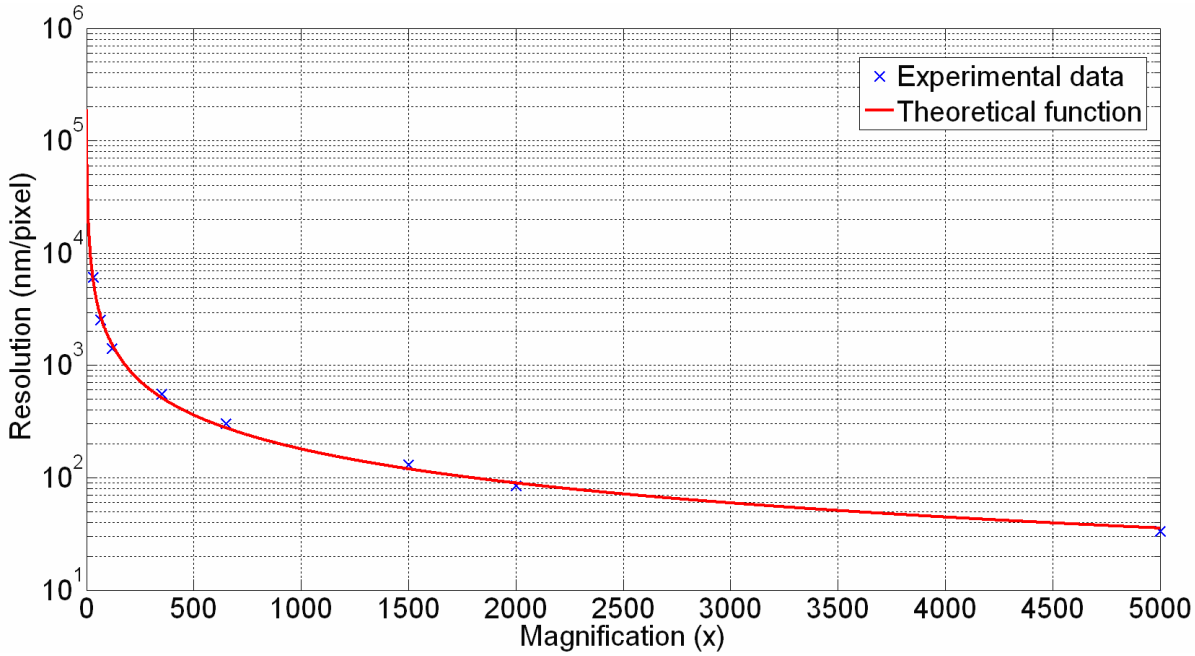

Fig. 4.9: SEM output resolution as a function of magnification

Although it was stated above that the SEM resolution is between 1 nm and 20 nm, it is not exactly truth. The output resolution is not affected only by the microscope resolution, but also by the resolution of the computer image. However, as the image size (712 x 484 pixels) remains constant for all cases, it is evident that the output resolution is a function of the magnification. The function was determined from numerous of SEM images taken during this research as:

$$\text{Total resolution} = 1.90 \cdot 10^5 \cdot \text{Magnification}^{-1.01} \tag{4.2}$$

The resulting trend is plotted in fig. 4.9.

It is evident that only the highest possible magnification should be used to take measurements in order to minimize the measurement error.

However, the resolution is not the only source of the measurement errors. As the tool has a complex 3-dimensional shape, special attention must be paid to positioning of the tool. A tilt about any of the axis may cause a reduction of the measured dimensions. In fig. 4.10 is shown a relation between a relative error and the tilt (φ). The relative error was calculated as a ratio of the dimensional reduction and the real dimension. It was calculated from the following relation:

$$\text{Relative error} = (1 - \cos\varphi) \cdot 100\% \tag{4.3}$$

This means that if the cutting diameter of the Ø0.2 mm tool is measured and the tilt about the tool axis is 5°, the error will be 0.5 μm. Furthermore, if the effect of the output resolution is assumed, the total error is approximately 1 μm. This error is insignificant in compare with the measured diameter.

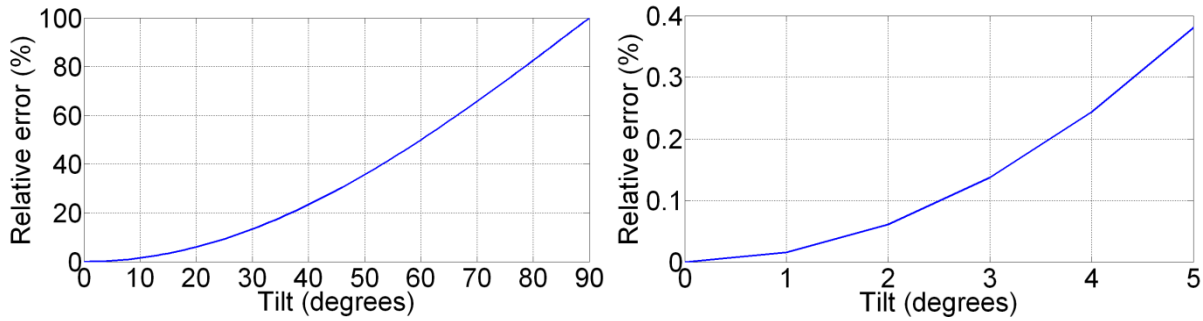

(a) The range of 0° - 90°

(b) Detail of the range of 0° - 5°

Fig. 4.10: Relative error caused by tilt of the sample

If smaller dimension, such as tool flank wear (VB) is measured, the magnification can be proportionally increased. This leads to an increase of the resolution and consequently in a reduction of the absolute error. The error caused by the tilt cannot be absolutely eliminated, but can be significantly reduced by carful setting of the tool within the microscope chamber.

Focusing is the last important source of measurement uncertainties. As the tool has a complex shape, it is difficult to focus accurately to the measurement plane. However, as the depth of field of SEM is typically larger than the one of common optical microscopes, it is more appropriate to use SEM for measurements of micro end-mills.

All the properties of the SEM make it a suitable measurement method for the current research. Another technique, which may be assumed for the tool measurements, is a confocal optical microscope [120]. Advantages of this technique are a high measurement speed and acquisition of 3D information about the tool. However, this type of microscope is currently not available in Cranfield university.

4.4.3 BLUM nano laser setting system

Fig. 4.11: Illustration of the BLUM nano laser setting system [113]

In the section 4.2 was briefly mentioned the BLUM nano laser setting system [113], which is a part of the KERN EVO machining centre located in Cranfield University. The system works on a principle of crossing the laser beam by a rotating tool as it is shown in fig. 4.11. During this research the system was found extremely helpful for a fast in-situ tool inspection. The system uses a visible red light laser with wavelength of 630-700 nm and with a power of

less than 1 mW. The repeatability of the system declared by the manufacturer is 0.1 μm and the manufacturer clams the system to be suitable for inspection of tools with cutting diameters down to 5 μm.

Except of setting of the tool, the BLUM nano was used in this research for fast measurement of tool wear. In this case, the tool wear is measured in sense of a reduction of the tool cutting diameter. The tool diameter was regularly measured after a defined milling distance, and then the tool cutting diameter reduction was calculated.

4.4.4 White light interferometer

The main interest of this research is a prediction of tool life. However, in the next section of this thesis are covered some experiments comparing performance of different types of tools (coated/uncoated, Ø0.2 mm and Ø1 mm). These experiments include a study of generated surfaces. Because of small depths and widths of cut typical for micro milling, conventional methods based on contact stylus measurements are inapplicable. On the other hand methods developed for characterization of nano-structured surfaces, such as atomic force microscopy (AFM), are inapplicable because of low lateral and vertical ranges. Furthermore, both AFM and stylus methods are based on scanning of the surface, and therefore, they are usually used only for characterisation of selected profiles.

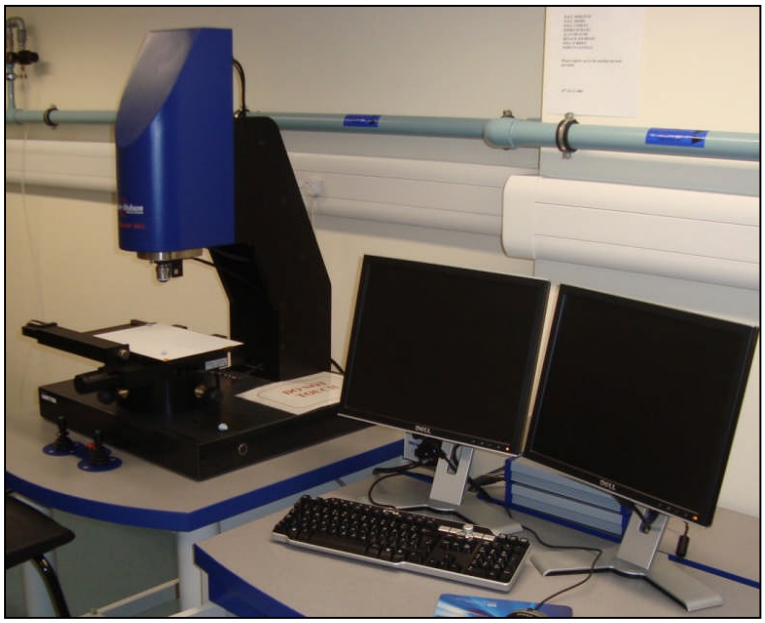

Fig. 4.12: Taylor Hobson Precision Talysurf CCI 6000 [121]

As the most appropriate measuring technique for the surfaces generated by micro milling was identified white light interferometry (WLI). The technique is based on interference of optical waves, and it is able to measure a surface over an area in a very short time (typically only tens of seconds). In this research was used Tailor Hobson Talysurf CCI 6000 [121], which is shown in fig. 4.12. The instrument is located in a temperature and humidity controlled environment to ensure minimum surface deviations due to environmental fluctuations. The instrument is equipped with 5 lenses with magnifications of 2.5x, 5x, 10x, 20x and 50x. However, in this research was used only the lens with the magnification of 50x. The vertical resolution (z) is 0.1 nm, measurement noise 0.05 nm, optical (lateral) resolution (xy) 0.4-0.6 μm, measurement area 0.36 mm x 0.36 mm and a maximum slope 27.7°. RMS repeatability is declared by the manufacturer to be 0.003 nm.

5. Experimental study of micro end-milling performance

5.1 Motivation and objectives

In chapter 2 was stated that micro milling has been developed from conventional milling by continuous scaling down. Therefore, it is assumed that main mechanisms are the same in both cases. However, it is also well known that different scaling factors play an important role on tool performance. For example, an increasing ratio between the cutting edge radius and the uncut chip thickness changes the proportion between ploughing and shearing mechanisms and may lead to a non-linear trend of maximum cutting forces. Another example is a rapid reduction of tool stiffness which can result in a poorer surface finish or in premature tool breakage.

The above mentioned effects are only a selection of all possible issues arising from scaling down. There are many other factors which may play more or less significant role in micro milling, and which are not yet fully understood.

Therefore, the main aim of this chapter is:

To familiarize with micro milling process and identify significance of scaling effects on micro milling performance.

This is, however, very broad aim and it would not be feasible to answer all the important questions in this research. In order to gain strong confidence in the measured data, large number of repetitions on different machine tools and in various (but well monitored and controlled) environments would be necessary. Furthermore, different materials and different tools (e.g. tools with various cutting edge radii) should be used for study of specific effects. This is, however, not possible, and therefore, the tests presented here give only a brief insight into micro milling. The main attention is paid to issues related with prediction of tool life. This includes study of tool wear and cutting forces.

Furthermore, micro milling process lies in a shadow zone between nano and macro world. It was found that measurements in this zone are the most difficult ones. In many cases

measuring methods developed for applications in macro scale has not sufficient resolution, but on the other hand, the methods developed for nano applications are too slow and suffers from low range. Therefore, the secondary objective of this chapter is:

To verify reliability of used measurement methods, and if possible, suggest more suitable ones.

Results arising from this secondary objective will be used later in this research for design of verification tests.

5.2 Experimental method

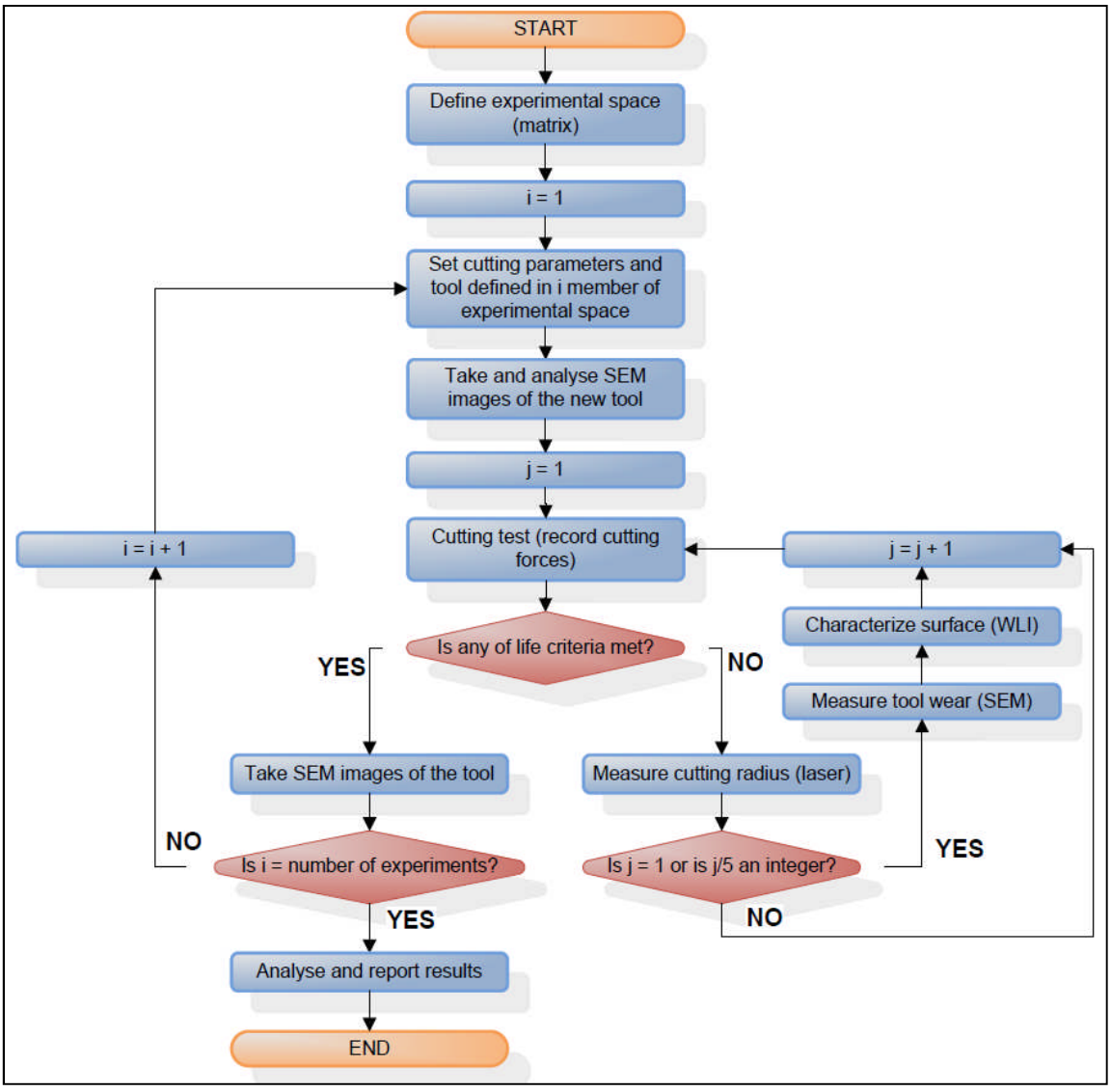

Fig. 5.1: Experimental plan (flowchart)

In fig. 5.1 is illustrated the experimental procedure used in this chapter. In the first step are planned all the experiments performed in this chapter. This includes: decision on number of experiments (see section 5.2.1) and definition of cutting parameters (see section 5.2.2).

Workpiece used in this research is the same one as described in section 4.3. This means that in the case of Ø1 mm tool the cutting length per test is 80 mm and in the case of Ø0.2 mm tool the length is 15 mm. All tests in this research are run as dry milling. This is because an application of a coolant/lubricant increases the number of input parameters and consequently results in higher process uncertainty.

Tests are performed as side milling. After each cut the tool is moved perpendicularly to feed direction with a step equal to the defined width of cut. Cutting forces are measured during every test (see section 5.2.3). After that the tool is cleaned by alcohol and pressurized air and measured by laser. Furthermore, after every fifth cut the tool and workpiece are removed from the machine tool for detailed inspection. SEM images of the tool are taken and analyzed, and generated surface is measured by WLI. This approach is repeated until any of the defined life criteria is reached. After that, the broken tool is inspected by SEM. This procedure is performed for every experiment defined in the experimental space until all tests are done.

Finally life criteria must be set. Two types of criteria are used in this research. The first one is tool breakage. This criterion is expected to be more relevant for Ø0.2 mm tools, where the tool is more likely to break. The second criterion is related to tool wear. It can be either related to absolute wear measure (e.g. $VB_B \geq VB_{B\ max}$ or $\Delta D_c \geq \Delta D_{c\ max}$ etc.) or to relative measure (e.g. $\frac{\Delta D_c}{D_c} \cdot 100\% \geq$ *Specified %*). In this research the second type of criterion is set as:

$$\frac{\Delta D_c}{D_c} \cdot 100\% \geq 5\% \tag{5.1}$$

Where D_c is the cutting diameter and ΔD_c is a reduction of the cutting diameter.

5.2.1 Definition of experimental space

The experiments presented in this chapter are planned as comparison tests and they are not supposed to be used for mapping of output measures. Therefore, the experimental space is

reduced to one set of tests for each tool type. On the other hand, more than one tool type must be used. In this research are analysed four different types of tools. The first type is uncoated square end-mill with diameter of 1 mm. This tool represents a large tool which can be classified as a macro end-mill. The second tool type used in this research is uncoated square end-mill with diameter of 0.2 mm. This tool represents one of the smallest micro end-mills currently available in the market, and machining with this tool is expected to be strongly affected by all scaling effects. The third and fourth tool types are commercially coated end-mills with both 0.2 mm and 1 mm diameters. These two types are included in this research in order to investigate the effects of the coating in micro milling. The commercial coatings currently applied in micro milling were identified as identical with the ones developed for conventional machining. However, as all the scaling effects are not yet fully understood, it is possible that these coatings will not perform as expected and in result they will have negative or negligible effect.

Because of concerns about the repeatability of micro milling process, each cutting test is repeated three times. Three repetitions were chosen as a minimum number of experiments which can indicate an issue with repeatability.

Hence, the complete number of experiments performed in this chapter is twelve as they are summarized in tab. 5.1.

Tab. 5.1: Experimental space (summary of experiments ran in this chapter)

No.	Tool type	Cutting speed	Feed	Depth of cut	Width of cut
1	Ø0.2 mm (uncoated)	v_1	f_{z1}	a_{p1}	a_{e1}
2	Ø0.2 mm (uncoated)	v_1	f_{z1}	a_{p1}	a_{e1}
3	Ø0.2 mm (uncoated)	v_1	f_{z1}	a_{p1}	a_{e1}
4	Ø0.2 mm (coated)	v_1	f_{z1}	a_{p1}	a_{e1}
5	Ø0.2 mm (coated)	v_1	f_{z1}	a_{p1}	a_{e1}
6	Ø0.2 mm (coated)	v_1	f_{z1}	a_{p1}	a_{e1}
7	Ø1 mm (uncoated)	v_2	f_{z2}	a_{p2}	a_{e2}
8	Ø1 mm (uncoated)	v_2	f_{z2}	a_{p2}	a_{e2}
9	Ø1 mm (uncoated)	v_2	f_{z2}	a_{p2}	a_{e2}
10	Ø1 mm (coated)	v_2	f_{z2}	a_{p2}	a_{e2}
11	Ø1 mm (coated)	v_2	f_{z2}	a_{p2}	a_{e2}
12	Ø1 mm (coated)	v_2	f_{z2}	a_{p2}	a_{e2}

5.2.2 Definition of cutting parameters

The cutting parameters recommended by tool supplier [38] for steels with hardness of approximately 30 HRC are summarized in tab. 5.2. However, the cutting conditions are derived directly from macro milling and do not respect specifics of micro milling. The submicron feed per tooth (f_z) recommended by the supplier for Ø0.2 mm tools is almost four times smaller than the cutting edge radius which is usually between 1.5 μm and 2 μm. Also the recommended depth of cut (a_p) looks excessive in comparison with values typically used in research publications. Therefore, cutting conditions for micro milling recommended by tool manufacturer are assumed unrealistic and they are not used in this research.

Table 5.2: Cutting parameters recommended by UNION TOOL co. [38]

Tool diameter (mm)	v_c (m·min^{-1})	f_z (mm/tooth)	a_p (mm)	a_e (mm)
Ø0.2	20 - 40	0.00033 - 0.00066	0.3	0.02
Ø1.0	35 - 40	0.0015 - 0.0018	1.5	0.1

The main aim of these tests is a comparison of performance of tools with two different cutting diameters. Therefore, it is advantageous to relate the cutting parameters to the cutting diameter (D_c) instead of choosing specific values for each tool type. The only exception is cutting speed which is kept constant for all tests. The definition of the speed is done in three steps. First, the rotational speed for the tool with diameter of 0.2 mm is chosen. Then the cutting (circumferential) speed is calculated from relation 5.2. Finally, the rotational speed for the tool with diameter of 1 mm is calculated. This approach is applied because the speed used by the machine tool is expressed as rotational speed and not as cutting speed.

$$v_c[m \cdot min^{-1}] = \frac{2 \cdot \pi \cdot rpm[min^{-1}] \cdot \frac{D_c[mm]}{2}}{1000} \tag{5.2}$$

The rotational speed for the tool with cutting diameter of 0.2 mm was set to 25 000 rpm. This value was chosen because the machine tool shows extensive vibrations when speeds over 35 000 rpm are used. Hence, higher rotational speeds may cause undesirable process instabilities. To the rotational speed of 25 000 rpm and cutting diameter of 0.2 mm corresponds the cutting speed of 15.71 m·min^{-1}. As it was mentioned above, this cutting speed is kept constant also for the tool with diameter of 1 mm. Hence, by a reverse calculation was obtained rotational speed of 5 000 rpm for the large tool.

The feed rate, the depth of cut and the width of cut are defined by relations 5.3, 5.4 and 5.5 respectively. These relations are based on previous experience of technical and research staff (namely Mr. John Hedge and Dr. Tan Jin).

$$f_z[mm/tooth] = 0.02 \cdot D_c[mm] \tag{5.3}$$

$$a_p[mm] = 0.5 \cdot D_c[mm] \tag{5.4}$$

$$a_e[mm] = 0.1 \cdot D_c[mm] \tag{5.5}$$

Finally, the numerical values used in these experiments are summarized in tab. 5.3.

Table 5.3: Cutting parameters used in these tests

Tool diameter (mm)	RPM (min^{-1})	f_z (mm/tooth)	a_p (mm)	a_e (mm)
Ø0.2	25 000	0.004	0.1	0.02
Ø1.0	5 000	0.02	0.5	0.1

5.2.2 Analysis of cutting forces

The cutting force is perhaps the most important measure used for analysis of any cutting process. Therefore, it is the first measure which is monitored and analyzed during these tests. The cutting forces are measured by KISTLER dynamometer (see chapter 4). Three force components are measured in x, y and z directions. An example of a measured force signal is shown in fig. 5.2. The measured signal was compensated for a drift and disassembled as it is shown in fig. 5.3, where the red part of the signal corresponds to force acting on the first cutting edge and the blue part corresponds to the force acting on the second cutting edge. This procedure facilitates to study the forces acting on each of the cutting edges separately, and hence, achieve deeper understanding of the process.

The disassembled signal was further processed and maximum, minimum and root mean square (rms) values for each cutting edge engagement (each red or blue block in fig. 5.3) were calculated. These values were saved in a matrix in which every line has the following format: [number of engagement, $F_{x\,min}$, $F_{x\,max}$, $F_{x\,rms}$, $F_{y\,min}$, $F_{y\,max}$, $F_{y\,rms}$, $F_{z\,min}$, $F_{z\,max}$, $F_{z\,rms}$, $F_{tot\,min}$, $F_{tot\,max}$, $F_{tot\,rms}$]. Then average values and standard deviations for the whole milling distance, excluding first and last 2% of the signal, were calculated and used to plot force trends. The initial and termination periods of the measurements were excluded because they

are affected by transition effects (see fig. 5.1) which are not studied in this research. In the case of the experiments presented in this research these transition zones represent only approximately 2% of the whole signal, and therefore, they are not assumed to have a significant effect on tool life.

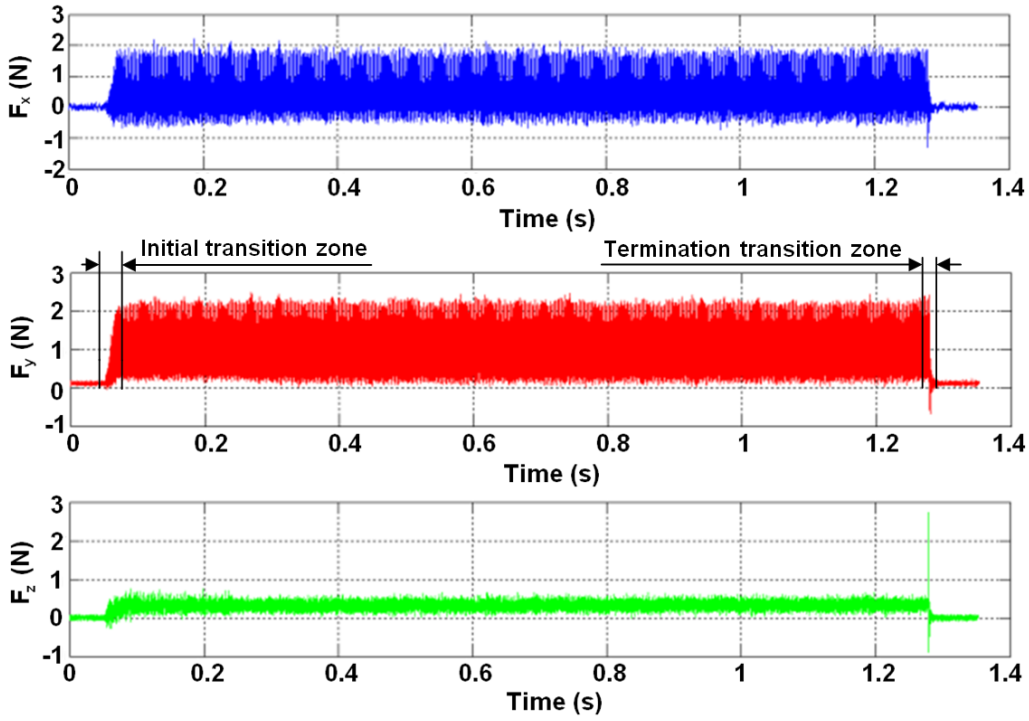

Fig. 5.2: An example of force signal measured during tests with Ø0.2 mm micro end-mill

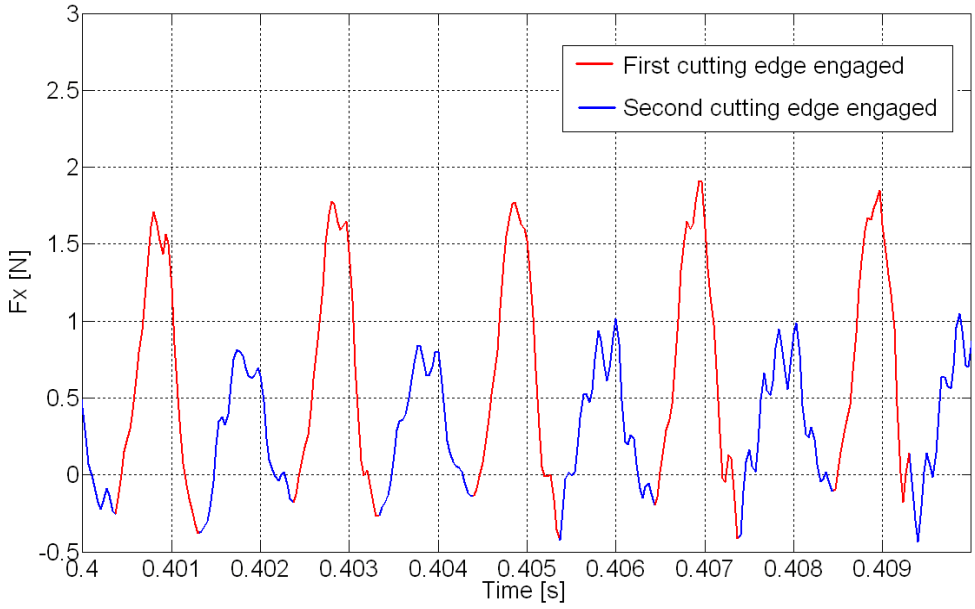

Fig. 5.3: Example of a disassembled force signal in feed direction

5.2.3 Analysis of tool wear

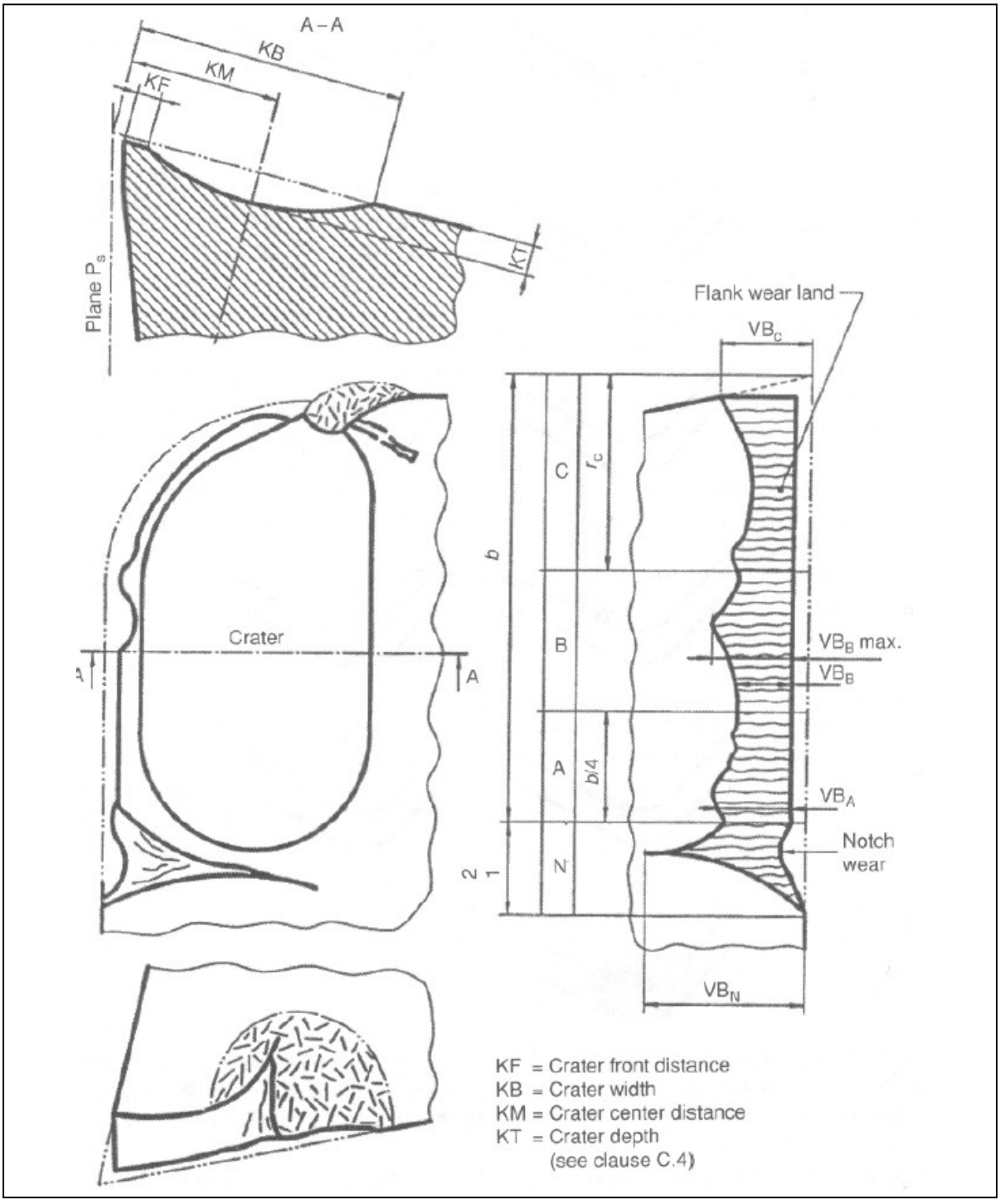

Fig. 5.4: Typical wear pattern of carbide tool [15]

Tool wear is another important factor which must be monitored and analysed. In fig. 5.4 is illustrated a typical wear pattern of carbide tools. Two main types of wear can be typically distinguished as: the flank wear and the crater wear. According to Stephenson and Agapiou

[15] the flank wear is usually characterized by four measures: VB_B, VB_Bmax, VB_N and VB_C. Crater wear is characterised by its maximum depth (KT), distance of the maximum depth from the original face (KM), the crater front distance (KE) and crater width (KF).

If these measures will be presented in the wear patterns, they all will be measured and analysed. All the values will be measured periodically after every five cuts. This frequency of measurements is chosen because of two main reasons. First, tool life is not well known and higher frequency of measurements reduces a risk of missing important information. Secondly, for each of these measurements the tool must be removed from the machine tool. This increases experimental time, costs and also uncertainty. This is undesirable, and therefore, the measurements should be reduced to a minimum. Hence, one measurement per five cuts was chosen as a reasonable compromise.

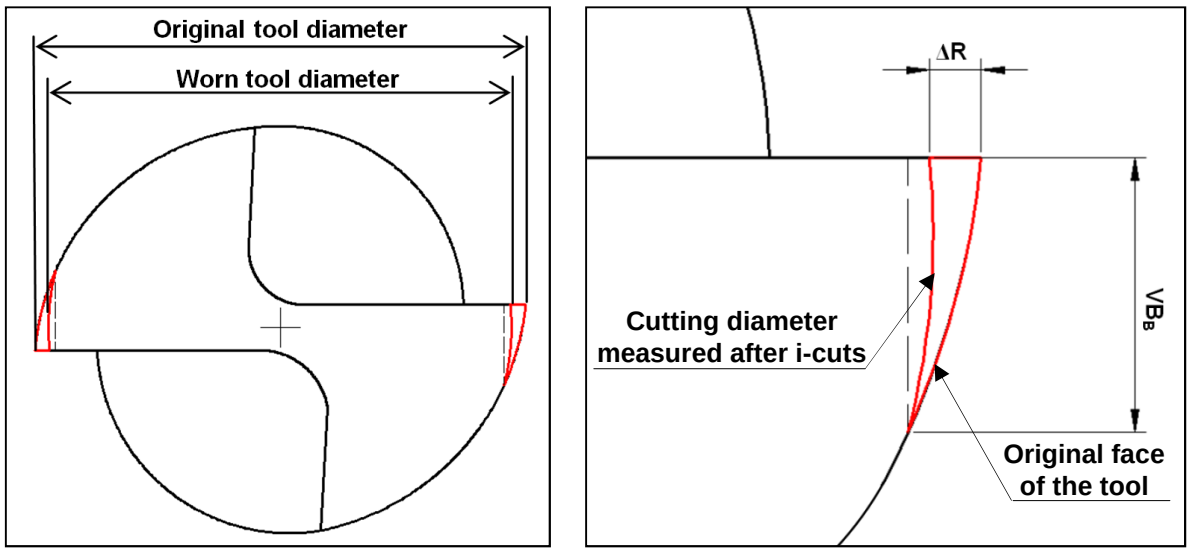

(a) Illustration of tool wear (b) Detail of a cutting edge

Fig. 5.5: Illustration of tool wear and tool cutting radius reduction

Because of very small measures characterizing tool wear (increments of less than 1 μm per five cuts are expected) and complex shape of the tool, SEM imaging was chosen as the most appropriate measuring method (see discussion in chapter 4). However, the SEM is a time consuming and expensive method. Therefore, it is often not applicable in an industrial environment. Furthermore, frequent removal of the tool from the machine tool increases risks and costs. Therefore, it is worth to investigate other possibilities of characterizing tool wear. In this research it is proposed to use BLUM laser setting system (see chapter 4). It is assumed

that the system can be used for measurements of cutting diameter reduction ($\Delta D_c = 2 \cdot \Delta R$), and then ΔR can be analytically related to VB_B as it is illustrated in fig. 5.5. This method seems to be a promising alternative to SEM measurements. The main advantages of the laser measurements are: low time and cost demands, and no need for tool removal. On the other hand, disadvantages are: lower resolution and less information about tool wear. In order to investigate possibilities and reliability of this approach, all tools are measured by the laser after every single cut in three locations ($l_1 = \frac{1}{6} \cdot a_p$, $l_2 = \frac{1}{2} \cdot a_p$, $l_3 = \frac{5}{6} \cdot a_p$) as they are illustrated in fig. 5.6.

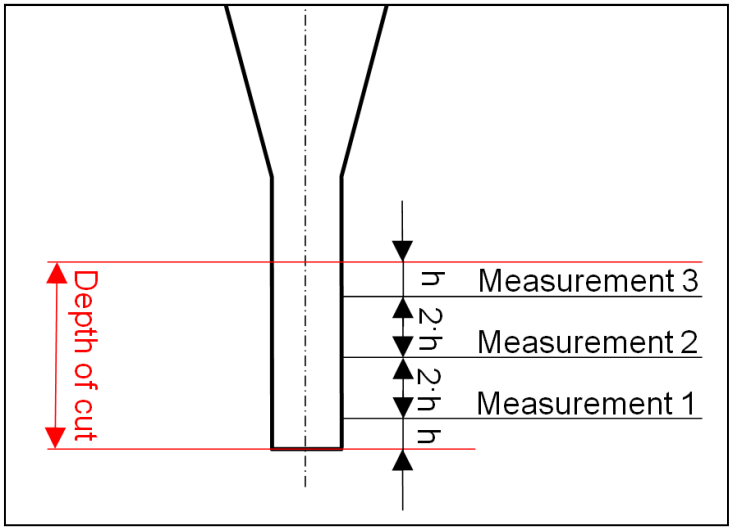

Fig. 5.6: Illustration of laser measurement locations

Except of the quantitative wear measurements and study of wear patterns, wear mechanisms are also studied in this research. In conventional cutting are typical three main mechanisms of tool wear: mechanical (can be further classified as abrasion, chipping and surface fatigue), adhesive and thermal [122]. Because of low cutting temperatures presented in micro milling, it is not expected to observe any type of thermal wear. On the other hand, mechanical wear (especially abrasion and micro chipping) are expected to be the dominant wear mechanisms. This, however, must be confirmed experimentally, and therefore, all SEM images taken during these tests are analysed for characteristic of signs different wear mechanisms.

5.2.4 Analysis of generated surface quality

Generated surface roughness is the last characteristic analysed during these experiments. All measurements are performed on Tailor Hobson Talysurf CCI 6000 white light interferometer (for further details see section 4.4.4). This measurement method allows analysing areal surface parameters instead of traditionally used profile parameters.

During this research are analysed only side walls. This is because only a very small surface is generated on the bottom and it is not possible to measure it. The reason for inability of measuring the bottom surface is a short focal length of the used method and difficulties of surface roughness measurements under sharp angles. However, also the information about the side wall surface roughness is valuable. These surfaces are generated in such products as micro channels.

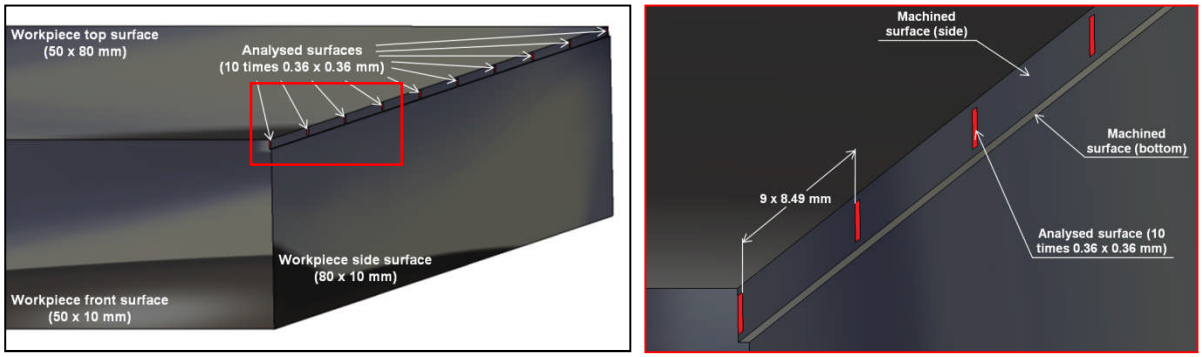

Fig. 5.7: Illustration of generated surface and WLI measurement points (Ø1 mm tools)

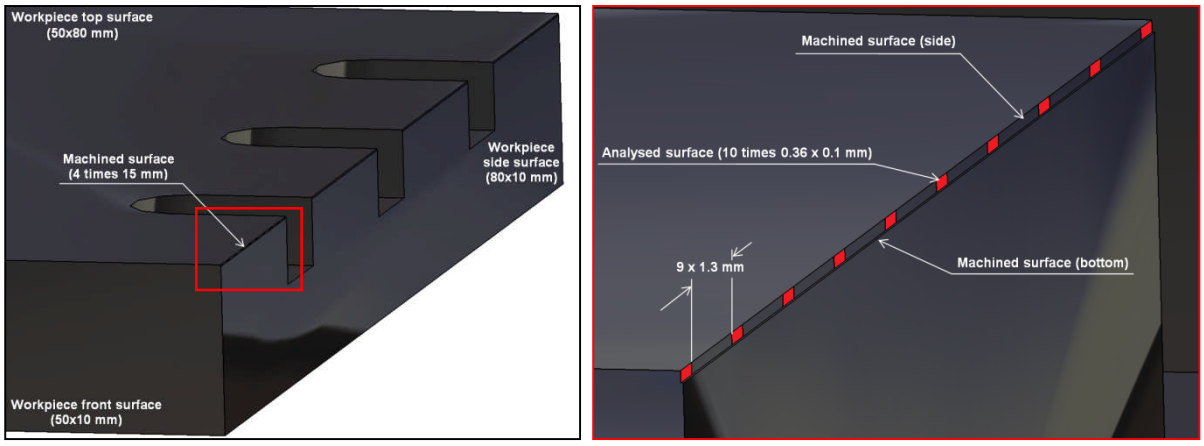

Fig. 5.8: Illustration of generated surface and WLI measurement points (Ø0.2 mm tools)

However, the WLI is limited in size of the measured area (0.36 mm x 0.36 mm). Therefore, the measurements are taken only in 10 separated locations as it is illustrated in fig. 5.7 and fig. 5.8. The parameter measured during this research is the areal average surface deviation (S_a). Although the other surface parameters might be of interest in some applications, this one is the most common measure of surface quality used in research and industry.

5.3 Results and discussion

5.3.1 Wear patterns and wear mechanisms

(a) Flank wear

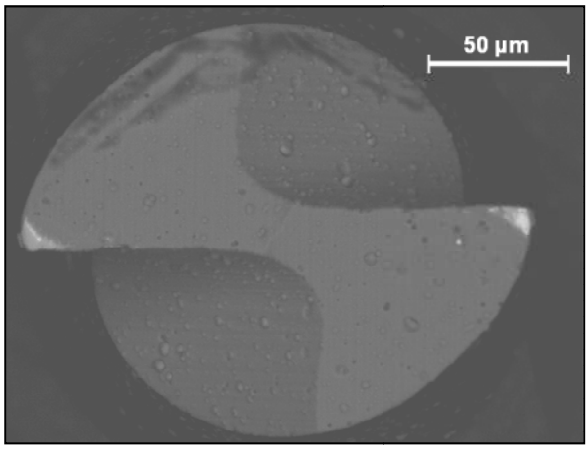

(b) Nose wear

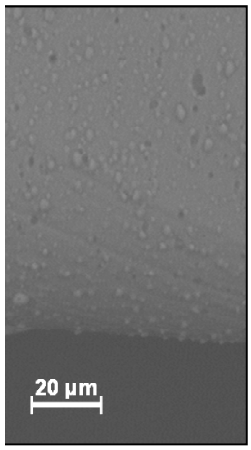

(c) Rake wear

Fig. 5.9: Example of tool wear (Ø0.2 mm coated tool, BSE images)

Independently on the test case, all wear patterns show similar characteristics. The flank wear is easily observable in all test cases. In all cases the flank wear shows its maximum near to the tool tip and minimum on the top of the cut (see fig. 5.9a). Notch wear was not observed in any case. Nose wear was also observed in all tested cases (fig. 5.9c). On the other hand, any sign of wear was not observed on the rake faces (see fig. 5.9b). Hence, craters are highly unlikely to form in micro milling. No difference in wear patterns were observed between Ø1 mm tools and Ø0.2 mm tools.

Three main wear mechanisms observed during these experiments are:

- micro chipping of the cutting edge,
- abrasive wear,
- material adhesion.

Micro chipping of the cutting edge

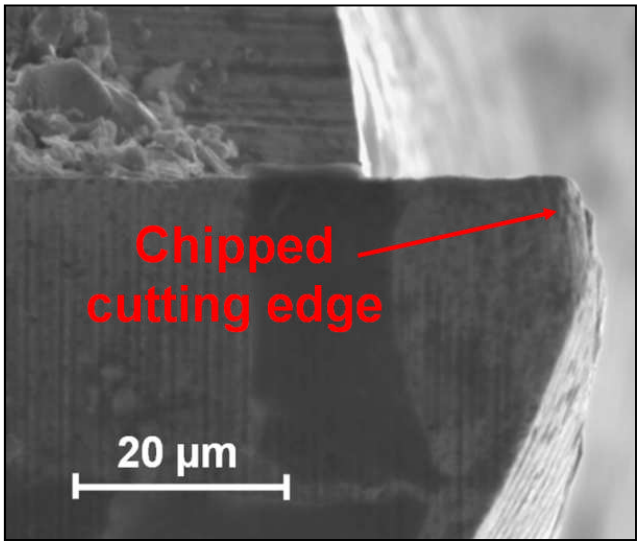

Fig. 5.10: Magnification of a chipped cutting edge (front view)

Milling is an intermittent process. This results in cyclic impacts which can initiate small cracks which can lead to chipping of the cutting edge. Especially in the initial phase of machining the risk of edge chipping is high. This is because of small contact area between the cutting edge and the workpiece leading to high stress. Characteristic sign of the presence of this mechanism is rapid reduction of the tool cutting diameter. Also the new cutting edge

surface is rougher than the one generated by abrasion. An example of chipped cutting edge is shown in fig. 5.10.

Chipping was identified in all of the tested cases. However, in the tests with Ø1 mm tools it was found to be significant only in relatively short initial phase, as in the later phase abrasion becomes more important. This was also confirmed by quantitative measurement presented later in this chapter. Furthermore, in all cases the chipping was identified mainly on the cutting edge tip. This is because this part of the cutting edge experience the highest impact energy.

Abrasive wear mechanism

Abrasion is the second wear mechanism observed during the tests. Because it is generated by ploughing of hard micro particles over the tool cutting edge, the generated surface is typically smoother than in the case of chipping (which is caused by sudden breakage of the edge). It can also be identified by its typical marks in the direction of the tool movement, see fig. 5.11. The abrasive wear gradually decreases the tool cutting diameter and can cause geometrical inaccuracies of the machined part. Furthermore, because a larger surface of the flank face is in contact with the workpiece, a poorer surface quality and higher forces are likely to be generated. Abrasive wear was observed with all types of tools used in these experiments. However, coated tools show significantly lower wear rates than uncoated ones.

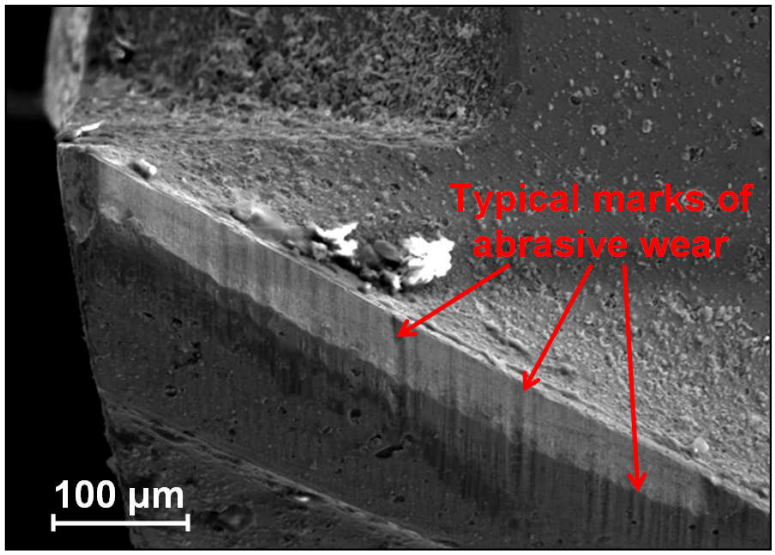

Fig. 5.11: An example of surface generated by abrasion

Material adhesion and Build-up-edge

Although material adhesion is not a typical wear mechanism, it may lead to build-up-edge (BUE) which can cause chipping and breakage of the cutting edge. Furthermore, BUE generally leads to poorer cutting edge quality and also may increase the cutting edge radius. Both of them affect cutting mechanism and the final product quality. Therefore, it is important to understand if this mechanism is present in micro milling. In several cases the SEM images taken during these tests confirmed this mechanism. Two examples of back-scattered electron images are shown in fig. 5.12. In the first figure is shown an uncoated tool with a little amount of adhered material. In this case it is not expected to have an significant effect on the cutting mechanism. However, in the second case, shown in fig 5.12b, is a well developed BUE. Such amount of adhered material already significantly changes the cutting edge and can have a serious effect on cutting process. It should also be mentioned that BUE was more often observed in the case of Ø0.2 mm tools than in the case of Ø1 mm tools. This, however, does not mean that the BUE is presented only in micro milling.

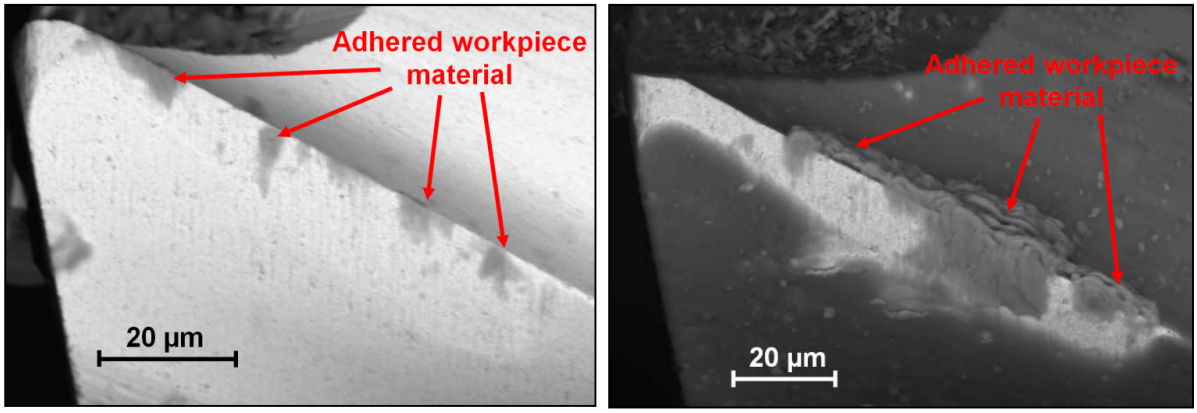

(a) An example of adhered material on an uncoated Ø0.2 mm micro end-mill

(b) An example of developed BUE on a coated Ø0.2 mm micro end-mill

Fig. 5.12: Examples of adverted workpiece material on a cutting edge

5.3.2 Comparison of SEM and laser measurements of tool wear

In this subsection is compared wear measured by SEM and BLUM laser system. In fig. 5.13 is shown a reduction of the cutting tool diameter as functions of an average flank wear VB_B. The measured values are compared with theoretical functions which have been achieved graphically for each tool dimension. Both theoretical functions, for Ø0.2 mm and

Ø1 mm tools, show linear trends and can be expressed by equations 5.6 (for Ø0.2 mm tool) and 5.7 (for Ø1 mm tool) respectively.

$$\Delta D_C^{\emptyset 0.2mm} = 0.380 \cdot VB_B^{\emptyset 0.2mm} + 0.0058 \tag{5.6}$$

$$\Delta D_C^{\emptyset 1mm} = 0.336 \cdot VB_B^{\emptyset 1mm} + 0.435 \tag{5.7}$$

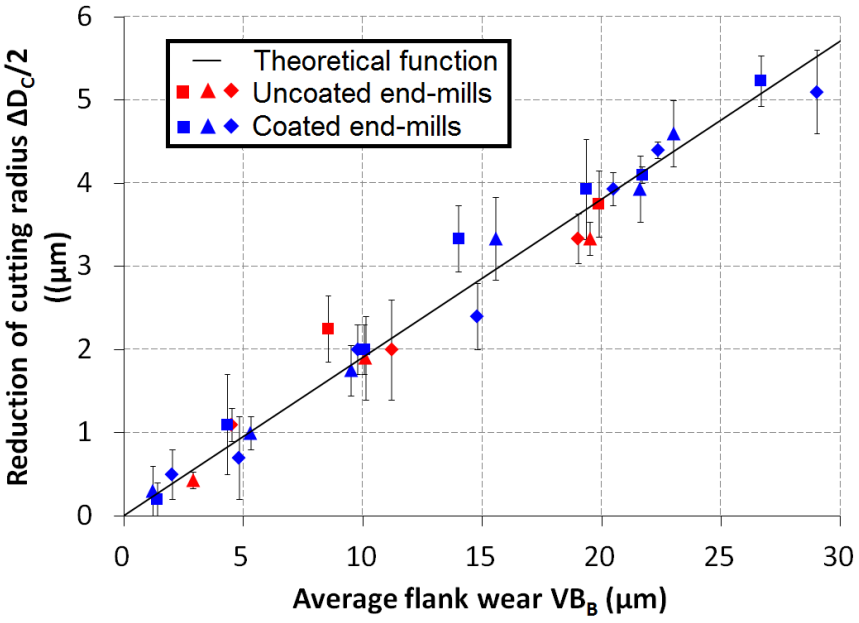

(a) Ø0.2 mm end-mills

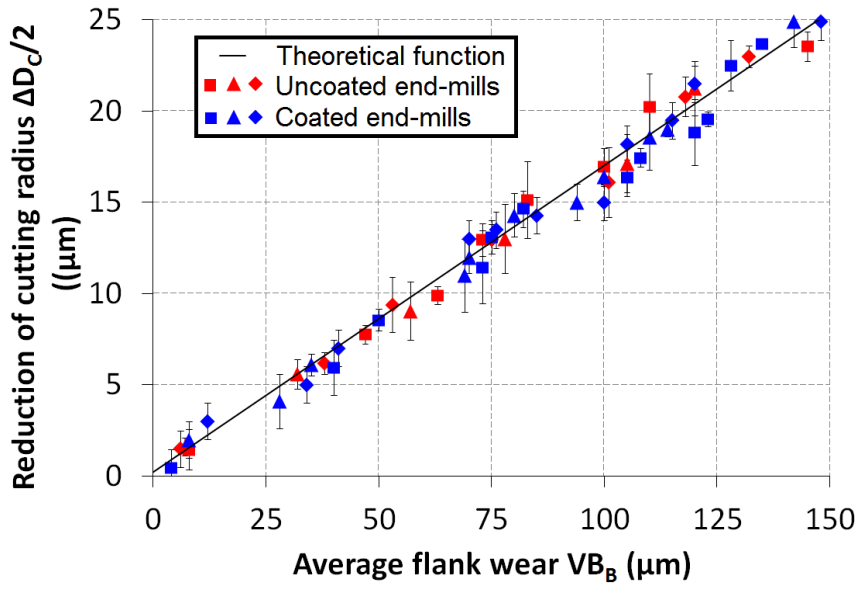

(b) Ø1 mm end-mills

Fig. 5.13: Relation between cutting tool diameter reduction and average flank wear

The measured values were always measured on three tools of the same type and in three locations as it is illustrated in fig. 5.6. The error bars in fig. 5.13 illustrate a difference between maximum and minimum measured values, where each data point represents an average value measured on a single tool. It is evident, that in all four studied cases, the measured values follow the theoretical function. An average absolute error for each of the four cases was calculated from equation 5.8, where *N* is a total number of data points.

$$E_{abs} = \frac{\sum_N abs(y_{measured} - y_{theoretical})}{N} \tag{5.8}$$

Another way of analysing the error is an average error calculated from equation 5.9. In this case the data point errors can gain both positive and negative values. This analysis gives an indication about distribution of the data points round the theoretical function. This is because positive and negative values subtract from each other and results in a small value. Hence, if the values are equally distributed below and above the theoretical function, the resulting error is equal to zero.

$$E = \frac{\sum_N (y_{measured} - y_{theoretical})}{N} \tag{5.9}$$

Interesting information gives also a relative error. This is calculated from equation 5.10 and gives information about significance of the error.

$$E_{\%} = \frac{\sum_N abs\left(\frac{y_{measured} - y_{theoretical}}{y_{theoretical}}\right)}{N} \cdot 100\% \tag{5.10}$$

All three types of errors are summarized in tab. 5.4. In all cases the relative error does not exceed 10%. This error is assumed to be acceptable for fast tool inspections. Furthermore, the error *E* is in all cases less than 100 nm (except Ø1 mm coated tool). This signalizes an even distribution of the measured values around the theoretical function.

Hence, the BLUM laser setting system was found to be a reliable and time effective alternative to SEM measurements of tool wear. It is also assumed to be more suitable for industrial applications, where it is not possible to remove the tool for periodic checks. This method also facilitates to inspect the tool more frequently than SEM. Therefore, in the rest of

this research the tool wear will be inspected only by BLUM laser system. Only in the cases were more detailed analysis is required SEM will be used to support the results.

Table 5.4: Summary of the calculated errors

Tool type	E_{abs} (µm)	E (µm)	$E_{\%}$ (%)
Ø0.2 mm (uncoated)	0.19	-0.013	9.4%
Ø0.2 mm (coated)	0.21	0.057	8.9%
Ø1 mm (uncoated)	0.56	0.026	5.8%
Ø1 mm (coated)	0.62	-0.12	6.9%

5.3.3 Quantitative analysis of tool wear

In fig. 5.14 is shown measured wear as a function of the milling distance. Each data point in the graphs represents an average value measured on three tools of the same type. The error bars illustrates standard deviations calculated for each data point. Furthermore, linear trends of the wear progression are also plotted in the graphs. In the first graph are compared tools with the cutting diameter of 0.2 mm (coated and uncoated). Both tool types show linear trend of wear progression. However, the coated tools wear slower than the uncoated. The reduction of tool wear was an expected benefit of the coating and can also be observed in the graph comparing Ø1 mm tools.

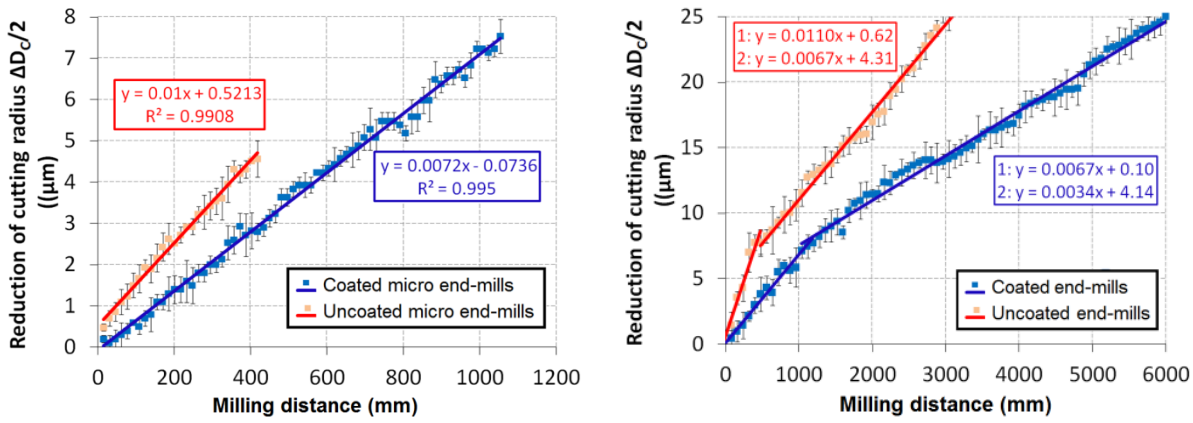

(a) Ø0.2 mm end-mills (b) Ø1 mm end-mills

Fig. 5.14: Comparison of wear progress of uncoated and coated tools for cutting conditions $v_c = 15.71$ m·min^{-1}, $f_z = 0.02 \cdot D_c$, $a_p = 0.5 \cdot D_c$, $a_e = 0.1 \cdot D_c$

In the case of Ø1 mm tools the wear trends show two main stages. Within each of the stages wear progresses linearly. However, in the first stage it is faster than in the second one. This difference is most likely because of different mechanisms dominating the first and the

second stage respectively. When the tool is new, the cutting edge is very sharp. Hence, the contact area between the cutting edge and the workpiece is very small. This can lead to extensive stresses and consequently in cutting edge chipping. When the wear progresses the contact area increases and chipping is less probable to appear. On the other hand abrasion is assumed to become dominant. These results in reduction of wear progression.

In the case of Ø1 mm tools an application of the coating has resulted in reduction of wear by ratio of 1.6 in the first phase and 2.4 in the second phase. Whereas in the case of Ø0.2 mm tools the ratio was found to be only 1.4. This indicates a lower effect of the coating on reduction of wear in the case of micro end-mills. It is also evident that the coating effect is significantly higher in the second phase (observed only in the case of Ø1 mm tools) than in the first one. This is assumed to be because of lower effect of the coating on prevention of chipping than abrasion. However, this was not further analysed in this research, and therefore, it cannot be confirmed.

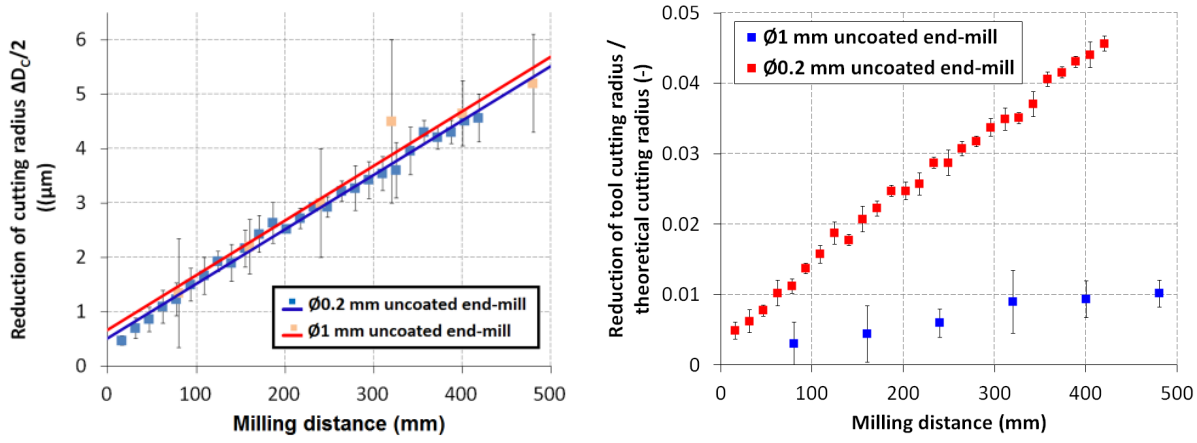

(a) Wear progress

(b) Ratio of tool wear/ tool diameter

Fig. 5.15: Comparison of wear progress of Ø0.2 mm and Ø1 mm uncoated tools for cutting conditions $v_c = 15.71$ m·min^{-1}, $f_z = 0.02 \cdot D_c$, $a_p = 0.5 \cdot D_c$, $a_e = 0.1 \cdot D_c$

In fig. 5.15 is compared cutting radius reduction of uncoated end-mills with diameters of Ø1 mm and Ø0.2 mm. The first graph shows absolute values (as measured). In this case is not observed any significant difference between the values. This observation is not surprising because a length of cut (distance over which the cutting edge is in a contact with the

workpiece) is the same for both Ø1 mm and Ø0.2 mm. This can be proven from the following equation:

$$Length\ of\ cut = \frac{milling\ distance}{f_z} \cdot acos\left(\frac{R_c - a_e}{R_c}\right) \cdot R_c \tag{5.11}$$

By substitution of a_e and f_z by relations 5.3 and 5.5 will this equation get the following form:

$$Length\ of\ cut = \frac{milling\ distance}{0.04} \cdot acos(1 - 0.2) \tag{5.12}$$

From the equation 5.10 is evident that the length of cut is in this particular case not dependent on the cutting radius (or cutting diameter) and only variable in this equation is milling distance. Hence, it is clear that if the milling distance is the same for both studied cases, also the length of cut will be the same.

However, different situation can be observed when the cutting diameter reduction is related to the tool cutting radius. In fig. 5.10b are plotted ratios of cutting radius reduction and nominal cutting radius. It is evident that the ratio is significantly higher in the case of Ø0.2 mm tools. Hence, the effect of wear on tool performance is clearly higher in the case of micro milling than in the case of macro milling.

5.3.4 Cutting forces

The next quantity analysed during these tests is cutting force. The measured maximum forces as functions of milling distance are plotted in fig. 5.16 (uncoated Ø0.2 mm tools) and fig. 5.17 (uncoated Ø1 mm tools). In all cases the forces acting on one cutting edge are higher than the forces acting on the second one. It is assumed to be because of tool run-out which leads to different uncut chip thickness for each of the cutting edges. Although this effect was observed in both cases (Ø0.2 mm and Ø1 mm tools), its relative effect is significantly higher when the smaller tools are used.

Another thing observed in the force signal is an occasional sudden increment of the force acting on one cutting edge. This increment is usually compensated by reduction of the force acting on the second cutting edge. This behaviour is well identifiable in the case of second

Ø0.2 mm tool. This behaviour agrees with to observations of BUE. Although this effect of BUE is also observed in the case of 1 mm tools, its effect is significantly less important.

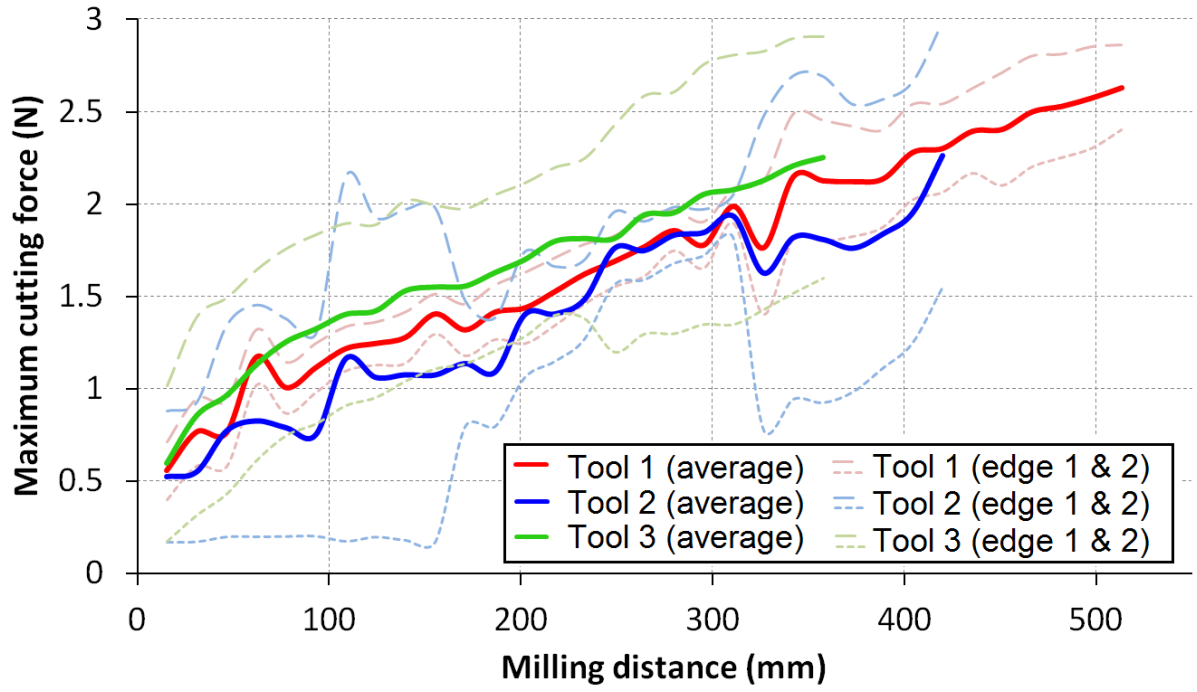

Fig. 5.16: Cutting forces generated by Ø0.2 mm tools

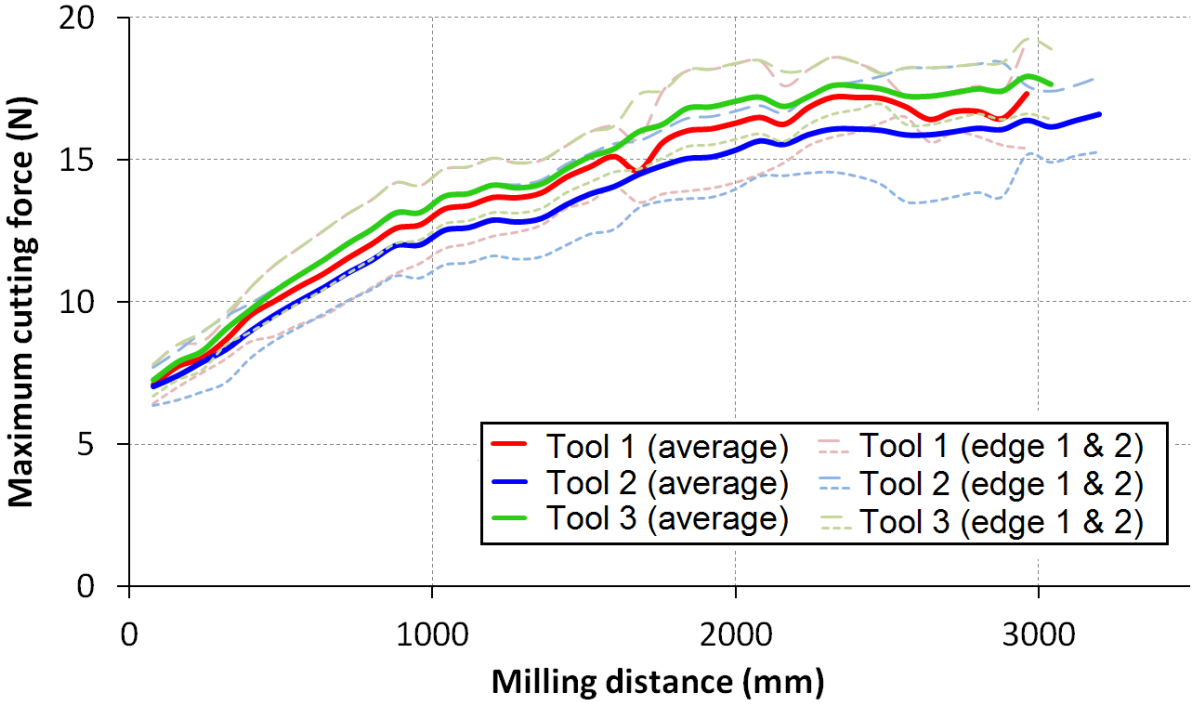

Fig. 5.17: Cutting forces generated by Ø0.2 mm tools

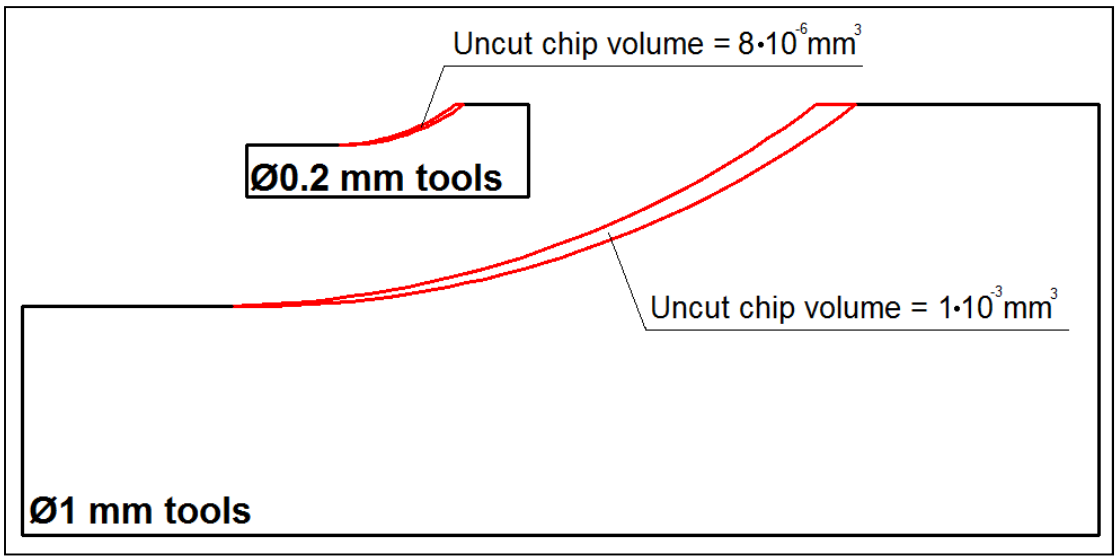

Fig. 5.18: Comparison of uncut chip cross-sections

The maximum cutting force is approximately 5 times higher when Ø1 mm tools are used than in the case of Ø0.2 mm tools. This ratio is, however, much lower than the ratio between uncut chip volumes, which was estimated to be approximately 125, see fig. 5.18. This disproportion between the acting force and the removed volume indicates crucial differences in cutting mechanisms. It is presumably caused by an effect of cutting edge radius which is usually negligibly low in the case of conventional milling.

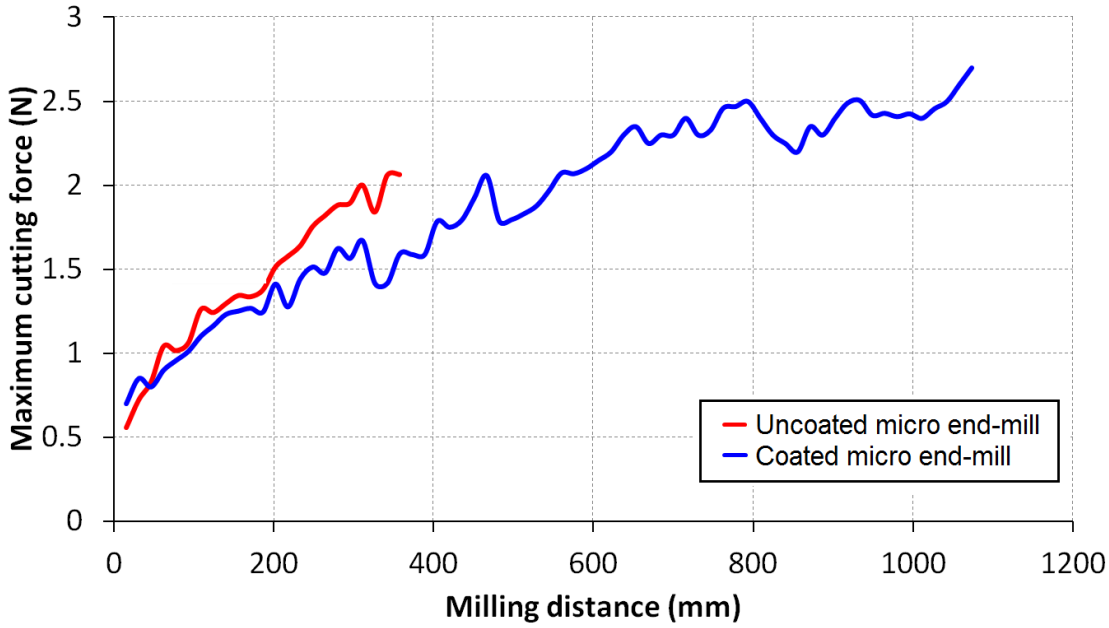

Fig. 5.19: Comparison of maximum forces acting on coated and uncoated Ø0.2 mm tools

In fig. 5.19 are compared average maximum forces measured during machining by coated and uncoated Ø0.2 mm micro end-mills. The forces acting on the new uncoated tools were found to be lower than the forces acting on the coated tools. The difference between the initial cutting forces is 0.1 N. However, because the uncoated tools wear faster, also the forces increase faster. Therefore, the force acting on a worn tool is lower when the coated tool is used.

5.3.5 Generated surface

Next quantity which was measured during these experiments was generated surface roughness. The measured S_a values are plotted as functions of milling distance in fig. 5.20. In all tested cases the coated tools had generated rougher surfaces than the uncoated tools. This was expected because the coated tools have always larger cutting edge radius than uncoated ones. Furthermore, same as in the case of tool wear the surfaces generated by Ø1 mm tools show two easily distinguishable phases. The milling distance of the first phase is approximately the same as in the case of tool wear (~700 mm in the case of the uncoated tools and ~1100 mm in the case of the coated tools). Hence, there is a clear correlation between tool wear and surface roughness. In the first phase the surface roughness grows significantly faster than in the second phase. This is observable as with the uncoated as with the coated tools. This is also same as in the case of tool wear. However, in contrast with tool wear the uncoated tools show lower increase of surface roughness than the coated tools.

As it was explained above, the lower surface roughness in the case of uncoated tools is assumed to be because of the smaller cutting edge radius. Therefore, the cutting edge radii were measured during these experiments. The new uncoated tools were found to have cutting edge radii of approximately 0.5 µm while the new coated tools had the radii of approximately 1.5 µm. This corresponds with the thickness of the coating measured in chapter 4; the thickness of the coating was found to be approximately 1 µm. These cutting edge radii were measured after each five cuts and no growing or reducing trends were found. Hence, the cutting edge radius of the uncoated tool remains smaller than the cutting edge radius of the coated tool during whole tool life. However, it must be mentioned that these measurements are highly inaccurate because of many reasons such as: variation of the radius over the cutting edge, not perfectly circular shape of the cutting edge, very small dimension of the radius etc.

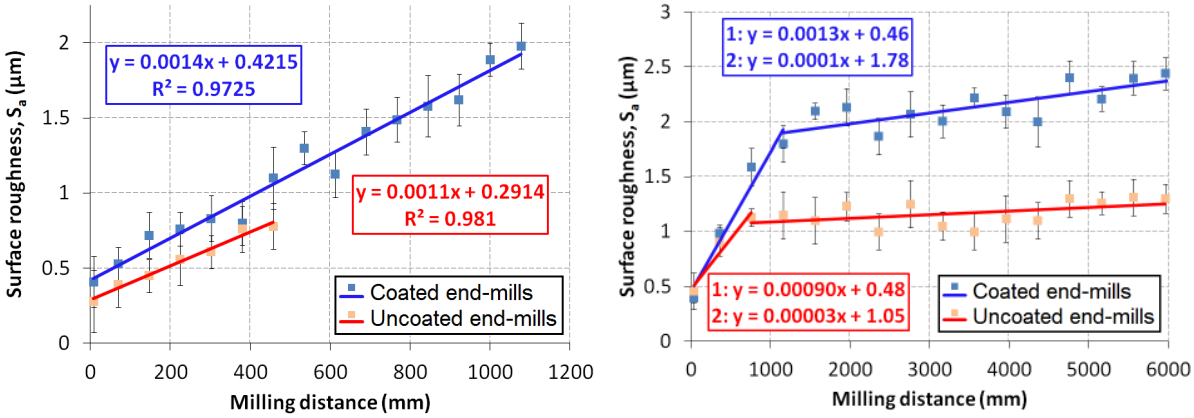

(a) Ø0.2 mm end-mills (b) Ø1 mm end-mills

Fig. 5.20: Comparison of surface roughness of uncoated and coated tools for cutting conditions $v_c = 15.71$ m·min^{-1}, $f_z = 0.02 \cdot D_c$, $a_p = 0.5 \cdot D_c$, $a_e = 0.1 \cdot D_c$

The surface generated by Ø0.2 mm tools has generally lower roughness than surface generated by Ø1 mm tools. However, in the case of the coated tools the difference is negligible. On the other hand in the case of uncoated tools the surface generated by Ø1 mm tools is approximately 1.6 times rougher than the one generated by Ø0.2 mm tools (when new tools are used). This advantage of using micro end-mills is, however, paid by faster reduction of surface quality with increasing milling distance in the case of Ø0.2 mm tools. In the case of uncoated tools the surface roughness increases approximately 1.2 times faster when Ø0.2 mm tools are used. This may be caused by higher effects of tool wear on tool performance in the case of micro milling.

In fig. 5.21 are compared surface topographies generated by an uncoated tool with the cutting diameter of 1 mm. On the left side figure is shown a typical surface generated during the first phase (see fig. 5.21a) as on the right side figure is shown a surface generated during the second phase (see fig. 5.21b). Evidently the surface generated during the first phase has different character from the surface generated during the second phase. Except higher peak-to-valley distance, the second case also shows significantly larger plastic deformations. It is assumed that this is caused by a larger contact area between the flank face and the workpiece. This leads to increase of importance of ploughing mechanism which typically results in higher plastic deformations.

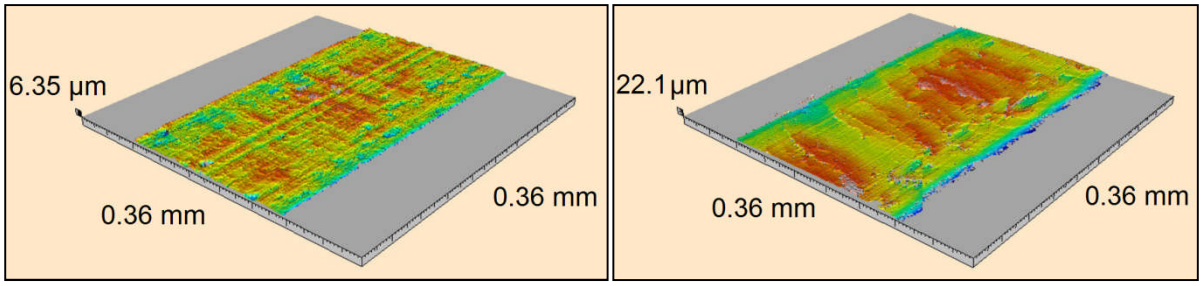

(a) Surface generated by a new tool (b) Surface generated by a worn tool

Fig. 5.21: Illustration of surface generated by new and worn coated Ø1 mm tool

5.3.6 Tool breakage

One of the main issues of micro milling identified during these experiments is tool breakage. This was observed only when tools with the cutting diameter of 0.2 mm were used. Hence, it is a clear difference between macro and micro milling. The main reason for the tool breakage in the case of micro milling is a significant increase of bending stress when the tool diameter is reduced.

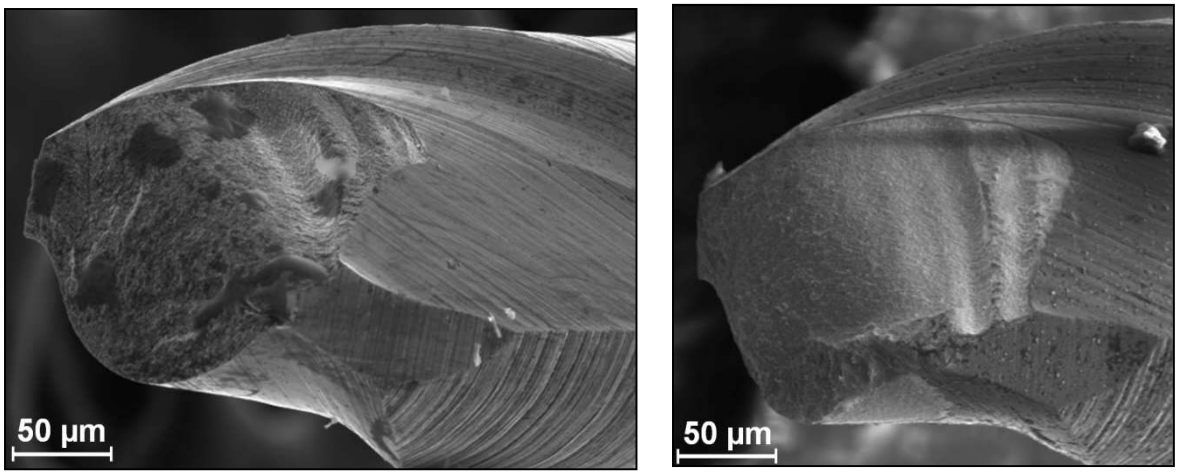

(a) Uncoated tool (b) Coated tool

Fig. 5.22: SEM micrographs of broken Ø0.2 mm micro end-mills

Two examples of broken tools are shown in fig. 5.22. Both examples show no plastic deformations. This indicates brittle fracture which is difficult to predict. From the previous sections is clear that no of the measured quantities shows any signal of imminent tool breakage. Furthermore, the breakage seems to appear randomly. In tab. 5.5 are summarised milling distances when tool breakage appears. In the third column of the table are listed critical forces (maximum force in the moment of tool breakage). In both studied cases

(uncoated, coated tools) the values show broad variations. Hence, clearly the milling distance cannot be used as a criterion of tool life.

Table 5.5: Comparison of milling distances and maximum cutting forces in break of uncoated and coated Ø0.2 mm micro end-mills.

	Milling distance to tool breakage (mm)	Critical force (N)
Uncoated tool no. 1	360	2.62
Uncoated tool no. 2	430	2.74
Uncoated tool no. 3	520	2.69
Coated tool (AlTiN) no. 1	950	3.58
Coated tool (AlTiN) no. 2	1250	3.03
Coated tool (AlTiN) no. 3	1520	3.01

The tool coating was found to have significantly beneficial effect on tool life. The coated tools break approximately 2.5 times later than the uncoated ones and withstand approximately 1.2 times higher forces. This observation signalise that the coating does not only prevent tool wear, but also has a positive effect on crack initialisation. It should, however, be mentioned that this effect of the coating is not yet fully exploited and should be extensively researched in the future.

5.4 Summary

In this chapter are presented results of tests comparing performance of Ø0.2 mm micro end-mills and Ø1 mm end-mills. In both cases were used coated and uncoated tools. The tests have confirmed that in all cases the dominant wear mechanism is abrasion. However, also cutting edge chipping and adhesion was observed during the tests. No significant differences in wear patterns were observed, and therefore, it may be concluded that the knowledge gained from conventional milling is also valid in micro milling.

The quantitative wear measurements have confirmed that coating has significantly beneficial effect on tool wear in both studied cases. In the case of 0.2 mm tools, the coating was found to have also a positive effect on tool breakage. The coated micro end-mills withstand higher cutting force than uncoated, and therefore, break later. It is suggested that the coating covers surface defects generated during tool manufacturing. However, the effects of coating on preventing tool breakage are not yet fully understood, and further research should be performed in the future.

It was also found that monitoring technique based on SEM imaging is extremely inefficient and requires frequent tool removals. Therefore, a new wear monitoring method based on laser tool cutting diameter reduction measurements was investigated in this research. It was proven that this method is fast and reliable. Therefore, this method will be used in all wear measurements in the rest of this thesis.

Micro milling cutting forces were found significantly higher than expected. It is assumed that this is caused by increased effect of cutting edge radius. Furthermore, the coating was found to have a positive effect on the cutting force. Although the initial cutting force is higher in the case of coated micro end-mills (presumably because of larger cutting edge radius), it grows slower.

Surface roughness generated by new Ø0.2 mm tools is generally the same as the one generated Ø1 mm tools. However, when the smaller tools are used the quality of the surface reduces faster than if the larger tools are used.

Premature tool breakage was identified as a biggest challenge of micro milling. Tool breakage was not observed in any case of Ø1 mm tools. Hence, it is evidently a new issue which is typical only when very small micro end-mills are used. Furthermore, tool breakage was found to be very difficult to predict (it seems to appear randomly with no relation to maximum force or milling distance). It is assumed to be affected by the tool dimensional tolerances and other process uncertainties. This topic will be further investigated in the rest of this research.

6. Modelling of cutting forces in micro milling

6.1 Motivation and objectives

Lack of a reliable tool performance prediction method is one of the major drawbacks of micro milling. Therefore, the main objective of this research was set to develop a method able to predict tool life. Such method is assumed to help industrialists with planning of their manufacturing strategies and with an estimation of product costs and delivery times. Besides product quality, this information is the most important for an increase of micro milling competitiveness.

The method developed in this research is based on a theoretical modelling. The main advantage of such a method is in an elimination of frequent interactions with production process. Furthermore, experimental methods often suffer by large uncertainties. This generally leads to necessity of a large number of repetitions and consequently to an increase of the production costs and time. However, the theoretical modelling also faces its challenges. The main difficulty is in obtaining of its input data. Although, these inputs vary for different methods, cutting force can be assumed as a common one for all of the methods.

Therefore, in this chapter is introduced a numerical cutting force prediction method. This method is based on an empirical relation between the cutting force and the uncut chip area as it is typical for all analytical and mechanistic models (see literature review in chapter 2). The fundamental relations between the cutting force and the uncut chip area are adopted from literature. However, the method used in this research estimates the uncut chip area by a time dependent numerical approach instead of usually used analytical formulations. The numerical approach is expected to give higher flexibility and versatility of the model than the fully analytical methods.

Hence, the main objective of this chapter is:

To develop a versatile cutting force prediction method suitable for tool stress analysis.

6.2 Fundamental relations

The method introduced in this chapter is fundamentally based on an analytical cutting force model developed originally by J. Tlusty and P. MacNeil [123]. Their model for prediction of cutting forces in conventional milling was presented in 1975. Since that time the model has been improved by various researchers. Bao and Tansel have reconsidered the original formulation of tool path and proposed more accurate analytical relations [22]. They also have developed an analytical formulation of tool run-out [21]. However, their model has remained 2-dimensional as the original one. The implementation of the third force component was proposed by Zaman et. al. in 2006 [61]. They have presumed that the tangential force component is normal to the cutting edge, and therefore, it can be disassembled to an axial component and a component perpendicular to both, axial and radial one. Furthermore, Zaman et. al. as well as Bao et. al. have validate their models for micro milling. Both publications clam a good agreement of the predicted data with the experimental ones. This confirms a suitability of this cutting force formulation for applications in micro milling.

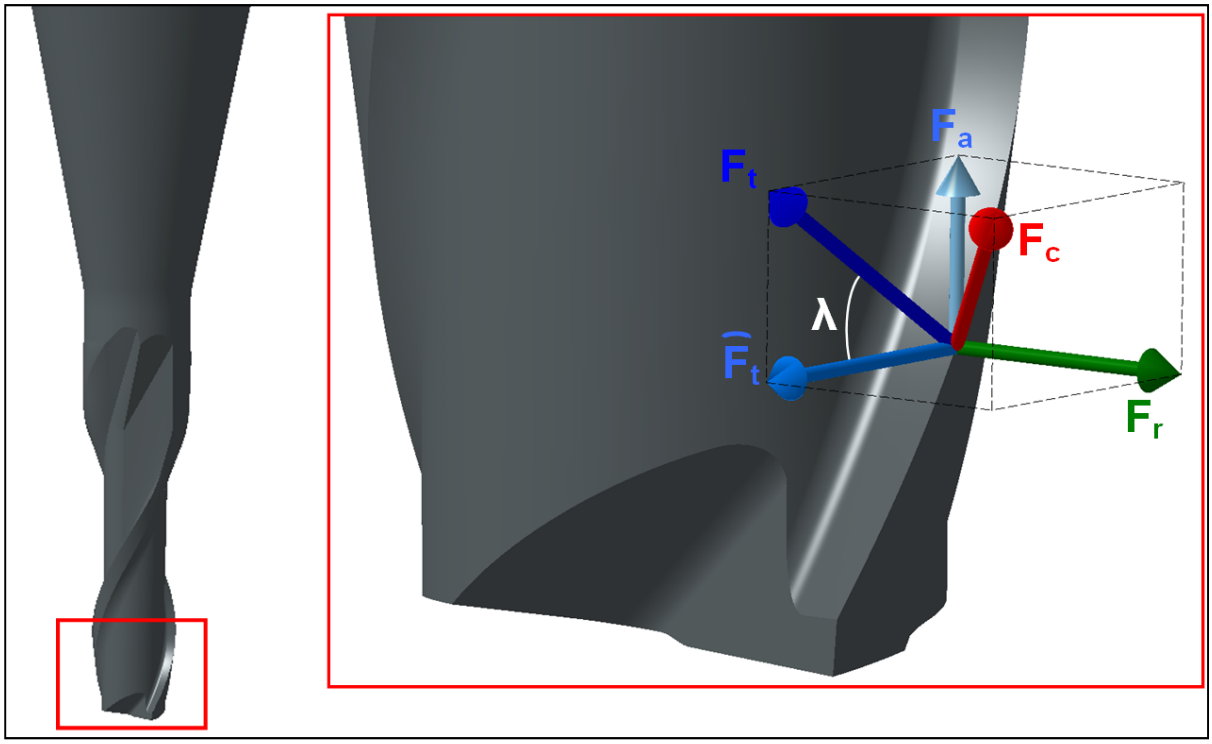

Fig. 6.1: Illustration of elemental force components in general cutting edge position

The cutting force formulation used in this research is closest to the one presented by Zaman et. al. Hence, the formulation includes three cutting force components (F_r, $\widehat{F}_t$, F_a) as

they are illustrated in fig. 6.1. However, as the method proposed in this research uses a numerical estimation instead of an analytical expression of the uncut chip area as it was used in the original model, it is more suitable to express the cutting force in the form of elemental forces (a force per a small, well defined, portion of the cutting edge). Hence, the fundamental relations used for modelling of the cutting forces used in this research are the following ones:

Relation 1 (assumption): The instantaneous elemental tangential cutting force component (dF_t) is proportional to instantaneous elemental uncut chip area (dA), and can be expressed by the following relation:

$$dF_t(z,t) = K_m \cdot dA(z,t) \tag{6.1}$$

where K_m ($N \cdot mm^{-2}$) represents a specific cutting force, which can be explained as a cutting force needed to cut $1\ mm^2$ of a specific workpiece material with a specific tool. K_m is usually obtained from a few initial cutting tests.

Relation 2 (assumption): The instantaneous elemental radial cutting force component (dF_r) is proportional to the instantaneous elemental tangential cutting force component:

$$dF_r(z,t) = q \cdot dF_t(z,t) = q \cdot K_m \cdot dA(z,t) \tag{6.2}$$

where q in this equation represents proportionality constant and it is also obtained from the initial cutting tests.

Relation 3 (assumption): The axial cutting force component (dF_a) and the tangential cutting force component in the plane perpendicular to the tool axis ($d\widehat{F_t}$) can be expressed as:

$$dF_a(z,t) = \sin(\beta) \cdot dF_t(z,t) = \sin(\beta) \cdot K_m \cdot dA(z,t) \tag{6.3}$$

$$d\widehat{F_t}(z,t) = \cos(\beta) \cdot dF_t(z,t) = \cos(\beta) \cdot K_m \cdot dA(z,t) \tag{6.4}$$

where β is the helix angle.

Relation 4: The total elemental cutting force (dF_c) is a vectorial summation of all elemental components. This can be expressed by vectorial the following equation:

$$\overrightarrow{dF_c} = \overrightarrow{dF_t} + \overrightarrow{dF_r} = \overrightarrow{dF_t} + \overrightarrow{dF_a} + \overrightarrow{dF_r} \tag{6.5}$$

Relation 5: Any component of cutting force is calculated as an integral of corresponding elemental cutting force components over tool cutting edge. This can be expressed as:

$$F_t(t) = \int dF_t(z,t) = \int_{z_1}^{z_2} K_m \cdot w(z,t) \cdot dz(t) \tag{6.6}$$

$$F_r(t) = \int dF_r(z,t) = \int_{z_1}^{z_2} q \cdot K_m \cdot w(z,t) \cdot dz(t) \tag{6.7}$$

where $K_m(z)$ and $w_i(z)$ are functions of axial location.

6.3 Transformation of coordinate systems

The forces calculated by this model are related to the tool coordinate system (CS). This CS is a Cartesian system with its vertical axis coincident with the tool rotational axis and x-axis parallel to the tool rake face. On the other hand workpiece is usually defined in a different CS. These two CS are in a relative movement to each other. The main issue is that the measured cutting forces are usually defined in the workpiece CS. This is because the force sensor is attached to the workpiece and not to the spindle. Therefore, if the measured and the calculated forces shall be compared (e.g. during experimental verification or in intelligent monitoring systems) they must be transformed to a united CS.

In fig. 6.2 is shown a cross-sectional view of the tool in a general position with highlighted instantaneous cutting force components related to the tool CS ($F_t \cdot cos\beta$ and F_r). Additionally, corresponding force components related to the workpiece (F_x and F_y) are also shown in this figure. The axial force component $F_a = F_t \cdot sin\beta$ is in this particular case identical to F_z (in fig. 6.2 F_z and F_a are not shown because they are perpendicular to the drawing plane).

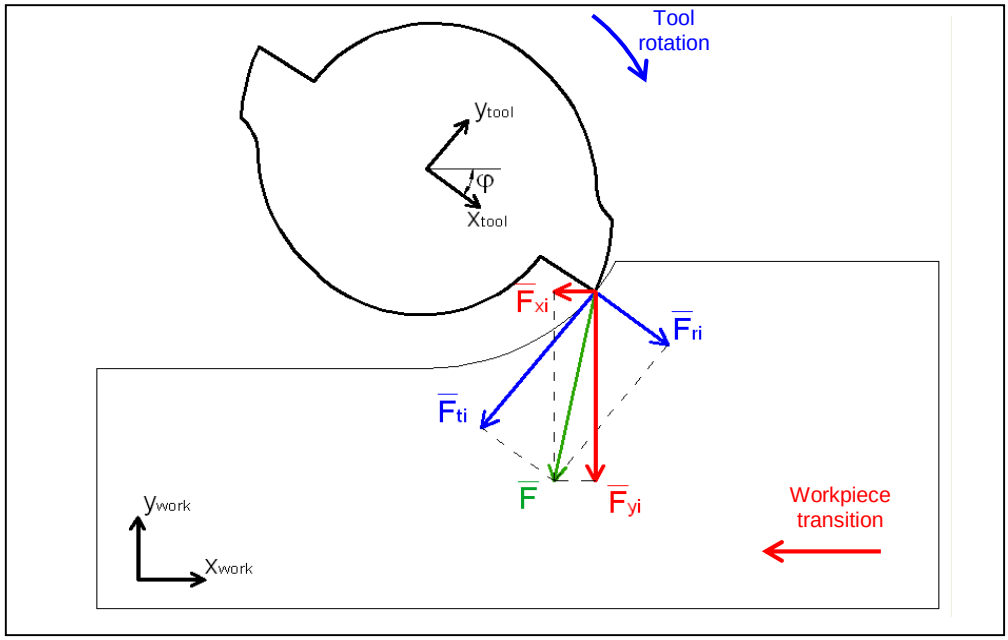

Fig 6.2: Schematic view of instantaneous cutting force components in general position

It is evident that the magnitude of instantaneous total force is independent on the choice of coordinate system. Hence, the vectors of cutting force components related to the tool and the workpiece CS, respectively, can be mathematically expressed:

$$\vec{F} = \overrightarrow{F_t} + \overrightarrow{F_r} = \overrightarrow{F_t} \cdot cos\beta + \overrightarrow{F_r} + \overrightarrow{F_a} = \overrightarrow{F_x} + \overrightarrow{F_y} + \overrightarrow{F_z} \tag{6.8}$$

For clarity the graphical representation of this relation is shown in fig. 6.3.

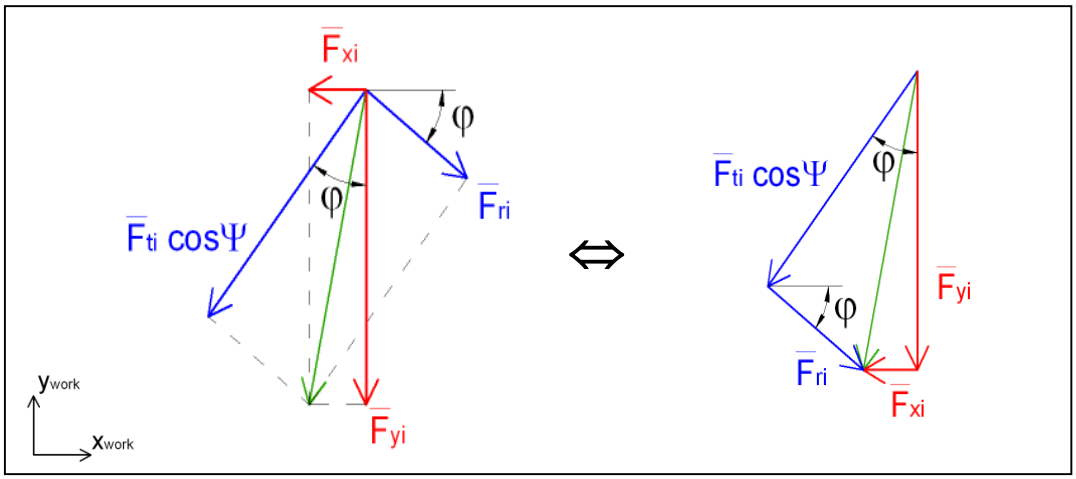

Fig 6.3: Graphical representation of the force components vector summation

From the figure it is easy to derive the following expressions:

$$F_x = cos\varphi \cdot F_r - sin\varphi \cdot (F_t \cdot cos\beta) \tag{6.9}$$

$$F_y = sin\varphi \cdot F_r + cos\varphi \cdot (F_t \cdot cos\beta) \tag{6.10}$$

$$F_z = F_a = F_t \cdot cos\beta \tag{6.11}$$

where φ is the instantaneous angular position of the tool.

This system of three equations can be advantageously expressed in a matrix form as following:

$$\begin{Bmatrix} F_x \\ F_y \\ F_z \end{Bmatrix} = \begin{bmatrix} cos\varphi & -sin\varphi & 0 \\ sin\varphi & cos\varphi & 0 \\ 0 & 0 & 1 \end{bmatrix} \cdot \begin{Bmatrix} F_r \\ F_t \cdot cos\beta \\ F_a \end{Bmatrix} \tag{6.12a}$$

or symbolically:

$$\{F_{work}\} = \left[R_{z,\varphi}\right] \cdot \{F_{tool}\} \tag{6.12b}$$

where $R_{z,\varphi}$ is a transformation matrix for rotation about axis *z* with an angle φ.

This transformation relation is sufficient for the case illustrated in fig. 6.3. This case, however, illustrates only 3-axis milling (the tool moves only in lateral directions *x*, *y* and *z*). For the transformation of the cutting force in the case of 5-axis milling (tilts about *x* and *y* axes) two additional transformation matrixes ($R_{x,A}$ and $R_{x,B}$) are needed. These matrixes can be derived similarly as $R_{z,\varphi}$, and they will have the following form:

$$R_{x,A} = \begin{bmatrix} 1 & 0 & 0 \\ 0 & cosA & -sinA \\ 0 & sinA & cosA \end{bmatrix} \tag{6.13a}$$

$$R_{y,B} = \begin{bmatrix} cosB & 0 & sinB \\ 0 & 1 & 0 \\ -sinB & 0 & cosB \end{bmatrix} \tag{6.13b}$$

Hence, finally the calculated cutting force for the case of 5-axis milling can be transformed to workpiece coordinate system by the following relation:

$$\{F_{work}\} = [R_{x,A}] \cdot [R_{y,B}] \cdot [R_{z,\varphi}] \cdot \{F_{tool}\} \tag{6.14}$$

6.4 Method approach

Method is based on splitting tool cutting edge into small elements and on the application of relations from analytical geometry on each element. By this approach elemental chip areas are calculated for each time point. This approach facilitates modelling of the forces for various cutting edge geometries, even with variable helix angles. Different workpiece shapes and relative tool-workpiece movements can also be simulated.

After basic tool and workpiece geometries definition, the tool is rotated and translated. Tool-workpiece interaction is identified and the uncut chip thickness for each element of cutting edges is calculated. In the next step, is identified the constant q and the function $K_m(z)$. The total values of q and K_m are established through a small number of experiments. After total K_m is found, the relevant portion is distributed to each element. At this point cutting force components F_t, $\widehat{F}_t$ and F_a can be calculated for each edge element and the time step by the application of relations 6.1, 6.3 and 6.4. Force component F_r is than calculated by multiplication of F_t by the constant q as described in relation 6.2.

6.4.1 Tool and workpiece geometries definition (pre-processing)

Tool geometry in this research is defined as follows:

- Definition of the tool rotation axis.
- Definition of the tool cross-section. For modelling purposes the geometry can be simplified to definition of line representing rake face.
- Definition of local coordinate systems. Individual coordinate system is translated along the tool axis and pitched with respect to helix angle.
- Tool cross-section is adjusted to local coordinate systems.

The workpiece geometry used in this research is a simple block. It is defined by three planes perpendicular to each other.

Once tool and workpiece geometries are defined, they have to be adjusted to each other with respect with tool the initial position.

6.4.2 Determination of the theoretical chip areas

After the mathematical definition of the tool and the workpiece is completed, the uncut chip area for each element can be calculated. This is done by calculating the uncut chip thickness in every node and calculation of the area of the trapezoid defined by the uncut chip thicknesses of two neighbouring nodes, as sketched in fig. 6.4. As very shortly mentioned above, the method employed in this research uses transient analysis. The precise position of the tool in every instance is calculated and mathematically described. The relative cutting edge/workpiece position is checked for the following conditions:

- If the cutting edge element is out of the workpiece material, then the tool is moved into new position in next time step. No data are saved.
- If the cutting edge element is inside the workpiece material, then the position and number of the current rotation is saved and the tool is moved into new position in next time step.

This is repeated until the current time reaches time limit set by the user.

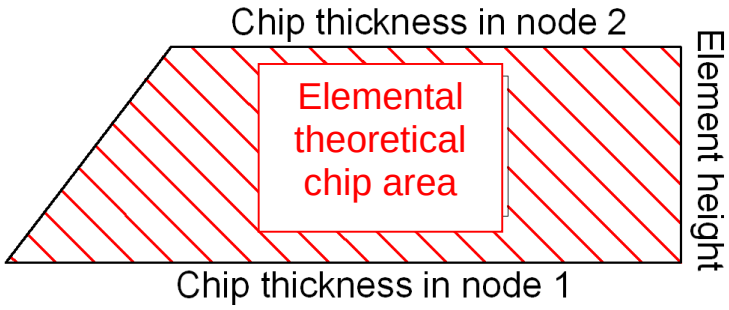

Fig. 6.4: Illustration of elemental theoretical chip area

In the next step the distance between each saved cutting edge element's position and interaction of the cutting edge with surface generated in previous cutting edge pass is calculated and saved.

The flowchart for the whole chip thickness calculation process is illustrated in fig. 6.5.

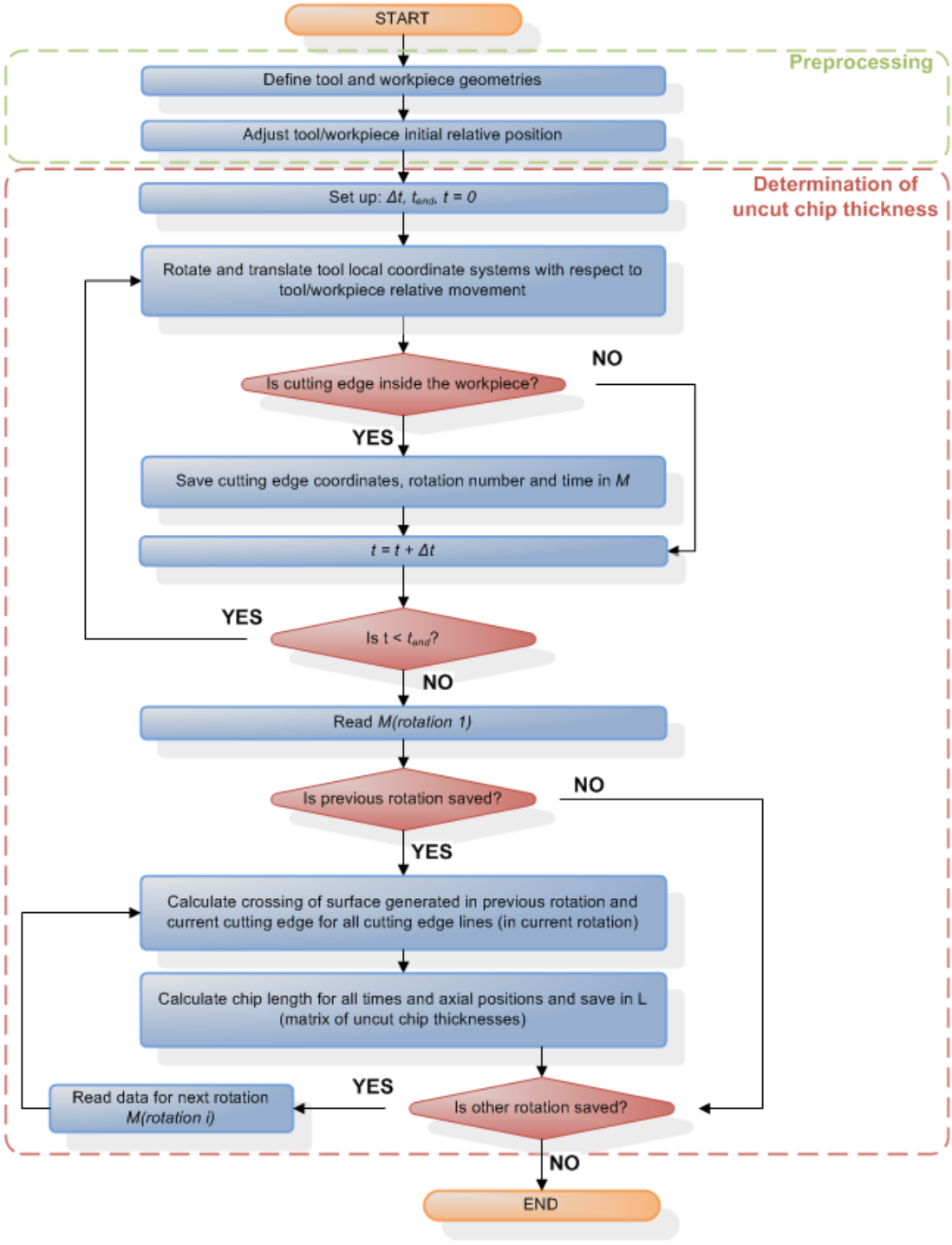

Fig. 6.5: Flowchart of theoretical chip thickness calculation

In fig. 6.6 two steps of the solution are graphically represented. Yellow surfaces illustrate tool rake faces, red surface illustrates a theoretical cutting area, blue lines show basic workpiece geometry, blue dots illustrate newly generated surface and grey dots illustrate surface generated in previous cutting edge pass.

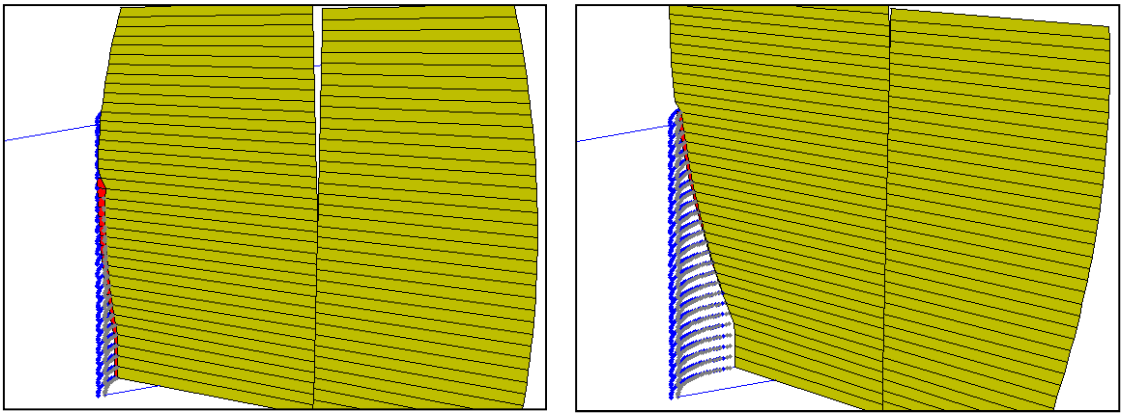

Fig. 6.6: MATLAB generated illustrations of the theoretical chip area calculation

Finally, it is a good practise to express the chip thickness *w(z, t)* function in form:

$$w(z,t) = W_a \cdot \hat{w}(z,t) \tag{6.15}$$

where W_a is magnitude and $\hat{w}(z,t)$ is normalized chip thickness as a function of axial position and time.

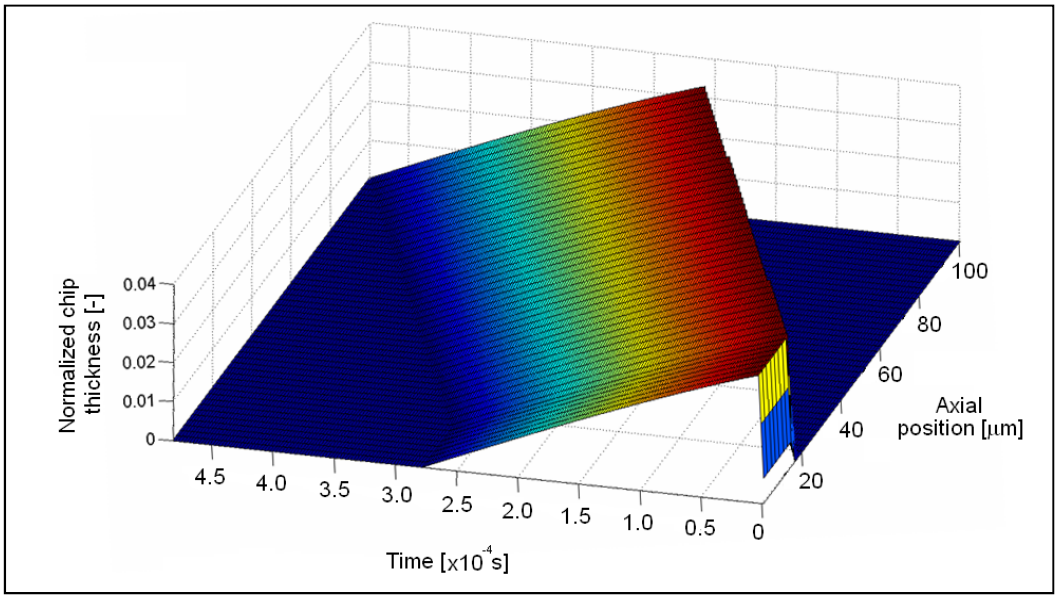

Fig. 6.7: Graphical representation of normalized chip thickness as function of axial position and time; down-milling, n = 10 000 rpm, f_z = 3 μm, a_e = 100 μm.

The advantage of the form 6.16 is easer application of the cutting force as a boundary condition in FEA. The typical shape of $\hat{w}(z,t)$ is shown in fig. 6.7.

6.4.3 Determination of the proportional constant *q* and the specific cutting force *Km(z)*

Function $K_m(z)$ is assumed to be a function of tool axial position and can be expressed as:

$$K_m(z) = K_{m\,tot} \cdot k(z) \tag{6.18}$$

where $K_{m\,tot}$ is total specific cutting force achieved experimentally and *k(z)* is a weighting function.

In this research function *k(z)* is assumed to be proportional to the amount of material in direction perpendicular to the cutting edge. Its shape for the Ø0.2 mm tools used in this research is shown in fig. 6.8.

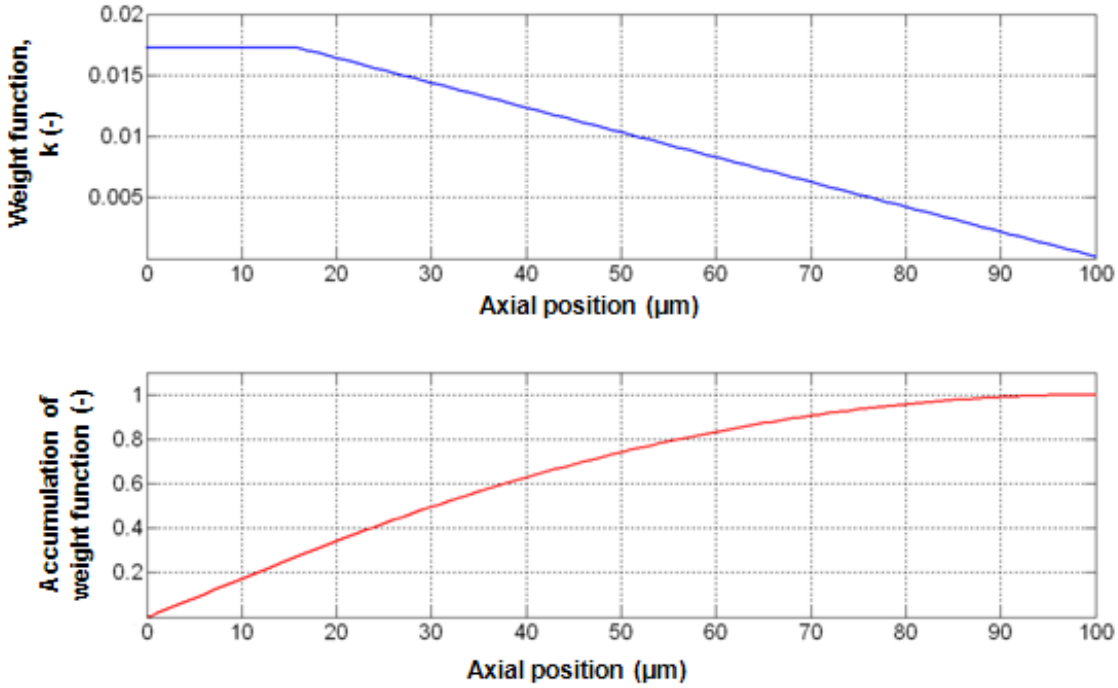

Fig. 6.8: Weight function *k(z)* and its accumulation

The total specific cutting force $K_{m\,tot}$ and the proportional constant *q* can be achieved from a few experiments. The experiments are designed as a full slotting. This is because of determination of rotational angle. Once the forces are measured they are implemented into the relation 6.12 where $\widehat{F}_t$, F_r and F_a are expressed by the relations defined in section 6.2. After reordering the equations will have the following form:

$$K_{m\,tot} = \frac{F_x}{cos\varphi \cdot q \cdot A - sin\varphi \cdot cos\beta \cdot A} \tag{6.19a}$$

$$q = \frac{F_y - cos\varphi \cdot cos\beta \cdot A \cdot K_{m\,tot}}{sin\varphi \cdot A \cdot K_{m\,tot}} \tag{6.19b}$$

$$K_{m\,tot} = \frac{F_z}{cos\beta \cdot A} \tag{6.19c}$$

From these equations it is already easy to get both $K_{m\,tot}$ and q.

Full slots with depths of 0.02 mm are milled by uncoated Ø0.2 mm micro end-mills. No lubrication is used during the tests to avoid uncertainties caused by air pressure and uneven friction. Cutting speeds and feeds used in the experiments are covered in tab. 6.1. They are chosen to include different cutting speeds and feeds. Every test was repeated three times and average values were used to determine $K_{m\,tot}$ and q.

Table 6.1: Cutting speeds and feeds used evaluation experiments and average in $K_{m\,tot}$ and q values

	cutting speed, v_c (m·s^{-1})	**feed, f_z (µm)**
Test 1	6.28	2
Test 2	15.71	2
Test 3	25.13	2
Test 4	15.71	4
Test 5	15.71	6

The determined specific cutting forces and proportional constants are plotted in fig. 6.9. The specific cutting force and the proportional constant were found to be linear functions of feed. However, no distinct dependency was found on the cutting speed. This is caused by different proportions of ploughing and shearing when uncut chip thickness (feed per tooth) is varied. However, no significant changes in proportion should appear when cutting speed is varied.

Therefore, in all future analyses the specific cutting force and the proportional constant will be expressed as functions of feed (f_z) in the following form:

$$K_{m\,tot} = -0.23 \cdot f_z + 2.95 \tag{6.20}$$

$$q = -0.02 \cdot f_z + 0.4833 \qquad (6.21)$$

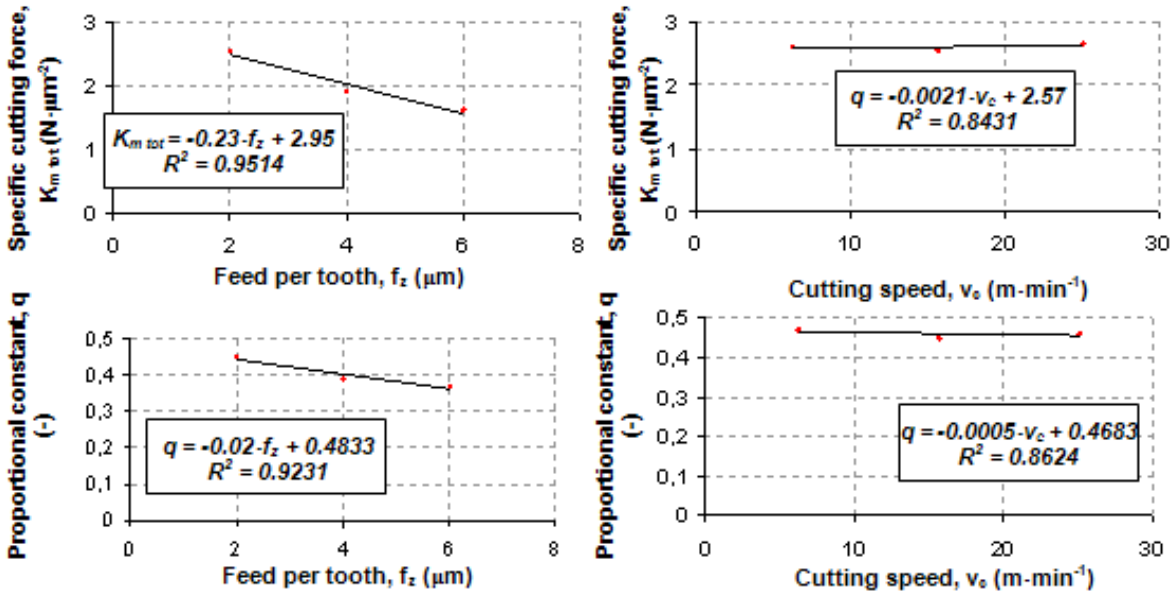

Fig. 6.9: Dependence of specific cutting force and proportional constant on feed per tooth and cutting speed respectively

6.5 Model verification

Developed modelling method was verified by a comparison of theoretical cutting forces with experiments.

Tools used in the verification experiments are uncoated Ø0.2 mm micro end-mills. Uncoated tools were chosen in order to minimize unpredictable effects caused by coatings. The experiments were performed as dry side milling. In all experiments constant width of cut 0.02 mm and depth of cut 0.1 mm was used. Four different cutting speeds were used: 6.28 m·min^{-1} (10 000 rpm), 12.56 m·min^{-1} (20 000 rpm), 18.85 m·min^{-1} (30 000 rpm) and 25.13 m·min^{-1} (40 000 rpm). Feed per tooth was 2 µm, 4 µm, 6 µm and 8 µm. Hence, there are sixteen different combinations of cutting speeds and feeds per tooth. Down-milling was used in all these experiments. Each of the combination was repeated 3 times.

An example of the comparison of theoretical and measured forces is shown in fig. 6.10. The cutting conditions used in the example case were v_c = 18.85 m·min^{-1}, f_z = 2 µm, a_e = 100 µm and a_p = 20 µm. The theoretical and measured forces show a good agreement. It was also noted that by the covering of tool run-out into model the agreement can be still improved.

The tool run-out is, however, different for each individual tool. Therefore, the procedure will not be covered in this study.

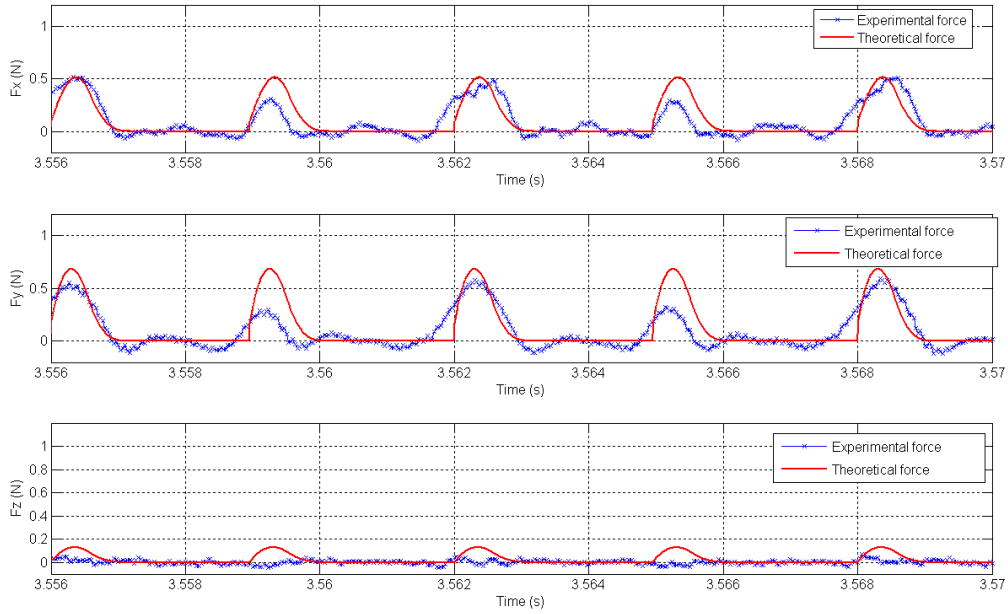

Fig. 6.10: Comparison of experimental and theoretical forces; down-milling, v_c = 18.85 m·min^{-1}, f_z = 2 μm, a_e = 100 μm and a_p = 20 μm

The relative errors for all verification tests were calculated as:

$$error = \frac{F_{measured} - F_{theoretical}}{F_{measured}} \cdot 100\% \qquad (6.22)$$

The errors for various cutting conditions are shown in fig. 6.11. The average error for evaluated cutting conditions is less than 15% and does not exceed 40%. This error is acceptable for future analyses covered in this work.

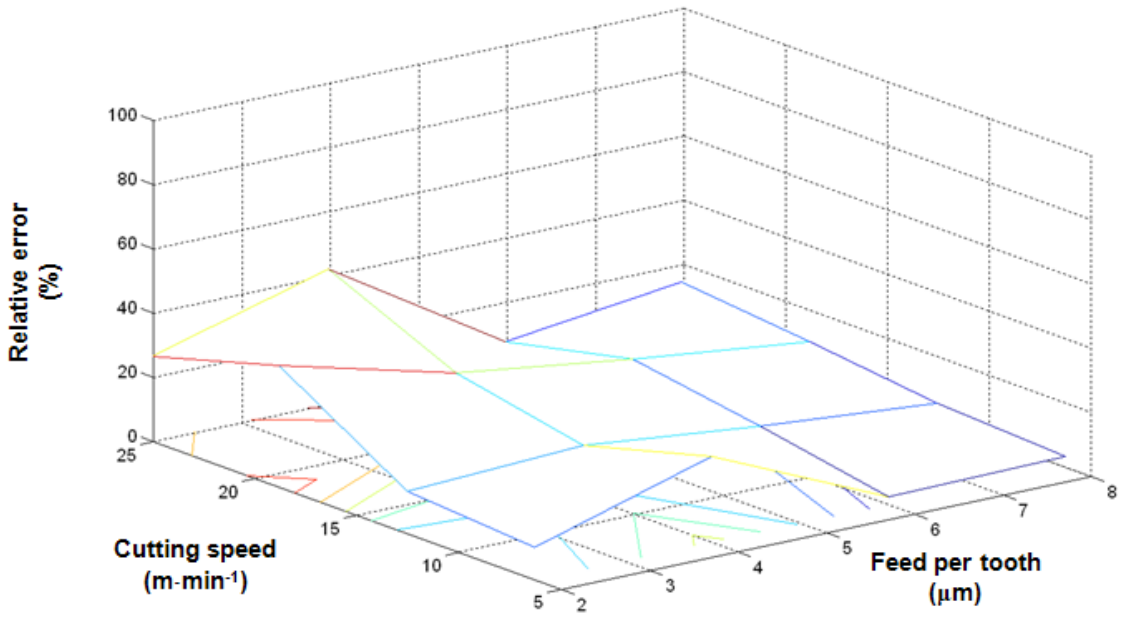

Fig. 6.11: Illustration of model error as a function of cutting speed and feed per tooth

6.6 Summary

In this chapter was presented a cutting force modelling method. This method is used in the following chapters for calculation of cutting forces needed for FEA. The method is based on analytical relations developed by J. Tlusty and P. MacNeil and further improved by M. T. Zaman. The forces are related to uncut chip area as it is typical for majority of cutting force models used in milling. It predicts cutting forces in tangential, radial and axial directions. The uncut chip area is calculated by numerical approach based on analytical geometry.

The method was experimentally verified and shows an average error of approximately 15%. Although some other researchers claim their models to be more accurate, this is the first model verified with as small tools as Ø0.2 mm (typically tools with diameters of 0.5 mm are used in literature). Hence, the tools used in this research have significantly lower stiffness which can affect accuracy of the force prediction. The maximum relative error is 40%. This error can be caused by many factors. However, as the most probable reason for such error is tool run-out. Although, this phenomenon has a strong effect on the cutting forces, it was not further studied in this research. The tool run-out can be caused by tool imperfections or by tool clamping. Therefore, the magnitude of tool run-out is unique for every special case. Therefore, it was not further studied in this research. However, this phenomenon should be

comprehensively studied in the future. Although, the model does not show perfect match with the experimental data, the average error of 15% is assumed to be acceptable for applications in the following chapters.

7. Analysis of tool dimensional tolerance effects on the failure of micro end-mills

7.1 Motivation and objectives

Micro milling process is basically the same as conventional macro milling. However, due to downscaling, various size effects appear and affect manufacturing process. One of the important effects is rapid reduction of tool stiffness and increase of stress generated by usual cutting conditions. Based on the cantilever beam theory, tool stiffness is proportional to the 4^{th} power of the tool diameter. Hence, even with small reduction of the tool diameter a significant increase of stress can be observed.

Measurements of tool dimensions covered in chapter 4 have shown large dimensional tolerances. This discovery was confirmed by various researchers from different research institutions. However, no research of the effects of the tool dimensional tolerance was found in literature.

Therefore, FEA is used to investigate the effects of the tool dimensional tolerance on stress distribution within the micro end-mill. An cutting force model presented in the previous chapter is used to estimate realistic 3D cutting forces which are used as boundary conditions in the FEA. Thanks to this approach various cutting conditions can be easily and quickly investigated and a critical feed, depth and width of cut can be estimated.

7.2 Measurements of micro end-mills

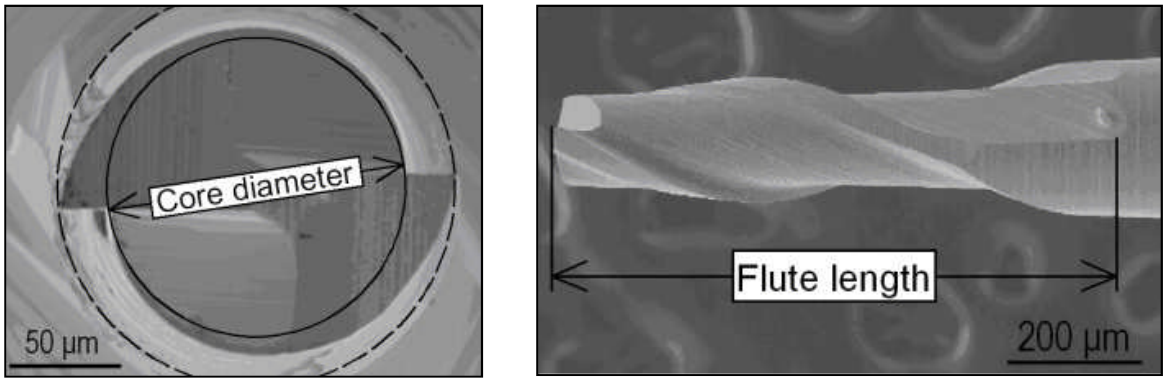

(a) Front view (b) Side view

Fig. 7.1: Illustration of the dimensions of a micro end-mill

Micro end-mills are commonly manufactured by micro grinding. This technology facilitates manufacturing of very small WC-Co end-mills with low costs and high material removal rates. However, due to a mechanical contact between the grinding wheel and the end-mill and relative positioning errors, inaccuracies of the final geometry often appear.

In order to determine these errors, 50 uncoated commercial micro end-mills with nominal cutting diameter of 0.2 mm were measured by SEM imaging. All the measured tools were taken from a single batch. The uncoated tools were used in order to isolate the tool manufacturing errors from the coating inaccuracies. Three main dimensions were of an interest: the core diameter, the cutting diameter and the flute length (see fig. 7.1). By the flute length is understood a distance from the tool tip up to the very end of the "chip pullout" geometry as it is shown in fig. 7.1b.

The measurements have confirmed large variations of these fundamental dimensions for individual tools. Histograms of the core diameters, the cutting diameters and the flute lengths are shown in figures 7.2, 7.3 and 7.4. All three histograms were normalized to one and compared with relevant theoretical normal distributions calculated from:

$$p(x;\mu,\sigma) = \frac{1}{\sigma \cdot \sqrt{2 \cdot \pi}} \cdot e^{-\frac{(x-\mu)^2}{2 \cdot \sigma^2}} \tag{7.1}$$

Where μ is the average dimension and σ is the standard deviation.

From the figures is evident that all measured data fits to the theoretical values. Therefore, upper and lower limits of the dimensions can be easily calculated from the following equation:

$$T_{1,2} = \mu \pm 3 \cdot \sigma \tag{7.2}$$

Table 7.1: Principal dimensions of Ø0.2 mm micro end-mills

Parameter	Value (µm)
Core diameter	132±10
Cutting diameter	183±8
Flute length	846±12

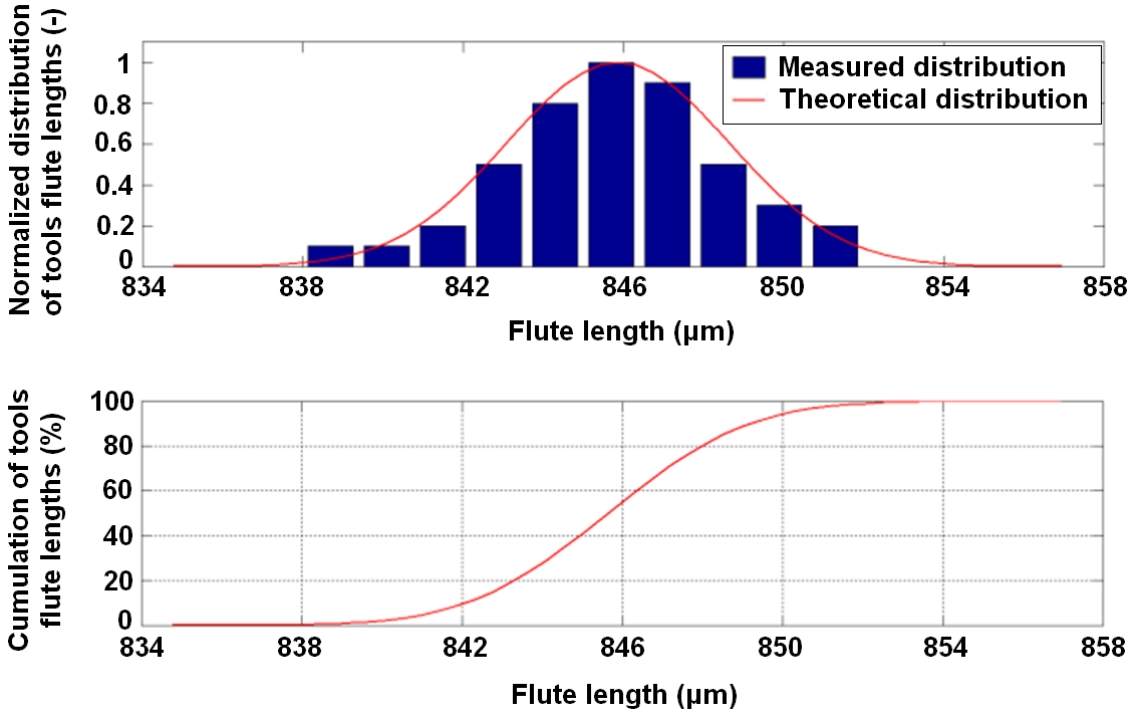

Fig. 7.2: The Measured and the theoretical distribution of the flute length

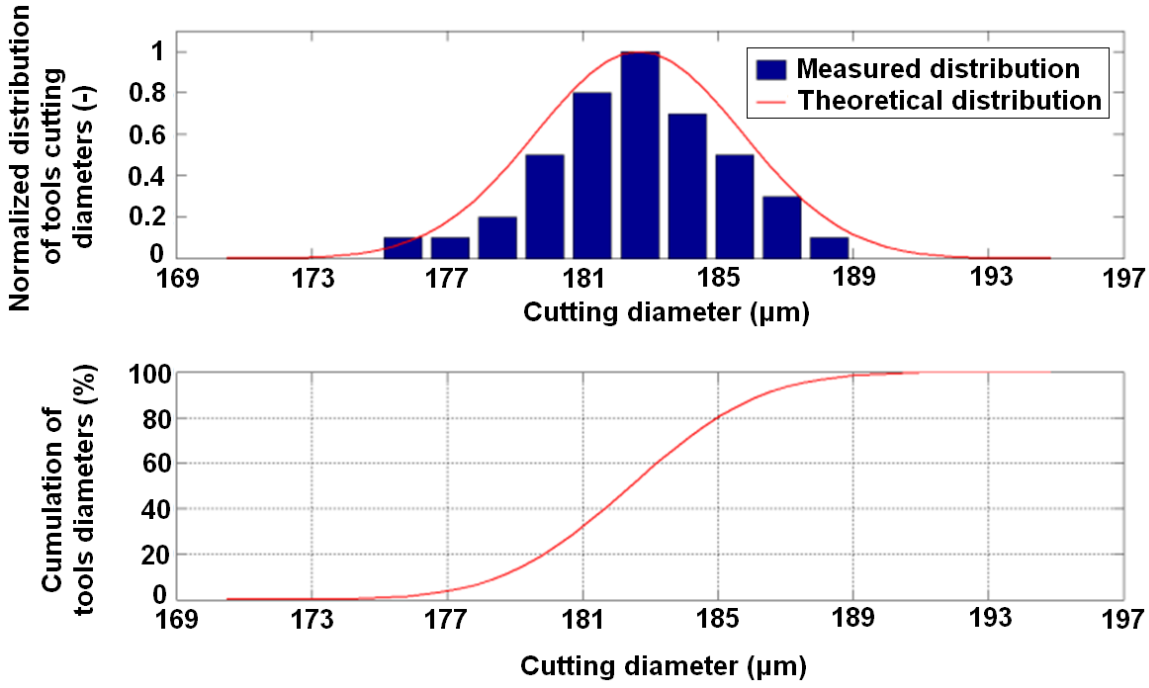

Fig. 7.3: The Measured and the theoretical distribution of the cutting diameter

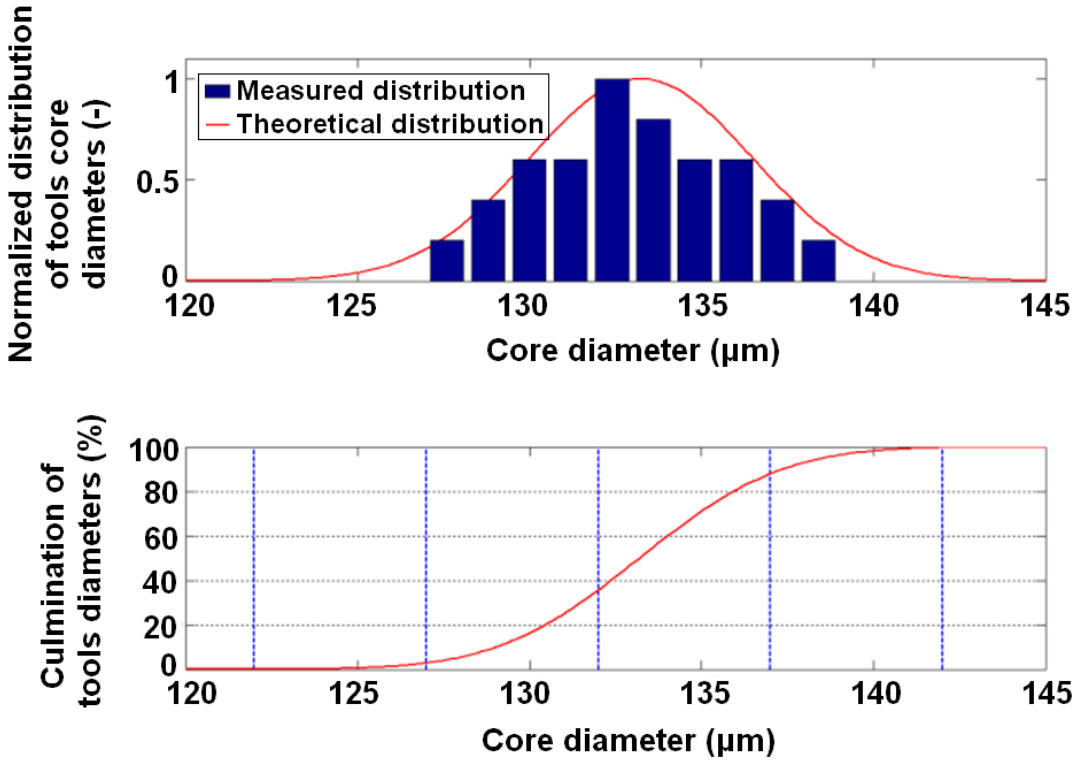

Fig. 7.4: The Measured and the theoretical distribution of the core diameter

The average dimensions and dimensional tolerances are listed in table 7.1. The tolerances of all three dimensions were estimated to be approximately 20 µm. This, however, represents nearly 17% difference between the smallest and the largest core diameter but only 2% difference in the case of the flute length. Although the cutting diameter tolerance represents 10% of the average value, it is assumed not to have an important effect on the tool stress. Therefore, further numerical analysis is performed only on tools with variable core diameter.

7.3 Finite Element Analysis

The geometrical model used in this research represents an average commercial Ø0.2 mm micro end-mill supplied by UNION TOOL. All tool dimensions used for the modelling purposes were achieved from SEM imaging. The main geometrical features and their dimensions were measured on all 50 tools and the average values were used in the model. Although, some concerns about the SEM measurement accuracy remain, the large number of the measured tools gives a good approximation of the real tool dimensions. Five models with core diameters of 122 µm, 127 µm, 132 µm, 137 µm and 142 µm were used in this study. All

other model dimensions were kept constant. Comparison of the geometrical model and real micro end-mill is shown in fig. 7.5.

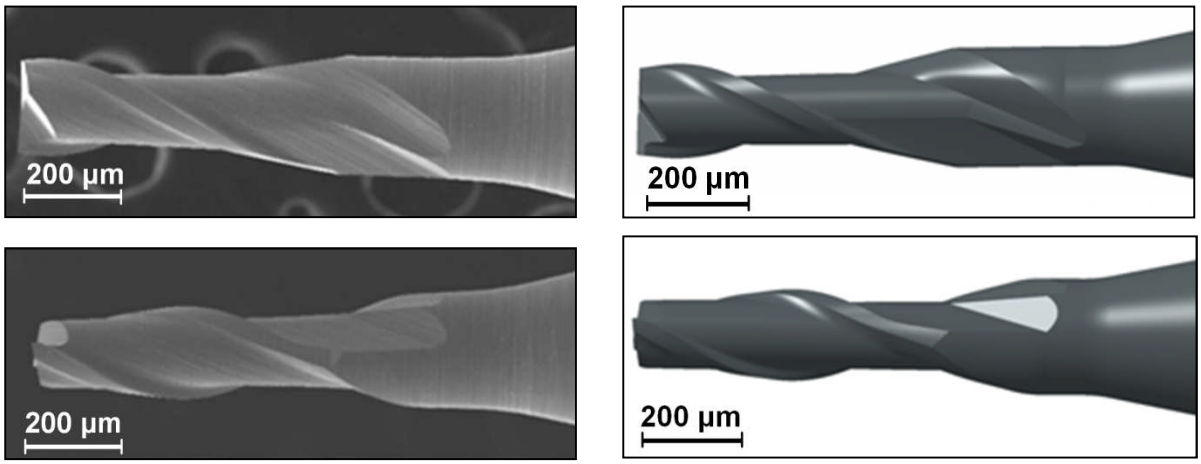

Fig. 7.5: Comparison of a real micro end-mill and its geometrical model

Material data used in the FEA are covered in table 7.2. The modulus of elasticity, Poisson ratio and density are taken from www.matweb.com [124] and correspond with measured tool material (94% WC and 6% Co).

As a criterion of tool failure was used transverse rupture strength (TRS). The value for ultra fine WC-Co, with 6% Co, was derived from data published in [125, 126].

Table 7.2: Material data used in FEA

Parameter	Value	Unit
Modulus of elasticity	6.45×10^{5}	MPa
Poisson ratio	0.22	-
Density	1.4653×10^{-8}	tonne mm^{-3}
Transverse rupture strength	$>3.6 \times 10^{3}$	MPa

The geometrical model was meshed by tetragonal elements with a mid-node. The elements with mid-node were used due to higher order accuracy comparing to commonly used linear elements. The cutting zone of the tool was meshed by very fine elements, while the neck zone of the tool was meshed with a coarse mesh as it is shown in fig. 7.6a. This is because high stress gradients are expected only in the cutting zone of the tool.

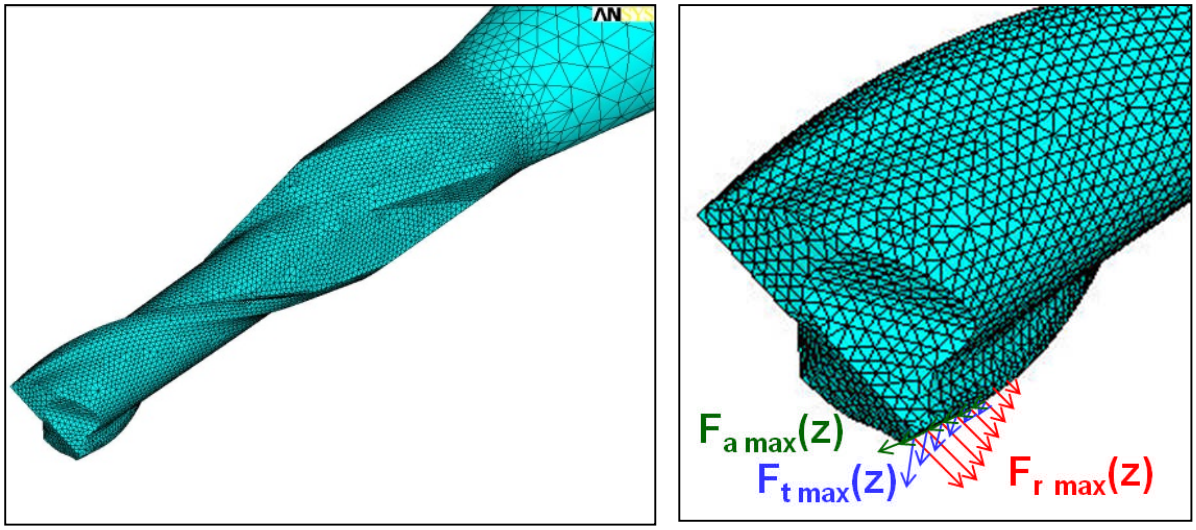

(a) Micro end-mill FE model

(b) Detail of the tool tip with highlighted applied force

Fig. 7.6: Micro end-mill FE model

All FEAs were run as static. This simplification can be used because of the very low tool inertia, and subsequent very fast tool response to any dynamic change in loads.

The tool was clamped in distance of 10 mm from the tool tip. This position well corresponds to clamping of a real tool.

The applied force was calculated by the model introduced in chapter 6 for various cutting conditions. The maximal cutting force was applied as a distributed load over the cutting edge as shown in fig. 7.6b. Three sets of simulations were carried out to investigate effects of feed per tooth (f_z), width of cut (a_e) and depth of cut (a_p). In the first set of simulations were used the following cutting conditions a_e = 20 µm, a_p = 100 µm and f_z = 1, 2, 4, 6 and 8 µm/tooth. In the second set of simulations a_p = 100 µm and f_z = 2 µm/tooth are kept constant and a_e = 10, 20, 40, 60 and 80 µm is variable. In the last set of simulations were used: f_z = 2 µm/tooth, a_e = 20 µm and a_p = 10, 50, 100, 150 and 200 µm. Chosen values cover typically applied cutting conditions for the assumed tool and workpiece combination.

Finally, the model was validated by demonstrating good correlation between the measured and predicted static tool stiffness.

7.4. Results and discussion

In this research was analyzed the first principle stress (σ_1) instead of commonly used equivalent stress (σ_{eqv}). This decision was made because σ_1 represents the maximum tensile stress within a point of a body (tool) which corresponds to the definition of transverse rupture strength as it was discussed in chapter 2.

Fig. 7.7 shows a typical calculated distribution of the first principal stress. Maximum tensile stress is in the location of the flute termination. The location of the maximum tensile stress corresponds with the location of real tool failure.

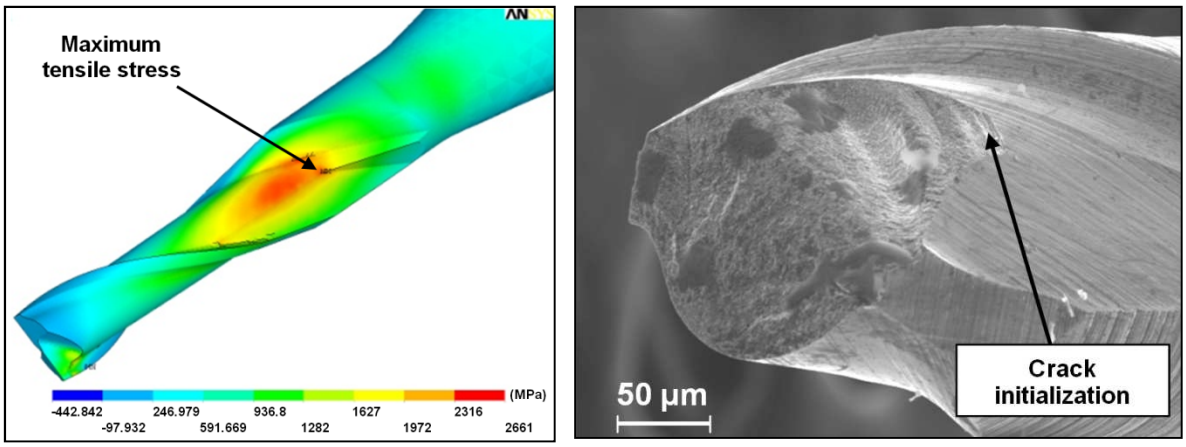

(a) Calculated stress distribution (b) An Example of a broken tool

Fig. 7.7: Tool stress analysis (f_z = 2µm, a_p = 100µm, a_e = 20 m)

Core diameter variations within analyzed tolerances have minimal effect on maximal tensile stress location. However, large effect on stress magnitude was found.

In fig. 7.8 the relation between feed per tooth and maximal tensile stress within the tool is shown. The red dashed line represents TRS of WC-Co. If the tensile stress is higher than the TRS, the tool is assumed to fail. From fig. 7.8 it is evident that the typical core diameter tolerance of Ø0.2 mm micro end-mill has a great effect on tool performance. In the case of a micro end-mill with a core diameter of 142 µm, it is expected to withstand nearly 4 µm/tooth. However, the tools with core diameter of 122 µm are likely to break on 2 µm/tooth. This spread of usable feeds is enormous and makes planning of optimal cutting conditions extremely difficult.

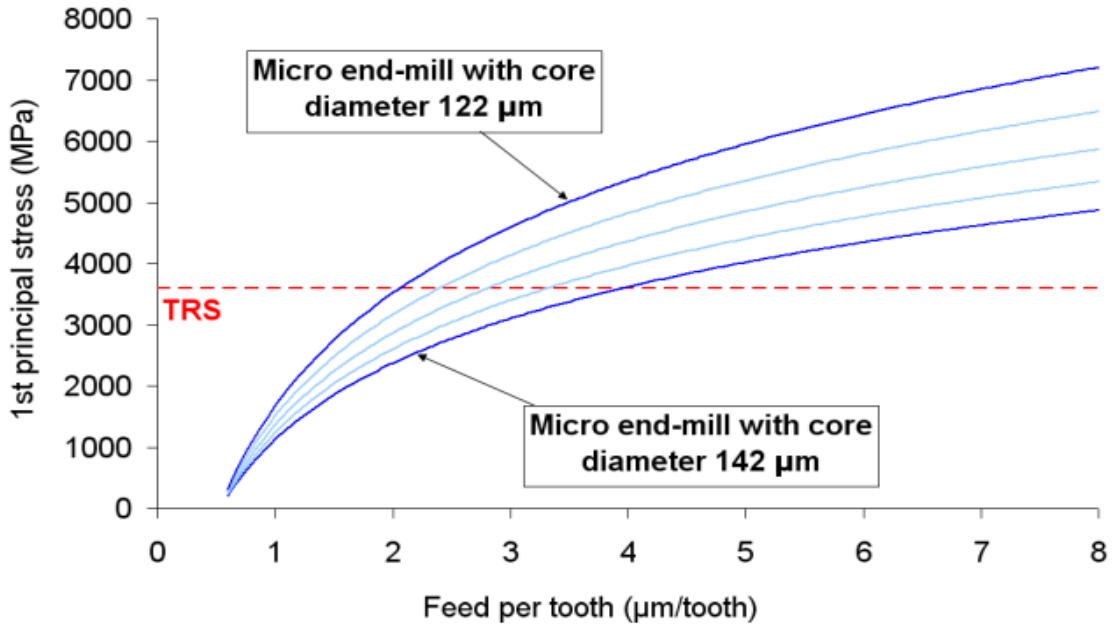

Fig. 7.8: Effect of feed on maximum tensile stresses in case of various core diameters (a_p = 100 µm, a_e = 20 µm)

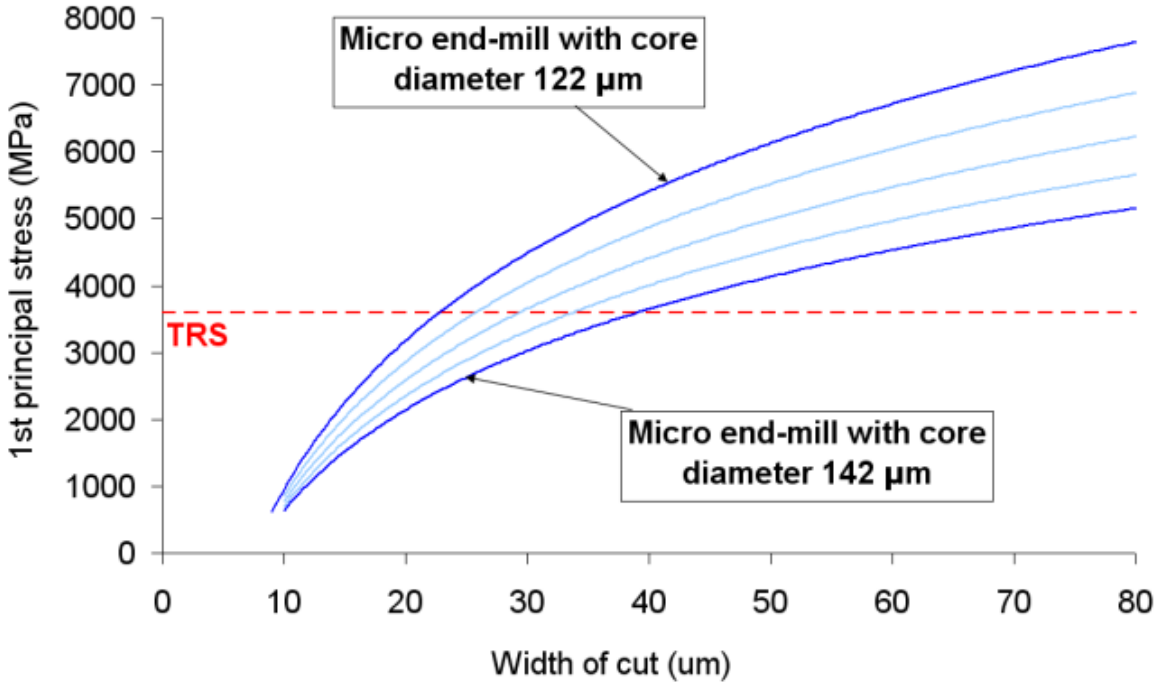

Fig. 7.9: Effect of width of cut on maximal tensile stresses in case of various core diameters (a_p = 100 µm, f_z = 2 µm/tooth)

The same conclusions may be drawn also for other cutting conditions. Fig. 7.9 plots the relationship of maximum tensile stresses with width of cut. In this case the spread of critical width of cut is from 22 µm to 40 µm.

Finally, the relationship between the minimum tensile stress and the axial depth of cut is shown in fig. 7.10. Also in this case the stress grows with increasing depth of cut. However, the difference among the maximum stresses in tools with different core diameters is not as high as in the cases of width and feed. Shallower characteristic of the depth-stress functions makes, however, the effect of the depth of cut on tool life very important. It was found that some of the considered tools reach the critical stress with depth of cut of 150 µm, and some others will not reach the critical value at all.

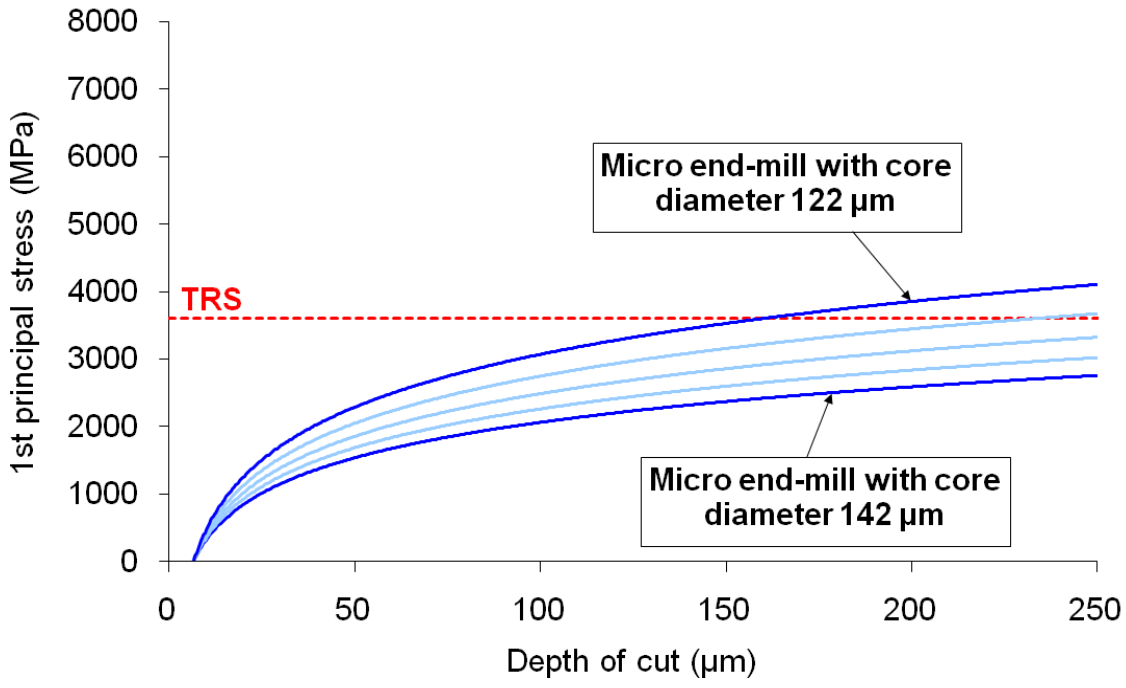

Fig. 7.10: Effect of axial depth of cut on maximal tensile stresses with various core diameters (a_e = 20 µm, f_z = 2 µm/tooth)

7.5 Summary

In this chapter was introduced the issue of micro end-mill tolerances. Three main dimensions (the flute length, the core diameter and the cutting diameter) were measured on 50 tools with nominal cutting diameter of 0.2 mm. Although all these tools were from a single batch, significant differences were found between the analysed tools. All three measured dimensions have approximately ±10 µm tolerances. This may seem tiny, but in the

relation with the average tool dimensions it represents a great challenge. The core diameter was determined as the most critical one. This is because the tolerance represents 17% of the average core diameter. On the other hand tolerance of the flute length represents only 2% of the average value, and therefore, it can be assumed as negligible.

FEA on the effect of the core diameter tolerances was performed as a set of static simulations. Models with five different core diameters were used in this research. The used core diameters were equally spaced between the largest and the smallest possible diameter, as they were identified by the measurements. In each set of simulations only one cutting condition was varied and other conditions were kept constant. The spread of maximum stresses is in all studied cases very wide. If cutting conditions are f_z = 2 µm, a_p = 100 µm and a_e = 20 µm, the maximum stress will be in range from 4 000 MPa to 6 000 MPa. This difference is caused purely by the core diameter tolerance. Hence, it is evident how important is the effect of the core diameter.

These results demonstrate the great difficulty in predicting tool failure in real micro milling situations. Therefore, the dimensional tolerances should always be kept in mind when predicting tool life.

8. Prediction of micro end-mill life

8.1 Motivation and objectives

Although micro milling was found to be a powerful manufacturing technology, it is not yet well accepted by industry. The main reason is a low predictability of tool performance. The micro end-mills were found to be liable for premature breakage and the final product quality is strongly affected by various uncertainties (e.g. machine tool dynamics, environmental fluctuations, workpiece and tool micro structure, quality of the cutting tool etc.).

Therefore, people in industry hesitate to use micro milling and keep using less capable, but more mature processes. This is fully understandable, as high risk of project failure is not acceptable for majority of industrial projects. The industrialists' concerns were confirmed by the research presented in the previous chapter. Although, the analysis of tool stress in the previous chapter is mainly theoretical, it is based on well established and reliable FEM. Therefore, the results give a good indication about this issue. It is evident that the tools, which are supposed to be the same, in the reality can perform very differently. This, however, makes it impossible to predict the micro milling outputs without application of probability and statistical methods. Such planning method is, however, not yet available, and therefore, planning of manufacturing strategy is very difficult and risky. Furthermore, no of the current monitoring techniques seems to be reliable for applications in micro milling. This is because of small dimensions, high rotational speeds and also typical characteristics of micro end-mills. It is nearly impossible to predict tool breakage from any of typically measured signals (force, acoustic emissions or measurements of tool wear). Tungsten-carbide is a fragile material and so tool breakage happens suddenly and unexpectedly. Finally, it is not possible to base micro milling strategies on experience, as it is usual in macro manufacturing.

All these reasons lead to the author's opinion that a prediction method is extremely important and it will not be possible to convince industry to use micro milling without it. Hence, an objective of this chapter is:

To develop a method for a prediction of micro end-mill life.

Tool life was chosen as one of the most influential factors affecting the final product costs. The main demands which the method should fulfil are:

- Tool life is predicated in a sense of probability of tool breakage and not as a single value,
- The method should have minimum interactions with the day-to-day production.

8.2 Method description

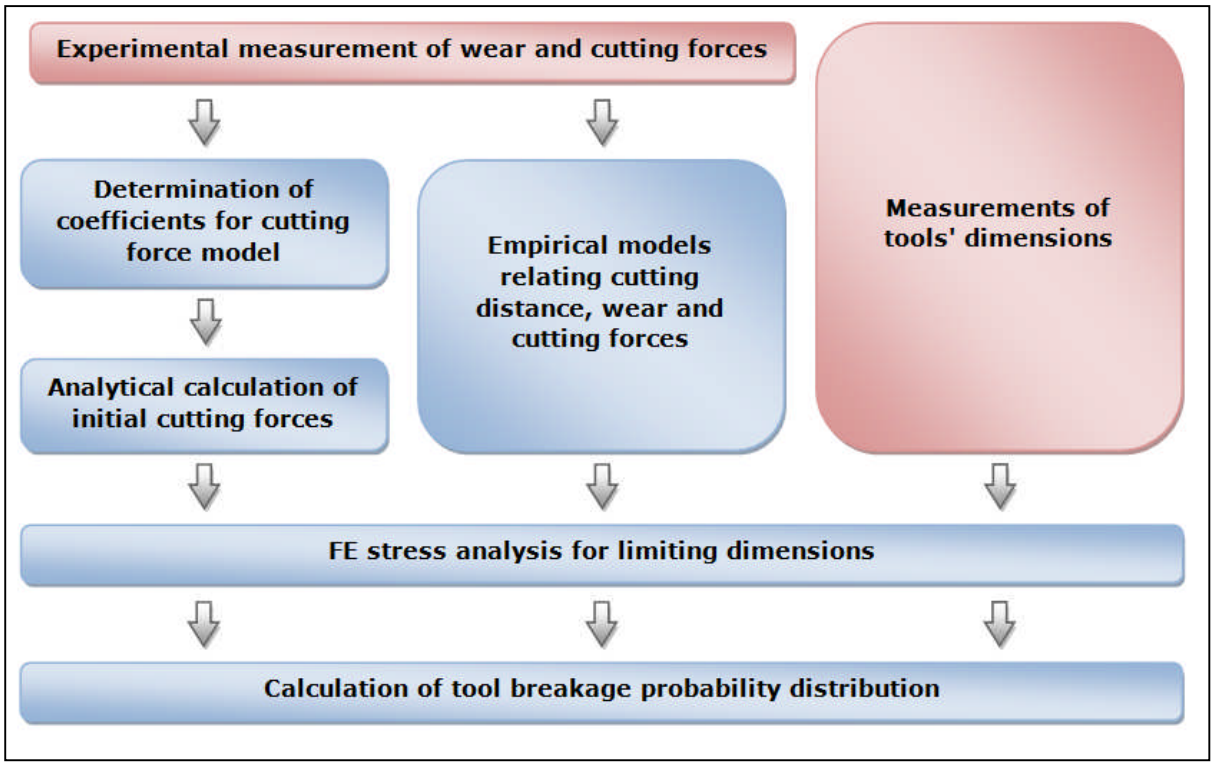

Fig. 8.1: Methodology for tool life (breakage) prediction

Micro milling is affected by a wide range of different input factors (e.g. application of lubrication, machine tool dynamics, cutting tool geometry and quality, cutting speed, feed, axial depth and width of cut etc.). Each of these factors has an effect on the outputs in form of product quality, manufacturing time and costs. These three outputs are the most important criteria for evaluation of the project risks and success. Their reliable prediction is, however, difficult and requires application of different types of methods for prediction of cutting forces, tool breakage, tool wear etc.

In this research are considered as variable only four input parameters: cutting speed, feed, width of cut and depth of cut. This does not mean that the other ones would not affect micro milling. All the other parameters are kept constant in this research, and their effects are not analysed. However, the method is designed to enable an implementation of further parameters in the future.

The method proposed here is an extension of the research presented in the previous chapter. It is based on an analysis of tool stress generated by various cutting conditions for tools with different tolerances. In this chapter it is further extended by implementation of tool wear effects, which was not assumed in the previous chapter. The results are then presented in a form of probability of tool breakage, as it will be explained later.

The method is divided into seven phases, from which two require experimental measurements and the rest is based on theoretical analyses. The sequence of the phases is illustrated in fig. 8.1 where the red blocks represent experimental phases and the blue ones represent theoretical phases. Furthermore, the measurements of tool dimensions do not interact with manufacturing process. Hence, the majority of operations used in this method do not interact with production.

8.2.1 Experimental analysis of wear and cutting forces

In the first phase of the method are required some experimental tests. These tests are used for determination of coefficients for models applied in the later phases. The required coefficients can vary depending on the chosen models (generally various types of models can be applied for prediction of wear or cutting forces; the models used in this research represent only one possible solution which the author assumes as the most suitable). Therefore, it is always important to design the experimental plan according to models used in the later phases.

In this particular research are used:

- An analytically/numerical method for prediction of cutting forces (see chapter 6),
- An empirical model for prediction of tool wear progression (see section 8.2.3), and
- Analytically/empirical model relating wear progression with increment of maximum cutting forces (see section 8.2.4).

8.2.2 Modelling of initial cutting forces

Cutting force is the first measure calculated in this method. The accuracy of its prediction strongly affects resulting tool stress and consequently reliability of tool breakage prediction. However, the force generally grows with increasing milling distance (time). This is mainly because of tool wear which changes cutting edge geometry and surface. The approach of relating the cutting force with tool wear is then described later in section 8.2.4.

Hence, in this section is predicted only the initial cutting force. This means the force at the very beginning of cutting process when the tool is new. This cutting force is predicted by the method presented in chapter 6. As was explained above in this thesis, this model requires two coefficients: the specific cutting force (K_m) and the proportional coefficient (q). Both of them were identified as linear functions of feed per tooth. Therefore, at least two sets of tests with different feeds are required for determination of K_m a q. The tools used for this purpose should be new and carefully checked for any defects. It is also strongly advised to repeat these tests at least three times because of repeatability issues. However, because the functions K_m (see equation 8.1) and q (see equation 8.2) were already determined in chapter 6 and the tools and workpiece material remain the same also in this chapter, the determination of the coefficients will not be further discussed here.

$$K_m = -0.23 \cdot f_z + 2.95 \tag{8.1}$$

$$q = -0.02 \cdot f_z + 0.4833 \tag{8.2}$$

8.2.3 Modelling of wear progression

Wear is another factor which must be considered during the prediction of tool life. It may be used in two manners. First, wear affects the cutting force. Generally, higher wear leads to higher force. Hence, wear is used as an input for the estimation of maximum cutting force as a function of milling distance or time. Secondly, wear affects product surface roughness which is another criterion which should be considered for determination of tool life. This means that if surface roughness exceeds the maximum allowed value the tool should be changed for a new one.

In chapter 5 were compared different types of tools. Part of the analysis was also a comparison of wear progression of different tools. In the case of Ø0.2 mm micro end-mills wear progression was found to follow a linear trend. Hence, the wear progression can be estimated from the following equation:

$$\Delta R_c = \mathrm{c_w} \cdot \Delta \mathrm{l} \tag{8.3}$$

where ΔR_c is a reduction of cutting radius (which is used in this research as a characteristic of tool wear), Δl is a milling distance and c_w is a constant coefficient, which can be called wear progression.

In the case of Ø1 mm end-mills two linear phases were identified. Wear progression is then expressed by two linear equations for each of the phases. Hence, the model will require three coefficients: c_{w1}, c_{w2} and l_{12}. The meaning of these coefficients is shown in fig. 8.2.

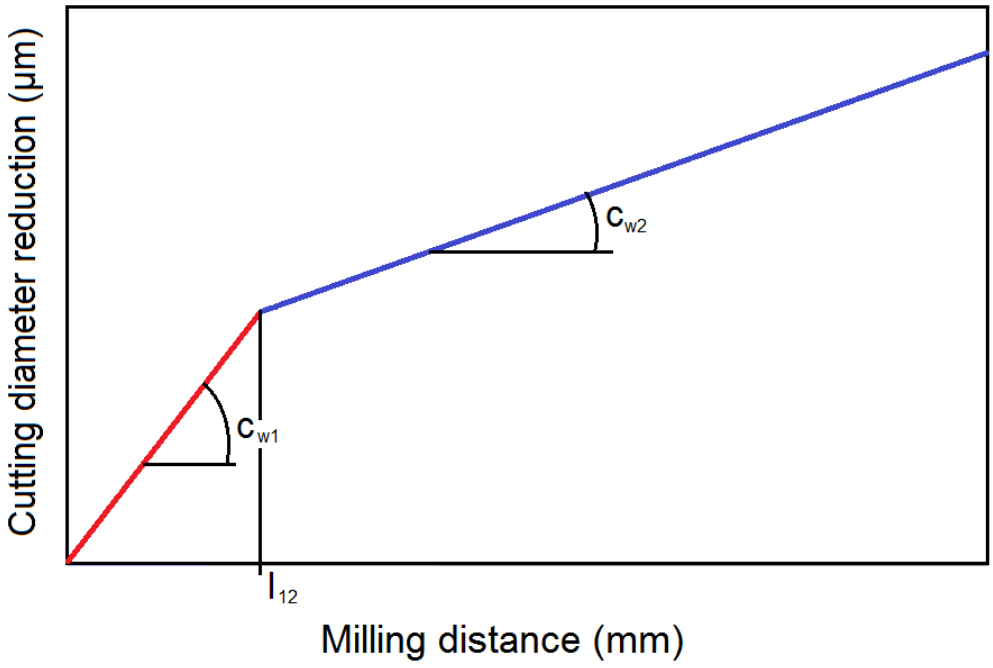

Fig. 8.2: Illustration of wear progression

However, the coefficients are generally functions of all input parameters. Hence, in the presented case four different parameters must be considered. In the most general case this would lead to 16 independent coefficients in a case of linear model and 256 different coefficients, if second order polynomial model would be used. Determination of each of these

coefficients would generally require one test. Similarly as in the case of coefficients for cutting force model, each test should be repeated at least three times. Hence, a large number of experiments would be required for this purpose. This is, however, usually not doable in industrial environment. Therefore, it is essential to determine a significance of each input parameter on tool wear. The experimental plan used for this purpose is summarised in tab 8.1. The experimental space contains eight members and each of the experiments is repeated three times. Hence, 24 test runs are needed.

Table 8.1: Design of experiments

Test no.	Speed (rpm)	Feed (µm/tooth)	Depth (µm)	Width (µm)
1	10 000	2	150	10
2	30 000	2	50	10
3	30 000	2	150	10
4	30 000	2	150	30
5	30 000	4	150	10
6	30 000	4	150	30
7	30 000	2	150	20
8	30 000	2	150	40

Wear in this research is expressed as a reduction of the tool cutting radius (ΔR_c) instead of the usually used VB_B value. This choice was made in order to simplify wear measurements as it was discussed in chapter 5. Thanks to this simplification more frequent measurements can be taken during the experiments. The wear progression in this case is calculated as followed:

$$c_w = average\left(\frac{R_{c_i} - R_{c_{i-1}}}{l_i - l_{i-1}}\right) \tag{8.4}$$

where R_{c_i} is the actual tool diameter; $R_{c_{i-1}}$ is the tool diameter measured in a previous step, l_i is the milling distance after the current step and l_{i-1} is the milling distance before the current step. Because only Ø0.2 mm tools are used in this research wear can be characterised by a single coefficient (c_w) which is a function of input parameters (see fig. 8.3).

Both, the cutting speed and the depth of cut show only a negligible effect on wear progression (see fig. 8.3a and 8.3b). However, if wear would be expressed in a usual way of wear rate (wear per unit of time) the speed would show a significant effect and could not be neglected. This would, however, lead to a need of a higher number of coefficients which would have to be determined experimentally. Therefore, in this research is used with

advantage wear progression instead of traditionally used wear rate. However, if the user wishes to use wear rate, he can easily calculate it from the following equation:

$$wear\ rate = wear\ progression \cdot rpm \cdot number\ of\ flutes \cdot f_z \tag{8.5}$$

The width of cut shows the dominant effect on wear progression (see fig. 8.3c). Therefore, two extra experiments are added into this analysis (a_e = 20 µm and a_e = 40 µm). These two extra experiments help to determine the trend function. By these experiments was confirmed a linear relation between wear progression and the width of cut.

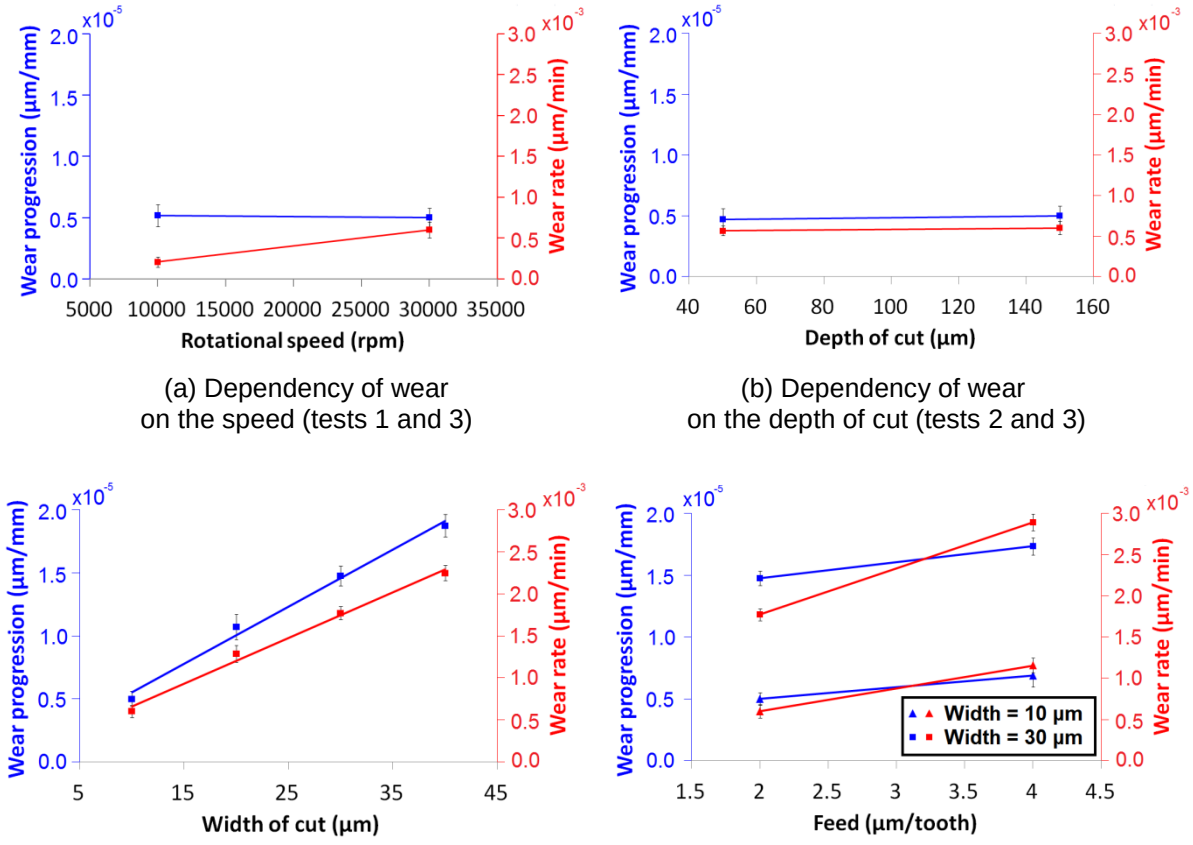

(a) Dependency of wear on the speed (tests 1 and 3)

(b) Dependency of wear on the depth of cut (tests 2 and 3)

(c) Dependency of wear on the width of cut (tests 3, 7, 4 and 8)

(d) Dependency of wear on the feed (tests 3 and 5, and tests 4 and 6)

Fig. 8.3: Illustration of wear progression and wear rates for different cutting conditions

The second most influential parameter is the feed. The resulting wear progressions and wear rates are plotted in fig. 8.3d. It is noticeable that the effect of feed is significantly lower than the effect of the width of cut. This, however, does not fit to an original expectation that feed will be the most influential parameter. This expectation was basically based on an

assumption that feed will have dominant effect on cutting forces which is one of the major factors affecting wear. For this reason are in fig. 8.4 plotted the initial cutting forces measured during these experiments. It is evident that also the initial cutting forces are dominantly affected by the width of cut. The second most important factor affecting the initial cutting force is the feed. It can be also noticed that the increased depth of cut leads to higher initial cutting forces. However, wear measured with different depths of cut do not show any change. This can be explained by larger length of cutting edge engaged during cutting. Thus, the force is distributed over a larger area, and therefore, the elemental force is not increased. Hence, because the depth of cut does not affect the elemental force it should not have any significant effect on tool wear.

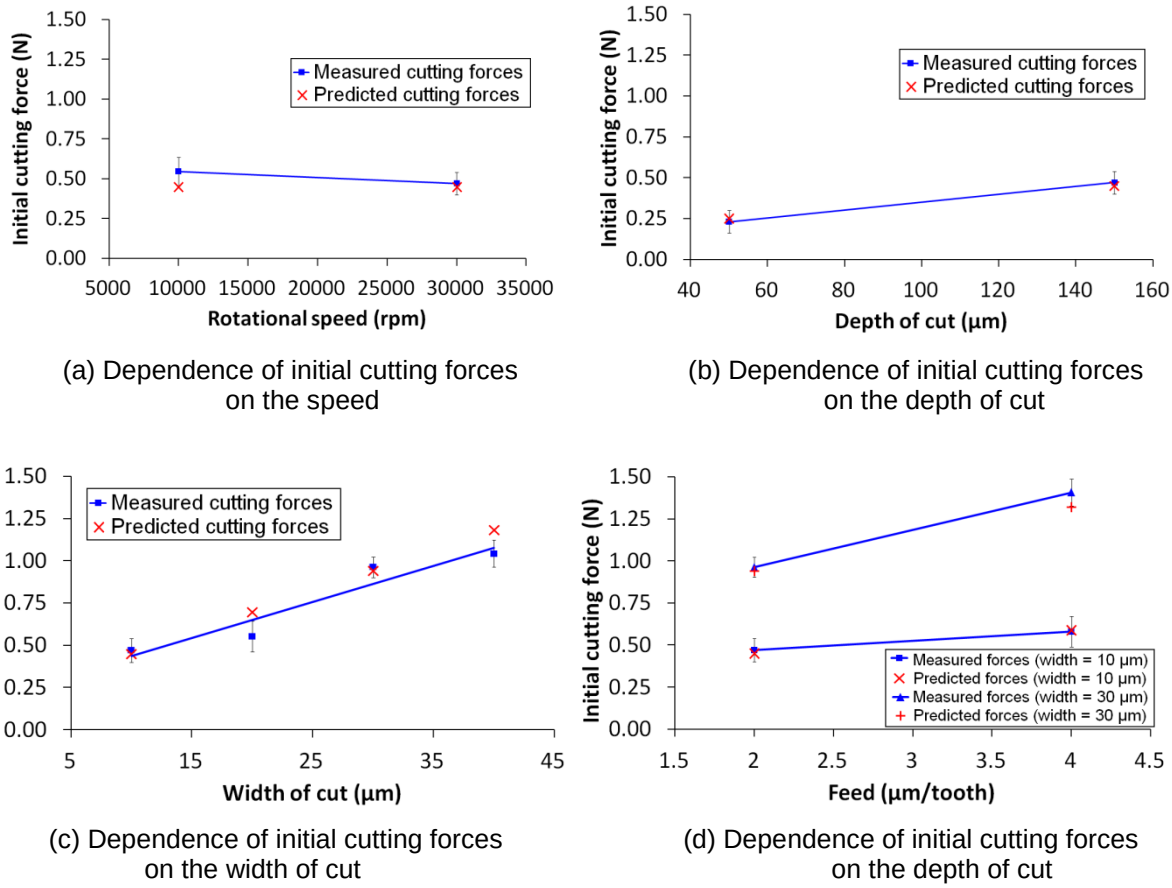

(a) Dependence of initial cutting forces on the speed

(b) Dependence of initial cutting forces on the depth of cut

(c) Dependence of initial cutting forces on the width of cut

(d) Dependence of initial cutting forces on the depth of cut

Fig. 8.4: Illustration of cutting forces for different cutting conditions

The last factor (rotational speed) has a reducing effect on the initial cutting force. This is presumably because the higher speed leads to higher cutting temperatures which can cause

material softening. However, because the temperatures in micro milling are generally low, the effect of the rotational speed is insignificant.

Hence, finally the wear progression empirical model can be determined. Because the experimental data shows only two influential factors (the width of cut and the feed) and both of them have linear effects on tool wear, linear model with two inputs can be used. The equation for prediction of tool wear will then have the following form:

$$c_w = c_1 \cdot f_z + c_2 \cdot a_e + c_3 \cdot f_z \cdot a_e + c_4 \tag{8.6}$$

In this equation are four coefficients which must be determined experimentally. Hence, the minimum number of experiments needed is four. By substituting feeds, widths of cut and cutting radius reductions from tests 3, 4, 5 and 6 are achieved the following values of the coefficients: $c_1 = 7.64 \cdot 10^{-7}\ mm^{-1}$, $c_2 = 4.53 \cdot 10^{-7}\ mm^{-1}$, $c_3 = 1.75 \cdot 10^{-8}\ \mu m^{-1}\ mm^{-1}$ and $c_4 = -1.41 \cdot 10^{-6}\ \mu m\ mm^{-1}$. The graphical interpretation of the relation among the coefficient c_w, the feed and the width of cut is shown in fig. 8.5.

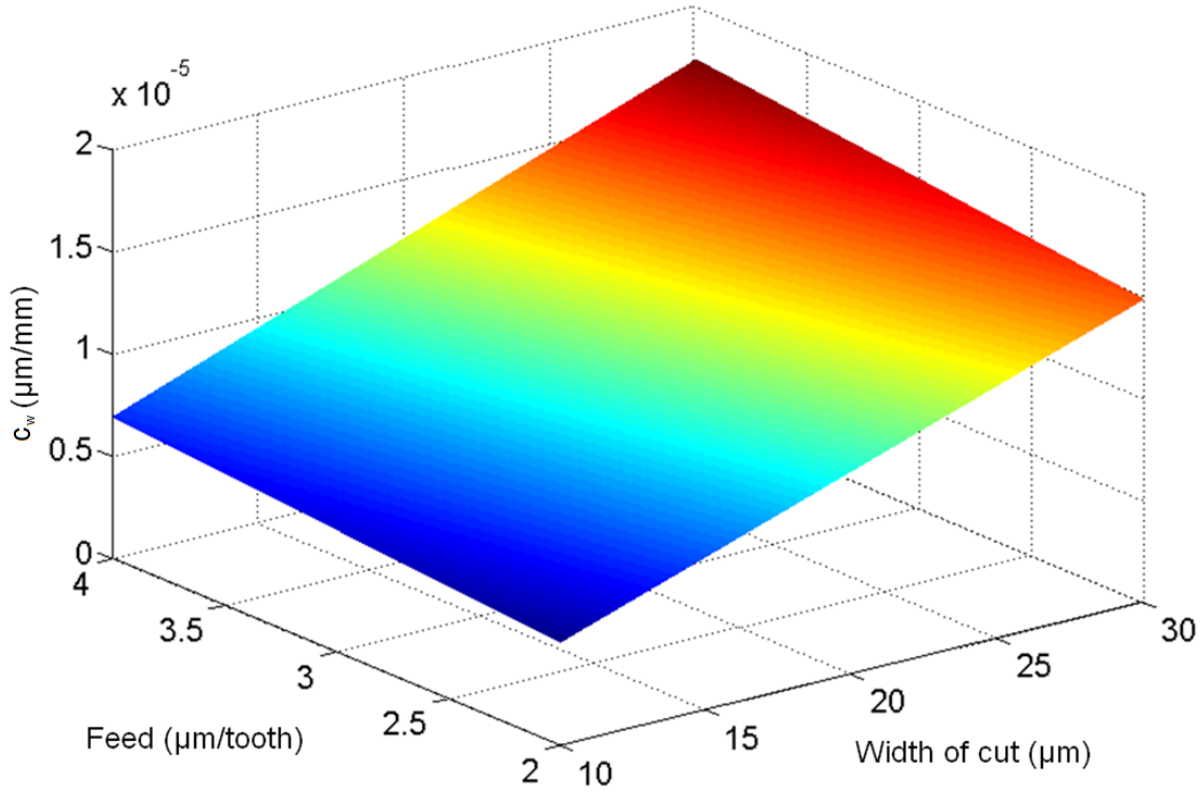

Fig. 8.5: Illustration of the dependency of the wear progression on the feed and the width of cut

Hence, finally the cutting radius reduction for any milling distance can be calculated from the following equation:

$$\Delta R_c = (c_1 \cdot f_z + c_2 \cdot a_e + c_3 \cdot f_z \cdot a_e + c_4) \cdot (l - l_0) + \Delta R_{c0} \tag{8.7}$$

Where l_0 is the milling distance at the end of the previous manufacturing phase and ΔR_{c0} is cutting radius reduction corresponding to l_0. These two members of the equation are relevant only in the case of variable cutting parameters or in the case of large tools (when the wear progresses with different rates in different phases – see fig. 8.2).

8.2.4 Relation between wear progression and cutting forces

In this moment are calculated the initial cutting force and the wear progression. However, for tool life prediction the force must be related to milling distance. For this purpose it is necessary to relate the cutting force increment to tool wear (which is already linked to the milling distance by equation 8.7). Mathematical expression relating the wear with the cutting force used in this research was derived by Archard in 1953 [127, 128]. The Archard wear equation is the most usually used wear model. It is a simple model relating wear volume (V) with a normal load applied on the wear surface (F_N) and sliding distance (s), see equation 8.8. The coefficient K is a material constant which must be determined experimentally.

$$V = K \cdot F_N \cdot \mathrm{s} \tag{8.8}$$

It should be noticed that the normal load applied on the relief land represents only a portion of the total cutting force. However, because the experiments performed in chapter 5 has confirmed no measurable effect of tool wear on the cutting edge radius, it may be assumed that the force related with chip formation is not affected by tool wear. Hence, the main reason for increment of the force is in the growing contact area on the relief land (the normal load is a product of the contact area and the contact pressure). Therefore, it is assumed that the Archard equation can be used for prediction of the total force increment.

Determination of wear volume

First of all must be determined the wear volume. The approximate volume is a product of the depth of cut (a_p) and the cross-sectional wear area (A_w). The mathematical expression of this product is the following:

$$V = a_p \cdot A_w \tag{8.9}$$

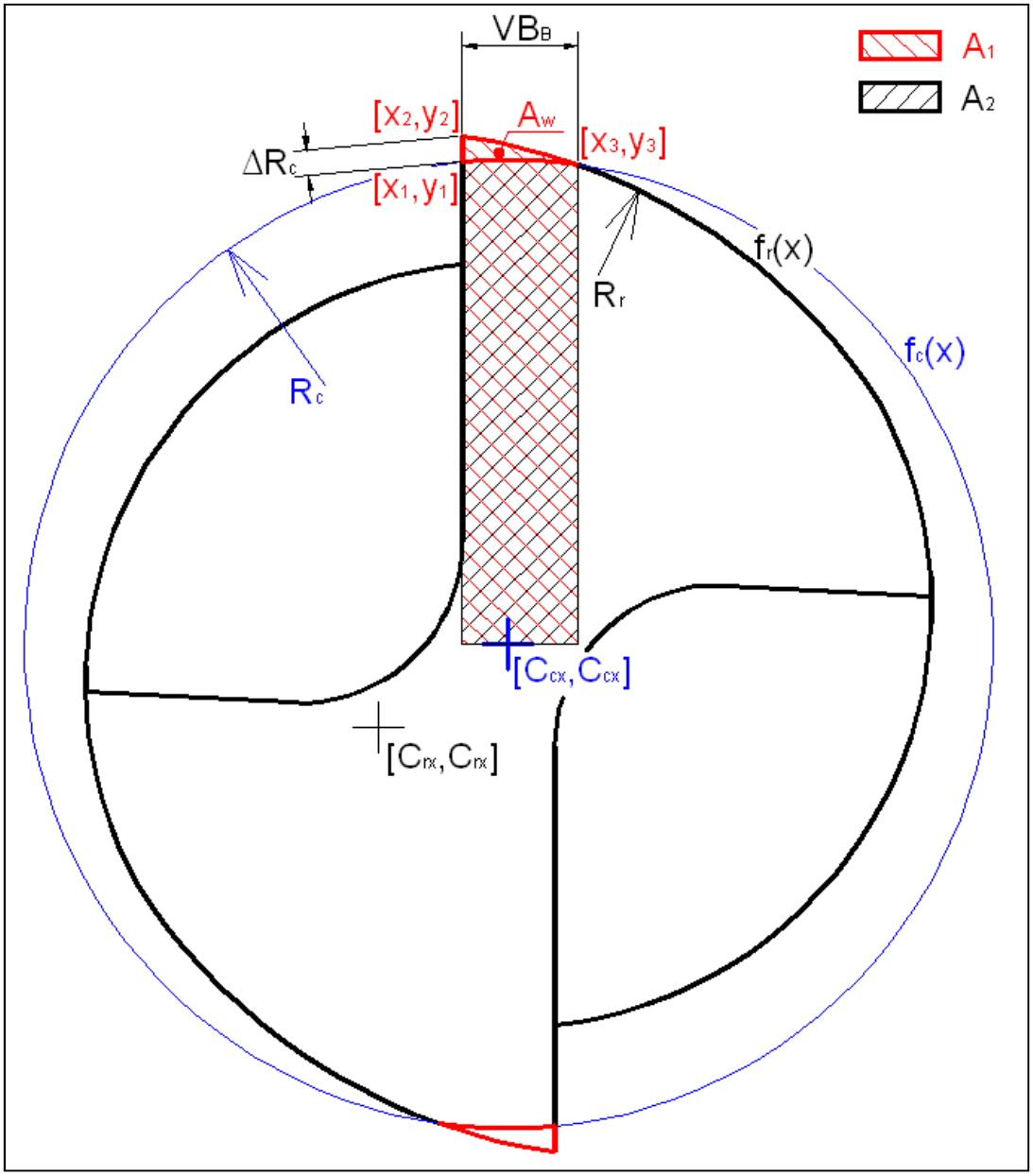

Fig. 8.6: Illustration of tool cross-section with highlighted dimensions relevant for wear volume calculations

Because the depth of cut is known, the only challenge is to calculate the cross-sectional wear area. For this purpose must be measured two tool features. The first feature needed for determination of the cross-sectional wear area is the centre of the tool cross-section (this is represented in fig. 8.6 by point C_c). The second needed feature is the profile of the relief land (represented by f_r in the fig. 8.6). The relief profile has usually circular shape, and therefore, it can be determined by its centre (C_r) and radius (R_r).

The other three important points highlighted in fig. 8.6 are:

- Intersection of rake face and actual cutting diameter [x_1, y_1],
- Original cutting edge tip [x_2, y_2], and
- Intersection of relief face and actual cutting diameter [x_3, y_3].

Hence, the wear cross-sectional area (A_w) can now be calculated from the following equation:

$$A_w = A_1 - A_2 = \int_{x_1}^{x_3} f_r(x) \cdot dx - \int_{x_1}^{x_3} f_c(x) \cdot dx \tag{8.10}$$

where $f_c(x)$ is defined by the actual cutting diameter ($D_c=2\cdot R_c$) with its centre [C_{cx}, C_{cy}] lying on the axis of rotation, and f_r is a relief face of the tool defined by its centre [C_{rx},C_{ry}] and radius (R_r). Because both of these functions are circular they can be described by the following equation:

$$f(x) = C_y + \sqrt{\mathrm{R}^2 - (\mathrm{x} - \mathrm{C_x})^2} \tag{8.11}$$

By integration of the equation 8.11 will be achieved the following equation for area bellow circular curve:

$$A_i = \left[C_y \cdot x + \frac{R^2}{2} \cdot asin\left(\frac{x - C_x}{R}\right) + \frac{R}{2} \cdot (x - C_x) \cdot \sqrt{1 - \left(\frac{x - C_x}{R}\right)^2} \right]_{x_1}^{x_3} \tag{8.12}$$

Hence, by substituting C_x, C_y and R by the measured values (C_{cx}, C_{cy}, R_c and C_{rx}, C_{ry}, R_r) the wear volume can be calculated. However, before it can be done, x_3 must be calculated.

Because this point represents an intersection of two circles (relief land profile and cutting edge path) it can be calculated from the following system of equations:

$$(x - C_{cx})^2 + \left(y - C_{cy}\right)^2 = {R_c}^2 \tag{8.13a}$$

$$(x - C_{rx})^2 + \left(y - C_{ry}\right)^2 = {R_r}^2 \tag{8.13b}$$

Another, more suitable, form of the equations 8.13 is the following:

$$x^2 + a_1 \cdot x + y^2 + b_1 \cdot y + c_1 = 0 \tag{8.14a}$$

$$x^2 + a_2 \cdot x + y^2 + b_2 \cdot y + c_2 = 0 \tag{8.14b}$$

where $a_1 = -2 \cdot C_{cx}$, $b_1 = -2 \cdot C_{cy}$, $c_1 = C_{cx}^2 + C_{cy}^2 - R_c^2$, $a_2 = -2 \cdot C_{rx}$, $b_2 = -2 \cdot C_{ry}$ and $c_2 = C_{rx}^2 + C_{ry}^2 - R_r^2$.

By subtracting the equation 8.14b from equation 8.14a will be achieved an expression of *y* in the following form:

$$y = d + e \cdot x \tag{8.15}$$

where $d = \frac{(c_2 - c_1)}{(b_1 - b_2)}$ and $e = \frac{(a_2 - a_1)}{(b_1 - b_2)}$.

And finally, by substituting the equation 8.15 to the equations 8.14a will be achieved a quadratic equation from which can be calculated desired x_3. This quadratic equation will have the following form:

$$(1 + e^2) \cdot x^2 + (2 \cdot d \cdot e + b_1 \cdot e + a_1) \cdot x + (c_1 + d^2 + b_1 \cdot d) = 0 \tag{8.16}$$

Determination of sliding distance

The sliding distance is a distance over which the cutting edge is in a contact with the workpiece. The total sliding distance can be calculated from the following equation:

$$s = \frac{l}{number\ of\ flutes \cdot f_z} \cdot s_{single} \tag{8.17}$$

where l is the total milling distance and s_{single} is the sliding distance of a single cut as it is illustrated in fig. 8.7. Because the cutting edge path is approximately circular, the s_{single} can be calculated as a length of circular section, which is given by the following equation:

$$s_{single} = \varphi \cdot R_c = acos\left(\frac{R_c - a_e}{R_c}\right) \cdot R_c \tag{8.18}$$

Hence, the final form of the equation 8.17 will be the following:

$$s = \frac{acos\left(1 - \frac{a_e}{R_c}\right) \cdot R_c}{number\ of\ flutes \cdot f_z} \cdot l \tag{8.19}$$

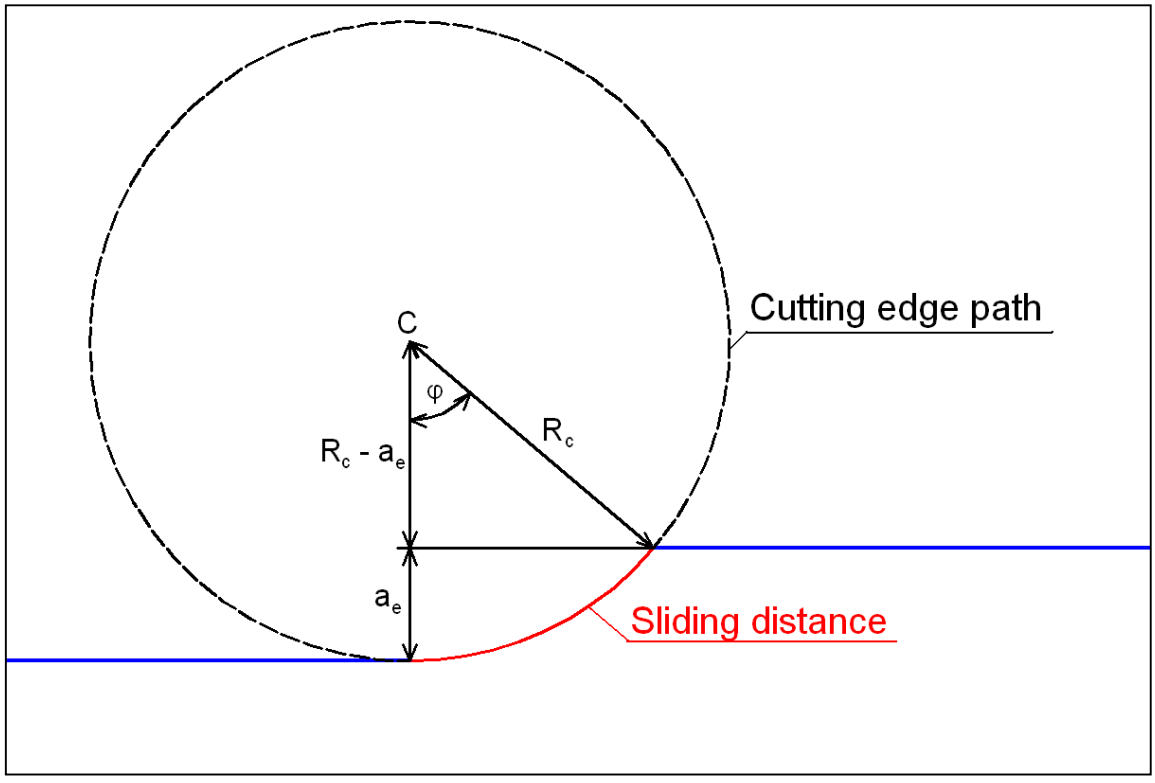

Fig. 8.7: Determination of sliding distance of a single cut

Determination of the coefficient *K*

The last member of the equation 8.8 which must be determined is the coefficient *K*. In this method is the *K* calculated from the following equation:

$$K = \frac{\Delta V}{\Delta s \cdot \Delta F_N} \tag{8.20}$$

where the symbol Δ means increment.

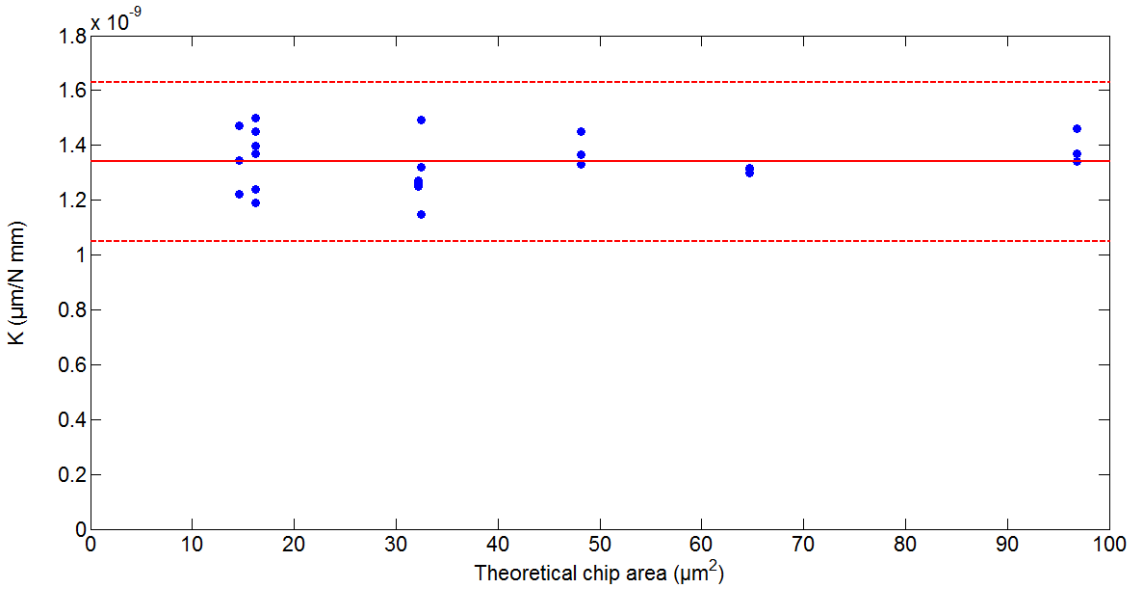

Fig. 8.8: Illustration of the relation between coefficient *K* and theoretical chip area

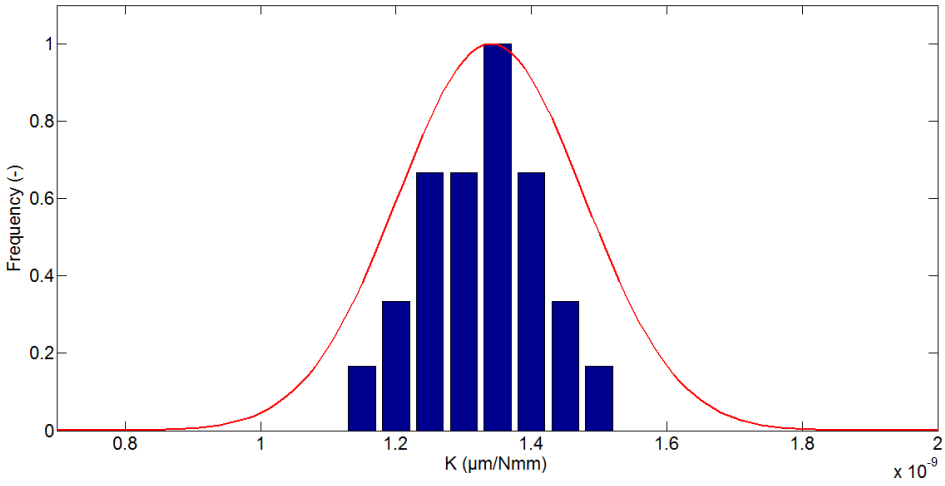

Fig. 8.9: Histogram of the coefficient *K*

The coefficient *K* was calculated for all experiments performed in this chapter. The results are plotted in fig. 8.8 as a function of the uncut chip thickness. It is evident that the coefficient *K* is independent on the uncut chip thickness. However, the calculated values show significant variations. The average value of K is $1.34 \cdot 10^{-9}$ µm^3 N^{-1} mm^{-1} and its standard deviation is $9.64 \cdot 10^{-11}$ µm^3 N^{-1} mm^{-1}. The statistical distribution of the coefficient K

is shown in fig. 8.9. From comparison of the empirical data with a theoretical distribution function is evident that the coefficient tends to have the normal distribution. Hence, a theoretical distribution can be calculated from equation 8.21; where $\overline{K}$ is the average value and Kstd is the standard deviation.

$$p(K|\overline{K}, K_{std}) = \frac{1}{K_{std} \cdot \sqrt{2 \cdot \pi}} e^{\frac{-(K-\overline{K})^2}{2 \cdot {K_{std}}^2}} \tag{8.21}$$

Total cutting force acting on a worn tool

As it was mentioned at the beginning of this section, the increment of the total cutting force is due to larger contact area. Hence, the force needed for generation of a chip remains approximately the same for the new as well as for the worn tool. The only force which is increasing due to tool wear is the normal (F_N) and the frictional force (F_T) acting on the tool relief face as it is illustrated in fig. 8.10. The normal force is acting approximately in radial direction and its magnitude is a product of contact pressure (p_N) and contact area ($A_{contact}$). The frictional force is proportional to the normal force and acts in the tangential direction. Because the contact area increases with tool wear, it is evident, that both of these forces will also have tendency to grow.

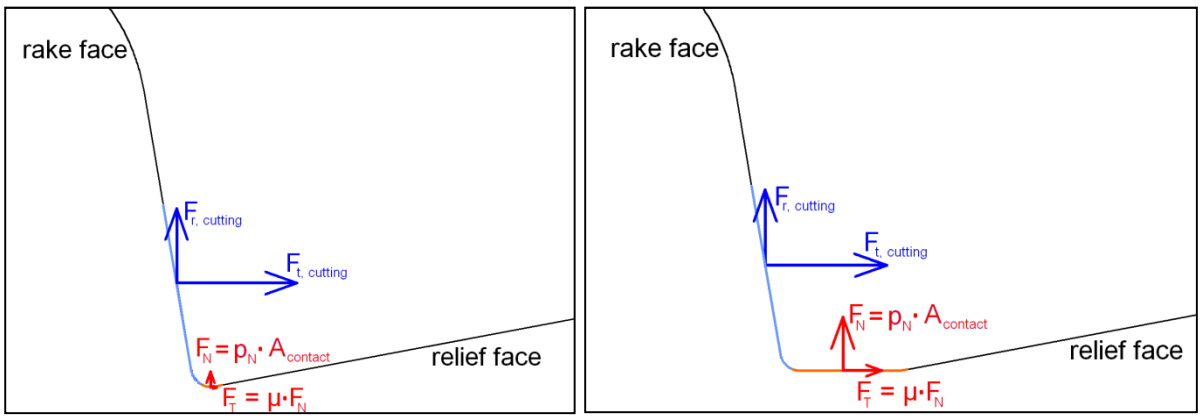

(a) Forces acting on a new tool (b) Forces acting on a worn tool

Fig. 8.10: Histogram of the coefficient *K*

Hence, the total force acting on the tool is a vectorial summation of the cutting force, the normal force and the frictional force (equation 8.22). The coefficient of friction used in this research for calculation of the frictional force is taken from Concise Metal Engineering Data Book [129] and its value is 0.5.

$$\vec{F} = \vec{F}_N + \vec{F}_T + \vec{F}_{r,cutting} + \vec{F}_{t,cutting} + \vec{F}_{a,cutting} \tag{8.22}$$

8.2.5 Prediction of maximum stress

Hence, in this moment the force as a function of milling distance can be calculated. This is very useful information and can be easily compared with experimental data. However, the forces themselves do not show anything about tool performance. As it was discussed in the previous chapter, micro end-mills show large dimensional tolerances. This results in a broad range of maximum stresses within unique tools. Hence, it is evident that the quantity which can be used for tool life prediction is the maximum bending stress and not the cutting force.

The stresses are calculated by static FEA in the same manner as it was described in chapter 7. The tool is loaded by maximum cutting force which is distributed over the cutting edge. This is done for both minimum and maximum core diameters. Once this is done, the average maximum stress (equation 8.23) and the standard deviation (equation 8.24) can be calculated.

$$\overline{\sigma^1} = \frac{\sigma^1_{\max core} + \sigma^1_{\min core}}{2} \tag{8.23}$$

$$\sigma^1_{std} = \frac{\sigma^1_{\max core} - \overline{\sigma^1}}{3} \tag{8.24}$$

Because the measured tool dimensions show normal statistical distribution, and because the stress calculations are based on a linear analysis, it is evident that also the maximum bending stress will be normally distributed. Therefore, it is not needed to repeat the stress analysis for each possibility, and its distribution can be calculated from the following equation:

$$p\left(\overline{\sigma^1}\middle|,\ \sigma^1_{std}\right) = \frac{1}{\sigma^1_{std}\cdot\sqrt{2\cdot\pi}}\, e^{\frac{-\left(\sigma^1-\overline{\sigma^1}\right)^2}{2\cdot\ {\sigma^1_{std}}^2}} \tag{8.25}$$

Furthermore, because the static FEA is based on a solution of linear equations system, it is assumed that it is not necessary to calculate the stresses for every set of the cutting conditions. However, the cutting conditions affect the force distribution over the cutting edge and consequently location and direction of the resultant cutting force. Hence, the relation

between inputs (cutting conditions) and outputs (stresses) must be investigated. For this reason stresses evoked by application of various cutting conditions were calculated. Six different feeds (1 µm/tooth to 6 µm/tooth), six different widths of cut (10 µm to 100 µm) and six depths of cut (10 µm to 200 µm) were analysed in all possible combinations. Hence, 216 different sets of cutting conditions were analysed. The feed varies with a period of 216, the width of cut with a period 36 and the depth of cut with a period of 6. All these tests were analysed as for the tool with the largest core diameter (0.142 mm) as for the tool with the smallest core diameter (0.122 mm).

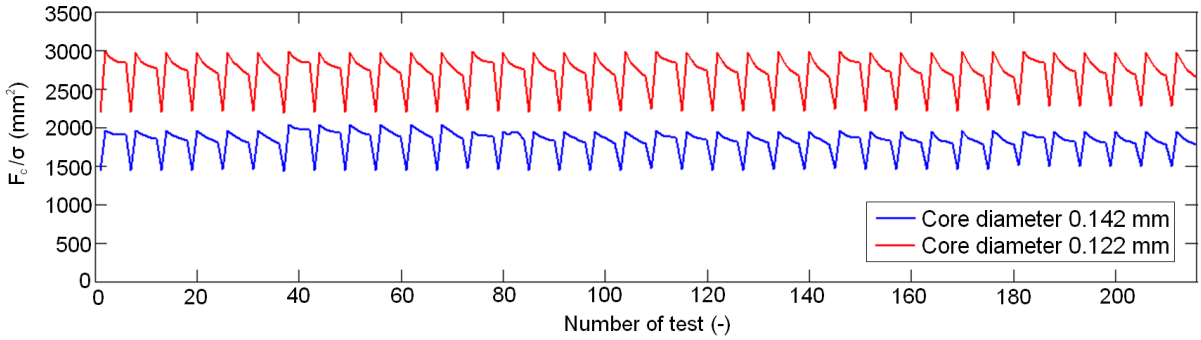

Fig. 8.11: Ratios between the cutting forces and inner stress

Once the stresses are calculated ratios between maximum cutting forces and maximum tensile stresses are analysed. The ratios for both, the smallest and the largest core diameter, are plotted in fig. 8.11. Both functions show clear period of 6 tests. This period corresponds to variation of the width of cut. However, some small differences between the "teeth" are distinguishable. Therefore, autocorrelation analysis was performed, see fig. 8.12. This analysis shows that the ratio is not affected by feed, and also the effect of the width of cut is negligible. The depth of cut is only input with a strong effect on this ratio. Furthermore, a difference between the ratios calculated for tools with the largest and the smallest core diameters remains constant.

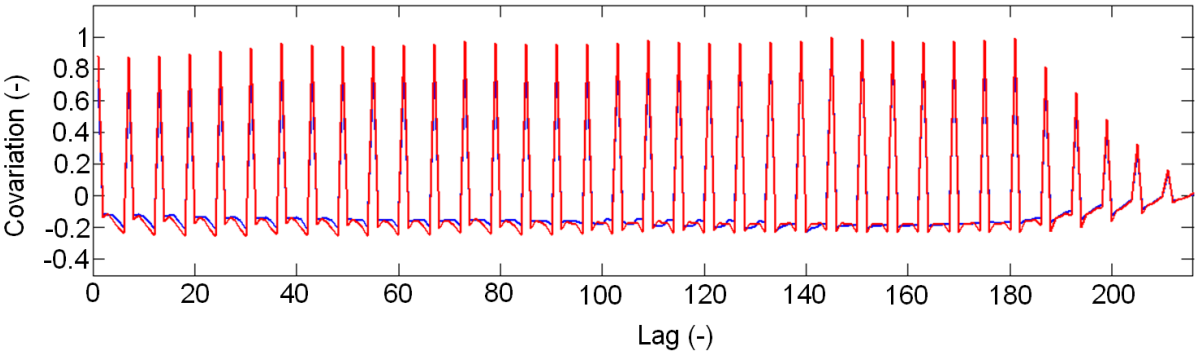

Fig. 8.12: Autocorrelation analysis

This is a very important finding for the analysis of the effect of tool wear. The feed does not affect the direction of the resultant force, and the width of cut has only a minor effect on the direction of the resultant force. Therefore, it may be concluded that the ratio between the forces and the stresses is mainly affected by the distribution of the applied force over the cutting edge. And because tool wear does not affect this distribution and has only a little effect on the force direction, the stresses within the worn tool do not require further FEA and they can be easily calculated from equation 8.26.

$$\sigma^1_{worn} = \frac{F_{worn}}{F_{new}} \cdot \sigma^1_{new} \tag{8.26}$$

These findings help to reduce the number of FEAs (and consequently computational time) needed for prediction of tool life.

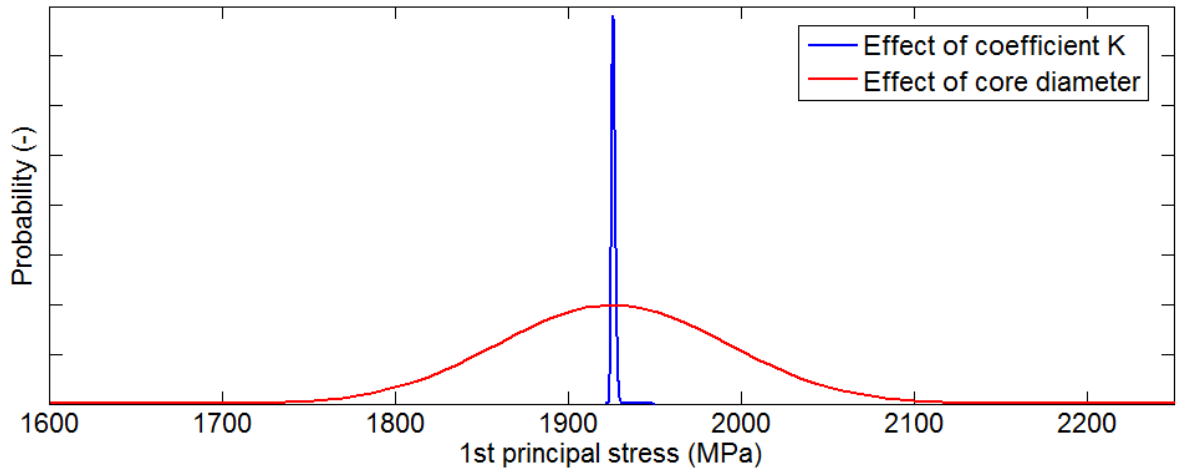

Fig. 8.13: The effects of the *K* and the core diameter on the range of possible stresses

Another important issue is that the stresses are affected by many input factors. They can be divided into two main groups: the tool dimensional tolerances and the effects causing variations of the cutting forces. In this research are used only two inputs in the manner of probability distribution: the coefficient *K*, used in calculation of the forces acting on the worn tool, and the tool core diameter. Each of them affects the resulting stresses. However, their importance is different. The stress variations caused by the variation of the *K* coefficient and the core diameter are illustrated in fig. 8.13. It is evident that if the variation of the core diameter has much stronger effect on the resultant bending stresses than the coefficient *K*. Actually, if the *K* coefficient would be assumed to be a constant (single value) it would not cause any significant error in the prediction of tool life. On the other hand, the variation of the core diameter causes theoretical variation of the resultant stress in a range of approximately 400 MPa. Hence, it is clear that this effect cannot be ignored.

Hence, in the case of these two inputs only one (core diameter) has a significant effect on the stress variation. However, real micro milling process is affected also by many other factors which may be assumed as statistically variable (other tool dimensions, effects of workpiece micro structure, coating variations, effects of lubrication, tool run-out etc.). For example, if the effects of two inputs on the stress variation would be the same, the total range of possible stresses would be three times wider than the range of the stresses caused by a single variable input.

Calculation of the probability of maximum stress appearance

Hence, it is important to explain how the probability of maximum stress appearance is calculated. In fig. 8.14 is the approach illustrated on an example where two different variable inputs are assumed. In the first phase are calculated the probability distributions of the input parameters (e.g. two different tool dimensions). These distributions are achieved from the tool dimensional measurements as it was explained in the previous chapter. In fig. 8.14a are these probability distributions represented by the blue functions. From these distributions are for FE stress analysis are from these distributions important only four cases. The first case for which the stresses need to be calculated is a tool with the minimal first input and the minimal second input. In the second case is the first input minimal and the second input maximal. In the third case the first input is maximal and the second input is minimal. And finally, in the

last case the first input is maximal and the second input is also maximal. Once FE models for each of the above given cases are prepared, the maximum stresses are calculated. Then the probability distributions are calculated from the equations 8.23 to 8.25. In fig. 8.14a are these probability distributions illustrated by the red functions.

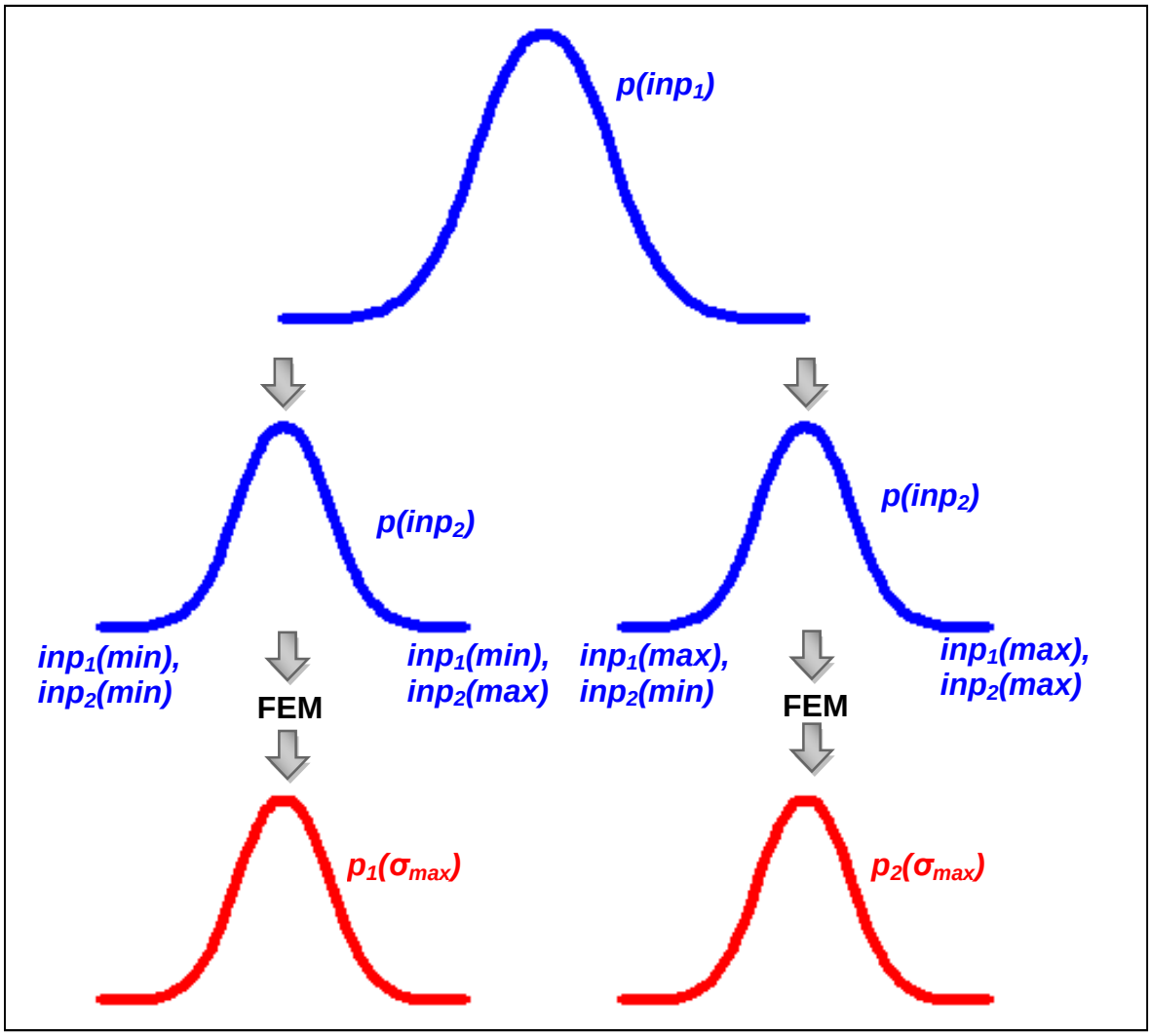

(a) Phase 1: Calculation of limiting stress distributions

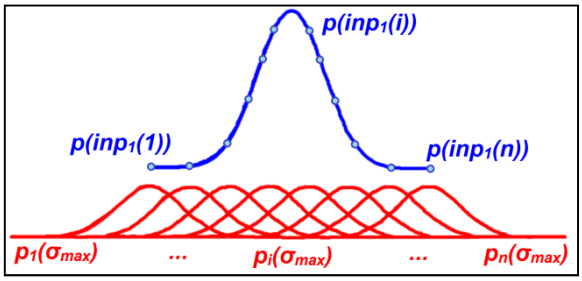

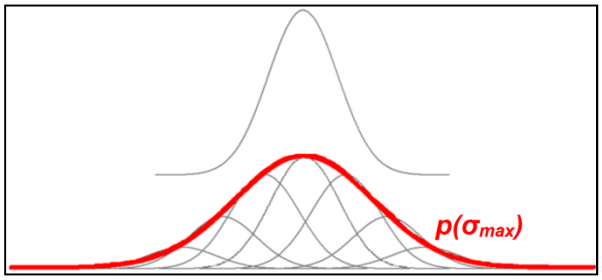

(b) Phase 2: Calculation of other stress distributions

(c) Phase 3: Consideration of the first input probability distribution

Fig. 8.14: Principle of calculation of statistically distributed maximum stress

In the second phase are calculated all the other stress probability distributions. This phase is illustrated in fig. 8.14b. In a general case, the range of $p_1(\sigma_{max})$ will be different from the range of $p_2(\sigma_{max})$. This is because of a non-linear relation between the maximum stress and tool dimensions (e.g. the maximum stress of a cantilever beam reduces with 3rd power of the beam diameter and grows with 2nd power of the beam length). Hence, in the ideal case, all the other probability distributions should be calculated by FEA in the same manner as the maximum stress probabilities for the limiting dimensions. This would, however, require extensive computational time. Therefore, a simplification in a form of an assumption of a linear growth of the probability range is proposed to be used. This simplification will obviously cause an error in skewness (see fig. 8.15) of the total probability distribution. However, because this error has no effect on the possible minimum and maximum possible σ_{max}, it is assumed to be acceptable. In this phase should be followed this approach:

1. Calculate the range of the possible maximum stresses for the first probability distribution (minimum input 1).
2. Calculate the range of the possible maximum stresses for the second probability distribution (maximum input 1).
3. Define the range of stresses for which shall be calculated the probability distributions. This range is restricted by the average σ_{max} from the first and second probability distribution.
4. Calculate constant a defining increment of the probability range. This is done from the following equation:

$$a = \frac{average\left(\sigma^1_{max,2}\right) - average\left(\sigma^1_{max,1}\right)}{range_2 - range_1} \tag{8.27}$$

5. Define step size $\Delta\sigma_{max}$.
6. Sweep through the possible stresses from $average\left(\sigma^1_{max,2}\right)$ to $average\left(\sigma^1_{max,1}\right)$ with step $\Delta\sigma_{max}$ and calculate the relevant probability distributions as followed:
    a. Average possible σ_{max}:

$$\text{average}(\sigma_{\max}(i)) = \Delta\sigma_{\max}(i-1) + \Delta\sigma_{\max} \tag{8.28}$$

b. Minimum possible σ_{max}:

$$\min\left(\sigma_{\max}(i)\right) = \text{average}\left(\sigma_{\max}(i)\right) - \frac{a \cdot range_1}{2} \tag{8.29}$$

c. Maximum possible σ_{max}:

$$\max\left(\sigma_{\max}(i)\right) = \text{average}\left(\sigma_{\max}(i)\right) + \frac{a \cdot range_1}{2} \tag{8.30}$$

d. Theoretical standard deviation from equation 8.24.

e. Probability distribution for i-th step from equation 8.25.

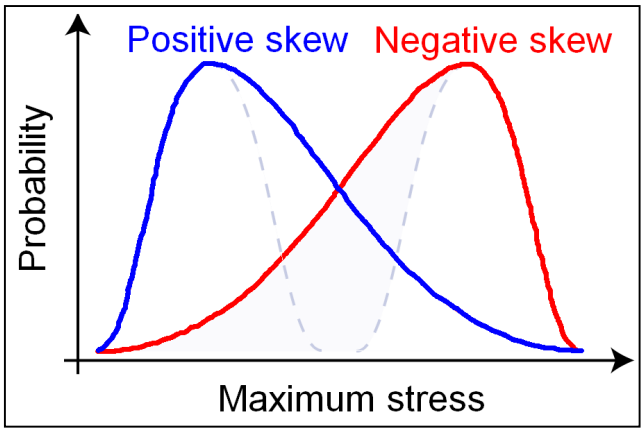

Fig. 8.15: Illustration of the skewed probability function

Finally, in the last stage the total probability distribution of the maximum stress appearance is calculated. This is done in the following three steps:

1. Each of the distributions calculated in the previous phase is multiplied by corresponding probability of appearance of the first input (see fig. 8.14c – grey functions).
2. Then the combined probability distribution is calculated by summing the probabilities of appearance of each possible maximum stress. Hence, the probability of appearance of the relevant maximum stress can be calculated from the following equation:

$$p(\sigma_{max}^{1}(j)) = \sum_{i=1}^{n} p_i(\sigma_{max}^{1}(j)) \tag{8.31}$$

3. However, it is evident that the calculated probability will not give in total 100%. This is because each of the separate probability distributions gives in total 100%. Hence, the sum of all probabilities will be a product of number of used probability distributions and 100%. Furthermore, each of the probability distributions was already scaled by the probability of the first input in the step. Hence, it is evident, that the resultant probability distribution calculated from equation 8.31 must be "scaled". For this reason is used the following equation for each of the possible σ_{max}:

$$p(\sigma_{max}^{1}(i)) = \frac{p(\sigma_{max}^{1}(i))}{\int p(\sigma_{max}^{1}) \cdot \mathrm{d}\sigma_{max}^{1}} \tag{8.32}$$

8.2.6 Prediction of tool breakage

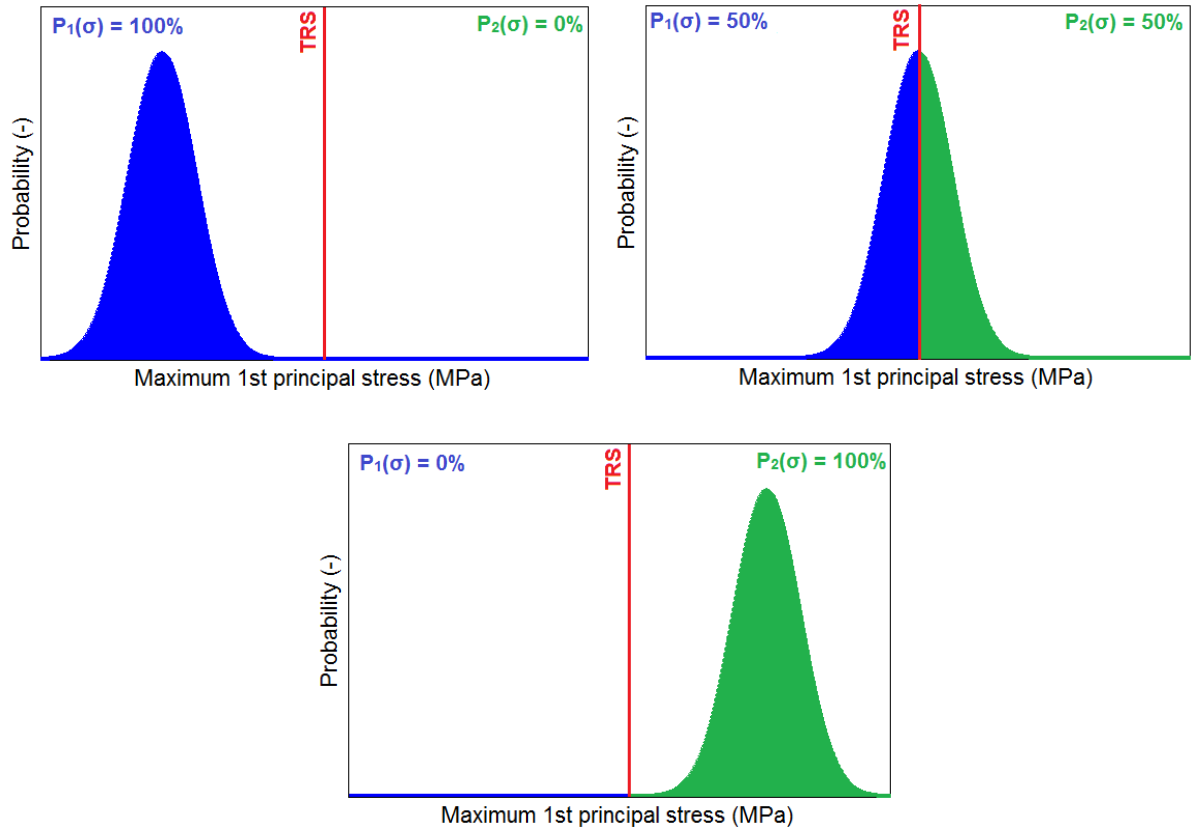

Fig. 8.16: Determination of tool breakage

Finally, the risk of tool breakage as a function of milling distance (time) is calculated. This is done by comparison of maximum stress probability distribution with a breakage criterion for every time step. This is repeated until all theoretical stresses reach the criterion. Same as in the previous chapter, transverse rupture strength (TRS) is used as the criterion. Three different situations are illustrated in fig. 8.16. In the first case all possible stresses are lower than TRS, and hence, the probability (risk) of tool breakage is 0%. In the second case some of the possible stresses are lower and some other higher than TRS. Hence, the risk of tool breakage is higher than 0% but lower than 100%; the specific case illustrated in the figure shows 50% risk of tool breakage. The third illustrated case shows the situation when all possible stresses are higher than TRS. Hence, the risk of tool breakage is 100%.

The risk of tool breakage for each step is then equal to cumulative probability function which can be calculated from the following equation:

$$P(\sigma_{max}^{1}) = 100\% \cdot \int_{TRS}^{\infty} p(\sigma_{max}^{1}) \cdot \mathrm{d}\sigma_{max}^{1} \tag{8.33}$$

The solution of the equation (8.33) is then illustrated in fig. 8.17.

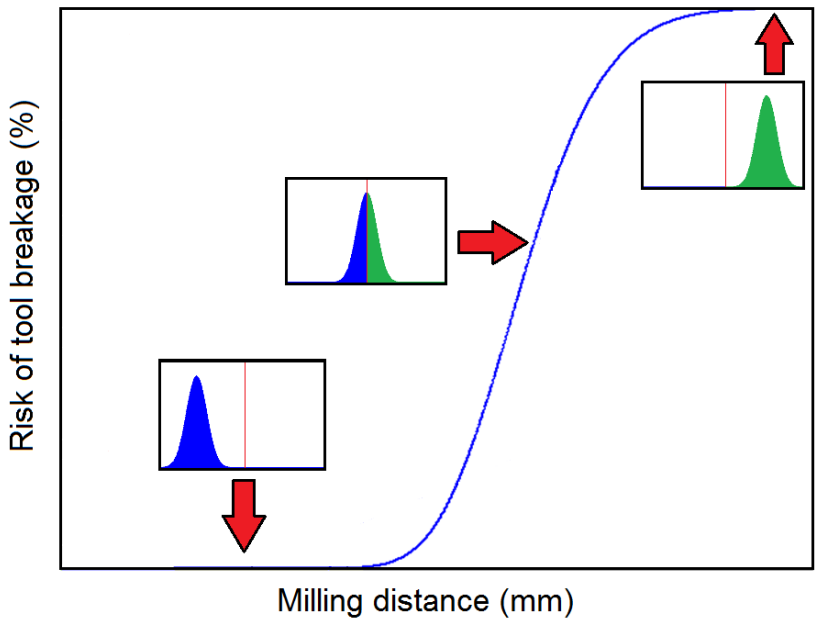

Fig. 8.17: Illustration of a typical risk function of tool breakage

8.3 Method validation

Validation is an important part of this chapter. It is essential to prove the validity of the method. However, evidently a comprehensive validation would require tests with a large number of repetitions (ideally hundreds of repetitions). This is basically because of the statistical character of the method. Furthermore, the validation should be conducted with many different cutting conditions to prove its versatility. This is, however, not possible to do in this research due to high costs of micro end-mills and long experimental times. Therefore, only a limited validation is performed here. However, the validation tests were chosen as they would cover as large variety of cutting conditions as possible.

Tool wear, cutting forces (dependent on the milling distance), maximum stresses and tool life are predicted for three different sets of conditions and then compared with experimentally achieved data. The cutting conditions used in these tests are listed in tab. 8.2. To achieve a statistically relevant data each of the tests was repeated 15 times. Although this number of repetitions is still relatively low for reliable statistical study, it is assumed to be a good compromise between economical factors of the experiments and the achieved information. Because the force model used in this research is not sensitive to the rotational speed and also the experimental study in 8.2.3 shows no significant effect of the speed, only one speed is used in all experiments. All the other parameters are varied from very high values (e.g. $a_p = 100\ \mu m$) down to very low values (e.g. $a_p = 10\ \mu m$).

Tab 8.2: Cutting parameters used for verification

	Feed (µm/tooth)	Width of cut (µm)	Depth of cut (µm)	Speed (rpm)
Test 1	2	10	50	30 000
Test 2	4	20	100	30 000
Test 3	2	90	10	30 000

8.3.1 Results and discussion

In the first step of this study are calculated initial cutting forces. The calculated values and measured values are compared in tab. 8.3. The measured values are in all analysed cases in a good agreement with the measured forces. The relative error does not exceed ±10% in any of the cases. This indicates a suitability of the force model for the tool life prediction.

Tab. 8.3: Comparison of measured and calculated initial cutting forces

	Average measured cutting forces (N)	Calculated cutting force (N)	Relative error
Test 1	0.198	0.181	-8.58%
Test 2	0.685	0.705	2.92%
Test 3	0.129	0.121	-6.20%

Another important quantity which is analysed in this study is wear progression. The measured and calculated wear (in form of reduction of cutting radius) is plotted in fig. 8.18. The measured data are the average values and the error bars represent standard deviations. In all three cases the calculated wear is in a good agreement with the measured data. However, it should be noticed that a large variation of the measured wear was found. This variation is, however, not captured by the currently used wear model. It is assumed that the variation can affect the tool life in the same manner as the tool dimensional tolerances. Therefore, the effect of wear variation should be further studied in the future, and if necessary another model should be proposed.

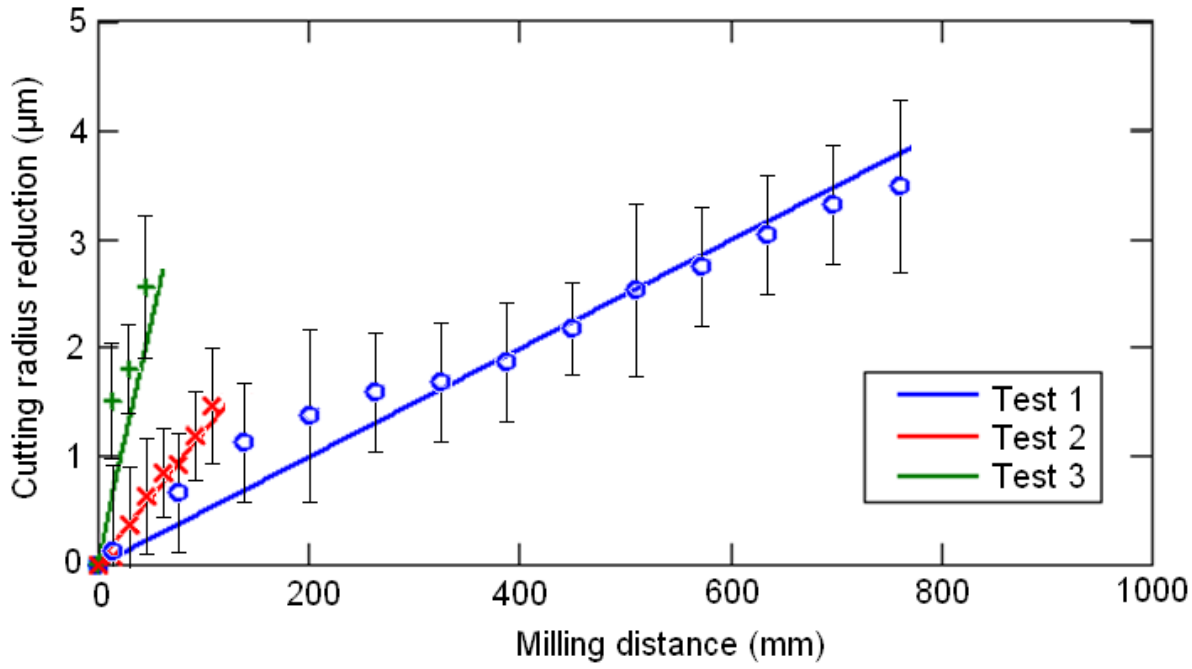

Fig. 8.18: Comparison of calculated and measured wear

In the next step of the method is calculated maximum cutting force as a function of milling distance. This is the first step in which is applied a probabilistic approach. Therefore, the results are presented as a probability distribution of the maximum cutting forces for different

milling distances. In fig. 8.19 are plotted the predicted and the measured distributions of the maximum cutting forces for the first set of the cutting conditions for three different milling distances: 100 mm, 500 mm and 1 000 mm. The measured cutting forces are presented in a form of counts the maximum cutting force in one of five equally distributed bins.

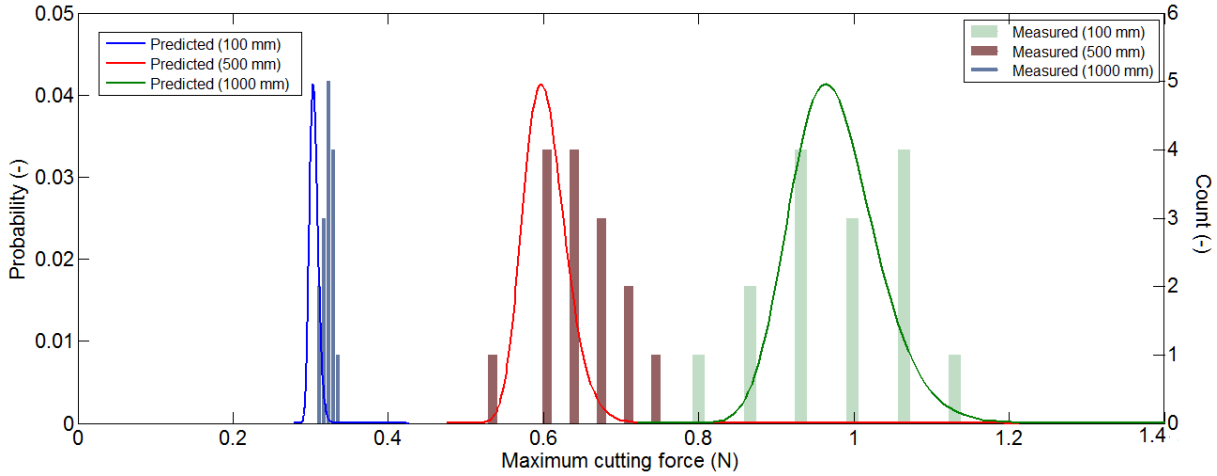

Fig. 8.19: Comparison of the predicted and measured cutting forces acting on the worn tools; test 1

In all three analysed cases the measured forces are in a good agreement with the predicted ones. However, for milling distance of 100 mm the predicted forces are shifted down against the measured values (the average of predicted values is 0.03 N lower than the average of the measured values). After the milling distances of 500 mm and 1 000 mm the agreement of the predicted and measured forces is significantly better. Similar agreements of the results were also achieved with the other two test cases. Hence, it may be concluded that the method gives valid predictions of the cutting forces for various milling distances.

Once the cutting forces are estimated for different milling distances, the stress analysis can be performed. The calculated stresses, however, cannot be compared with experimental data because these are impossible to measure.

In fig. 8.20 are plotted the maximum bending stresses for test 1. Same as in the case of cutting forces, the stress probability distributions for three different milling distances are shown (100 mm, 500 mm and 1 000 mm). TRS is also shown in the figure. As it was already explained above, the TRS represents a critical value over which the tool is predicted to break. It is evident that for the first two milling distances none of the possible stress is higher than

TRS. Hence, in these two cases the probability of tool breakage is zero. However, in the case of the third milling distance (1000 mm) some of the possible stresses are already higher than TRS. This means that some of the tools are likely to break.

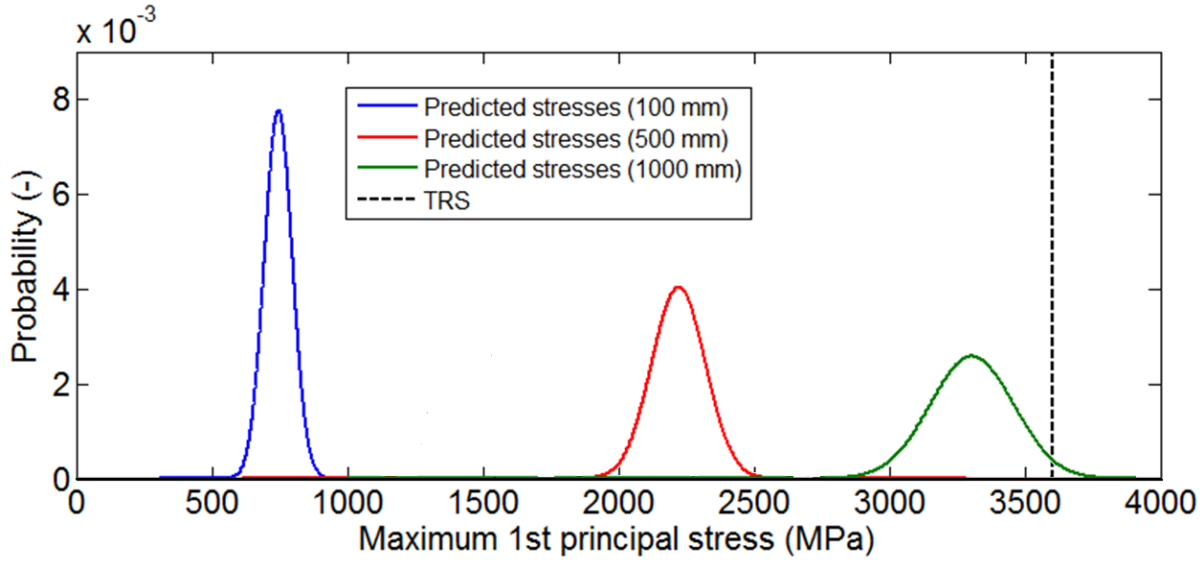

Fig. 8.20: Calculated maximum bending stress, test 1

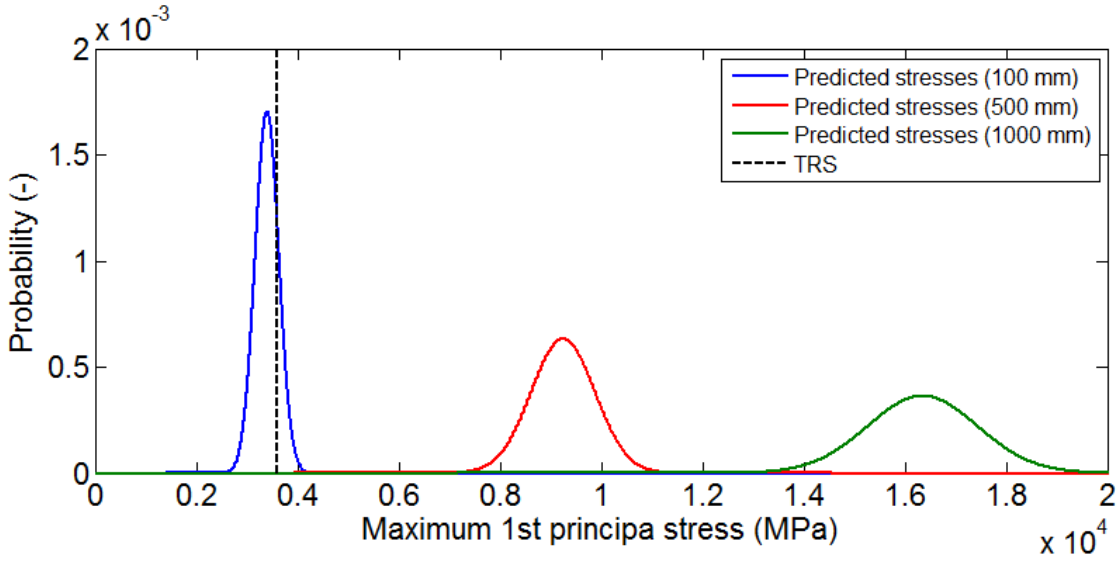

Fig. 8.21: Calculated maximum bending stress, test 2

In the second test case more aggressive cutting conditions are used. Hence, the tools will break much sooner. This is confirmed by the graph plotted in fig. 8.21. In this particular case, all tools are expected to break before reaching milling distances of 500 mm. At the reality there is already approximately 25% probability that the tool will break after milling distance

of 100 mm. Even worse situation can be observed when the third set of cutting parameters is used, see fig. 8.22. In this case, nearly all tools are predicted to break before reaching milling distance of 100 mm.

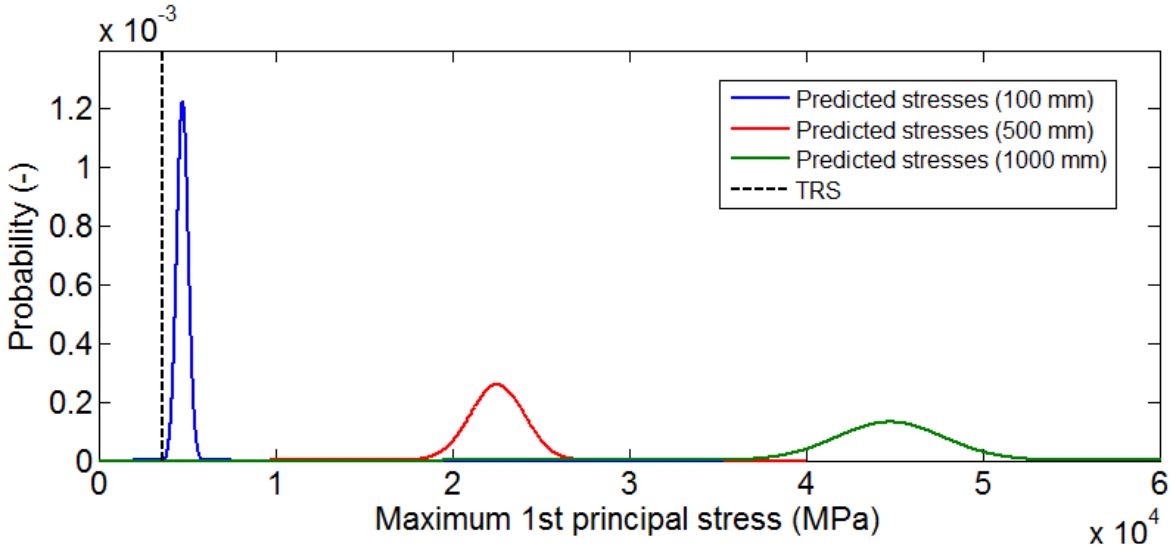

Fig. 8.22: Calculated maximum bending stress, test 3

Based on the stress calculations, tool life is predicted. The measured and calculated lives for all three tested cases are compared in tab. 8.4 and fig. 8.23. The predicted and measured tool lives are in all three cases in a good agreement. However, some of the real tools fail out of the predicted range. It is assumed, that the prediction accuracy can be further improved by including the effects of the other dimensional tolerances (flute length, cutting diameter, cutting edge termination geometry etc). This is, however, a topic for the future research.

Tab. 8.4: Comparison of measured and predicted tool lives

	Cutting distance	**Broken tools**	
		Predicted	Measured
Test 1	610 mm	0 %	7 % (1 tool)
	970 mm	25 %	20 % (3 tools)
	960 mm	50 %	40 % (6 tools)
	1060 mm	75 %	80 % (12 tools)
	1690 mm	100 %	93 % (14 tools)
Test 2	70 mm	0 %	13 % (2 tool)
	105 mm	25 %	20 % (3 tools)
	115 mm	50 %	53 % (8 tools)
	130 mm	75 %	93 % (14 tools)
	210 mm	100 %	100 % (15 tools)
Test 3	60 mm	0 %	13 % (2 tool)

	70 mm	25 %	40 % (6 tools)
	75 mm	50 %	86 % (13 tools)
	78 mm	75 %	100 % (15 tools)
	105 mm	100 %	100(15 tools)

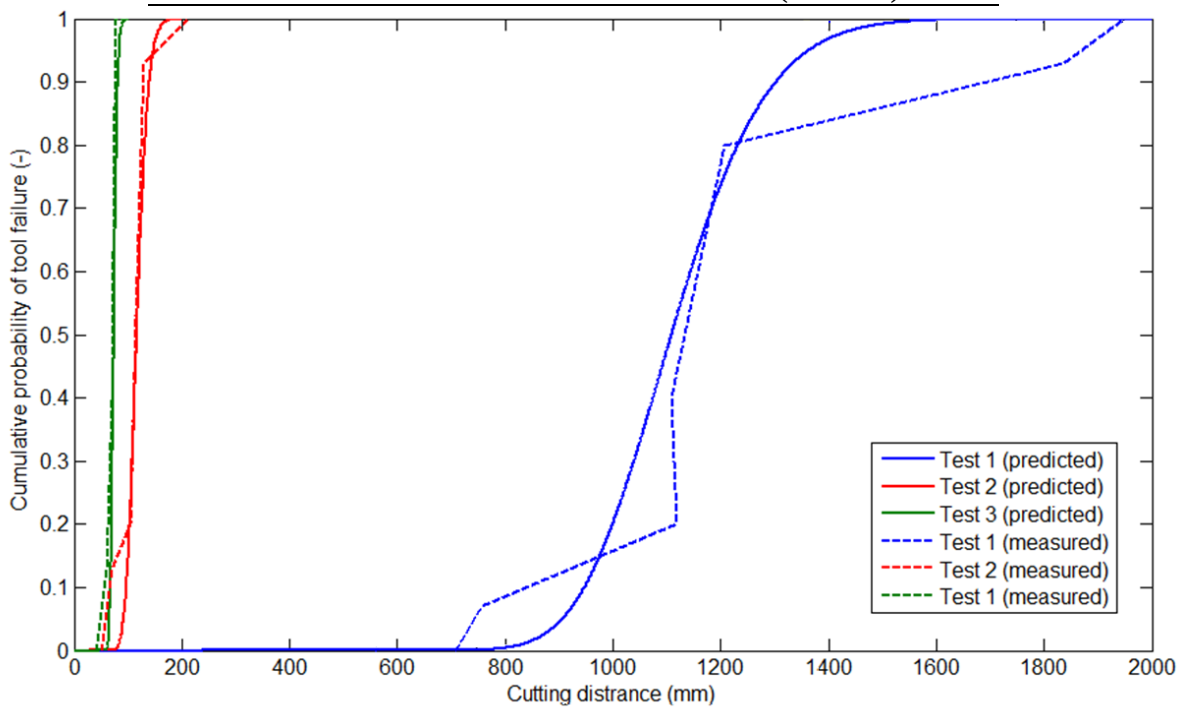

(a) Whole range

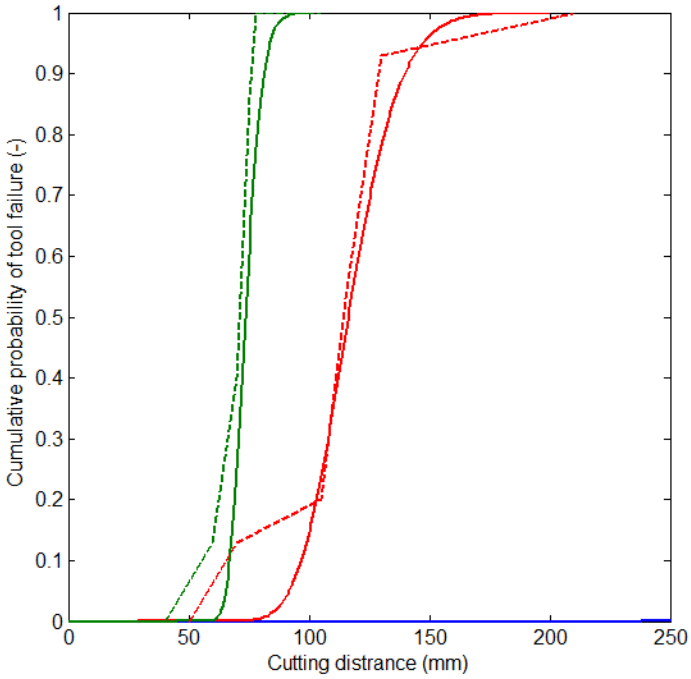

(b) Detail

Fig. 8.23: Illustration of predicted and real tool lives

Finally, volume removed per a single tool was calculated for all three tested cases. If the first set of cutting conditions is used, the tool is predicted to break after removing 0.31 mm^3 - 0.84 mm^3. In the case of the second set of cutting parameters the removed volume is 0.14 mm^3 - 0.42 mm^3. In the last case one tool removes 0.054 mm^3 - 0.095 mm^3. Hence, it is clear that by choosing the first set of cutting conditions the highest material volume per tool can be removed. On the other hand, the risk zone is the largest one. This information is extremely important for cost estimation.

8.4 Summary

In this chapter was presented a new tool breakage prediction method. The method is based on a theoretical modelling with consideration of tool/process tolerances. Unlike any other prediction method, this method gives statistical results instead of a critical distance (distance after which all tools are expected to break). Hence, the user receives information about the risk of tool breakage and the decision if he will accept that risk is up to him. The method is assumed to help production engineers to plan their manufacturing strategies and estimate the final product costs and manufacturing times. The method can also be implemented into cutting parameters optimisation algorithms which can help to set up the most efficient cutting strategies. Such application of the method is, however, not yet developed and represents a challenge for the future research.

The theoretical results achieved by the presented method were compared with three sets of experiments. In all tested cases the theoretical results well agreed with the experimental ones. This indicates a reliability of the method. However, further validation is still required for more complex manufacturing strategies. Especially a case with variable input parameters (e.g. two different widths of cut are applied sequentially on one tool) should be tested. Before the method can be applied for this type of applications, it still needs further improvements. The main issue of the current method is the prediction of tool wear. If tool life for micro milling with variable depth of cut is of interest the wear must be predicted for small sections of the cutting edge. Hence, discretised model similar to the one used for cutting force should be used.

However, although the method still needs improvements and some of the models may be reconsidered in future, it represents the first method able to predict micro end-mill life. The

main contribution of knowledge of this method is in application of currently available deterministic models together with a probabilistic approach. Hence, the novelty is in expressing tool life as a risk of tool breakage.

Furthermore, the issue of process uncertainties is common for all micro-manufacturing processes. Therefore, it is assumed that some of the principles presented in this chapter can also be applied to other processes. For example in the case of micro wire EDM, the wire width has its tolerances which affect significantly wire vibrations and breakage. Hence, clearly the probabilistic approach should be applied.

9. Methodology for micro end-mill design

In this chapter is introduced a methodology for micro end-mill design. This methodology is based on the knowledge gained during this research and explains the most important issues related to the tool design. In the first section of this chapter is discussed the current state and its deficiencies. This discussion justifies the need of a new systematic approach. In the second section are then discussed the main factors which must be considered during the tool design. This is followed by the methodology and explanation of its steps. In the final part of this chapter is provided a case study showing an application of the methodology.

9.1 Motivation and objectives

Up to now it was explained in this thesis that scaling down of the tool brings new challenges such as: premature tool breakage, large dimensional tolerances etc. In the previous chapters these effects were studied on typical commercial tools. These tools, however, do not reflect the special needs of micro milling. At the beginning of this research were compared two different types of end-mills. The first tool type was a micro end-mill with diameter of 0.2 mm as the second tool type had the diameter of 1 mm. From SEM images acquired during this research was found that both tool types look the same and that the Ø0.2 mm tools are only proportionally scaled down, see fig. 9.1. This was also confirmed by a study of tools available in the market. The suppliers offer the same tool types for both micro and macro scales (see literature review presented in chapter 2).

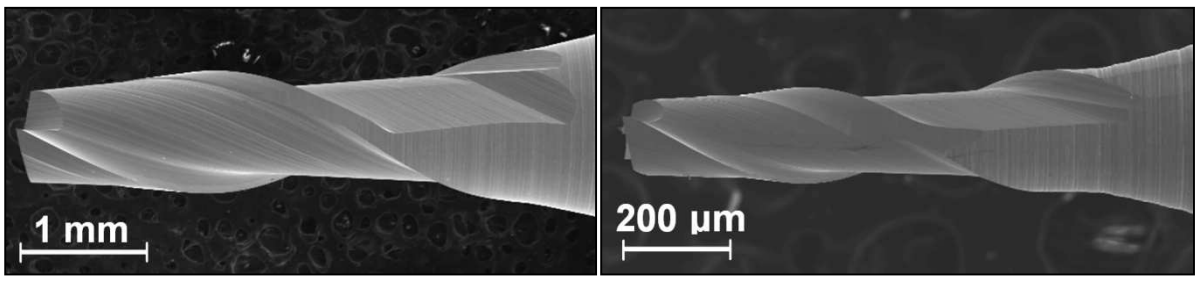

(a) Ø1 mm end-mill (b) Ø0.2 mm end-mill

Fig 9.1: Comparison of Ø0.2 mm and Ø1 mm end-mills

The author of this thesis, however, believes that the tool design is an important factor affecting tool performance, and therefore, much higher attention should be paid to this topic. A systematic and knowledge based designing method is crucial for successful industrial

applications of micro milling. The systematic approach considering all scaling effects and micro milling challenges was, however, not found in literature. Therefore, the main objective of this chapter is:

To develop a systematic and knowledge based method for design of micro end-mills.

9.2 Design challenges

The main issue of micro end-mills is that the current tools are not designed with respect of their needs. It is generally believed that what works in macro scale will also work in micro scale. However, In many cases this is not truth. There are many differences between micro and macro milling. These differences are usually not caused by different mechanisms but by their different importance. Some of the effects which can be easily ignored in macro scale have devastating effects in micro scale. On the other hand some effects which are important in macro scale are insignificant in micro scale. Therefore, in this section are discussed different factors and their effects.

9.2.1 Bending stiffness and maximum bending stress

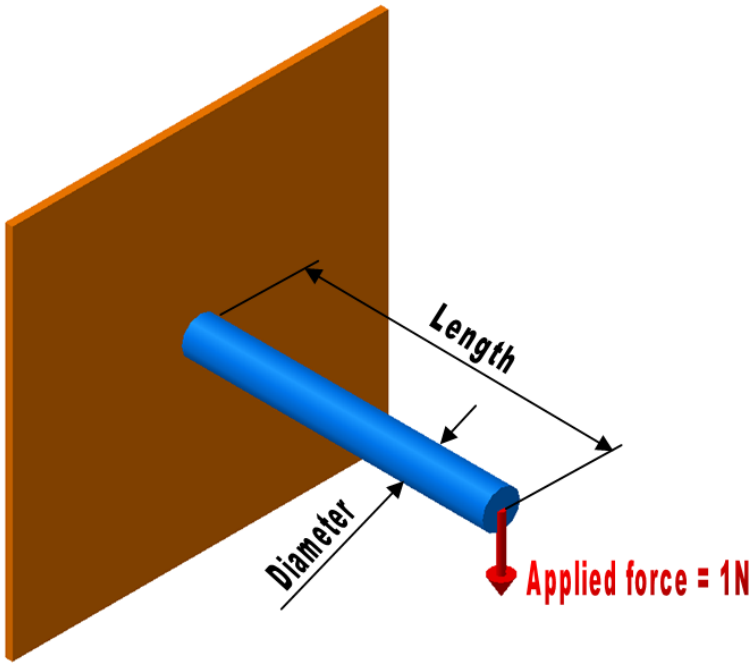

Fig 9.2: Illustration of a cantilever beam

As it was already explained in the previous chapters, maximum bending stress is the main factor affecting tool breakage. In the previous chapters stress distribution was calculated by FEM and the maximum stress was compared with TRS (if the maximum stress is higher than TRS, the tool is assumed to break). However, it was not yet explained how it is related to the tool diameter and the tool length. For this reason an analytical solution of maximum stress in a cantilever beam with a circular cross-section, as it is illustrated in fig. 9.2, is used here. Although the real tool shape is much more complex, this simple example can indicate an importance of the tool dimension effects on tool breakage.

The maximum bending stress of this simple beam can be calculated analytically from equation 9.1, where F is the applied force, d is the beam diameter and l is the beam length.

$$\sigma_{max} = \frac{F}{S_y} \cdot l^2 = \frac{32 \cdot F}{\pi \cdot d^3} \cdot l^2 \tag{9.1}$$

It is evident that with decreasing beam diameter and increasing beam length maximum stress (σ_{max}) will increase. For illustration the resulting stresses for beams with length of 1 mm and diameters from 0.1 mm to 1 mm are plotted in fig. 9.3a. Clearly the maximum stress rapidly increases with decreasing diameter. On the other hand, the beam length has a reverse effect. In fig. 9.3b is shown the maximum bending stress as a function of the beam length for beams with diameter of 0.2mm.

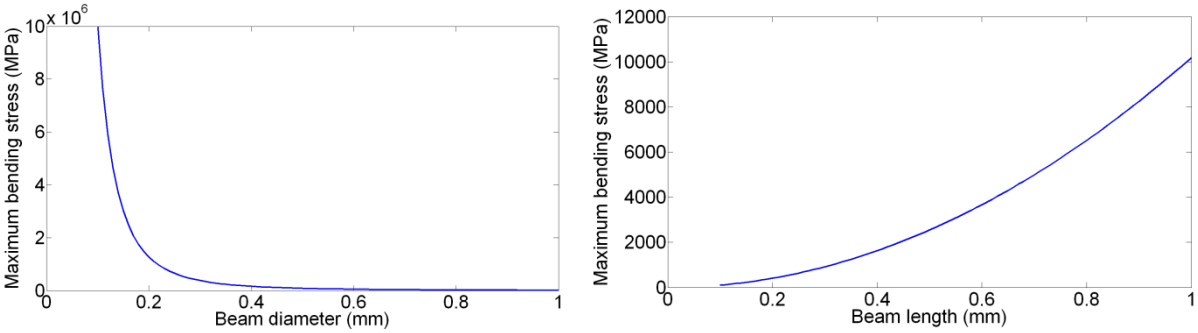

(a) Stress as a function of diameter; l = 1 mm (b) Stress as a function of length, D = 0.2 mm

Fig 9.3: Maximum bending stress as a function of a beam dimensions

Another important characteristic is tool stiffness. The lower stiffness results in larger tool deformations which can negatively affect the final product accuracy and generated surface quality. Therefore, it is important to keep stiffness as high as possible. However, similarly as

in the case of maximum bending stress, stiffness is also a function of tool dimensions. Relation 9.2 is used for calculations of bending stiffness of different cantilever beams and the resulting trends are then plotted in fig. 9.4. From the figure it is evident, that smaller beam diameter and the larger beam length result in lower stiffness. This trend is stronger in the case of very small diameters (e.g. stiffness of a beam with diameter of 0.5 mm is only 16 times lower than stiffness of a beam with 1 mm diameter, however, beam with diameter of 0.1 mm has already 626 times lower stiffness than beam with diameter of 0.5 mm) . Hence, it is evident that in the case of micro end-mills with diameters bellow ~0.3 mm a strong attention must be paid to this issue.

$$k = \frac{F}{\delta} = \frac{3 \cdot E \cdot I_y}{l^3} = \frac{3 \cdot \pi \cdot E \cdot d^4}{64 \cdot l^3} \tag{9.2}$$

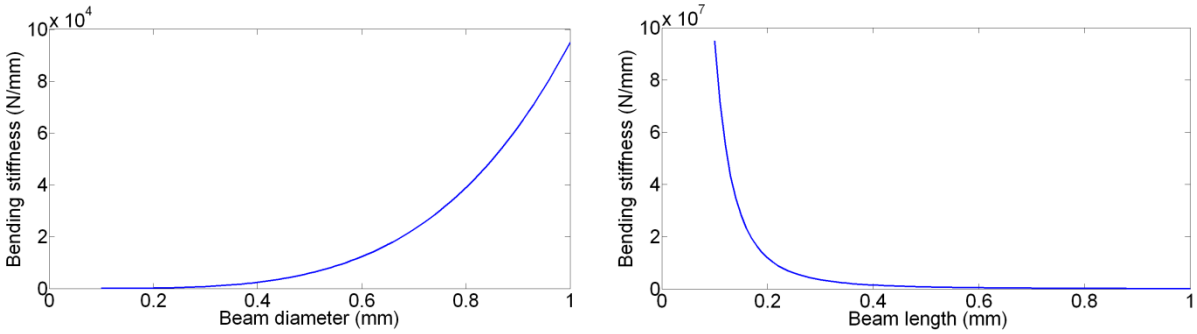

(a) Stiffness as a function of diameter; l = 1 mm (b) Stiffness as a function of length, D = 0.2 mm

Fig 9.4: Stiffness as a function of a beam dimensions

The last characteristic which can be illustrated on the cantilever beam is the natural frequency. Because milling is a dynamic process it is important to keep in mind dynamic properties of the tool. Tool chatter is a dangerous phenomenon which can cause unpredictable tool performance and even premature tool breakage. It is always good practice to keep the first natural frequency as high as possible. Furthermore, the natural frequencies may be used for recommendations of suitable speeds (the rotational frequency, and its multiplies, should never be closed to any of tool natural frequencies). The first natural frequency of a circular beam can be calculated from equation 9.3. This equation is applied to the same beam dimensions as in the previous two cases (maximum stress and bending stiffness) and the resulting trends are plotted in fig. 9.5. Evidently, with decreasing tool diameter and

increasing tool length the first natural frequency will tend to be lower. Hence, also in this case higher attention must be paid to the tool design in micro scale, than in macro scale.

$$n_0 = \frac{1}{2 \cdot \pi} \cdot \sqrt{\frac{k}{m}} = \frac{d}{8 \cdot \pi \cdot l^2} \cdot \sqrt{\frac{3 \cdot E}{\rho}} \tag{9.3}$$

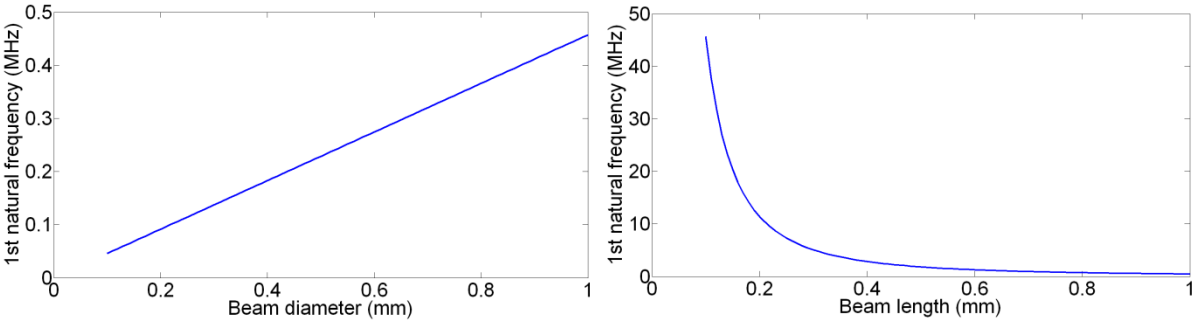

(a) 1st natural frequency as a function of diameter; l = 1 mm

(b) 1st natural frequency as a function of length, D = 0.2 mm

Fig 9.5: 1st natural frequency as a function of a beam dimensions

On the simple example of a cantilever beam were demonstrated three important issues related to micro end-mill design. The maximum bending stress, bending stiffness and the first natural frequency are three factors affecting tool breakage. Tools with very small diameters and long lengths (a typical micro end-mill) represent the worst possible case for all of them.

9.2.2 Rake angle and depth of flutes

Another important challenge is an appropriate design of tool cutting edges. Tt is important in any cutting process to keep cutting forces as low as possible. The higher forces result in higher tool wear and premature tool breakage. Therefore, it is absolutely essential to keep the forces in mind during tool design. However, because of various size effects and higher effect of the tool chatter it is more difficult to control the forces in micro scale than in macro scale. Common practice of cutting force reduction is using of a positive rake angle. It is well known fact, that positive rake angles result in shearing dominant cutting mechanism which generates lower forces than ploughing dominant cutting (typical for negative rake angles). It was already mentioned in chapter 2 that chip formation in micro scale differs from the one in macro scale. It is because of scaling down of the process, and therefore, increasing role of the

cutting edge radius. Chosen feed depends on the used tool, workpiece material and required surface quality. However, typical feeds in micro milling of steels are between 2 μm/tooth and 8 μm/tooth. The cutting edge radii of coated micro end-mills achievable by current technologies are usually between 1.5 μm and 2 μm. Hence, the dimensions of the uncut chip thickness and the cutting edge radius are closed to each other. This is very different from macro cutting where the cutting edge radius is usually significantly smaller than the uncut chip thickness, and therefore, the effect of the cutting edge radius can be neglected.

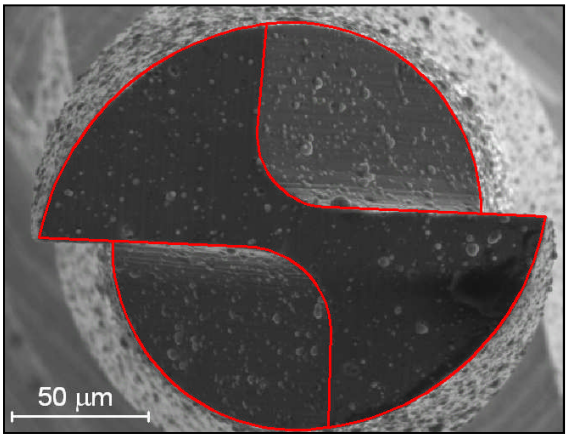

(a) Micro end-mill cross-section

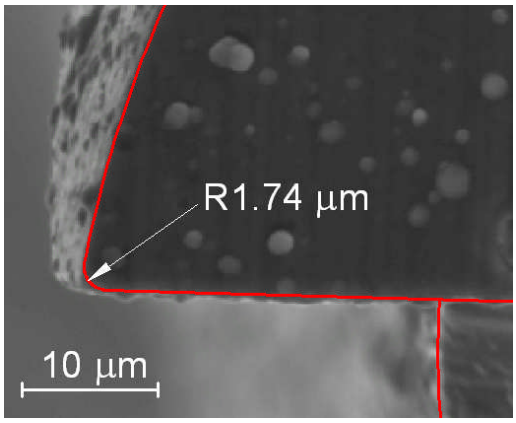

(b) Detail of the cutting edge

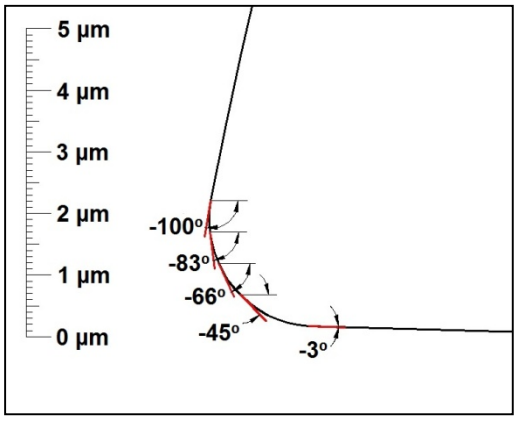

(c) Illustration of the rake angles over the cutting edge radius

Fig 9.6: Illustration of the rake angles in micro milling

In fig. 9.6 is shown a detail of a typical micro end-mill cutting edge. It is evident that the rake angle is gradually decreasing over the cutting edge radius. It is also difficult to define transition point between rake face and relief face. This makes it difficult to predict whether

the rake angle will have demanded effect on tool performance. Hence, an analysis of chip formation is an essential part of micro end-mill designing method. Comprehensive understanding of chip formation is also important for determination of minimum cutting flute depth and can help to prevent extensive cutting edge chipping. Furthermore, the results of the analysis can be used for recommendations of suitable cutting conditions (especially feeds).

Because of the small dimension and complex character of micro milling, it is difficult to analyse the chip formation experimentally. Therefore, chip formation FEA seems to be the most appropriate approach.

9.2.3 Tool unbalance effect

Another important issue is tool unbalance. Unbalance of any rotating part results in additional radial forces. The tool unbalance is mainly caused by the tool imperfections. However, in some cases the unbalance can be caused by the design itself, e.g. inappropriate single-flute tool design. An important question is how significant the unbalance forces are in the case of micro end-mills? For this purpose can be the unbalance modelled as a concentrated mass located on the tool cutting diameter. In this case the force can be approximately calculated from equation 9.4 where m_e is the unbalance mass in kilograms, r is the distance of the unbalance mass from the centre of rotation in millimetres and $\dot{\omega}$ is a rotational speed in rotations per minute.

$$F_r = \frac{m_e}{r} \cdot v^2 = \frac{4}{3.6 \cdot 10^6} \cdot m_e \cdot r \cdot \pi^2 \cdot \dot{\omega}^2 \tag{9.4}$$

It is evident that with increasing tool dimensions the unbalance mass and its distance from the centre of rotation will most likely increase. Therefore, in this section the tool unbalance mass is expressed as a ratio of the unbalance mass and the beam total mass (see equation 9.5). Same as in the previous section, the effect of the tool unbalance is illustrated on the case of a cantilever beam.

$$\frac{m_e}{m_{beam}} = \frac{m_e}{\pi \cdot r^2 \cdot l \cdot \rho} = 0 \div 0.5 \tag{9.5}$$

The r in the equation 9.5 is equal to the beam diameter (equal to the cutting diameter of the tool), l is the beam length and ρ is the density ($\rho_{WC\text{-}Co} = 14\ 653\ kg \cdot m^{-3}$).

Finally a deflection (δ) of the beam can be calculated from equation 9.6.

$$\delta = \frac{F_r}{k} \tag{9.6}$$

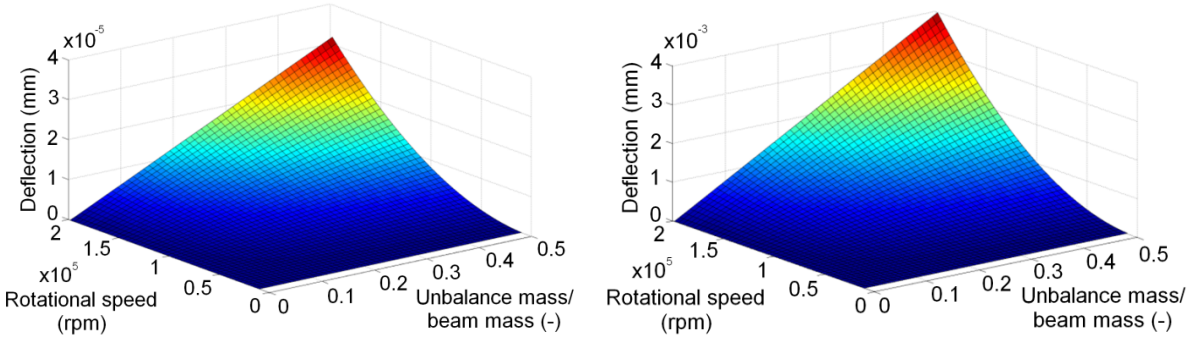

(a) Ø0.2 mm end mill (b) Ø1 mm end mill

Fig 9.7: Relation between tool deflection and unbalance for different speeds and ratios of unbalance mass/tool mass

The unbalance mass is located on the tool cutting diameter because this case represents the worst possible situation. The effect of unbalance is analysed on rotating beams with diameters of 0.2 mm and 1 mm. The beam length is in both cases 1 mm. Hence, the stiffness of the first beam is 152 $N \cdot mm^{-1}$ and of the second one $94.98 \cdot 10^3$ $N \cdot mm^{-1}$. It means that stiffness of the beam with diameter of 1 mm is approximately 625 times higher than stiffness of the beam with 0.2 mm diameter. The analysis was performed for different rotational speeds from 1 rpm up to 200 000 rpm. The resulting deflections are shown in fig. 9.7. The calculated deflections for the beam with diameter of 0.2 mm are approximately 100 times lower than in the case of the beam with diameter of 1 mm. Hence, it may be concluded that the effect of unbalance is much lower in the case of micro milling than it is in the macro scale. Furthermore, in the case of the beam with diameter of 0.2 mm realistic deflections caused by the unbalance are in the order of tens of nanometres. This is assumed to have a negligible effect on cutting process and tool life. Therefore, the unbalance is not an issue in micro milling and a designer does not have to pay a special effort to this topic.

9.2.4 Helix angle effects

On the other hand much higher attention must be paid to optimization of the helix angle. Two reasons why the helix angle affects cutting performance significantly more in micro scale than in macro scale are:

- Rapid increase of bending stress with decreasing tool diameter makes locations of any stress concentrators crucial. Optimization of the helix angle can help to relocate the main stress concentrators (in the flute termination zone) more appropriately.

- Generally the portion of the tool which is in a contact with the workpiece is much higher in micro milling than in macro milling. This is illustrated in fig. 9.8 where a tool with diameter of 1 mm and a tool with diameter of 0.2 mm, both with helix angle of 30°, are compared. In both cases the assumed depth of cut is 0.2 mm. This depth of cut can be used as in macro as in micro milling. In the case of the tool with diameter of 1 mm the maximum peripheral angle engaged in cutting is only 13°, whereas in the case of the tool with diameter of 0.2 mm it is 66°. Hence, it is evident that the effect of the helix angle on the resulting cutting forces is significantly higher in the case of micro milling. Therefore, proper helix angle optimization is absolutely crucial for the tool performance.

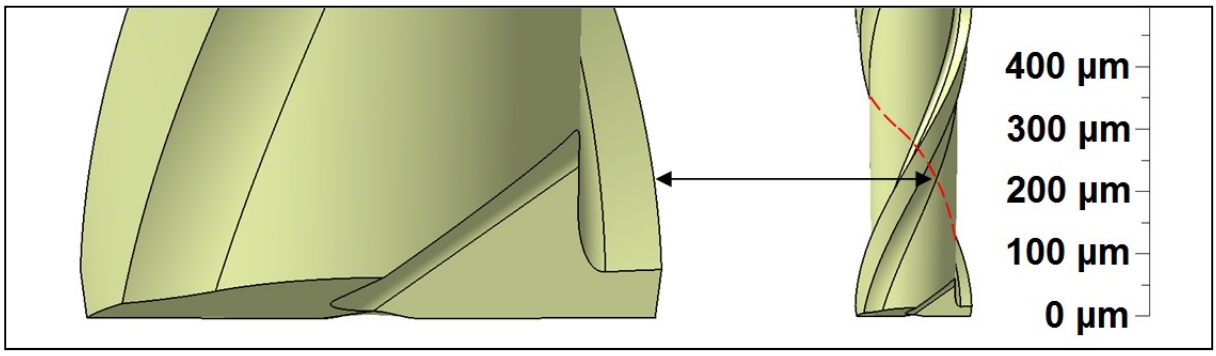

Fig 9.8: Illustration of the micro and macro tools engagement

9.2.4 Critical zones of micro end-mills

Based on the experience gained during the experimental part of this research two critical zones were identified as they are highlighted in fig. 9.9a. The first critical zone represents the cutting edge which is in direct contact with the workpiece. The repeated impacts and the

sliding of the flank face over the generated surface cause tool wear. This results in increasing cutting forces which lead to higher bending stresses. For illustration a typical cutting edge of a micro end-mill after removing approximately 2 mm^3 of steel is shown in fig. 9.9b. However, the tool geometry has only a low effect on abrasive tool wear. This wear mechanism is dominantly affected by the tool and the workpiece materials and chosen cutting conditions. On the other hand, the tool geometry has a significant effect on the initial cutting edge chipping. An example of a poor cutting edge design is shown in fig. 9.10. In this case, the manufacturer has prioritize positive rake angle, and therefore, designed the cutting edge with a “beak”. This, however, results in extensive stress and consequently in cutting edge chipping.

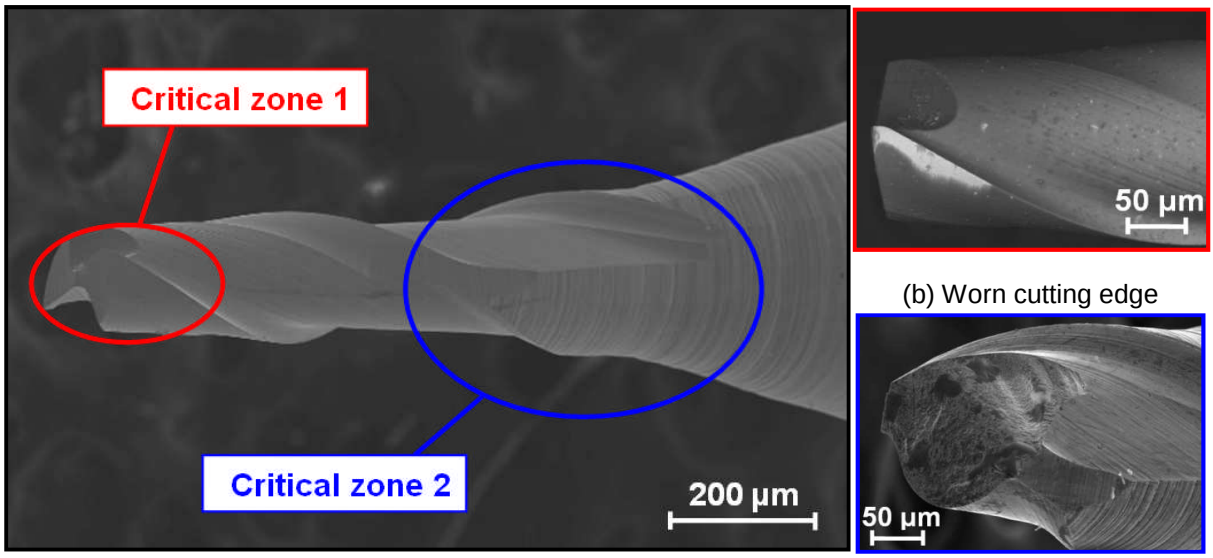

(a) Critical zones

(b) Worn cutting edge

(c) failed tool

Fig 9.9: Micro end-mill critical zones

Another critical zone of the tool was identified in the transition between the cutting part and the neck. In this location the cutting edges are terminated. This leads to stress concentrations. These transition geometries are usually copied from macro end-mills, in which case the bending stresses are low. However, as it was already discussed above, the situation in micro milling is different. The bending stresses are high and often lead to premature tool breakage (see an example of a broken micro end-mill in fig. 9.9c). Therefore, much higher attention to an analysis of the stresses and carful design of the transition geometry is absolutely essential. Although optimization of the dimensions can result in a

certain reduction of bending stress, it is usually not sufficient. It is assumed that new geometrical solutions can be very beneficial.

Hence, it is clear that the design of micro end-mills requires much higher effort than it is in the case of macro end-mills.

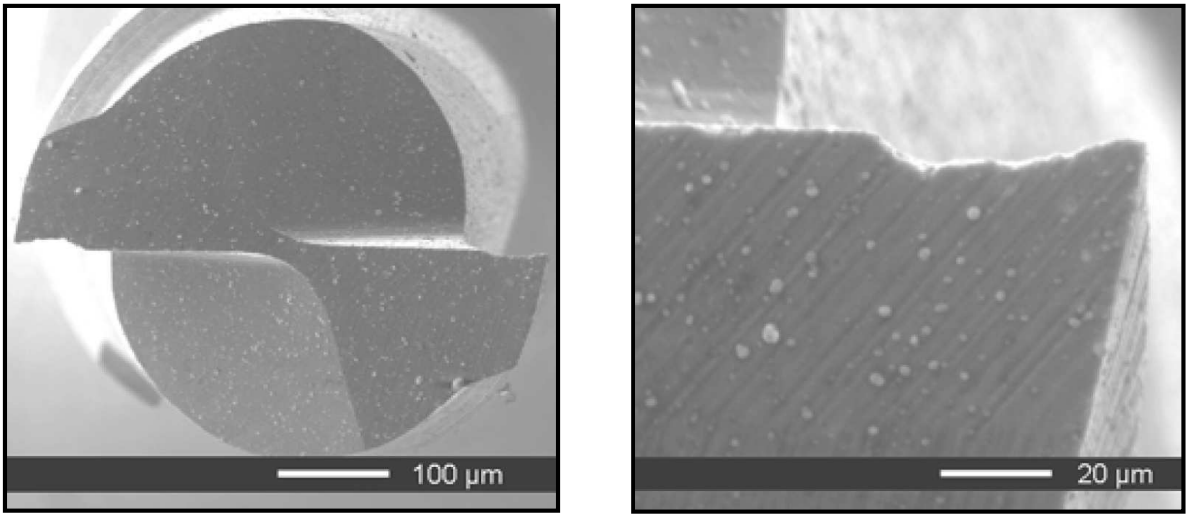

Fig 9.10: An example of poor cutting edge design [40]

9.2.5 Roughing and finishing applications

Another important issue which must be considered is tool application. Two different cases can be distinguished as roughing and finishing. Although all the challenges described above are the same for both of these cases, there are some different demands on each of the tool designs.

Roughing tools

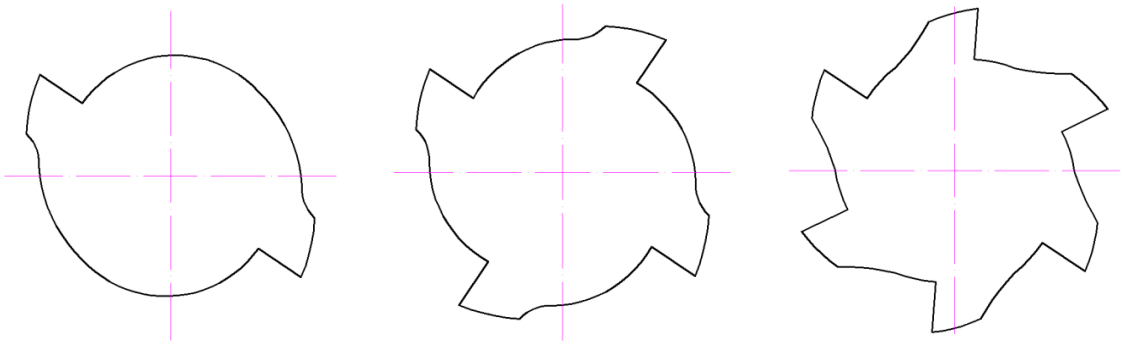

(a) 2-flutes tool (b) 4-flutes tool (c) 6-flutes tool

Fig 9.11: Cross-sections of the tools with different numbers of cutting flutes

The roughing tools are commonly used for removing of maximum workpiece material in the shortest possible time. Surface finish is usually not the primary issue. Therefore, during designing of the roughing tool a special attention should be paid to minimization of bending stress. Furthermore, in roughing process are usually required higher feed rates than in the case of finishing. One of the possible solutions is an increase of the flute depth. This solution would facilitate an increase uncut chip thickness. Another possible solution is an incensement of number of flutes. In fig. 9.11 are shown some of the possible cross-sections of the roughing tools with different numbers of flutes. Evidently the feed per rotation can be almost six times higher in the case of the tool with six flutes comparing to the tool with a single flute. However, it must be remembered that the incensement of the number of flutes will most likely change the stress distribution and in some cases this modification can result in extensive bending stresses. Therefore, FEA should be always used for study of the suggested modification effects.

Finishing tools

On the other hand, tools for finishing operations are required to produce the best possible surface finish. Furthermore, volume removed during finishing operation is much lower than in roughing. Hence, the feed rates typically used for finishing operations are set to low values. This is because lower feed rates are assumed to produce lower surface roughness. This phenomenon is illustrated in fig. 9.12. It is assumed that in the best possible case the generated surface will copy the cutting edge path. This is of course a simplified assumption, and at the reality the surface roughness will be affected by many other factors, however, for an illustration of the feed rate effect this simplification is acceptable. Hence, in this simplified case, the side wall surface generated by any feed x mm/tooth will look like the blue line in fig. 9.11 and surface generated with a halved feed will look like the red line. In the second case the peak-to-valley distance is approximately four times smaller than in the first case. Similar effect of the feed is also on the bottom generated surface. Hence, clearly the lower feeds are preferable for finishing operations.

On the other hand, tool deflections may result in lower uniformity of the generated surface. The deflection is a function of applied force and stiffness. However, because the applied force (cutting force) will never be absolutely same in two rotations (because of

various dynamic effects), the bending will have a tendency to fluctuate. Hence, the cutting edge path will vary during the cutting process. This effect cannot be fully eliminated, but it can be reduced by increasing tool stiffness. Hence, stiffer tools are preferable for finishing operations.

These two factors lead to an obvious conclusion that the finishing tools should have generally lower depths of flutes than roughing tools.

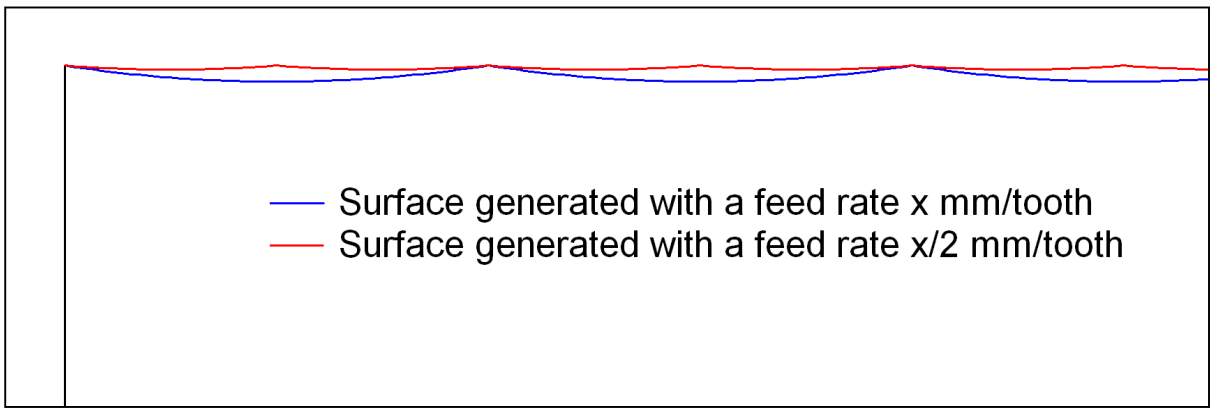

Fig 9.12: Illustration of the effect of feed rate on the generated surface

Another issue is the tool run-out. It is generally not possible to manufacture a perfect tool and a perfect spindle. Therefore, the tool run-out will always be presented in any milling process. In fig. 9.13a is shown a cross-section of a tool with two flutes with an illustration of run-out effect. Clearly, the first flute follows a different tool path than the second flute. This will result in a rougher surface finish. However, the effect of the tool run-out on the generated surface can be minimised by a single flute tool design as it is illustrated in fig. 9.13b. Such tool is also presumed to be stiffer. On the other hand, it is most likely that the single flute tool will experience an unbalance. However, as it was explained above, unlike in the case of macro milling in real micro milling the effect of unbalance is not an issue. Hence, the single flute designs should be assumed as a possibility for finishing operations.

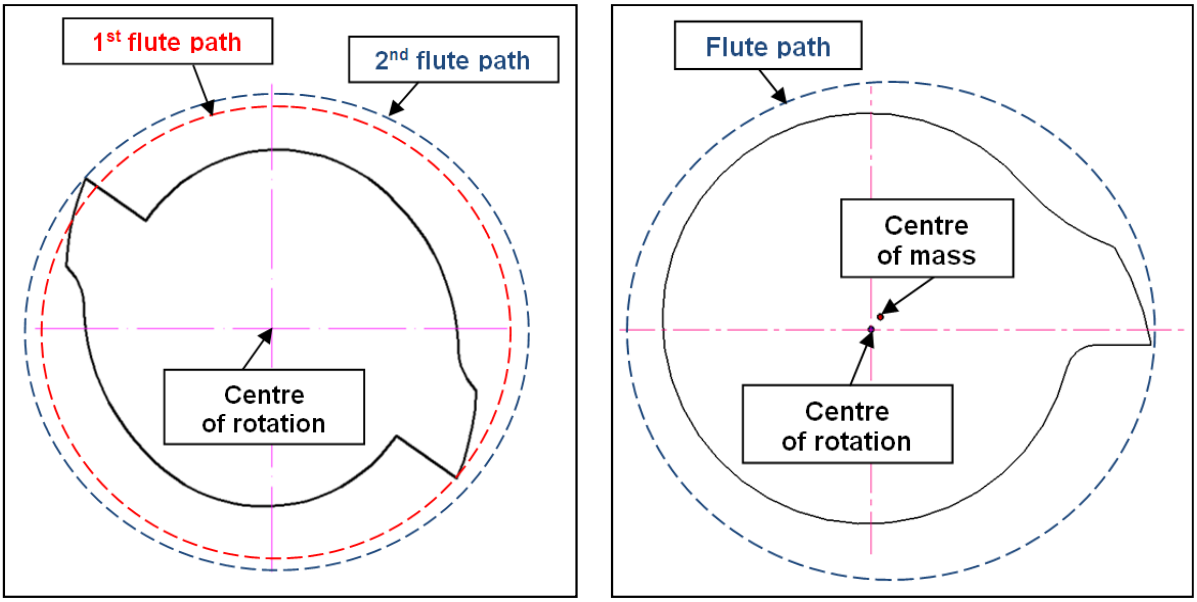

(a) 2-flutes tool (b) Single flute tool

Fig 9.13: Illustration of the effect of the tool run-out

9.2.6 Consideration of workpiece material

Except of the cases described in the previous subsection, the designer must always consider workpiece material which will be dominantly cut by the designed tool. It is evident that the tool which shall be used for cutting of hardened steel must be designed differently than the tool used for cutting of soft materials like aluminium or copper. In the case of hard materials the specific cutting energy is significantly higher, and therefore, the feeds are usually set to low values. Therefore, in this case the designer can consider reduction of the flute depth. Generally the reduction the flute depth results in larger tool core, and this is advantageous for tool stiffness. On the other hand, in the case of soft materials, the tool does not have to be as stiff but usually are used higher feeds. Hence, in this case the core diameter can be reduced and the depth of flute increased.

This is not as important in the case of macro milling, where the tool stiffness is usually high, and therefore, the risk of tool breakage is minimal. Hence, the macro tools can be designed with unified dimensions for wide range of applications. However, in the case of micro milling, special tools should be designed for various applications. This highlights an increasing importance of systematic and reliable methods for micro tools design.

9.2.7 Manufacturing difficulties

Any designer of any product should always keep in mind manufacturing process of the proposed product. Because of generally lower number of suitable micro manufacturing processes, it is even more important in the case of the micro products. The micro end-mill represents one of the geometrically most complex products currently available on the market. Therefore, manufacturing possibilities of the designed micro end-mill is absolutely crucial.

Manufacturing of micro end-mills is also difficult because of its low stiffness. Most widely used micro grinding (mechanical machining) generates large forces which result in tool imperfections and dimensional uncertainties. The consequence of this was already discussed in the previous two chapters (unpredictability of tool performance). Evidently, a possible solution is to reduce MRR. This is, however, not preferable for industry because it leads to higher unit costs.

Another possible solution is to use some of the other manufacturing processes (e.g. micro-EDM, FIB or micro-LBM). These processes are non contact and do not generate any significant forces. However, micro-EDM and FIB are even slower and more expensive than micro grinding. Hence, it would be justifiable for industry only in the case that the tool life would be significantly extended and the tools could be sold for higher prizes. On the other hand, micro-LBM is a fast manufacturing process, but is not yet mature.

Each of the possible processes has its strong sides and its weaknesses. The chosen process affects the possible geometrical complexity, the minimum feature size, surface quality and tolerances. Hence, the tool design cannot be done without consideration of chosen manufacturing process.

9.3 Method description

In the previous section were discussed main factors which must be taken in account during the micro end-mill design. The aim of this section is to organize designing process into a systematic approach dealing with all the identified challenges. Whole designing process is based on theoretical analyses whenever they are applicable. For clarity, the method approach is illustrated in fig. 9.14. It consists of seven stages before the tool prototyping and final experimental verification. Such method is assumed to be more cost effective than methods

based purely on experimental studies. It does not require frequent and time consuming interactions with production process neither large initial investments. The theoretical analyses also give comprehensive information about the tool, which often cannot be gained experimentally. If needed, this information can be effectively used for tracking an issue of the final product instead of chaotic redesigning.

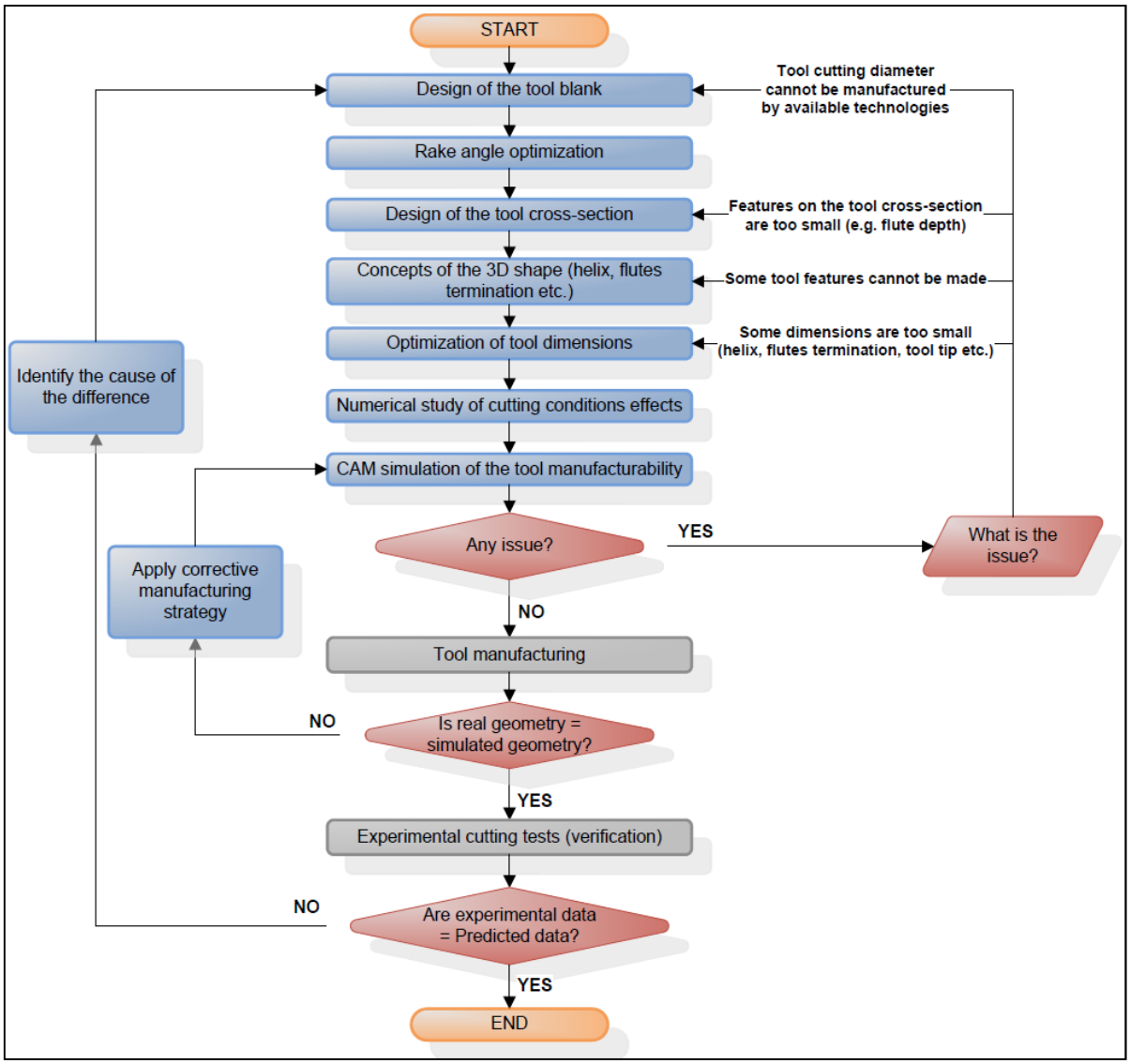

Fig 9.14: Methodology for micro end-mill design

9.3.1 Design of the tool blank

The flowchart describing this phase of tool design is illustrated in fig. 9.15. This method is described in its general form and it can be applied for optimisation of various dimensions (not only related to the tool blank).

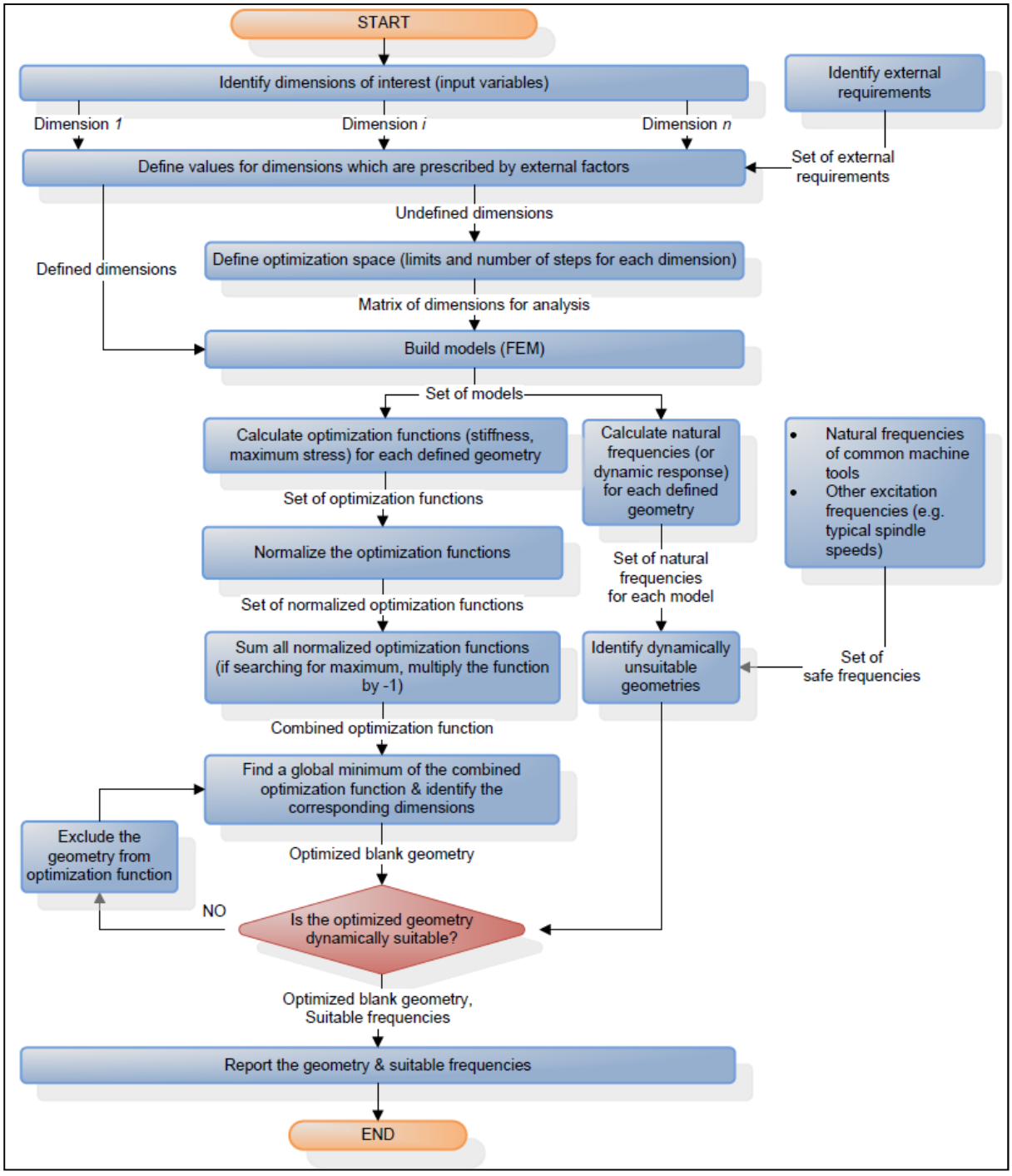

Fig 9.15: The tool blank optimization method

In the first stage of this method the tool blank is optimized. The main tool dimensions, such as the cutting diameter and the maximum cutting length, are defined. Furthermore, the neck angle and a fillet radius between the neck and the cutting part should also be numerically optimized. The location between the neck and the cutting part represents a stress

concentrator and in combination with an inappropriate design of other tool features can lead to premature tool breakage. Last dimensions which must be decided in this stage are the shank diameter and the shank length. These dimensions are not critical for the tool functionality. However, they may affect the tool dynamics and consequently cutting forces or machined surface. The shank diameter is also one of the factors affecting economical success of the new tool because it must fit in clamping systems used in the targeted market. Therefore, clamping systems should be analysed and considered during the blank design.

Hence, in the most general case, six dimensions should be considered. However, usually some of the dimensions are restricted by customer/market requirements, and cannot be changed. The cutting diameter is usually given by applications. Therefore, this dimension is given and cannot be changed without a serious reason. Most usually the minimum cutting diameter is restricted by tool manufacturing technology or tool fracture properties.

Two optimization parameters are considered during the blank design. The first one is maximum tensile stress, which should be kept as low as possible. On the other hand stiffness should be as high as possible. The third parameter which should also be considered during the tool blank design is a range of safe frequencies. This is not a typical optimisation parameter like the other two. It is more important for recommendations of operating cutting parameters, and it is more application related.

9.3.2 Rake angle optimization

Once the tool blank is designed and all its dimensions are defined, the cutting mechanism should be studied. This is especially important in micro milling because of various size effects. It is generally not possible to use an experience as it is typical in macro scale cutting. In this method FEA of cutting process (chip formation) is proposed as the best solution. It is mainly because of deeper insight into cutting process than it is possible by experimental investigation.

During this phase should be studied:

- The effect of the tool rake angle on chip formation
- The effect of applied cutting conditions on chip formation

Based on the information achieved from FEA, the most appropriate rake angle can be chosen. Furthermore, the information about chip flow can be used for decision on the flute depth. These two dimensions are the most important for the tool cross-section design.

9.3.3 Design of the tool cross-section

Once the tool blank is designed and the chip formation mechanism understood the tool concepts should be proposed. This is done in two separate steps. In the first step the tool cross-section is proposed and in the second step the 3-dimensional shape is proposed.

Hence, first the tool cross-section must be designed. This step requires designer's intuition and experience. However, the cross-section should always be designed with a respect of assumed tool manufacturing method. Generally, it is always advantageous to use simple designs because these are easier to make. On the other hand, the tool cross-sectional area should be the largest possible (without affecting the tool functionality). The most important dimensions in this phase are: rake angle, depth of flute and clearance angle. Furthermore, in this phase the designer must think about the applications of the proposed tool. Based on this he should choose the number of flutes.

9.3.4 Concepts of the 3D shape of the tool

This is the second conceptual phase of designing process. In this phase are designed all 3D features of the micro end-mill. Same as in the previous phase, also this phase requires an experience and imagination of the engineer. It is generally advantageous to propose several concepts which are compared and optimised in the following step.

9.3.5 Optimisation of tool dimensions

This phase is generally the same as the optimisation of the tool blank. Therefore, the flowchart presented in section 9.3.1 can be followed also in this phase. The optimisation functions are the same: maximum bending stress and bending stiffness. However, the input dimensions are different (can vary from design to design).

9.3.6 Numerical study of cutting conditions effects

Once, the novel tool is designed it should be analysed for its sensitivity to different cutting conditions. Two analyses are proposed:

1) Analysis of tool sensitivity to direction of the applied force. This is very important especially in the case of micro milling, where the process uncertainties and tool tolerances can cause variation of the cutting force direction. Hence, clearly the sensitivity should be as low as possible. In ideal case the stiffness and maximum stress should not vary when the force is applied in different directions. For this purpose can be used FE stress analysis of the optimised tool with unit force applied in different directions (from fully tangential to fully radial).
2) Analysis of tool sensitivity to different cutting conditions. In this analysis the tool should be loaded by cutting forces (calculated by method presented in chapter 6) for different cutting conditions. This analysis should identify the most suitable cutting conditions which should be used with the proposed tool design. This analysis is important because some micro end-mill designs can perform well with one set of cutting parameters, but they can be absolutely unsuitable for another set.

9.3.7 CAM simulation of the tool manufacturability

This is the last theoretical phase of the method. It is generally used to verify manufacturability of the new tool. However, it can also be used for estimation of tool manufacturing time and costs. The CAM simulations can also be used for development of new manufacturing strategies (application of new technologies and optimisation of process parameters).

9.4 Case study: Dual helix tool with freeform flute termination

In this case study is presented a practical application of the proposed methodology. Particular analyses are used for design of a micro end-mill with a nominal cutting diameter of 0.2 mm and cutting length of 0.5 mm. These dimensions were chosen because they are the same ones as those of the commercial end-mills used all through this research. This makes it easier to compare predicted performance of the new tool with performance of the commercial ones.

The example represents a roughing tool designed for manufacturing of micro moulds. Hence, a typical workpiece material machined by this tool is similar steel as the one used in the previous chapters.

9.4.1 Design of the tool blank

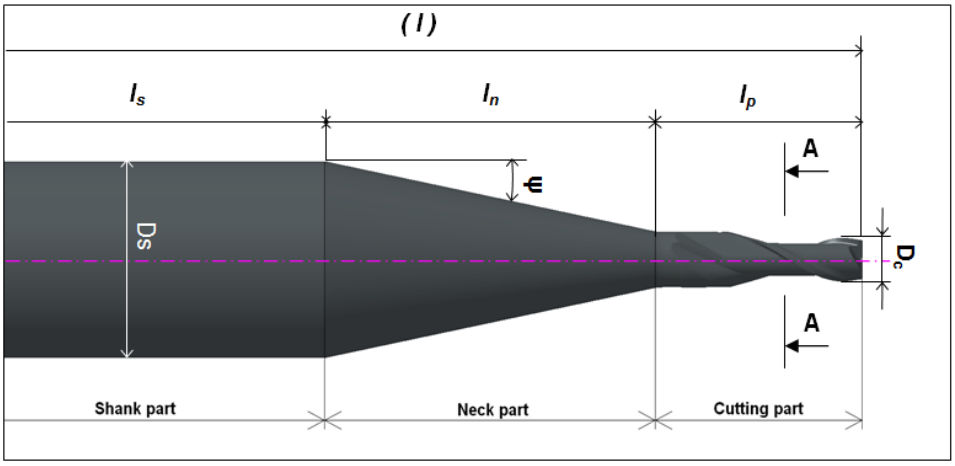

(a) Overall view of a typical micro end-mill

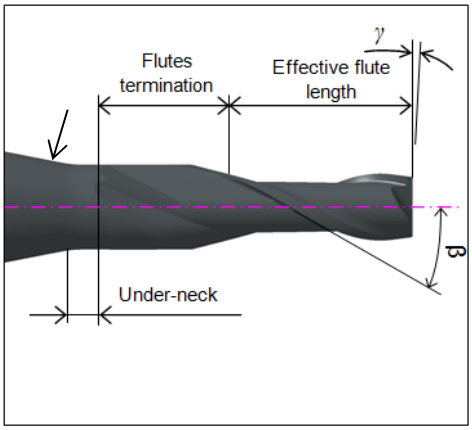

(b) Detail of tool cutting zone

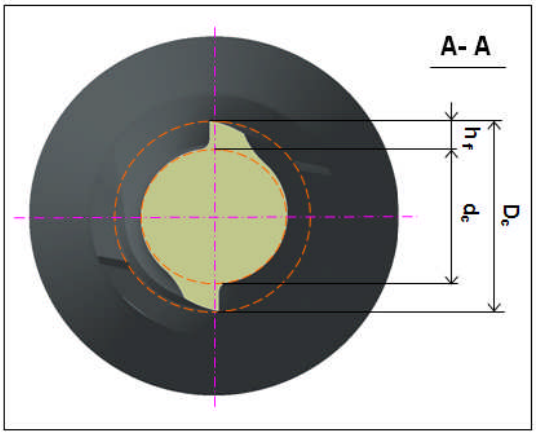

(c) Cross section view

Fig 9.16: Illustration of micro end-mill geometry

In the first phase, the tool blank must be designed. According to the methodology this involves an optimisation of the main tool dimensions with respect to maximum stress and stiffness. Natural frequencies of the tool blank should be also considered in this phase.

The first step of the methodology is an identification of the dimensions which can be optimized. In fig. 9.16 is shown a typical micro end-mill with its main dimensions. In total 15 different dimensions can be identified in the figure. However, not all of them are relevant for the tool blank design. Only the following eigth must be considered: total tool length (l), shank length (l_s), neck length (l_n), cutting part length (l_p), shank diameter (D_s), cutting part diameter (D_c), neck angle (ψ) and fillet radius (r). Furthermore, the total length and the neck length are dependent on some of the other dimensions. Hence, only six dimensions are independent.

However, in the reality not all of these six parameters can be varied. The shank diameter is defined by standard tool holders (or customer requirements). Furthermore, the total length, the cutting length and the cutting diameter are in this study kept constant.

Hence, only two dimensions are considered as variable inputs: the neck angle and the fillet radius. The upper and lower limits for the neck angle are set to 5° and 40° respectively, and an analysis step is 5°. This means that eight different neck angles are analysed. The studied fillet radii are between 0 mm and 1 mm with a step of 0.25 mm. Hence, the total optimisation space has eight by five members as it is illustrated in tab. 9.1.

Tab. 9.1: Optimization space

Fillet \ Neck angle	5°	10°	15°	20°	25°	30°	35°	40°
0.00 mm	OUT 11	OUT 12	OUT 13	OUT 14	OUT 15	OUT 16	OUT 17	OUT 18
0.25 mm	OUT 21	OUT 22	OUT 23	OUT 24	OUT 25	OUT 26	OUT 27	OUT 28
0.50 mm	OUT 31	OUT 32	OUT 33	OUT 34	OUT 35	OUT 36	OUT 37	OUT 38
0.75 mm	OUT 41	OUT 42	OUT 43	OUT 44	OUT 45	OUT 46	OUT 47	OUT 48
1.00 mm	OUT 51	OUT 52	OUT 53	OUT 54	OUT 55	OUT 56	OUT 57	OUT 58

For each of the members are calculated three different outputs: stiffness, maximum tensile stress and the first natural frequency.

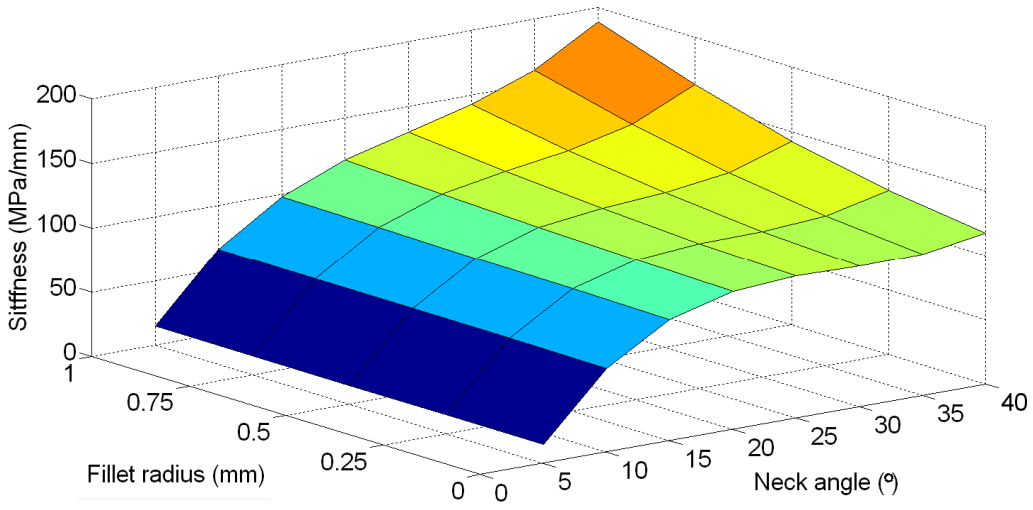

Fig 9.17: Predicted effect of the neck angle and the fillet radius on bending stiffness

In fig. 9.17 is plotted stiffness as a function of the fillet radius and the neck angle. The function has a non-linear trend in both directions. Generally it can be concluded that bigger neck angle together with bigger fillet radius result in higher stiffness.

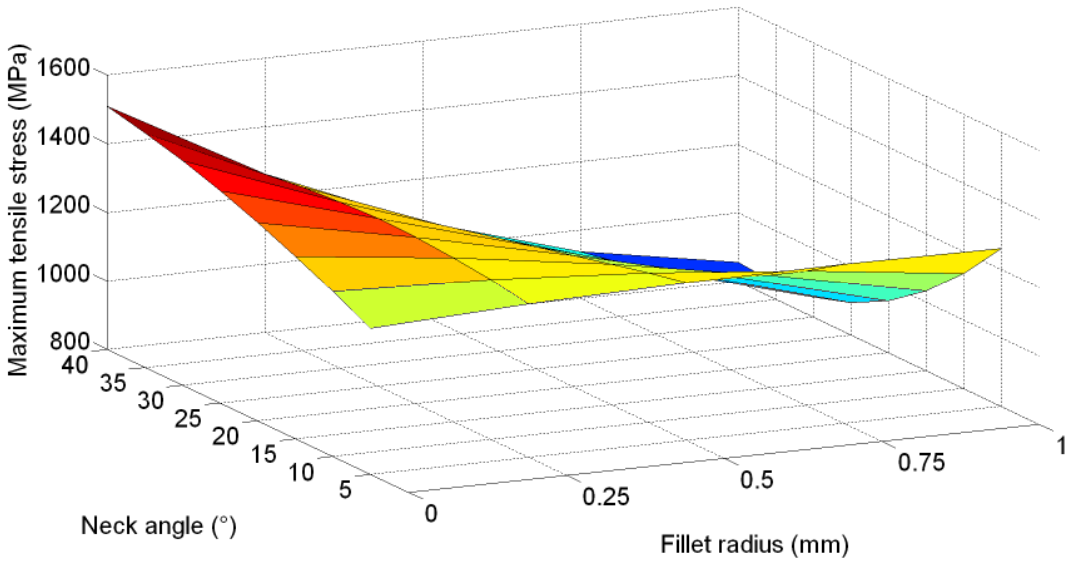

Fig 9.18: Predicted effect of the neck angle and the fillet radius on maximum tensile stress

The graph in fig. 9.18 shows results of the stress analysis. Also in this case, the best combination is the largest neck angle and the largest fillet radius. However, the trend of this function is not as obvious as in the case of stiffness. In the case of absence of fillet radius (r = 0 mm) the maximum stress has growing tendency with increasing neck angle, as in the case of r = 1 mm, the trend is reverse. This shows the importance of this analysis.

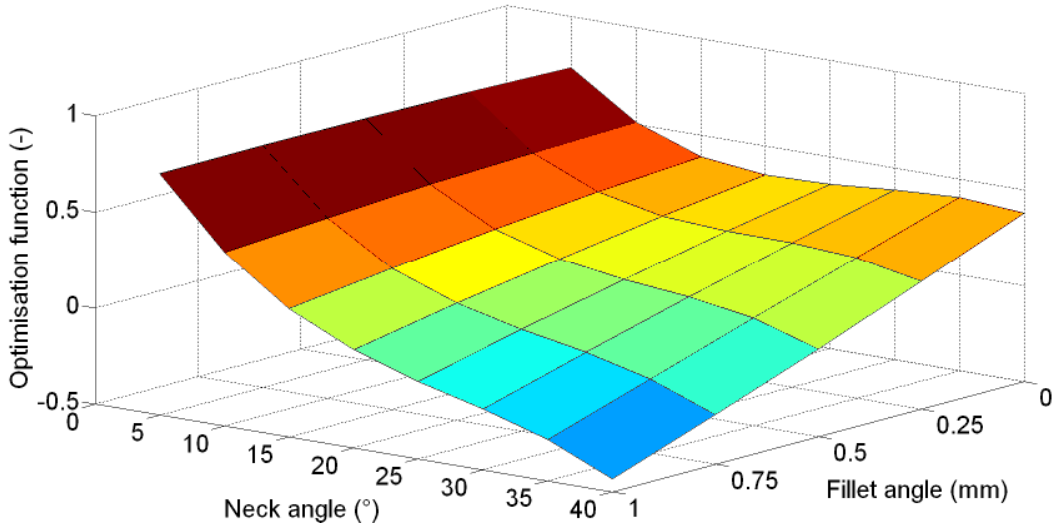

Fig 9.19: Combined optimisation function

Although in this particular case the optimal solution is evident (the largest fillet radius and the largest neck angle), in some other cases it might not be as simple. Especially in the case when more dimensions are considered, the relations might become more complex and the decision is more difficult. Therefore, it is always a good practice to follow the next step of the methodology and calculate the combined optimisation function. Such function is plotted in fig. 9.19. As expected, this function has its minimum when the radius of 1 mm and the neck angle of 40° is used.

Except stiffness and tool maximum stress the first natural frequency is analysed in this case study. The relation between the first natural frequency and the neck angle is shown in fig. 9.20. From the figure is evident that he fillet radius has no recognizable effect on the frequency. On the other hand, the natural frequency has a decreasing tendency with increasing neck angle. Rapid reduction of the frequency may be observed especially for angles <20° and then the reduction slows down. However, the natural frequency was found to be sufficiently high in all studied cases. For example for neck angle 20° the frequency is 8 500 Hz. This frequency is much higher than a usual tool rotational speeds (usually the exciting frequencies are up to 2 000 Hz). Therefore, this characteristic does not affect tool performance and further analysis is not necessary.

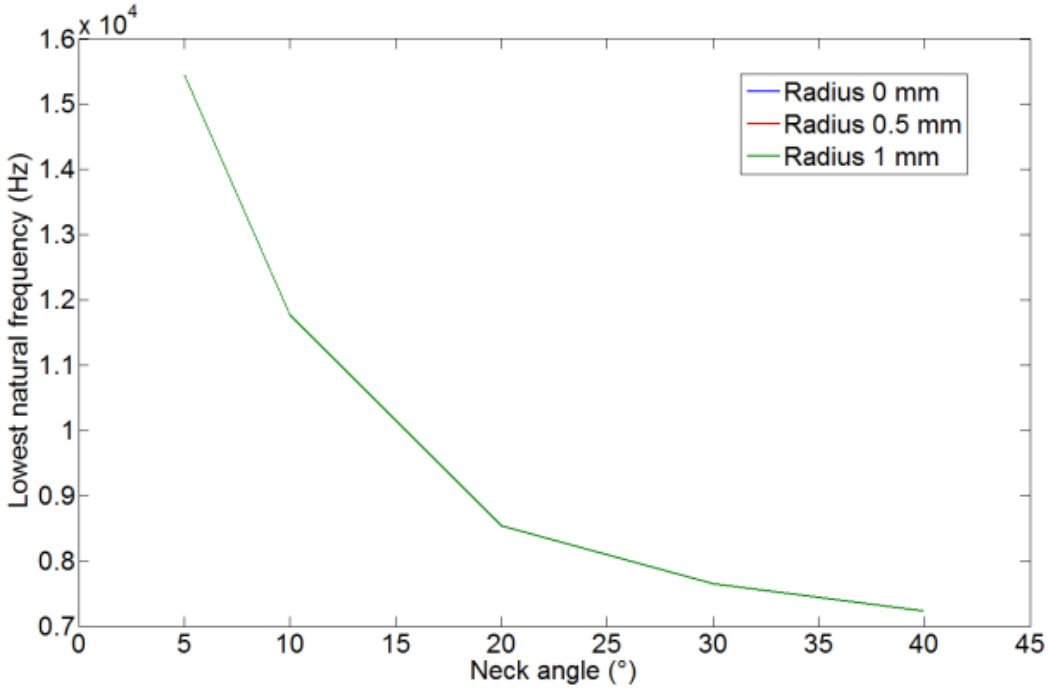

Fig 9.20: Predicted effect of the neck angle and the fillet radius on the first natural frequency

The final tool blank proposed in this case study is shown in fig. 9.21. According to the theoretical results the most appropriate neck angle would be 40° and fillet radius 1 mm. However, because of concerns with tool manufacturability halved neck angle (20°) is actually used.

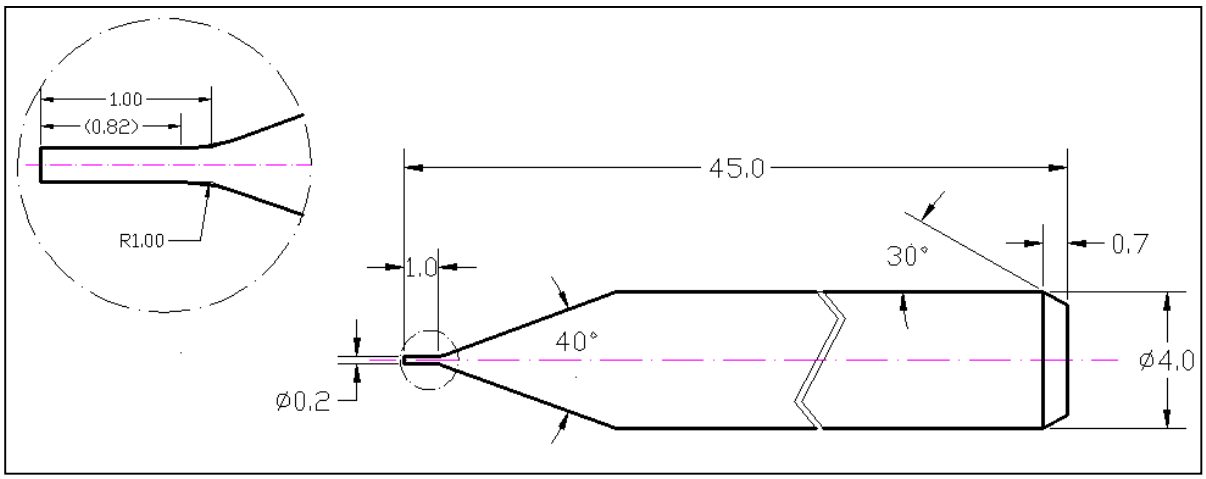

Fig 9.21: Micro end-mill blank

9.4.2 Rake angle optimisation

The next phase of the methodology describes an approach of designing rake angle. FEA is suggested as the main analysis tool for this phase. In this section is presented a practical use of this approach and discussed its pitfalls and difficulties.

Except of rake angle optimization, the calculated data can be also used for estimation of minimum flute depth. This dimension is much more critical in micro milling than it is in conventional milling. Evidently, the main attempt is to provide sufficient space for fluent chip removal. Hence, bigger flute depth seems to be more suitable. Insufficient flute depth can lead to chip stacking, what can lead to undesirable BUE effect. On the other hand there is a clear relation between the core diameter and flute depth. Any increase of one of these dimensions will result in reduction of the second one. However, as tool stiffness was mentioned as of the main issues, the core diameter should be as large as possible. These two requirements (maximum flute depth and maximum core diameter) are contradictory. FEA is assumed to give a useful indication for solving this issue.

Description of the FE model

Two-dimensional explicit transient FEM analysis with arbitrary Lagrangian-Eulerian formulation (ALE) was used for an analysis of chip formation. The ALE formulation was used only on the part of the model, where are expected large deformation (see fig. 9.22). The ALE formulation was chosen because of its suitability for solving large deformations involving contacts. Comparing to traditional adaptive meshing techniques, the mesh based on ALE formulation has fewer elements, and therefore, it is computationally less expensive. Furthermore, application of this formulation reduces a risk of appearance of singular (highly distorted) elements which cause computational instabilities.

The whole model contains approximately 5 000 elements; depending on a feed rate used in the particular case. The analysed rake angles vary from -10° up to +10° with a step of 5°. All the rake angles are analysed for feeds of 2 μm/tooth, 4 μm/tooth and 6 μm/tooth. The rotational speed used for all analyses is 30 000 rpm and the depth of cut is 100 μm. The tool is modelled as a rigid body with prescribed rotation and translation. Depth of flute used in the analyses is 20 μm. The cutting edge radius was measured from different micrographs acquired during this research and the average value of 1.5 μm was used in all of the analysed cases.

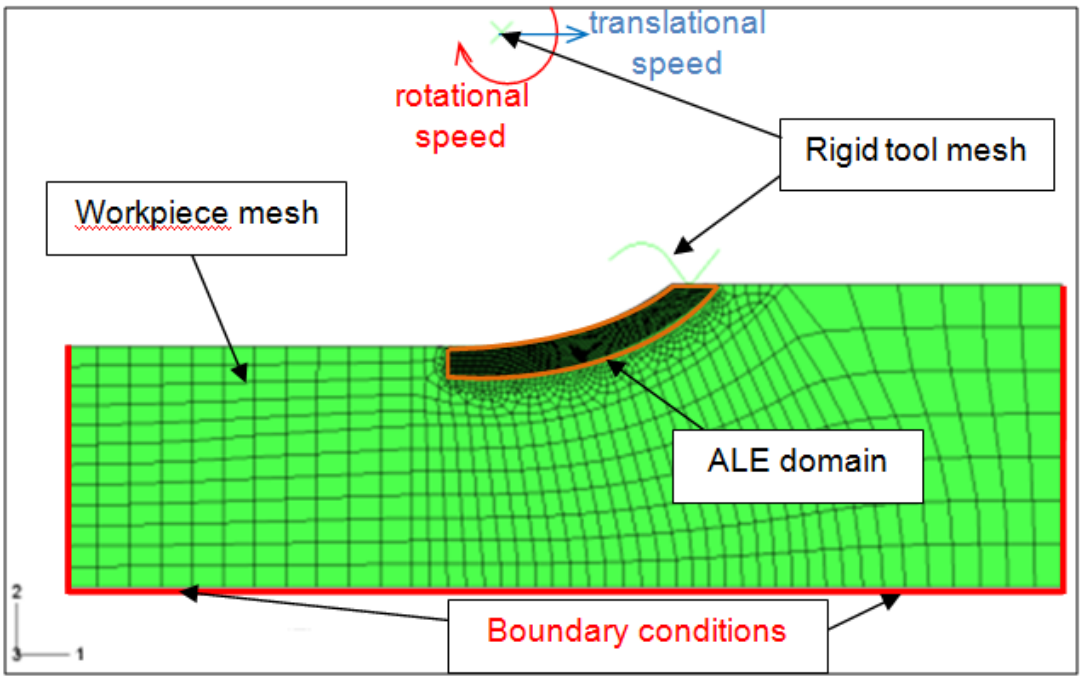

Fig 9.22: Finite element model used for analysis of chip formation

Workpiece material used in this analysis is 42CrMo4 steel. The material model used in this research is Johnoson-Cook material model [130]. This model was developed for modelling of plastic behaviour of ductile materials and is the most widely used model in chip formation analysis. The yield limit in this model is given by:

$$\sigma = \left(A + B \cdot {\varepsilon_p}^n\right) \cdot \left(1 + C \cdot ln\frac{\dot{\varepsilon_p}}{\dot{\varepsilon_0}}\right) \cdot \left[1 - \left(\frac{T - T_0}{T_{melt} - T_0}\right)^m\right] \tag{9.7}$$

where ε_p is the equivalent plastic strain, $\dot{\varepsilon_p}$ is the equivalent plastic strain rate, T is the temperature, and A, B, C, n, m, T_0, T_{melt} and ε_0 are material parameters. The material parameters were adapted from Pantalé [102] and are listed in tab. 9.2.

Table 9.2: Johnson–Cook material law parameters for the steel 42CrMo4 [102]

Constant	Value	Unit
A	595	MPa
B	580	MPa
C	0.023	-
n	0.133	-
m	1.03	-
$\mathbf{T_{melt}}$	1 793	K
$\mathbf{T_0}$	300	K

Except of the plasticity model, damage law is necessary to simulate unsteady-state metal cutting. Johnson-Cook damage law [131] is used in this research. The damage is calculated for each element and is defined by:

$$D = \sum \frac{\Delta\varepsilon_p}{\varepsilon_p^f} \tag{9.8}$$

where $\Delta\varepsilon_p$ is the increment of the plastic strain and ε_p^f is the equivalent fracture strain.

The expression for the equivalent fracture strain is given by:

$$\varepsilon_p^f = \left(D_1 + D_2 \cdot e^{D_3 \cdot \sigma^*}\right) \cdot \left(1 + D_4 \cdot ln\frac{\dot{\varepsilon_p}}{\dot{\varepsilon_0}}\right)\left[1 - D_5 \cdot \left(\frac{T - T_0}{T_{melt} - T_0}\right)^m\right] \tag{9.9}$$

The parameters D_1, D_2, D_3, D_4, D_5 were again taken from Pantalé [102] and they are listed in table 9.3.

Table 9.3: Fracture parameters for the 42CrMo4 steel [102]

Constant	Value
$\mathbf{D_1}$	1.5
$\mathbf{D_2}$	3.44
$\mathbf{D_3}$	-2.12
$\mathbf{D_4}$	0.002
$\mathbf{D_5}$	0.1

The classical Coulomb friction is used to model the tool-workpiece contact zone. According to this law two bodies are assumed to stick together if $T_t < \mu \cdot T_n$ and slip if $T_t = \mu \cdot T_n$; where T_t and T_n represent magnitudes of the tangential and normal force and μ is a friction coefficient. The friction coefficient used in this work was again adapted from Pantalé [102] and its value is 0.3.

Results and discussion

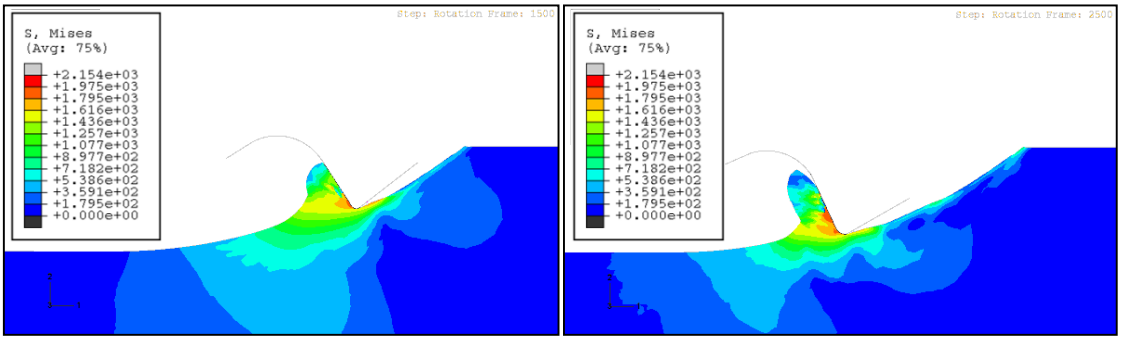

(a) The tool with the rake angle -10°, position 1

(b) The tool with the rake angle -10°, position 2

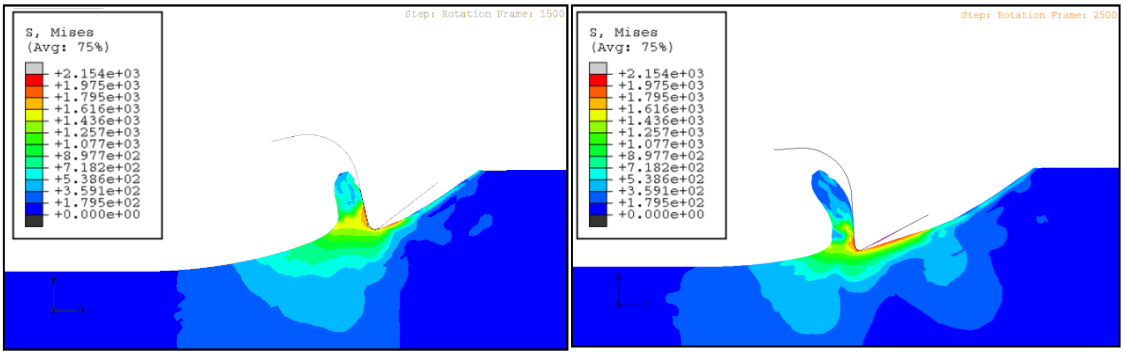

(c) The tool with the rake angle +10°, position 1

(b) The tool with the rake angle +10°, position 2

Fig 9.23: Results of the chip formation analysis

As first it should be mentioned that the stresses and the forces calculated in this analysis cannot be verified experimentally. The main reason for this is the two-dimensionality of the model. Hence, the modelled cutting process does not represent an oblique cutting (typical for milling) but an orthogonal cutting. However, the analysis results can be used as an indication of the rake angle effects. It is also worth to mention that the same simplification is used by majority of researchers and it is assumed to be reliable. The reason for using 2D orthogonal model is the extreme demand of computational power needed for simulating 3D cutting process. Furthermore, with the current computational methods it is not possible to use parallel processing for such type of analysis, and therefore, an increase of number of processors does not lead to required reduction of computational time.

In fig. 9.23 are shown stress distributions calculated for tools with the rake angles of -10° and +10° respectively. In both cases are shown two different positions, the first position is in approximately middle of the cut and the second one in three quarters. The feeds are in both cases 6 μm/tooth. Hence, these two cases represent the maximum and the minimum analysed rake angles and the largest analysed feed (and also uncut chip thickness). Hence, no of the other analysed cases should result in a larger chip. It is evident that in the case of the tool with rake angle of -10° the chip is significantly more massive. Its cross-sectional thickness is approximately 25% larger than in the case of the tool with rake angle of +10°. On the other hand, the chip is approximately 25% shorter than the one formed in the second case. Another thing which can be identified from fig. 9.23 is that the maximum equivalent stress generated in the chip is approximately same in both analysed cases. This indicates that the modification of the rake angle will not have a significant effect on properties of the generated surface.

Another important factor is the maximum cutting force. In fig. 9.24 are plotted the calculated forces as functions of the rake angle. The forces are calculated for three different feeds. From these results, it is evident that the effect of the rake angle is significantly stronger in the case of larger feeds. When the feed of 6 μm/tooth is used, the difference between the maximum cutting forces is ~ 25%, whereas in the case of 2 μm/tooth the difference is only ~7%. This is a very important finding with a significant effect on the tool design. Generally, in the case of roughing tools, when larger feeds are desirable, it is always a good practice to use the maximum positive rake angle, while in the case of finishing tools even negative rake angles can be considered as suitable. The results well correspond to the preliminary

expectations that the effect of the rake angle is not significant for very small uncut chip thicknesses.

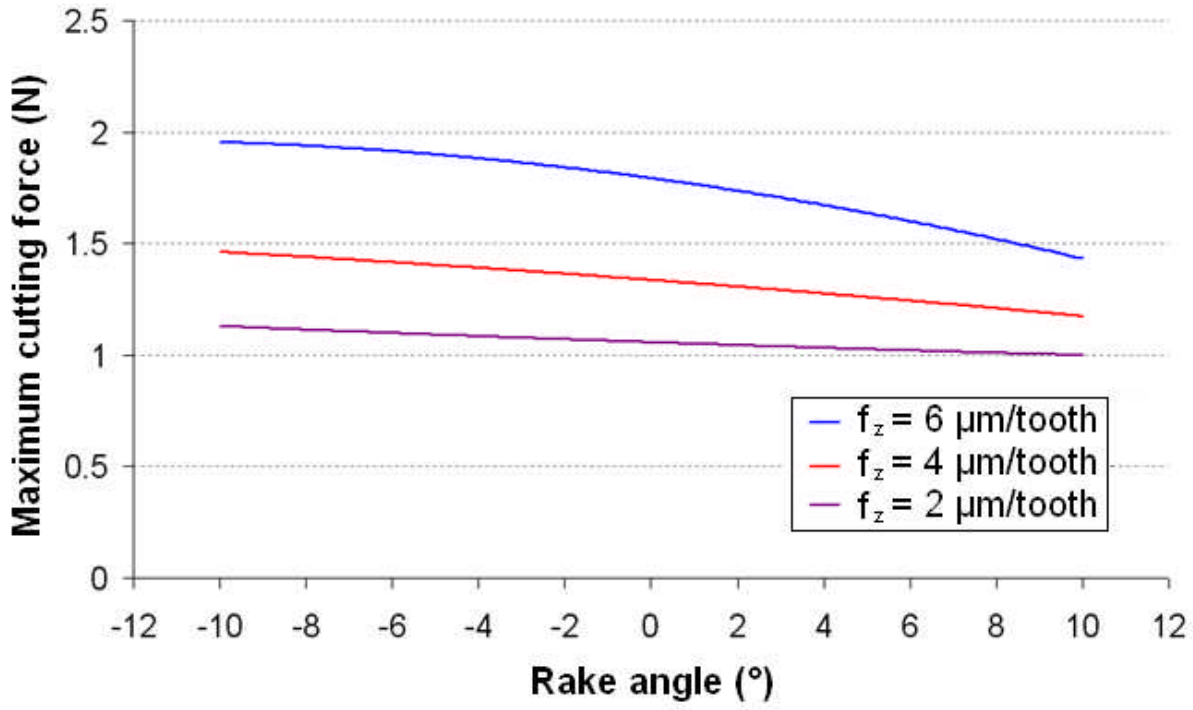

Fig 9.24: The effect of the rake angle on the resulting cutting force

Because the designed tool in this case study is proposed for roughing operations, larger feeds are desirable. Hence, obviously the largest positive rake angle should be used. Therefore, the rake angle of +10° will be used in the next step. Furthermore, the simulations indicate a suitability of the flute depth of 20 µm.

9.4.3 Design of the tool cross-section

In the previous section were chosen two main dimensions of the tool cross-section. The final cross-section shape is designed so that the cross-sectional area would be the largest possible (without limiting the tool functionality). In fig. 9.25 are compared the cross-sections of the proposed tool (red) and the commercial tool (black).

The proposed cross-section has simpler geometry and more robust geometry than the commercial tool. The novel design takes in considerations the manufacturing limitations and promise higher stiffness than the commercial design. Also, unlike the commercial design the novel design has a positive rake angle.

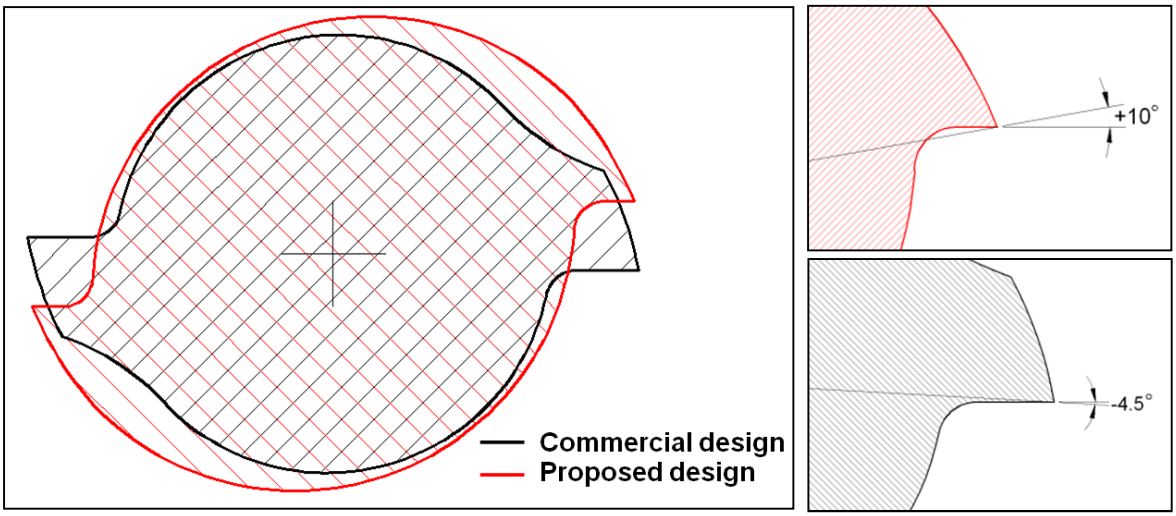

Fig 9.25: Comparison of the proposed and commercial micro end-mill cross-sections

9.4.4 Concepts of the 3D shape

This phase of tool design is the most innovative one. It desires an intuition and experience with designing of similar products. Generally the designer should come with several possible solutions which will be further analysed and optimised. In this case study are assumed three different design concepts. All three are based on a free-surface termination of the cutting edges. This solution enables maximum smoothing of the transition between the core and outer tool diameters. Hence, the most dangerous sharp edges and corners can be eliminated. The proposed concepts are shown in fig. 9.26.

The first concept (fig. 9.26a) is the simplest one. In this case the cutting edge continues through the transition zone with an unchanged angle as it is defined for the cutting zone. Simultaneously tool core is gradually changing until it reaches the cutting diameter. Than the transition zone is meshed by small surfaces defined by 3D sp-lines. This approach enables to produce a smooth transition between the core diameter and the outer diameter. The design concept with highlighted transition zone is shown in fig. 9.26b.

The second concept is based on an assumption that the continuation of the cutting flute, as it was done in the first concept, affects a large portion of the tool circumference. This is, however, not desirable. Therefore, the helix in this case is fluently transformed to the edge parallel with the axial direction. Also in this case, the transition zone is defined by a mesh of sp-lines with fluent shapes. This design concept is shown in fig. 9.26c.

The last design concept is a compromise between the previous two. In this case the cutting edge helix angle is fluently transformed into a much shallower termination helix angle. In this design concept the termination helix angle is 10°. This design concept is shown in fig. 9.25d.

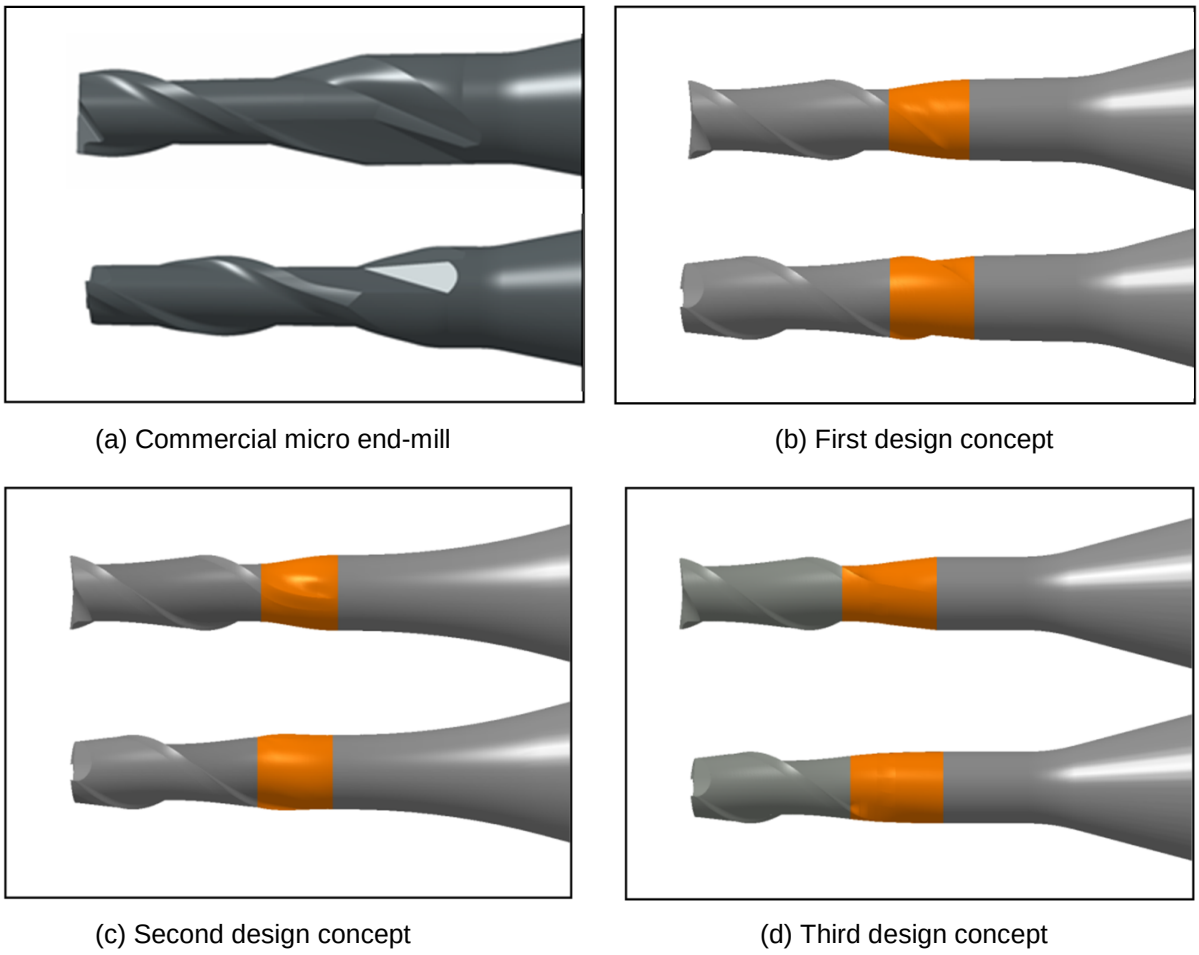

(a) Commercial micro end-mill

(b) First design concept

(c) Second design concept

(d) Third design concept

Fig 9.26: Design concepts of new micro end-mills

9.4.5 "Chip pullout"

In this stage it is good to mention one of the common mistakes of industrial tool manufacturers. All industrial manufacturers spend time and effort on designing of so called "chip pullouts". This geometric feature is assumed to lead the removed chip away from the cutting zone and pull it out to space. A typical example of this geometry is shown in fig. 9.27a. And the expected chip flow is illustrated in fig. 9.27b.

The "chip pullout" geometry is usually copied from macro tools and its effects on the tool breakage are not analysed. However, it is questionable whether it has any positive effect in

the case of micro milling. Chips formed during micro milling are very light, e.g. chip formed during full slotting with feed of 6 μm/tooth and axial depth of 100 μm is approximately 1.8μg. Hence it might be assumed that once the chip is fully removed from the workpiece it wiil be pulled by air flow. Thus, a study of the air flow can give an idea about chip disposal.

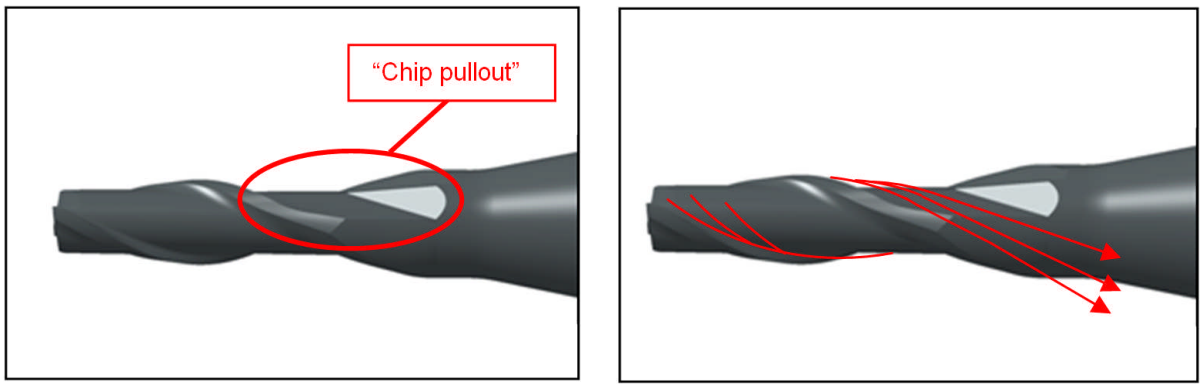

(a) A typical geometry of chip pullout (b) Expected path of a removed chip

Fig 9.27: Pullout of commercial tools

For this purpose is used a CFD analysis of air flow around a rotating micro end-mill. The analysis is performed with FLUENT 6.3. Classical k-ε turbulent model with enhanced wall treatment is used in this study. Starting CFD mesh has about 1 million cells with high mesh density in the zone closed to the tool; average cell edge length in this zone is 1 μm. Adaptive remeshing technique is used during the simulations. This technique automatically refines the mesh always when an increment of pressure inside a cell exceeds a critical value. This approach is commonly used in CFD analyses and helps to minimize a numerical error.

Five different rotational speeds analysed in this study are: 1 rpm, 10 rpm, 100 rpm, 1 000 rpm and 10 000 rpm. In fig. 9.28 are shown streamlines for two limiting speeds (1 rpm and 10 000 rpm). In the first case, the streamlines tend to follow the cutting edges. Hence, in this case the chip can theoretically rich the location of chip pullout. However, this speed is unrealistically low and would never be used in any machining process. On the other hand, the speed of 10 000 rpm represents a realistic case. However, all streamlines in this case are in planes perpendicular to the axis of rotation and do not show any tendency of following the cutting edge. Hence, the chip is predicted to flow away immediately after it is fully separated from the workpiece. Similar air flow trends are clearly noticeable already with low speeds of 10 rpm.

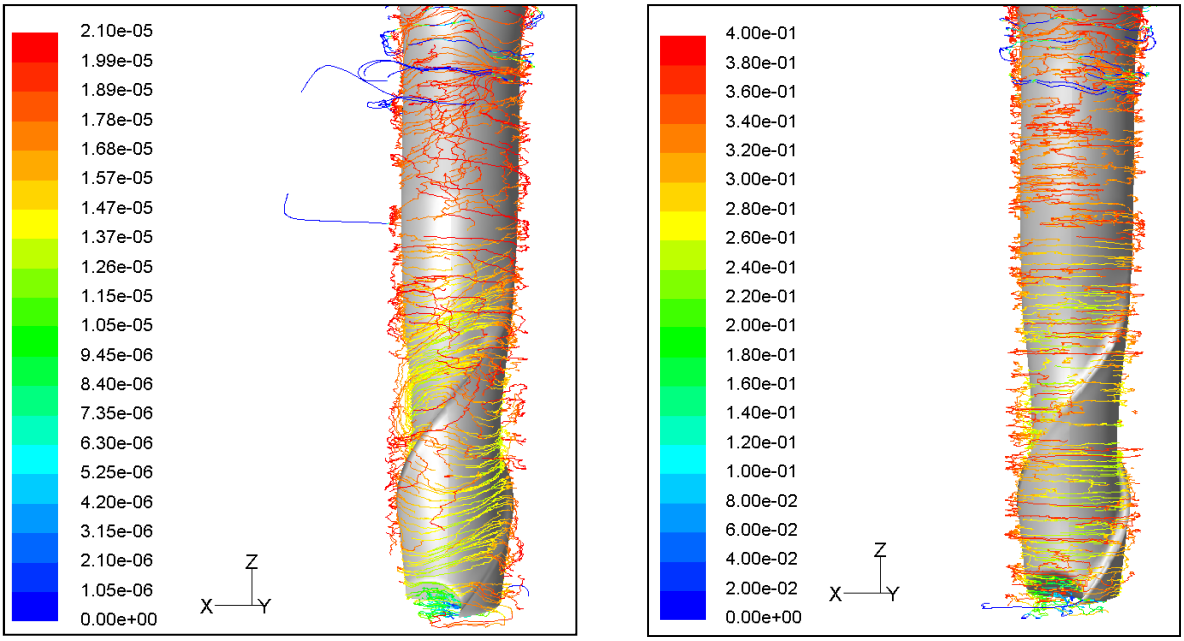

(a) Tool rotation of 1 rpm

(b) Tool rotation of 10 000 rpm

Fig 9.28: Air flow inducted by the tool rotation

Hence, the results of this study indicate that realistically the chip will never reach the location of the pullout. Hence, an effort of designing these geometrical features has no positive effect on cutting process and it should not be included in micro end-mill designs.

Finally, it should be noticed that the simulations presented here are very simplified comparing to the real life situations. However, the assumption about pointlessness of the complicated pullouts was confirmed by some other researchers (P. Li and A. Massimiliano) who have used high speed cameras in their research. Their observations confirm that the chips flow away immediately after they are separated and do not follow the cutting edge up to the pullout geometry.

9.4.6 Optimisation of tool dimensions

The next step of the micro end-mill design is an optimization of the tool dimensions. In this cases study are optimised only two dimensions: the helix angle and the transition length (see fig. 9.29 to fig. 9.31). However, in some other cases more dimensions might be considered.

For this purpose all three concepts with different helix angles and transition lengths are analysed by static FEA. The helix angles vary from 10° up to 50° with a step of 10°. The

transition lengths vary from 100 µm up to 500 µm with a step of 100 µm. Hence, 25 simulations are run for each tool. The applied cutting parameters used in this study are: f_z = 2 µm/tooth, a_e = 20 µm and a_p = 100 µm. The cutting forces are applied in the same manner as it was presented in chapter 7. Therefore, it will not be further discussed here. It is just worth to mention that the variable helix angle affects the force distribution over the cutting edge as well as the total cutting force and its direction. Hence, the cutting force must be calculated specially for each of the analysed cases.

Although the methodology states that both stiffness and maximum bending stress should be considered as optimisation parameters, in this case study is analysed only the stress. This is because the tool is proposed for roughing, and therefore, the stiffness is not an important issue. Generally the quality and accuracy of the semi-finished product is not as crucial. The main reason for roughing is a removal of a majority of the unwanted material. This manufacturing phase is usually planed to reduce the work load for finishing operations. This shows that the methodology should always be used with a consideration of the tool applications and it should not be blindly followed step by step.

The resulting maximum stresses for the first concept are shown in fig. 9.29. It is evident that the stress reduces with increasing helix angle and decreasing transition zone length. However, in the case of the shallowest helix angle can be observed an increase of the maximum stress on both limiting transition lengths of transition. The function reaches its minimum when the shortest transition length is combined with the largest helix angle. However, this would cause difficulties during the tool manufacturing, and therefore, it was decided to use helix angle of 40° and the transition length of 200 µm.

The other two concepts show different trends of the stress. Generally, they also show stress reduction with increasing helix angles and decreasing transition lengths. However, there is no increase of the stresses in the case of combination of short transition lengths and shallow helix angles. On the other hand, a clear saddle can be observed when the transition length is approximately 300 µm and helix angle is over 30°. Same as in the previous case it is assumed that the tool with the helix angle of 50° would be difficult to manufacture with the current manufacturing methods. Therefore, the transition length of 300 µm and the helix

angles of 40° are chosen for these two tool designs. The results of the analyses for the versions 2 and 3 are shown in figs. 9.30 and 9.31.

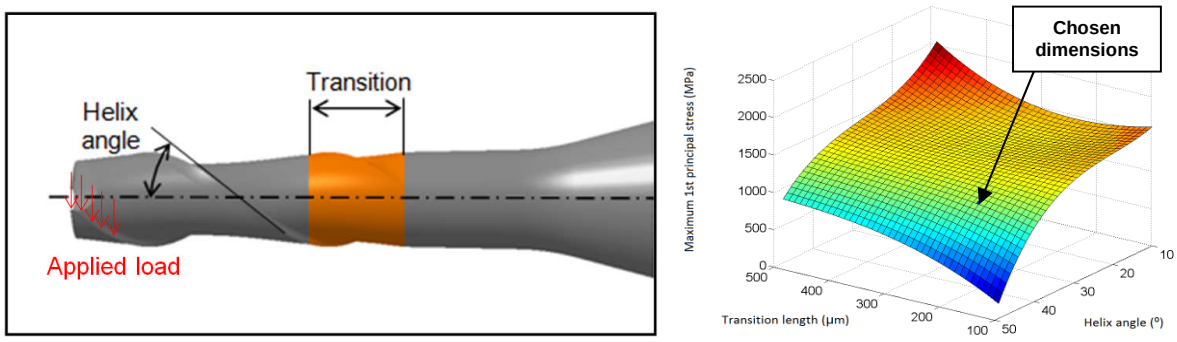

Fig 9.29: The dependency of the maximum tensile stress on the transition length and helix angle, design concept 1

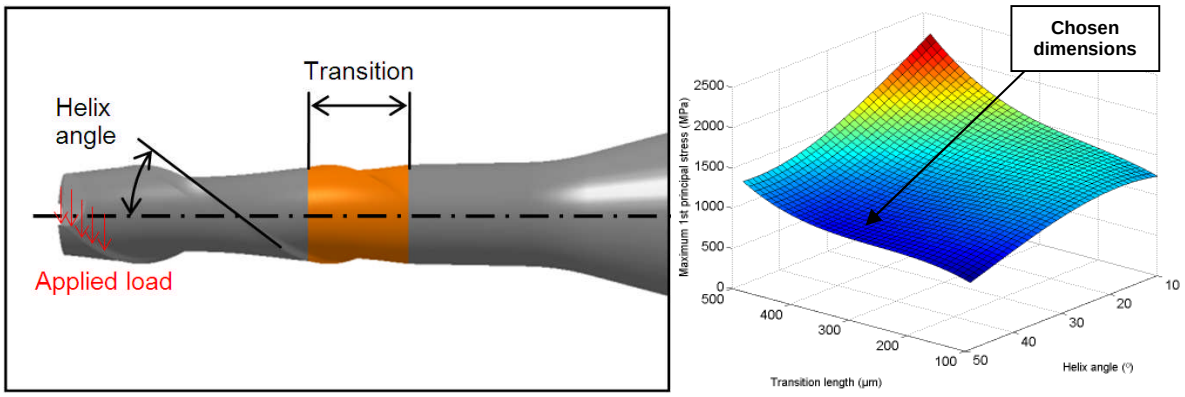

Fig 9.30: The dependency of the maximum tensile stress on the transition length and helix angle, design concept 2

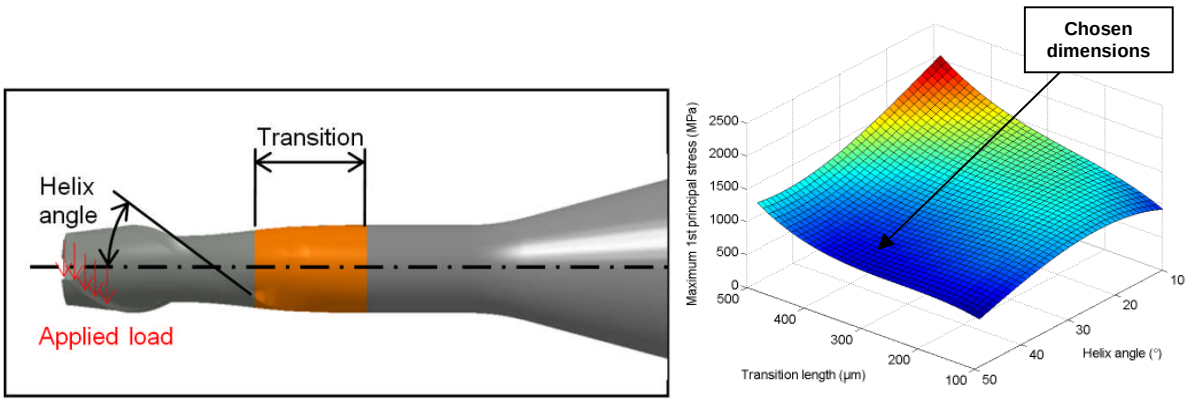

Fig 9.31: The dependency of the maximum tensile stress on the transition length and helix angle, design concept 3

9.4.7 Sensitivity analysis

The sensitivity of the tool to the applied force direction is another important factor which must be considered during designing process. The cutting force is influenced by many input factors such as tool wear, workpiece micro structure, machine tool vibrations or tool inaccuracies. All these factors are variable during cutting process, and therefore, it is impossible to predict the resultant cutting force direction absolutely accurately. In micro milling these uncertainties are significantly higher than in the case of macro milling. Therefore, micro end-mills should always have as low sensitivity to the cutting force direction as possible. This helps to increase the predictability of tool performance.

For this reason the optimized tool concepts were loaded by a unit force applied in different directions from 0° to 90°. The angle of 0° corresponds to a fully tangential force as the angle of 90° corresponds to a radial force. For the comparison reasons, the sensitivity of the commercial tool was also analysed. The results of this analysis are plotted in fig. 9.32. In the left graph is plotted tool bending stiffness as a function of the applied force angle. The commercial tool shows the lowest stiffness from all of the analysed cases. Furthermore, the difference between the maximum and the minimum stiffness of the commercial tool is 17 $N \cdot mm^{-1}$. This is more than in any other analysed case. Hence, clearly the commercial tool is more sensitive and has lower stiffness than any of the proposed tool designs. The tool design version 2 and 3 show very similar stiffness. However, the second version is less sensitive to the direction of the applied force. Therefore, from this point of view the second tool design is the most favourable. However, the third tool design is a good alternative.

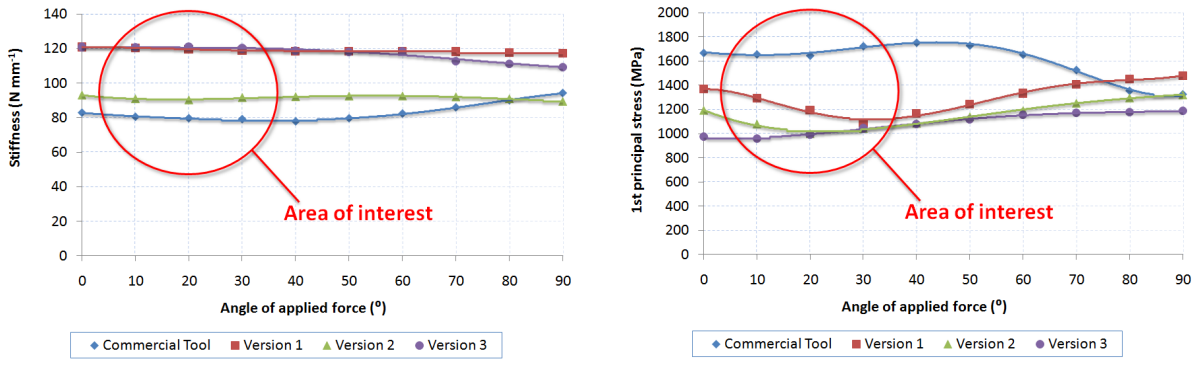

Fig 9.32: Dependency of the stiffness and maximum tensile stresses on the cutting force direction

The second graph shows the calculated maximum stresses. Obviously in this case the minimum values are preferred. Clearly the original design represents the worst of the tested cases. In this case the lowest stress is evoked by fully radial force. This is, however, absolutely unrealistic to appear during real machining process. At the reality, the experimental forces measured during this research always fit to range between approximately 10° and 30°. The lowest stresses on this range show the tool version 3. It also shows the lowest sensitivity to the direction of the applied force. Hence, from this point of view the third tool design is unbeatably the best one.

9.4.8 The cutting conditions effects on the tool inner stresses

Tab. 9.4: Cutting conditions used in a study of the novel designs

	Feed (µm/tooth)	Width of cut (µm)	Depth of cut (µm)
Test 1	4	20	50
Test 2	4	20	100
Test 3	4	20	150
Test 4	4	20	100
Test 5	4	60	100
Test 6	4	100	100
Test 7	2	20	100
Test 8	4	20	100
Test 9	6	20	100

In the subsection 9.4.6 the tool was analysed only for its response to one set of cutting parameters. However, in the real life various cutting conditions may be required. Therefore, in this section the tool is analysed for its response to three different sets of cutting parameters. The applied cutting parameters are listed in tab. 9.4 and they can be divided into three groups. The first three tests have variable depth of cut, whereas width and feed are fixed to 4 µm/tooth and 20 µm respectively. In the second group of tests are fixed the feed (4 µm/tooth) and the depth of cut (100 µm), whereas the width of cut is variable. In the last group is variable the feed. The width of cut is fixed to 20 µm and the depth of cut to 100 µm. In all cases were calculated resultant bending stresses. The same method as the one described in chapter 7 was used.

The maximum tensile stresses are shown in fig. 9.33. In all of the investigated cases the three new designs show significant decrease of stresses. The average stress reduction comparing to the commercial tool is: 40% for the design no. 1, 42% for design no. 2 and 46%

for design no. 3. Hence, this study confirms the findings from the previous section that the third tool design is the most promising one.

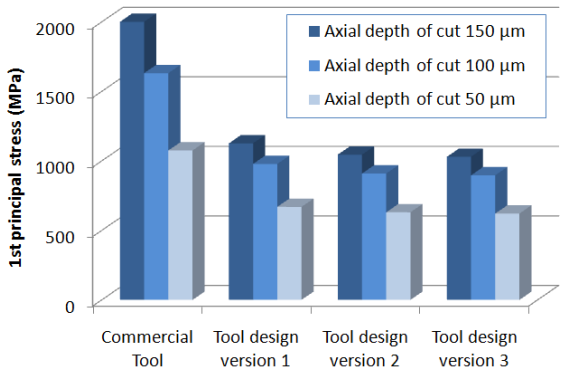

(a) The effect of the depth of cut on the inner stresses

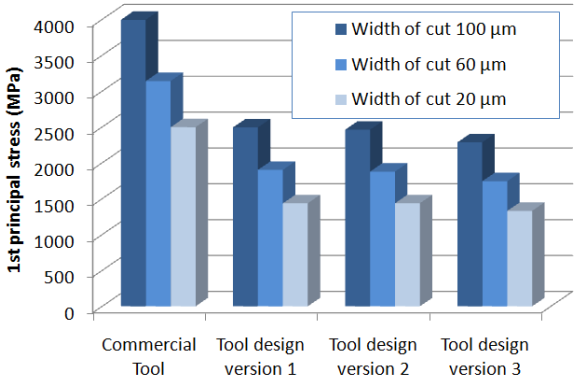

(b) The effect of the width of cut on the inner stresses

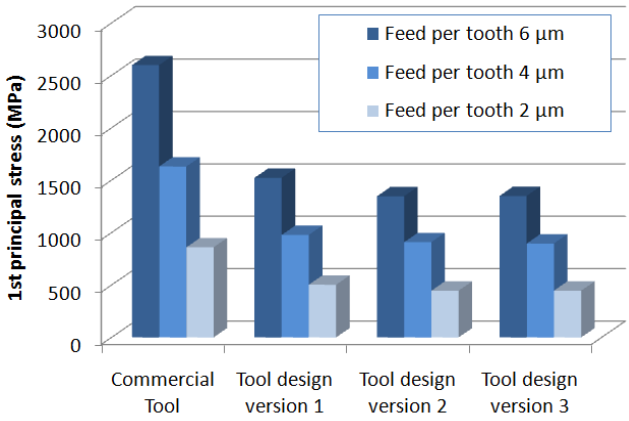

(c) The effect of the feed on the inner stresses

Fig 9.33: The effects of the cutting conditions on the tools inner stresses

9.5 Summary

In this chapter is presented a systematic methodology for designing of micro end-mills. The methodology is based on the knowledge gained during the experimental and theoretical research covered in the previous chapters. It takes in consideration the major challenges of micro end-milling. The chapter is divided into three major parts. In the first part are comprehensively discussed all the main factors which must be considered during the tool design. In the second part is proposed the methodology for designing of micro end-mills, and in the third part is the method demonstrated on a case study.

In the case study is designed a roughing tool. The tool is a dual helix micro end-mill with the cutting diameter of 0.2 mm. The theoretical data covered in the case study show a great potential of the newly proposed design. The novel tool shows higher stiffness (~30%), lower maximum stress (~40%) and lower sensitivity than the original commercial design. However, it must be mentioned that the theoretical results are not verified.

The presented method is the first one which takes in account as wide range of different scaling effects and is designed with a respect of micro-milling challenges. Because a typical micro end-mill is extremely sensitive tool, it is expected that the tool manufacturers will have to change their policy and start to produce large variety of specialised tools. Therefore, it is expected that systematic methods, such as the one presented here, will be highly desirable in the near future.

10. Conclusions and recommendations

10.1 Conclusions

In chapter 3 were set four main objectives of this research. All these objectives follow one common aim of increasing reliability of micro milling process.

Objective 1: Identify the main factors affecting tool performance and develop an understanding of them

In the first stage of this research were performed benchmarking tests comparing performance of tools with two different cutting diameters. The first type of tools had cutting diameter of 0.2 mm. These tools were the smallest ones available in the market at the time of beginning of the research. On the other hand, the second tool type had cutting diameter of 1 mm. These tools are on a boundary between conventional and micro milling. Furthermore, in both cases were used coated and uncoated tools. This helps to investigate effects of the coating in micro milling. During the tests were measured all the major process characteristics such as cutting forces, wear progression and generated surface roughness.

Wear patterns observed during the tests have not confirmed any difference between various tool types. Hence, it may be concluded that the wear mechanisms in micro milling are the same as those in conventional milling. As the dominant wear mechanism was identified tool abrasion. However, also cutting edge chipping and adhesion of workpiece material on the cutting edge were observed during the tests. The adhesion was identified as a dangerous wear mechanism resulting in BUE. The force measurements also indicate that BUE appears frequently and has a strong effect on cutting process (sudden increase of cutting force acting on one cutting edge and reduction of the force acting on the second edge). However, experiments with higher cutting speeds, performed later in this research, have shown that BUE becomes less important if cutting speed is increased.

The force measurements have identified one of the major differences between micro milling and conventional milling. Although a theoretical volume removed per cut was reduced by 125 times when 0.2 mm tools were used, the maximum cutting force has reduced only 5 times. This indicates an enormous increase of specific cutting energy in the case of

micro milling. It is assumed that the main reason of this increase is the reduction of uncut chip thickness to the level closed to cutting edge radius. This leads to ploughing dominant cutting mechanism which generates higher cutting forces than shearing dominant mechanism (typical for conventional milling). However, this assumption needs to be further investigated.

Surface roughness generated by Ø0.2 mm and Ø1 mm tools was found to be approximately the same. This observation is contrary to geometrical surface roughness modelling methods (based on assumption that surface roughness can be calculated from the cutting edge path). Furthermore, with progressing tool wear the surface quality generated by Ø 0.2 mm tools reduces faster than in the case of Ø 1 mm tools.

One of the major issues of micro milling identified during this research is premature tool breakage. This issue was observed only when Ø0.2 mm tools are used. Hence, it is a clear difference between conventional and micro milling. Furthermore, it was found difficult to predict tool breakage in advance. Milling distance, removed volume or machining time do not show any signal of imminent tool breakage. As the main reason of this unpredictability were identified large dimensional tolerances of micro end-mills. Therefore, stress analysis is assumed to be essential for prediction of tool breakage.

The coating was found beneficial in both studied cases. It reduces tool wear and consequently it has also a positive effect on cutting force increments. Furthermore, in micro milling also a positive effect of the coating on tool breakage was observed. The coated tools withstand higher forces and break later than uncoated ones. It is assumed that the coating has an ability to cover surface imperfections in form of micro cracks and machining marks. The coating also smoothes sharp edges and corners, and therefore, reduces maximum stresses. The only negative effect of the coating was observed on the surface roughness. Surfaces generated by coated tools are generally rougher than surfaces generated by uncoated tools.

Objective 2: Based on the knowledge, propose a tool life prediction method

The knowledge gained from the experiments indicates importance of tool breakage prediction. This is different from conventional milling where no tool breakage was observed. Especially the very small micro end-mills with diameters bellow approximately 0.3 mm are extremely liable to break. The importance of this issue increases with reducing tool diameter.

Furthermore, it is not possible to prevent the small micro end-mills to break (this is because of continuous growth of cutting forces due to tool wear). Hence, clearly the tool life has a different meaning in micro milling than in conventional milling.

In this research was developed a systematic micro end-mill life prediction method. The method shows a great potential for industrial applications. Experimentally validation has shown a good agreement of predicted tool lives with the reality. The method is based on FE stress analysis and statistical analysis of real tool dimensions. The main novelty of this method is in application of statistical distribution of tool dimensions instead of using nominal ones as it is usual. Thanks to this approach, tool life is predicted in a form of risk of tool breakage.

Objective 3: Investigate possibilities of tool life extension through improvements of tool geometry

Tool geometry is another important issue of micro milling. Although it is well known fact that the reduction of tool diameter has strongly negative effect on bending stress and stiffness, the current tool designs do not respect it. The commercial micro end-mills were found to be a scaled down copies of conventional end-mills. This practice is, however, absolutely inappropriate and needs to be changed. It is evident that because of micro end-mill predisposition to premature breakage, micro end-mills must be designed with much higher attention than conventional tools. There is a large number of factors affecting tool life in micro scale. In this research were identified as the most critical:

- Tool wear, which leads to increase of cutting forces.
- Sharp geometric features in exposed zones (concave edges and sharp corners) representing dangerous stress concentrators.
- Low bending stiffness, which leads to higher machining errors and also to higher bending stresses.

Hence, it is evident that the challenge is to reduce tool bending stresses and increase tool stiffness. As the best solution seems to be reduction the number of sharp geometric features and the remaining ones relocate to less critical zones. One of the possible solutions is to use

designs with variable helix angles. Furthermore, the tool geometries should be designed with a minimum number of features and with the highest possible cross-sectional area.

Another important issue is tool sensitivity to the cutting force direction. Especially in the case of micro milling, the direction of resultant force is highly instable. This is because of high effect of various uncertainties, chatter, and also because of the effect of tool wear. Therefore, the micro end-mills should be designed with a low sensitivity to the resultant force direction.

On the other hand, the theoretical analysis indicates low importance of tool unbalance. This is very different from the conventional milling, where tool unbalance is an important issue causing machining errors. The finding that tool unbalance is not critical in micro milling opens new possibilities. Unbalanced single flute tools may be designed with maximized core cross-section. This can be used for new highly stiff designs which can significantly increase tool life.

The research also highlighted a need of specialised designs for various applications. This issue arise from extreme sensitivity of micro end-mills to various factors. This leads to necessity of a systematic designing method which can speed up and utilise development of new micro end-mills.

Objective 4: Develop a systematic methodology suitable for micro end-mill design

Based on the knowledge gained during this research a systematic methodology for micro end-mill design was developed. The main novelty of this method is in its broad scope of issues which are considered. In this sense it is the first systematic method tailored for micro end-mill design.

The method was presented on a case study in which a roughing dual helix micro end-mill was developed. The theoretical results achieved in this case study show approximately 45% reduction of bending stresses within the proposed tool comparing to the commercial one. This reduction was achieved by two main improvements of the tool geometry. First the tool cross-section was redesigned as a larger cross-sectional area was achieved. Secondly, the cutting edge termination zone was also redesigned so that a fluent termination could be achieved.

Main contributions of knowledge are:

- The effects of the coatings on micro end-mill life were identified. Except of well known effect on tool wear, a positive effect of coating on tool breakage was observed (the coated tools withstand higher cutting forces). This effect of the coating was not yet described in relevant literature by anyone else.
- The effects of dimensional tolerances on micro end-mill stresses were quantified. Although, the quality of micro end-mills is a well known issue, nobody has quantified it so far. The theoretical results in this thesis are the first ones identifying the scale of this effect.
- A new tool life prediction method was developed. The method is based on a new approach combining statistical analysis of tool dimensions and analytically-numerical models. This method is the first one able to give realistic prediction of micro end-mill life.
- Systematic methodology for designing of micro end-mills was proposed. Although, some of the researches have presented new micro end-mill designs, none of them has considered as wide range of scaling effects as it is presented in this thesis. Hence, the methodology is the first one considering various challenges including chip formation, tool breakage and manufacturability.

10.2 Recommendations for future research

The results and conclusions drawn from this research lead to the following recommendations for further research:

- Determination of cutting force model coefficients by FEA of chip formation.
- Further validation of the proposed methods.
- Extension of the tool life prediction method by implementation of other relevant factors.
- Exploitation of the methods by their implementation in commercial software.
- Development of novel coatings preventing tool breakage.

Determination of cutting force model coefficients

The method of cutting force determination shows a good agreement with experimental data. However, the weakness of the method is in determination of the specific cutting energy and the proportional constant. These coefficients are determined experimentally, and they are assumed to be the main cause of model errors. Furthermore, the coefficients must be determined from full slotting milling. This is, however, very difficult in the case of machining of hard materials with very small micro end-mills. It is assumed that in some cases it is not possible to achieve these coefficients experimentally at all. A possible solution of this issue is determination of the cutting force model coefficients from numerical simulations of chip formation. Such approach was recently proposed by S. Afazov [84]. This model is claimed to give accurate predictions of micro milling cutting force. It is recommended to exploit possibilities of this approach and implement it into the method used in this research.

Validation of the proposed methods

Although the methods developed in this research show high potential, they should be further validated. This is, however, a challenging task because of large variations of micro end-mills. For example, the tool life prediction method was validated by three different sets of tests (each with 15 repetitions). These tests have shown a good correlation with the predicted tool lives. However, further validation with more repetitions and wider range of cutting parameters is still required. Furthermore, a validation of the method for more complex machining strategies should be also performed.

Extension of the tool life prediction method

The tool life prediction method presented in this thesis shows a good agreement with experimental tests. The method, as it is presented here, implements the effect of tool dimensional tolerances and uncertainty of maximum cutting force progression. However, in real machining process are presented also other uncertainties such as tool run-out, cutting edge chipping, BUE or chatter. Their effects have not been studied in this research, but they are assumed to be important source of errors. Therefore, it is essential to continue in development of the method and implementation of the further factors.

Furthermore, the method in the current state predicts only tool life. Although, this is very important information for estimation of final product costs and machining times, further information about the product quality is required. Hence, it is suggested to implement the surface quality and product accuracy prediction method.

Exploitation of the methods

The methods (especially the tool life prediction method) give new opportunities for industry to predict product costs and delivering times. This information helps to increase the competitiveness of micro milling. However, before the potential of the proposed methods can be fully exploited, they must be offered to industry in an easy to use form. As the best approach seems an implementation of the methods into existing software. However, before this will be possible, the compatibility of the methods with existing approaches must be increased. For example, it is not comfortable to prepare the workpiece model by direct numerical prescription of the geometry as it was done here. It would be much more comfortable to use capabilities of existing CAD/CAM software. Furthermore, by combining the newly developed methods with capabilities of existing CAM software, new cutting parameters optimisation methods can be developed.

Development of novel coatings preventing tool breakage

During the experimental study included in this research was identified a new effect of tool coating. The coating helps to increase the critical force (force acting on the tool in the moment of breakage). It is assumed that the coating mask surface defects and smooth sharp edges. However, this effect of the coating was not further studied in this research. Therefore, it is recommended to research new coating materials and new coating structures. It is assumed, that by application of nano-layered tough coatings the tool life can be further improved.

References

1. Moreau, W.M., ed. *Semiconductor lithography*. 1988, New York: Plenum Press.

2. Harriot, L.R., *Next generation lithography.* Materials Today, 1999. **2**.

3. Uriarte, L., et al., *A comparison between microfabrication technologies for metal tooling.* Proceedings of the 1st International Conference on Multi-Material Micro Manufacture, 2005: p. 351-354.

4. Pham, D.T., et al., *Micro-EDM - recent developments and research issues.* Journal of Materials Processing Technology, 2004. **149**(1-3): p. 50-57.

5. Dornfeld, D., S. Min, and Y. Takeuchi, *Recent Advances in Mechanical Micromachining.* CIRP Annals, 2006. **55**(2): p. 745-768.

6. Masuzawa, T. and H.K. Tonshoff, *Three-Dimensional Micromachining by Machine Tools.* CIRP Annals, 1997. **46**(2): p. 8.

7. Masuzawa, T., *State of the Art of Micromachining.* CIRP Annals, 2000. **49**(2): p. 473-488.

8. Meijer, J., *Laser beam machining (LBM), state of the art and new opportunities.* Journal of Materials Processing Technology, 2004. **149**(1â€“3): p. 2-17.

9. Kruth, J.P., M.C. Leu, and T. Nakagawa, *Progress in Additive Manufacturing and Rapid Prototyping.* CIRP Annals - Manufacturing Technology, 1998. **47**(2): p. 525-540.

10. Bouchaud, J., *High Value MEMS market overview*, in *Symposium on Design, Test, Integration & Packaging of MEMS/MOEMS*. 2011: Aix-en-Provence, France.

11. MINAM, *Micro- and Nanomanufacturing Stratgic Research Agenda*. 2012 (in press). p. 30.

12. Bigot, S., P. Dorrington, and S. Dimov, *Manufacturing Routes Costs Comparison for Emerging Micro and Nano Technologies*, in *Multi-Material Micro Manufacture 2010*, B. Fillon, C Khan-Malek, and S. Dimov, Editors. 2010: Oyonnax. p. 199-202.

13. *Balzer's device for making millig-cutters.* Journal of the Franklin Institute, 1896. **142(6)**: p. 440-442.

14. I. Tansel, et al., *Micro-end-milling-I. Wear and breakage.* International Journal of Machine Tools & Manufacture, 1998. **38**: p. 1419-1436.

15. Stephenson, D.A. and J.S. Agapiou, *Metal cutting theory and practice*. Second ed. 2006, Boca Raton: CRC Tailor & Francis. 846.

16. Benavides, G.L., D.P. Adams, and P. Yang, *Meso-Machining Capabilities*. 2001, Sandia National Laboratories: New Mexico. p. 40.

17. Hale, L.C., *Principles and Techniques for Designing Precision Machines*, in *Lawrence Livermore National Laboratory*. 1999, University of California: Livermore. p. 493.

18. KERN Precision INC. 2011; Available from: www.kern-microtechnic.com.

19. Tansel, I., et al., *Micro-end-milling - II. Extending tool life with a Smart Workpiece Holder (SWH).* International Journal of Machine Tools and Manufacture, 1998. **38**(12): p. 1437-1448.

20. Tansel, I., et al., *Micro-end-milling - III. Wear estimation and tool breakage detection using acoustic emission signals.* International Journal of Machine Tools and Manufacture, 1998. **38**(12): p. 1449-1466.

21. Bao, W.Y. and I.N. Tansel, *Modeling micro-end-milling operations. Part II: tool run-out.* International Journal of Machine Tools and Manufacture, 2000. **40**(15): p. 2175-2192.

22. Bao, W.Y. and I.N. Tansel, *Modeling micro-end-milling operations. Part I: analytical cutting force model.* International Journal of Machine Tools and Manufacture, 2000. **40**(15): p. 2155-2173.

23. Bao, W.Y. and I.N. Tansel, *Modeling micro-end-milling operations. Part III: influence of tool wear.* International Journal of Machine Tools and Manufacture, 2000. **40**(15): p. 2193-2211.

24. Rahman, M., A. Senthil Kumar, and J.R.S. Prakash, *Micro milling of pure copper.* Journal of Materials Processing Technology, 2001. **116**(1): p. 39-43.

25. Chae, J., S.S. Park, and T. Freiheit, *Investigation of micro-cutting operations.* International Journal of Machine Tools and Manufacture, 2006. **46**(3-4): p. 313-332.

26. Takeuchi, Y., et al., *Development of a 5-Axis Control Ultraprecision Milling Machine for Micromachining Based on Non-Friction Servomechanisms.* CIRP Annals - Manufacturing Technology, 2000. **49**(1): p. 295-298.

27. Mikrotool Pte LTD. 2011; Available from: www.mikrotools.com.

28. Willemin-Macodel SA. 2011; Available from: www.willemin-macodel.com.

29. Makino. 2011; Available from: www.makino.com.

30. Kugler of America. 2011; Available from: www.kuglerofamerica.com.

31. Mori Seiki. 2011; Available from: www.moriseiki.com.

32. Bang, Y.-b., K.-m. Lee, and S. Oh, *5-axis micro milling machine for machining micro parts.* The International Journal of Advanced Manufacturing Technology, 2005. **25**(9): p. 888-894.

33. Nanowave. 2011; Available from: www.nanowave.co.jp.

34. Vogler, M.P., et al., *Development of meso-scale machine tool (mMT) systems.* Society of Manufacturing Engineers MS, 2002. **MS02-181**: p. 1-9.

35. Okazaki, Y., N. Mishima, and K. Ashida, *Microfactory---Concept, History, and Developments.* Journal of Manufacturing Science and Engineering, 2004. **126**(4): p. 837-844.

36. Kussul, E., et al., *Development of micromachine tool prototypes for microfactories.* Journal of Micromechanics and Microengineering, 2002. **12**(6): p. 795.

37. Performance Micro Tool. 2012; Available from: www.pmtnow.com.

38. UNION TOOL co. 2011; Available from: www.uniontool.com.

39. Tansel, I., et al., *Micro-end-milling-I. Wear and breakage.* International Journal of Machine Tools & Manufacture, 1998. **38**: p. 1419-1436.

40. Li, P., *Micro milling of hardened tool steels*. 2009, Technical University Delft: Delft

41. Torres, C.D., et al., *Analyzing the performance of diamond-coated micro end mills.* International Journal of Machine Tools and Manufacture, 2009. **49**(7-8): p. 599-611.

42. Kyocera. 2011; Available from: www.kyoceramicrotools.com.

43. Fang, F.Z., et al., *Tool geometry study in micromachining.* Journal of Micromechanics and Microengineering, 2003. **13**: p. 726-731.

44. Uhlmann, E. and K. Schauer, *Dynamic Load and Strain Analysis for the Optimization of Micro End Mills.* CIRP Annals - Manufacturing Technology, 2005. **54**(1): p. 75-78.

45. Li, P., et al., *Design of micro square endmills for hard milling applications.* The International Journal of Advanced Manufacturing Technology, 2012. **57**(9-12): p. 859-870.

46. Fleischer J., D.M., Kühlewein, Ruhs C., *Geometry optimization of micro milling tools*, in *Fourth International Confrence on Multi-Material Micro Manufacture*. 2008.

47. Davis, J.R., *Tool materials* 1995: ASM international. 289.

48. A. Aramcharoen, et al., *Evaluation and selection of hard coatings for micro milling of hardened tool steel.* International Journal of Machine Tools & Manufacture, 2008. **48**: p. 1578-1584.

49. M. W. Kim, et al., *Cutting performance of nanocomposite Cr-C-N, Cr-Si-N and Cr-Si-C-N coated tools for micro end-milling operation.* Current Applied Physics, 2009. **9**(2, Supplement 1): p. e201-e204.

50. Ducros, C., C. Cayron, and F. Sanchette, *Multilayered and nanolayered hard nitride thin films deposited by cathodic arc evaporation. Part 1: Deposition, morphology and microstructure.* Surface and Coatings Technology, 2006. **201**(1-2): p. 136-142.

51. Ducros, C. and F. Sanchette, *Multilayered and nanolayered hard nitride thin films deposited by cathodic arc evaporation. Part 2: Mechanical properties and cutting performances.* Surface and Coatings Technology, 2006. **201**(3-4): p. 1045-1052.

52. Settineri, L., et al., *Evaluation of wear resistance of AlSiTiN and AlSiCrN nanocomposite coatings for cutting tools.* Manufacturing Technology, 2008. **57**: p. 575-578.

53. Onikura, H., et al., *Fabrication of Micro Carbide Tools by Ultrasonic Vibration Grinding.* CIRP Annals - Manufacturing Technology, 2000. **49**(1): p. 257-260.

54. Kojima, A., W. Natsu, and M. Kunieda, *Spectroscopic measurement of arc plasma diameter in EDM.* CIRP Annals - Manufacturing Technology, 2008. **57**(1): p. 203-207.

55. Ho, K.H., et al., *State of the art in wire electrical discharge machining (WEDM).* International Journal of Machine Tools & Manufacture, 2004. **44**: p. 13.

56. Cheng, X., et al., *Tool fabrication system for micro/nano milling-function analysis and design of a six-axis Wire EDM machine.* International Journal of Advanced Manufacturing Technology, 2010. **46**: p. 9.

57. Jiwang, Y., et al., *Fabrication of micro end mills by wire EDM and some micro cutting tests.* Journal of Micromechanics and Microengineering, 2009. **19**(2): p. 025004.

58. Adams, D.P., et al., *Micromilling of metal alloys with focused ion beam–fabricated tools.* Precision Engineering, 2000. **25**: p. 7.

59. Malekian, M., S.S. Park, and M.B.G. Jun, *Tool wear monitoring of micro-milling operations.* Journal of Materials Processing Technology, 2009. **209**(10): p. 4903-4914.

60. Chern, G.-L. and Y.-C. Chang, *Using two-dimensional vibration cutting for micro-milling.* International Journal of Machine Tools and Manufacture, 2006. **46**(6): p. 659-666.

61. Zaman, M.T., et al., *A three-dimensional analytical cutting force model for micro end milling operation.* International Journal of Machine Tools and Manufacture, 2006. **46**(4): p. 353-366.

62. Bissacco, G., H.N. Hansen, and L. De Chiffre, *Size Effects on Surface Generation in Micro Milling of Hardened Tool Steel.* CIRP Annals - Manufacturing Technology, 2006. **55**(1): p. 593-596.

63. Aramcharoen, A. and P.T. Mativenga, *Size effect and tool geometry in micromilling of tool steel.* Precision Engineering, 2009. **33**: p. 6.

64. Uhlmann, E., S. Piltz, and K. Schauer, *Micro milling of sintered tungsten-copper composite materials.* Journal of Materials Processing Technology, 2005. **167**(2-3): p. 402-407.

65. Filiz, S., et al., *An experimental investigation of micro-machinability of copper 101 using tungsten carbide micro-endmills.* International Journal of Machine Tools and Manufacture, 2007. **47**(7-8): p. 1088-1100.

66. Gietzelt, T., L. Eichhorn, and K. Schubert, *Micromechanical structuring of polymers, metals and ceramics.* Proceedings of the 1st International Conference on Multi-Material Micro Manufacture, 2005: p. 329-332.

67. Zhou, L., et al., *Wear characterics of micro-end mill in high-speed milling of graphite electrode.* Key Engineering Materials, 2004. **259-260**: p. 858-863.

68. Liu, K. and S.N. Melkote, *Finite element analysis of the influence of tool edge radius on size effect in orthogonal micro-cutting process.* International Journal of Mechanical Sciences, 2006. **49**: p. 650-660.

69. Simoneau, A., E. Ng, and M.A. Elbestawi, *Chip formation during microscale cutting of a medium carbon steel.* International Journal of Machine Tools and Manufacture, 2006. **46**(5): p. 467-481.

70. Simoneau, A., E. Ng, and M.A. Elbestawi, *Surface defects during microcutting.* International Journal of Machine Tools and Manufacture, 2006. **46**(12-13): p. 1378-1387.

71. Ng, C.K., et al., *Experimental study of micro- and nano-scale cutting of aluminum 7075-T6.* International Journal of Machine Tools and Manufacture, 2006. **46**(9): p. 929-936.

72. Son, S., H. Lim, and J. Ahn, *The effect of vibration cutting on minimum cutting thickness.* International Journal of Machine Tools and Manufacture, 2006. **46**(15): p. 2066-2072.

73. Ikawa, N., et al., *Ultraprecision Metal Cutting -- The Past, the Present and the Future.* CIRP Annals - Manufacturing Technology, 1991. **40**(2): p. 587-594.

74. Robinson, G.M. and M.J. Jackson, *A review of micro and nanomachining from a materials perspective.* Journal of Materials Processing Technology, 2005. **167**(2-3): p. 316-337.

75. Ikawa, N., et al., *Minimum thickness of cut in micromachining: Ikawa, Naoya; Shimada, Shoichi; Tanaka, Hiroaki. Nanotechnology. 1992 Jan; 3(1): 6-9.* Precision Engineering, 1993. **15**(4): p. 300-300.

76. Shaw, M.C., ed. *Metal Cutting Principles*. 2005, Oxford University Press.

77. Woon, K.S., et al., *Investigations of tool edge radius effect in micromachining: A FEM simulation approach.* Journal of Materials Processing Technology, 2008. **195**(1-3): p. 204-211.

78. Shiari, B., R.E. Miller, and D.D. Klug, *Multiscale simulation of material removal processes at the nanoscale.* Journal of the Mechanics and Physics of Solids, 2007. **55**(11): p. 2384-2405.

79. Weule, H., V. Hüntrup, and H. Tritschler, *Micro-Cutting of Steel to Meet New Requirements in Miniaturization.* CIRP Annals - Manufacturing Technology, 2001. **50**(1): p. 61-64.

80. Liu, K., X.P. Li, and M. Rahman, *Characteristics of high speed micro-cutting of tungsten carbide.* Journal of Materials Processing Technology, 2003. **140**(1-3): p. 352-357.

81. Yuan, Z.J., M. Zhou, and S. Dong, *Effect of diamond tool sharpness on minimum cutting thickness and cutting surface integrity in ultraprecision machining.* Journal of Materials Processing Technology, 1996. **62**(4): p. 327-330.

82. Vogler, M.P., R.E. DeVor, and S.G. Kapoor, *On the modeling and analysis of machining performance in micro-endmilling, part I: surface generation.* Journal of Manufacturing Science and Engineering, 2004. **126**: p. 685-694.

83. Kim, C.J., J.R. Mayor, and J. Ni, *A static model of chip formation in microscale milling.* Journal of Manufacturing Science and Engineering, 2004. **126**: p. 710-718.

84. Afazov, S.M., S.M. Ratchev, and J. Segal, *Modelling and simulation of micro-milling cutting forces.* Journal of Materials Processing Technology, 2010. **210**(15): p. 2154-2162.

85. Sato, M., T. Ueda, and H. Tanaka, *An experimental technique for the measurement of temperature on CBN tool face in end milling.* International Journal of Machine Tools and Manufacture, 2007. **47**(14): p. 2071-2076.

86. van Luttervelt, C.A., et al., *Present Situation and Future Trends in Modelling of Machining Operations Progress Report of the CIRP Working Group [`]Modelling of Machining Operations'*. CIRP Annals - Manufacturing Technology, 1998. **47**(2): p. 587-626.

87. Ehman, K.F., et al., *Machining Process Modelling: A Review*. Journal of Manufacturing Science and Engineering, 1997. **119**: p. 655-663.

88. Tlusty, J. and P. MacNeil, *Dynamics of cutting forces in end milling.* CIRP Annals, 1975. **24**(1): p. 21-25.

89. Jin, T., D.J. Stephenson, and D.M. Allen, *A new approach in modelling the micro end milling process using variable specific cutting energy and force ratio*, in *ICRM2007 – 4th International Conference on Responsive Manufacturing*. 2007: Nottingham.

90. Cygax, P.E., *Dynamics of cutting forces in end milling.* Annals of the CIRP, 1979. **23**(2-3): p. 123-140.

91. Kline, W.A. and R.E. DeVor, *The effect of runout on cutting geometry and forces in end milling.* International Journal of Machine Tool Design and Research, 1983. **23**(2-3): p. 123-140.

92. M. T. Zaman, et al., *A three-dimensional analytical cutting force model for micro end milling operation.* International Journal of Machine Tools & Manufacture, 2006. **46**: p. 366-379.

93. Li, C., et al., *Modeling of three-dimensional cutting forces in micro-end-milling.* Journal of Micromechanics and Microengineering, 2007. **17**: p. 671-678.

94. Feng, H.Y. and N. Su, *A Mechanistic Cutting Force Model for 3D Ball-end Milling.* Journal of Manufacturing Science and Engineering, 2001. **123(23)**: p. 23-29.

95. Umbrello, D., R. M'Saoubi, and J.C. Outeiro, *The influence of Johnson-Cook material constants on finite element simulation of machining of AISI 316L steel.* International Journal of Machine Tools and Manufacture, 2007. **47**(3-4): p. 462-470.

96. Outeiro, J.C., D. Umbrello, and R. M'Saoubi, *Experimental and numerical modelling of the residual stresses induced in orthogonal cutting of AISI 316L steel.* International Journal of Machine Tools and Manufacture, 2006. **46**(14): p. 1786-1794.

97. Özel, T. and T. Altan, *Determination of workpiece flow stress and friction at the chip-tool contact for high-speed cutting.* International Journal of Machine Tools and Manufacture, 2000. **40**(1): p. 133-152.

98. Childs, T.H.C. and K. Maekawa, *Computer-aided simulation and experimental studies of chip flow and tool wear in the turning of low alloy steels by cemented carbide tools.* Wear, 1990. **139**(2): p. 235-250.

99. Raczy, A., et al., *An eulerian finite-element model for determination of deformation state of a copper subjected to orthogonal cutting.* Metallurgical and Materials Transactions A, 2004. **35**(8): p. 2393-2400.

100. Dirikolu, M.H., T.H.C. Childs, and K. Maekawa, *Finite element simulation of chip flow in metal machining.* International Journal of Mechanical Sciences, 2001. **43**(11): p. 2699-2713.

101. Bagci, E., *3-D numerical analysis of othogonal cutting via mesh-free method.* International Journal of the Physical Sciences, 2010. **6**(6): p. 15.

102. O. Pantalé, et al., *2D and 3D numerical models of metal cutting with damage effects.* Computer methods in applied mechanics and engineering, 2004. **193**: p. 4383-4399.

103. Movahhedy, M.R., Y. Altintas, and M.S. Gadala, *Numerical analysis of metal cutting with chamfered and blunt tools.* Transactions of the ASME, Journal of Manufacturing Science and Engineering, 2002. **124**(2): p. 178-188.

104. Movahhedy, M.R., M.S. Gadala, and Y. Altintas, *SIMULATION OF CHIP FORMATION IN ORTHOGONAL METAL CUTTING PROCESS: AN ALE FINITE ELEMENT APPROACH.* Machining Science and Technology, 2000. **4**(1): p. 15-42.

105. Arrazola, P.J., et al., *Finite element modeling of chip formation process with ABAQUS/Explicit 6.3,* in *VIII International Conference on Computational Plasticity*. 2005: Barcelona.

106. Olovsson, L., L. Nilsson, and K. Simonsson, *An ALE formulation for the solution of two-dimensional metal cutting problems.* Computers & Structures, 1999. **72**(5): p. 497-507.

107. Zienkiewicz, O.C. and R.L. Taylor, *The Finite Element Method: The Basis*. Vol. 1. 1967: McGraw-Hill. 708.

108. M. A. Salgado, et al., *Evaluation of the stiffness chain on the deflection of end-mills under cutting forces.* International Journal of Machine Tools and Manufacture, 2005. **45**(6): p. 727-739.

109. V. S. Rao and P.V.M. Rao, *Tool deflection compensation in peripheral milling of curved geometries.* International Journal of Machine Tools and Manufacture, 2006. **46**(15): p. 2036-2043.

110. Altintas, Y., ed. *Manufacturing Automation: Metal Cutting Mechanics, Machine Tool Vibrations, and CNC Design*. 2000, Cambridge university press.

111. Uriarte L., Z.M., Santiso G., Lopez de Lacalle L. N.,Albizuri J., *Evaluation of dynamic parameters of micro milling tools smaller than 0.3 mm in diameter,* in *1st International Conference on Multi-Material Micro Manufacture*. 2005. p. 325-328.

112. *Westwind Air Bearings*. 2009; Available from: www.westwind-airbearings.com.

113. BLUM Novotest. 2011; Available from: www.blum-novotest.de.

114. *MatWeb - Material property data*. 2010; Available from: www.matweb.com.

115. *General Carbide*. 2010; Available from: www.generalcarbide.com/grades.

116. *SSAB*. 2011; Available from: www1.ssab.com.

117. Kistler Instrument AG. 2012; Available from: www.kistler.com.

118. National Instruments. 2012; Available from: www.ni.com/dataacquisition.

119. Malekian, M., S.S. Park, and M.B.G. Jun, *Modeling of dynamic micro-milling cutting forces.* International Journal of Machine Tools and Manufacture, 2009. **49**(7-8): p. 586-598.

120. Pawley J., ed. *Handbook of Biological Confocal Microscopy*. 3rd Edition ed. 2006, Springer: Berlin. 988.

121. Taylor Hobson Ltd. 2011; Available from: www.taylor-hobson.com.

122. Childs, T., et al., *Metal Machining: Theory and Applications*. First Edition ed. 2000, London: Arnold Publishers. 408.

123. J. Tlusty and P. MacNeil, *Dynamics of cutting forces in end milling.* CIRP Annals, 1975. **24**(1): p. 21-25.

124. MatWeb - Material property data. 2012; Available from: www.matweb.com.

125. General Carbide. 2012; Available from: www.generalcarbide.com/grades.

126. Fang, Z.Z., *Correlation of transverse rupture strength of WCâ€“Co with hardness.* International Journal of Refractory Metals and Hard Materials, 2005. **23**(2): p. 119-127.

127. Archard, J.F., *Contact and Rubbing of Flat Surface.* Journal of applied physics, 1953. **24**(8): p. 981-988.

128. J.F. Archard and W. Hirst, *The Wear of Materials under unlubricated Conditions.* Proceedings of the Royal Society, 1958. **A-236**: p. 71-73.

129. Davis, J.R., *Concise Metals Engineering Data Book*. 1997: ASM International. 245.

130. G. R. Johnson and W.H. Cook, *A constitutive model and data for metals subjected to large strains high strain rates and high temperatures,* in *7th International Symposium on Balistics* 1983: The Hague. p. 541-547.

131. G.R. Johnson and W.H. Cook, *Fracture characteristics of three metals subjected to various strains.* Engineering Frature Mechanics, 1985. **21**(1): p. 31-48.

Appendix A: Publications arising from this research

A.1 International conference papers

1. D. Zdebski, D.M. Allen, D.J. Stephenson, J. Hedge, C. Ducros and F. Sanchette, *An analysis of the effects of nanolayered nitride coatings on the lifetimes and wear of tungsten carbide milling tools*, Proceedings of the Cranfield Multi-strand Conference, Cranfield, UK, May 2008, p. 281-286.
   url: https://dspace.lib.cranfield.ac.uk/handle/1826/3832

2. D. Zdebski, J. Hedge, T. Jin, S. Marson, P. Shore, D. J. Stephenson and D. M. Allen, *An initial study on the diamond planing process to produce micro grooves for a microfluidic device*, Proceedings of the 3rd International CIRP High Performance Cutting – Micromachining Conference, Dublin, Ireland, June 2008, Volume 2, p. 549-559, 2008.

3. D. Zdebski, D. M. Allen, D. J. Stephenson, J. Hedge, C. Ducros and F. Sanchette, *An analysis of the effects of nanolayered nitride coatings on the lifetime and wear of tungsten carbide micromilling tools*, Proceedings of 4M Conference, Cardiff, UK, September 2008, p. 179-182.

4. T. Jin, D. Zdebski, D.M. Allen and D.J. Stephenson, *Micromilling force prediction by coupling FE and analytical modeling approaches*, Proceedings of the Cranfield Multi-strand Conference, Cranfield, UK, May 2008, p. 263-268.
   url: https://dspace.lib.cranfield.ac.uk/handle/ 1826/3832

5. T. Jin, D. Zdebski, D. M. Allen and D. J. Stephenson, *A new approach for prediction of micro milling forces*, Proceedings of the 3rd International CIRP High Performance Cutting – Micromachining Conference, Dublin, Ireland, June 2008, Volume 2, p. 785-793, 2008.

6. D. Zdebski, D. M. Allen, D. J. Stephenson, *A numerical analysis of dimensional tolerance effects on the failure of micro end-mills*, Proceedings of 4M Conference, Bourge en Bresse, France, November 2010, p. 170-173.

7. D. Zdebski, S. Ratchev, D. J. Stephenson, D. M. Allen, *Prediction of cutting conditions effects on micro-milling performance*, Proceedings of ICOMM conference, Evanston, USA, March 2012, p. 499-506.

8. D. Zdebski, D. J. Stephenson, S. Ratchev, D. M. Allen, *Methodology for designing of micro end-mills*, 5th CIRP conference on High Performance Cutting, Zurich, Switzerland, June 2012, p. 150-155.

A.2 Journal papers

1. P. Li, D. Zdebski, H. H. Langen, R.H. Munnig Schmidt, A.M. Hoogstrate, J.A.J. Oosterling, T. Jin and D.M. Allen, *Micromilling of thin ribs with high aspect ratios*, Journal of Micromechanics and Microengineering, 2010, **20**(11).

Appendix B: An example of an analysis of a new micro end-mill

Every new tool used in this research was comprehensively analysed by SEM and EDS. This analysis is essential for good knowledge about tool geometry and material composition. The images were also used for qualitative evaluation of the tools. Any distinctly defected and abnormal tools were not used for further research.

The SEM images were also used during preparation of the tool models used for stress analyses. Furthermore, knowledge gained from the SEM analysis was used in chapter 7 for determination of the tool tolerances and in chapter 9 for FEA of chip formation.

B.1 SEM analysis

Every tool was studied from four different sides and from front. This method gives a very comprehensive knowledge about tool geometry. In the following figures are shown examples of SEM images of the tool from different sides. Magnifications used in this analysis are: 100x (representing overall tool geometry), 350x (detail of the tool tip) and 800x (detail of the cutting edge).

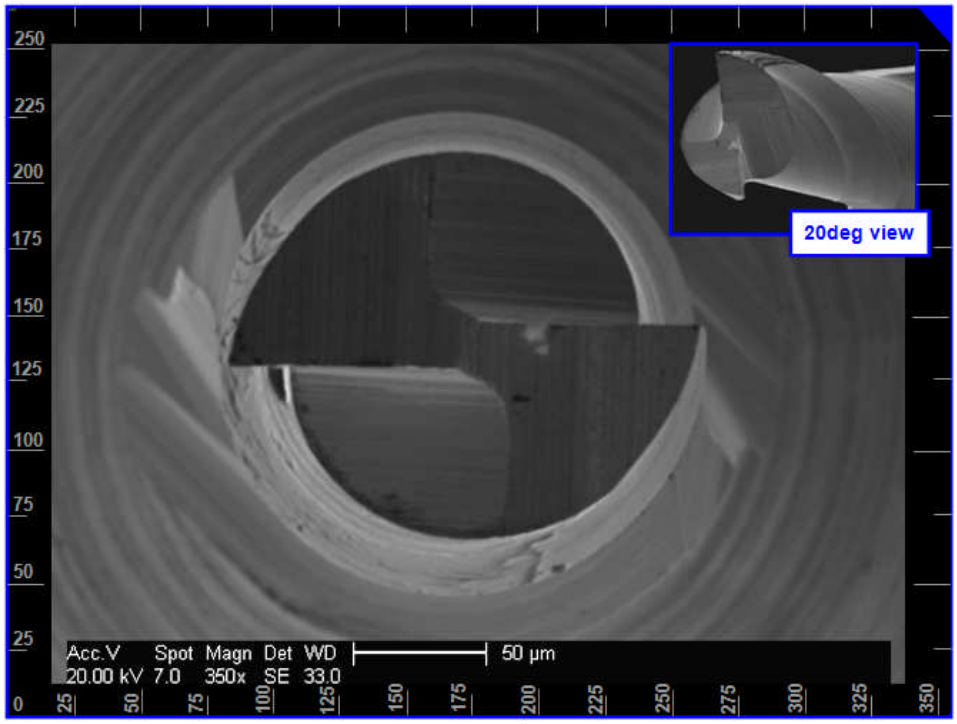

Fig B.1: Front view of Ø0.2mm uncoated tool (350 times magnified)

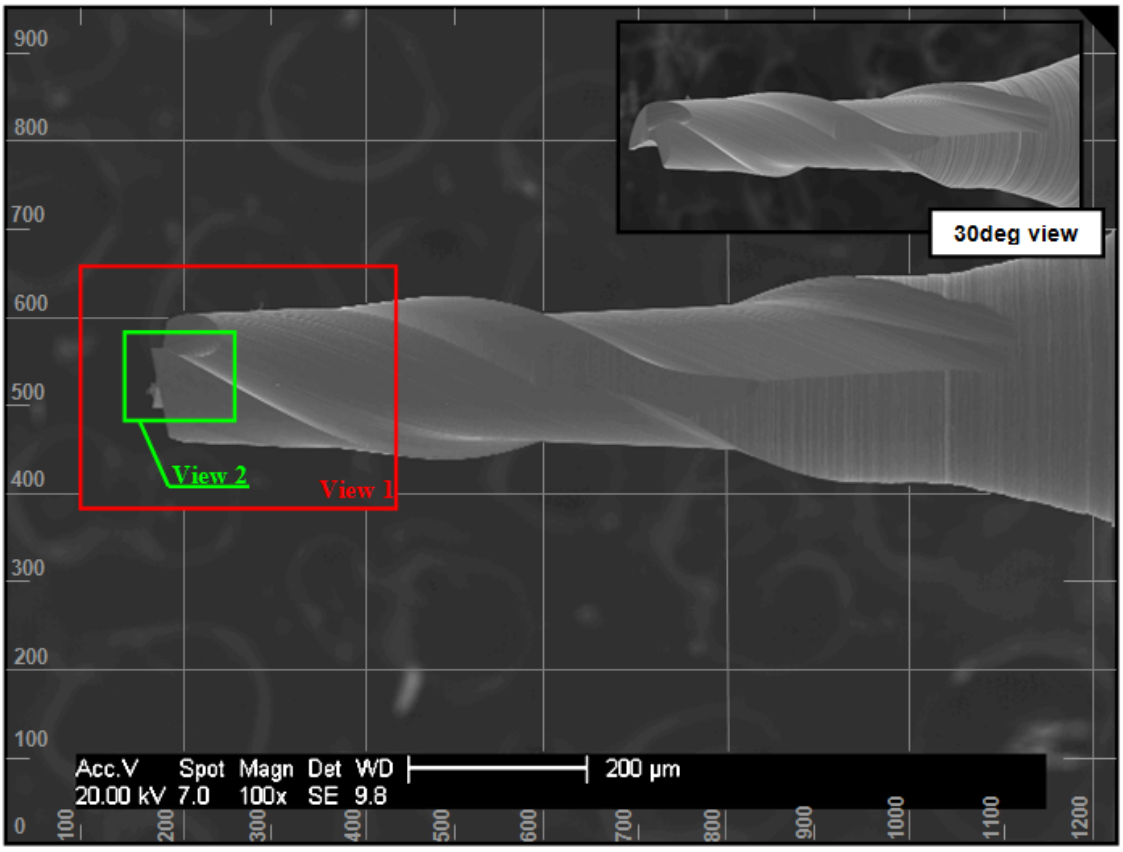

(a) Overall view (mag. 100x)

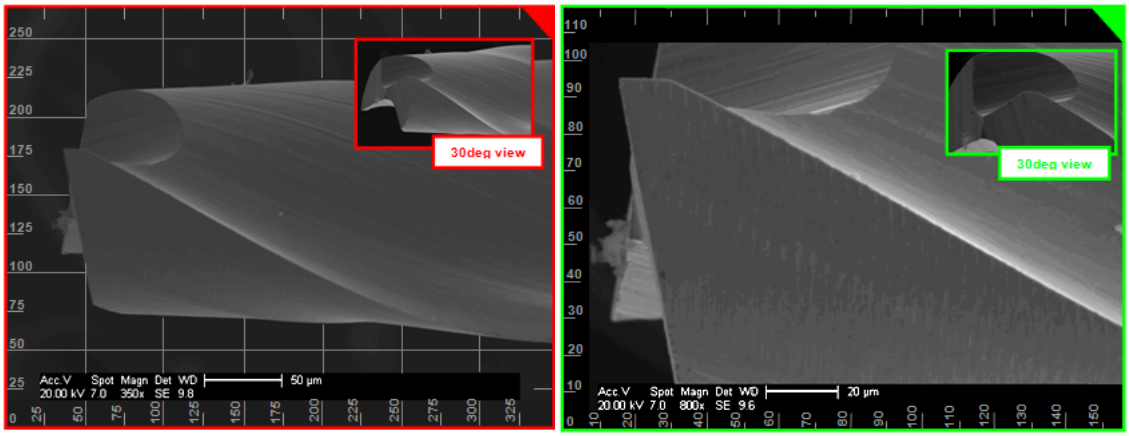

(b) Tool tip view (mag. 350x) (c) Cutting edge detail (mag. 800x)

Fig B.2: SEM images of first side of a typical uncoated micro end-mill

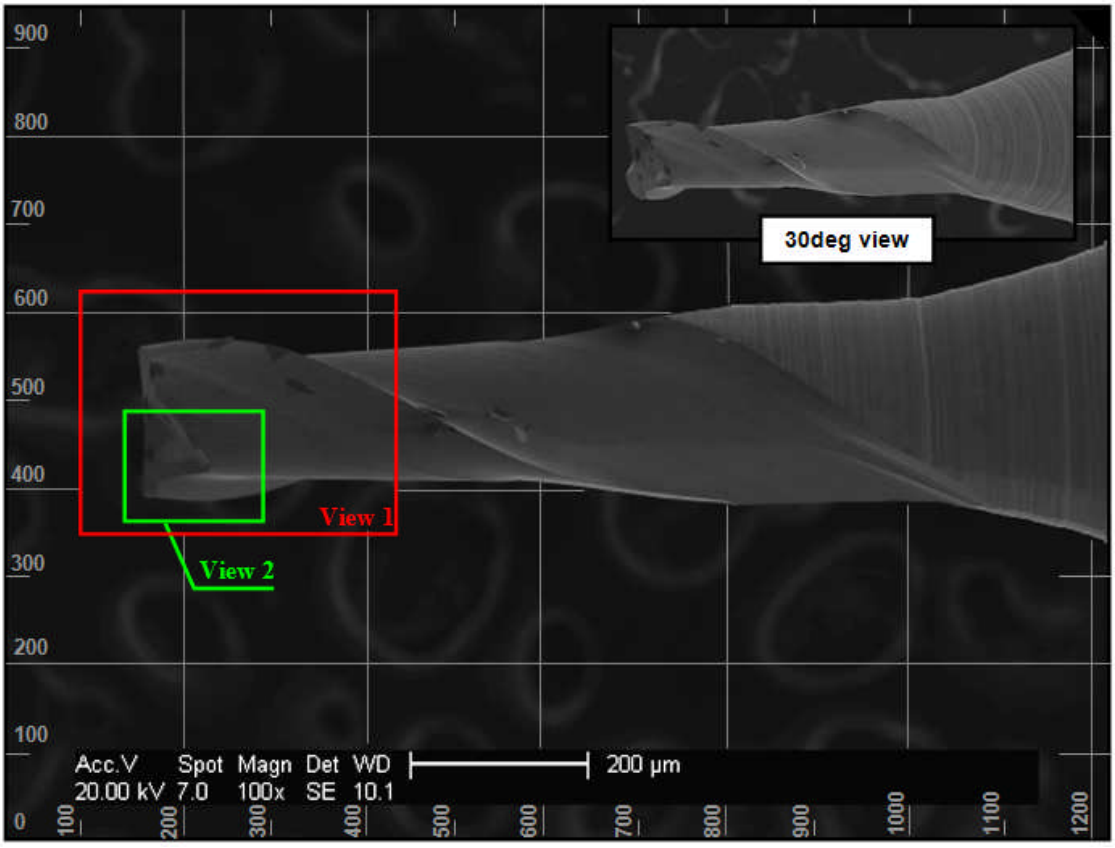

(a) Overall view (mag. 100x)

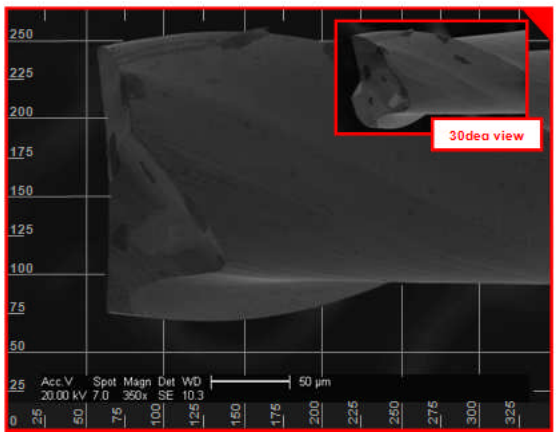

(b) Tool tip view (mag. 350x)

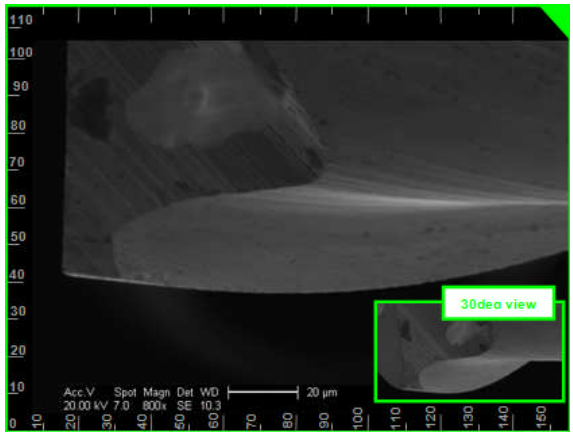

(c) Cutting edge detail (mag. 800x)

Fig B.3: SEM images of second side of a typical uncoated micro end-mill

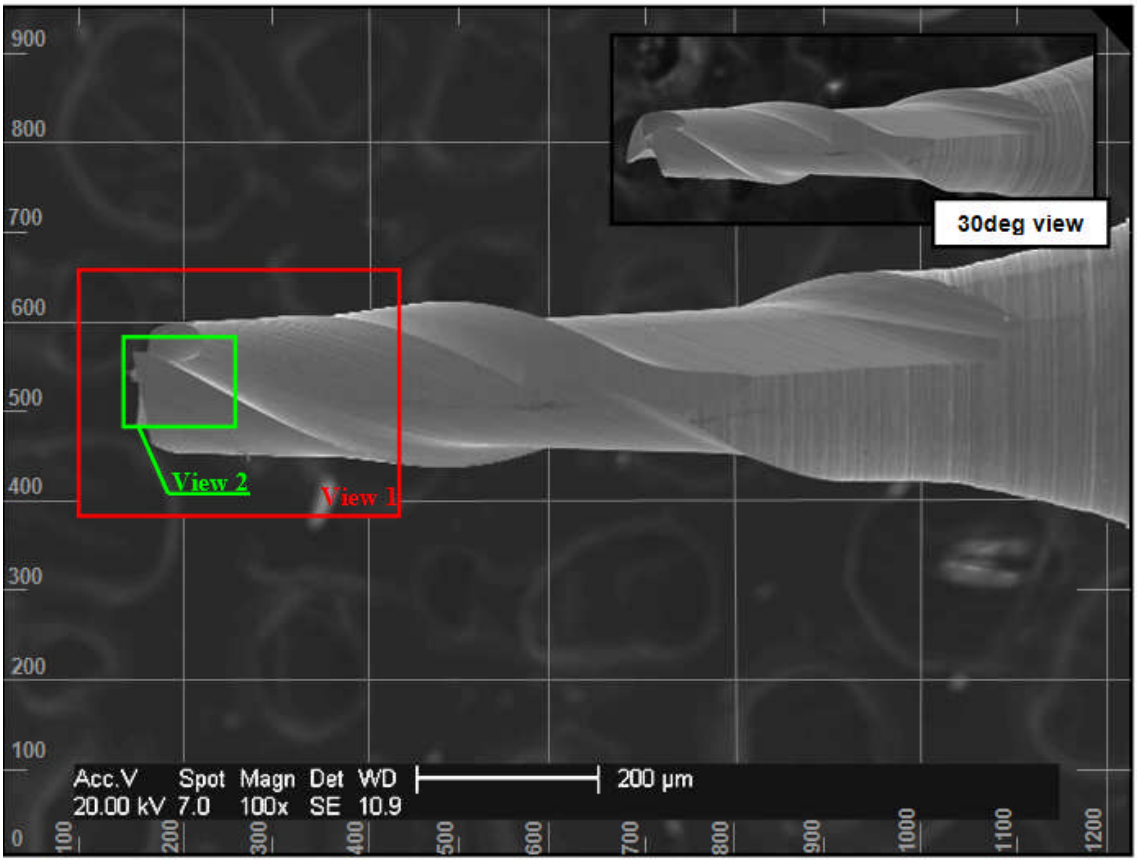

(a) Overall view (mag. 100x)

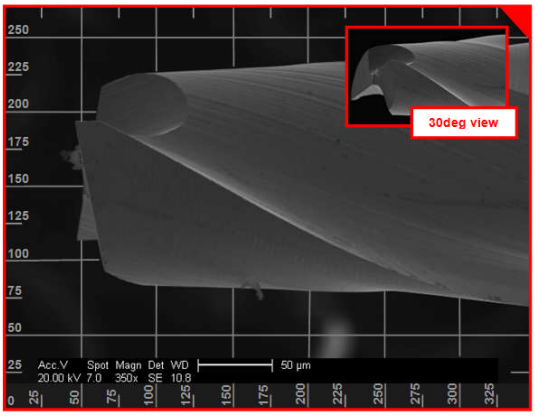

(b) Tool tip view (mag. 350x)

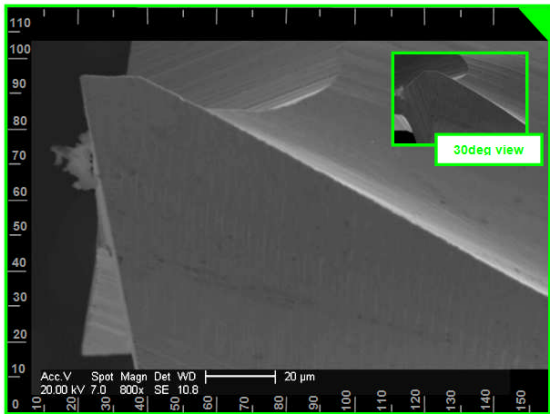

(c) Cutting edge detail (mag. 800x)

Fig B.4: SEM images of third side of a typical uncoated micro end-mill

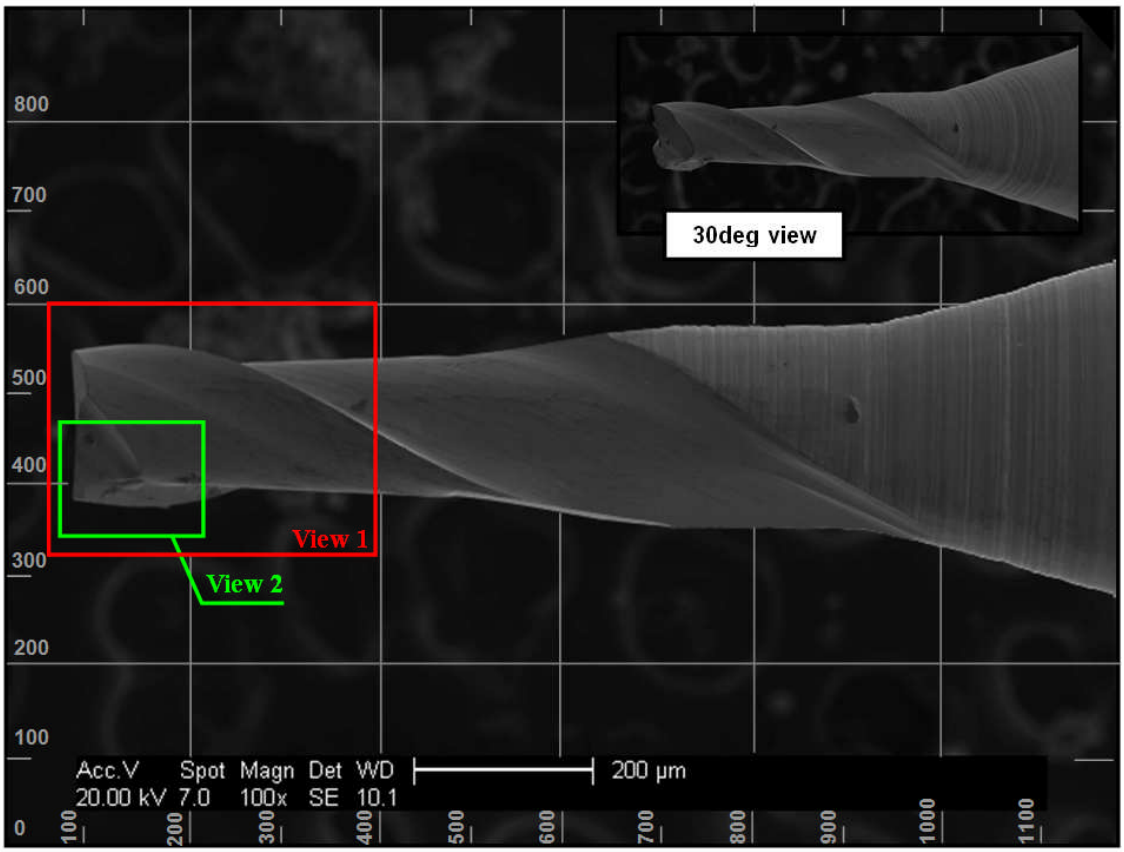

(a) Overall view (mag. 100x)

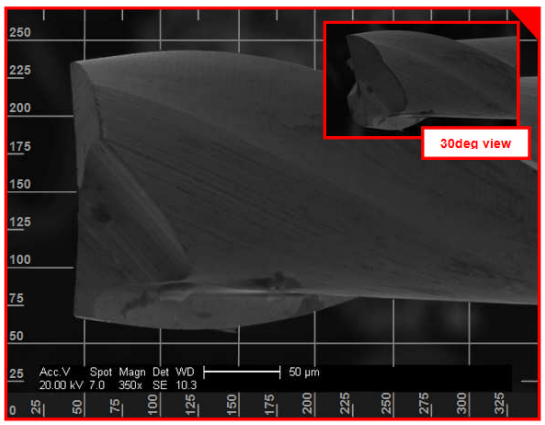

(b) Tool tip view (mag. 350x)

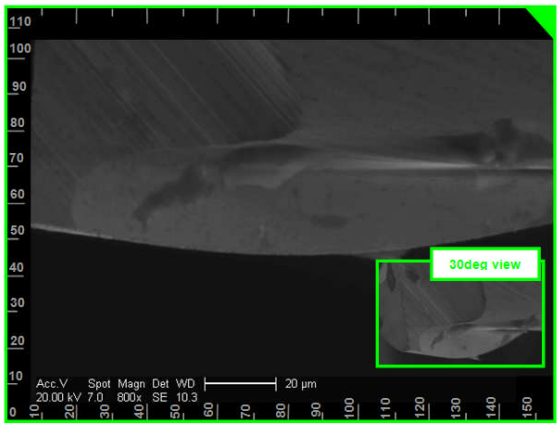

(c) Cutting edge detail (mag. 800x)

Fig B.5: SEM images of fourth side of a typical uncoated micro end-mill

B.2 EDS analysis

The second step of new tool inspection is EDS analysis. This, however, was not conducted with all new tools due to its time demands. Also, the material composition was found not to vary between unique tools as much as the geometrical features. Hence, it has no sense to investigate every tool with highly comprehensive EDS analysis.

The EDS analysis shown in this appendix consists of two steps. First was done a spectrum analysis in chosen locations. This helps to estimate quantity and distribution of material components.

An example of this analysis of tool tip is shown bellow.

Tab. B.1: Weight % of the chemical components – front view

Num. of spectrum / Chemical element	**C**	**W**	**Co**	**Cr**
Spectrum 1 (overall)	***12.09***	***82.73***	***4.88***	***0.31***
Spectrum 7 (overall)	***11.86***	***82.75***	***5.05***	***0.34***
Spectrum 2	*8.87*	*86.82*	*4.04*	*0.27*
Spectrum 3	*8.31*	*89.14*	*2.35*	*0.20*
Spectrum 4	*8.55*	*85.84*	*5.24*	*0.37*
Spectrum 5	*8.26*	*86.66*	*4.74*	*0.35*
Spectrum 6	*8.18*	*88.73*	*2.64*	*0.45*

After spectra analysis, maps of elements were analysed. A typical map is shown in fig. B.7. Furthermore, the distribution of elements was checked for its uniformity. This was done, by counting the elements in different locations of the tool. The distribution of the elements in this example is then plotted in fig. B.8. It is clear, that the distribution is fairly uniform and does not show any abnormalities.

These analyses were done on the tool tip and on all four sides of the tool.

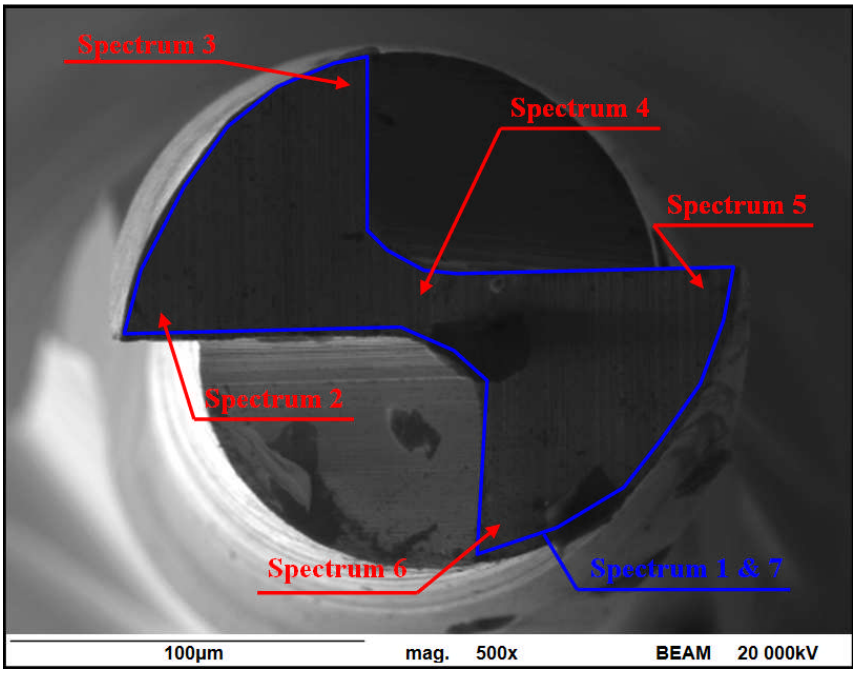

Fig B.6: Distribution of EDS spectra on a tool tip

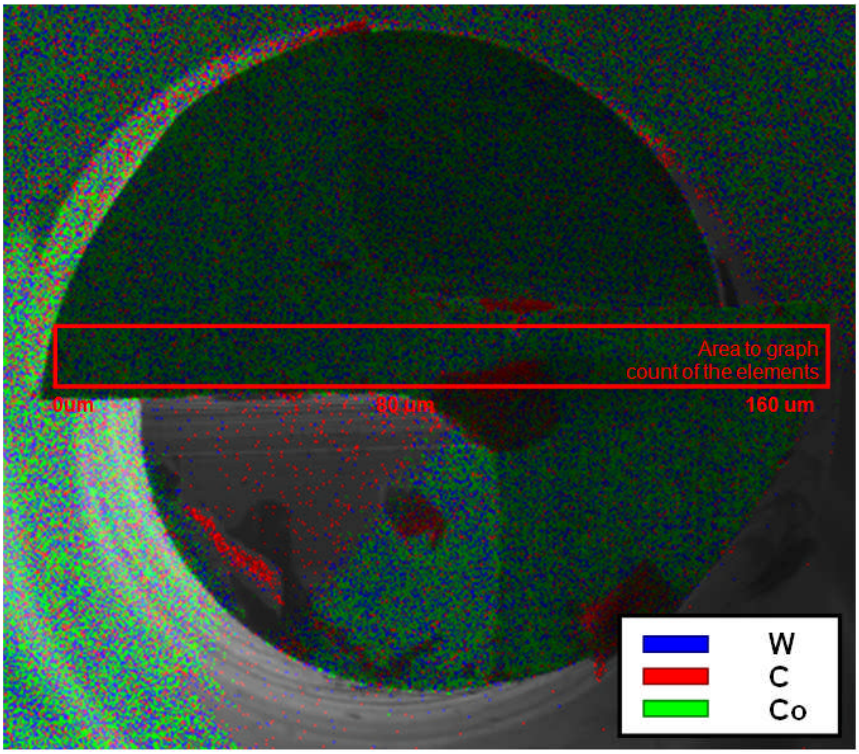

Fig B.7: Distribution of the chemical elements over the tool tip surface

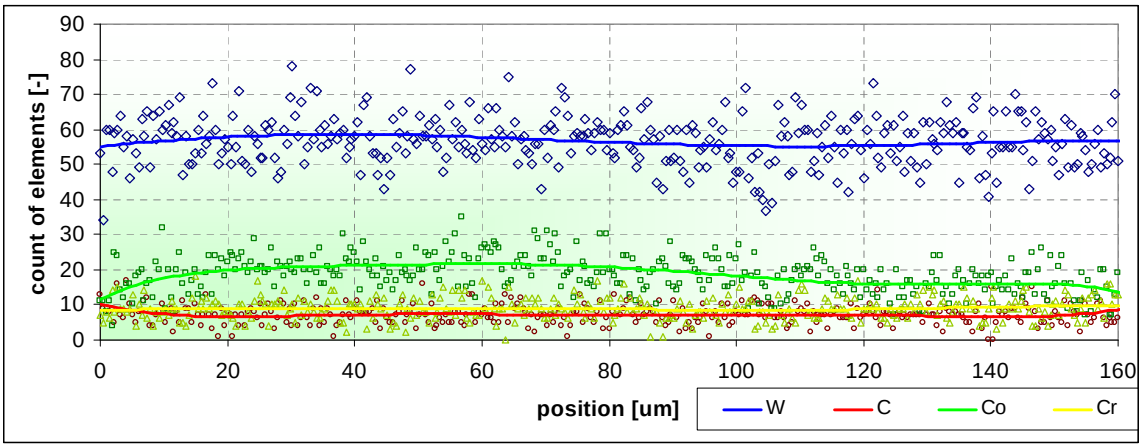

Fig B.8: Distribution of chemical elements on the tool tip